Ph.D. Dissertation

Community dynamics and photophysiological capabilities of diatoms in the water column and sediments of the Pacific Arctic region

太平洋側北極海の水柱および堆積物中における珪藻類の群集動態と光生理能力に関する研究

A thesis submitted in fulfillment of the requirements for the degree of
Doctor in Philosophy in Environmental Science

Yuri FUKAI

Course in Biogeochemistry, Division of Earth System Science
Graduate School of Environmental Science
Hokkaido University

Contents

Abstract

The Pacific Arctic has a broad shelf region, and the northern Bering and Chukchi Seas display among the highest daily primary productivity in the Arctic. The high primary productivity supports the rich marine ecosystems in this region through the food webs. In winter, sea ice is covered over the Arctic region, and light availability in the water column is limited, restricting primary production. After light environments are improved as the sea ice retreats, large microalgal blooms occur during spring and summer. Therefore, changes in sea ice dynamics can affect the timing and magnitude of algal bloom. However, few studies investigate the influence of the changes in the sea ice dynamics on the diatom communities, although diatoms often dominate the microalgal communities during blooms. Because the growth characteristics of diatoms differ among species and can affect the assimilation efficiency by zooplankton, a detailed assessment of changes in the diatom community is essential for considering its effects on marine ecosystems. Many diatom species can form resting stages under unsuitable conditions for growth. Since diatoms, including their resting stages, settle to the seafloor due to their heavy silica frustules, many viable diatoms can be found in the sediments, especially in shallow, high-productive regions. However, even though the Pacific Arctic has a shallow shelf area and a significant interaction between the water column and the seafloor, more knowledge is needed on the photophysiological response of viable diatoms in the sediments when the organisms are released into the water column. Hence, the potential of diatoms in the sediments for primary production has yet to be well-studied. In this study, we aimed to evaluate the effects of spatiotemporal changes in sea ice dynamics on the diatom community in the Pacific Arctic region. In addition, we tried to clarify the roles of diatoms in the sediments of this region in the primary production processes by assessing their photophysiology.

Firstly, we investigated the impact of two-year differences in sea ice dynamics on diatom community composition in the northern Bering Sea (chapters 2 and 3). In this region, the timing of the sea ice retreat in 2018 was earlier than in 2017. By comparing diatom communities in the summer water column, we found that their composition in the Chirikov Basin differed between 2017 and 2018. Typical spring-summer diatom species, such as *Chaetoceros socialis* complex, were dominant in 2017, whereas in 2018, cosmopolitan diatom species often found in the fall season, such as *Thlassionema nitzschioides*, were dominant. These differences in diatom assemblages during summer were most likely related to changes in the timing of the sea ice retreat, but detailed mechanisms of diatom community succession remained unclear. For further study, we assumed that viable diatom communities in the sediments reflected those in the water column before the observations and investigated these microalgal cells. Viable diatom communities in the

sediments south of St. Lawrence Island showed distinct differences between 2017 and 2018. Sea ice-associated diatoms accounted for a relatively high proportion in 2017, while they were hardly detected in 2018. On the other hand, the development of diatom blooms caused by *Thalassiosira* spp. probably occurred in the water column during 2018. In other words, while the light environment and habitat for sea ice-associated diatoms were unsuitable for their proliferation due to the earlier sea ice retreat period in 2018, diatoms such as *Thalassiosira* spp. actively grew in the water column after the sea ice retreat. These results suggest that spatiotemporal changes in sea ice dynamics in the Pacific Arctic region affect the diatom community composition during spring and summer blooms.

We then evaluated the impact of geographic differences in sea ice dynamics on diatom communities (chapter 4). Under the assumptions mentioned above, we investigated the viable diatom communities in sediments over the shelf of the Pacific Arctic. As a result, in the northern Bering Sea and the Chukchi Sea, where the open-water period is extended, open-water diatoms such as *Chaetoceros* spp. and *Thalassiosira* spp. were dominant. In contrast, sea ice-associated diatoms were prevalent in the southwestern Beaufort Sea, where sea ice existed for a relatively long period. Different diatom taxa may contribute to the bloom in the Pacific Arctic shelf depending on the timing of sea ice retreat and the associated light environment.

Our studies in chapters 3 and 4 revealed the existence of viable diatoms, including their resting stages, with extremely high concentrations in the Pacific Arctic sediments. Diatom resting stages are triggered by light exposure to germinate. Diatoms in sediments can proliferate after light irradiation, but dramatic changes in the light environment may be stressful for the microalgal cells. Therefore, the photophysiological response of diatoms in sediments to light exposure was assessed through laboratory culture experiments using sediments from the Chukchi Sea (chapter 5). After light exposure, diatoms in sediments actively grow throughout the incubation period, with *C. socialis* complex mainly contributing to the increase in the diatom community. Changes in the maximum quantum yield of photochemistry (F_v/F_m) in photosystem II, photosynthesis-energy (P-E) curve parameters, and microalgal pigment composition indicated that the physiology related to photosynthesis and photoprotection responded quickly after light exposure. Even when photosynthetic activity was reduced by intense light, it was restored within a few days, indicating a high degree of physiological plasticity of diatoms in sediments in response to light changes. To further study the interaction between diatoms in sediments and the water column, diatom communities in the sea surface and sub-surface of the Chukchi Sea were investigated during the autumn (chapter 6) when the sediments are likely to be resuspended due to strong wind events. First, diatoms were analyzed by scanning electron microscopy and DNA metabarcoding. Then, a correlation network analysis was performed after constructing a dataset with the advantage of both analytical techniques for diatoms. The results revealed that diatom resting stages, which

would be of sedimentary origin, were dominant in the surface and sub-surface layers of the southern Chukchi Sea. It also suggests that diatoms in sediments could be transported into the euphotic layer. Therefore, viable diatoms in the sediments of the Pacific Arctic shelf would have the potential to germinate and proliferate actively due to their high physiological plasticity and the unique environmental characteristics of the shallow shelf.

This thesis suggests that diatoms in the Pacific Arctic shelf significantly contribute to the biogeochemical processes not only through the downward transport of carbon and silicon (i.e., the biological pump) but also through a seeding role of sedimentary diatoms in the water-column primary production. In addition, diatom communities in the water column and sediments can readily alter their composition with changes in sea ice dynamics. Therefore, it is crucial to study how changes in diatom assemblages can affect biogeochemical cycles and marine ecosystems in the Pacific Arctic region, where climate change, including sea ice reduction, has been prominent recently.

CHAPTER 1 – General introduction

1.1. Brief introduction of microalgae and diatoms in the ocean

The ocean is the largest continuous ecosystem on Earth, and microscopic organisms are responsible for the biomass, abundance, and diversity of life there (de Vargas et al., 2015; Bar-On et al., 2018). Microalgae, "small single-celled algae," is one of the essential primary producers in the ocean. Despite the small cell size (typically from several to several hundred micrometers) of the primary producers, the ocean is responsible for more than 45% of global net primary production (approximately 50 Pg C y^{-1}) (Field et al., 1998). Although their habitats are ubiquitous in the world's oceans, for example, in the water column, in sediments, and in/under sea ice, the biogeographical characteristics of their dominant distribution relate to their cell size (Vincent et al., 2022). Pico-sized microalgae (typically 0.2–2 μm) distribute in the tropical and sub-tropical oceans with low nutrients and high temperatures, while nano-sized microalgae (typically 2–20 μm) can be potentially detected from temperate regions (Vincent et al., 2022). Larger-size microalgae, that is, micro-sized microalgae (typically 20–200 μm), grow mainly at high latitudes in spring and upwelling regions with rich nutrients (Vincent et al., 2022) and sometimes form large blooms.

Diatoms, one of the micro-sized microalgae, are a prominent member of microalgal blooms at high latitudes, including polar regions. Due to their fast growth rate (Edwards et al., 2015) and large cell size (~5 μm and up to 2 mm; Hoppenrath et al., 2009), diatoms play crucial roles in the carbon cycle in the ocean (Smetacek, 1999; Tréguer et al., 2018), and they contribute to approximately 40% of oceanic net primary production and about 40% of POC export (Nelson et al., 1995; Jin et al., 2006). They are also essential organisms for the ocean silica cycle because diatom frustules are made of the element (Tréguer and De La Rocha, 2013). Approximately 1400–1800 species belong to the marine diatoms (Sournia et al., 1991). However, more species would exist because 4,748 operational taxonomic units (OTUs) of diatoms are identified from the 18S rRNA gene-based analysis (Malviya et al., 2016). Thus, diatoms are the most widespread and diverse genera worldwide (Malviya et al., 2016). Diversity in diatom assemblages is sometimes affected by environmental factors. For example, the temperature is a significant factor in controlling diatom diversity in the expansive ocean area except for the shallow Pacific Arctic

shelf (Endo et al., 2018). The community composition of diatom genera is usually different among their habitats (Sakshaug, 2004). For example, in the Arctic, pennate diatoms and genus *Attheya* are often dominated in the sea ice (e.g., von Quillfeldt et al., 2003; Campbell et al., 2018) and on the sediments (e.g., von Quillfeldt et al., 2003), while in the open water, other centric diatoms, such as *Chaetoceros* and *Thalassiosira*, are dominant genera (e.g., von Quillfeldt, 2000; Sergeeva et al., 2010). Specific growth rates, photosynthetic efficiency, and sensitivity to environment differ among diatom species (e.g., Goldman, 1993; Kvernvik et al., 2018). In addition, assimilation efficiencies by copepods, one of the most dominant zooplankton in abundance and biomass, vary with diatom species (Abe et al., 2013). Therefore, changes in diatom community composition would influence primary productivity, energy transfer to zooplankton, and subsequent higher trophic levels in marine ecosystems, especially in diatom-dominant regions.

1.2. Introduction of the Pacific Arctic region

1.2.1. Brief introduction of hydrography in the Pacific Arctic region

The hydrographical environments from the northern Bering to the Chukchi Sea show complex characters (Danielson et al., 2017) (Figure 1.1). The Anadyr Water (AW), with low temperature, high salinity, and high nutrients, flows on the western side of the northern Bering and Chukchi Seas. The AW originates from subsurface water of the Bering Basin and flows through the Gulf of Anadyr. The winter-time intrusion of the Pacific-origin water to the lower layer of the Gulf of Anadyr is enhanced in the low sea ice production year due to southerly wind and a lower amount of dense water (Abe et al., 2021). Because the Pacific-origin water is known as subarctic intermediate nutrient pooled water whose nutrients are laden through upward turbulent around the Aleutian Islands (Nishioka et al., 2020), its inflow into the Gulf of Anadyr could enhance nutrient levels within the gulf. On the other hand, the Alaskan Coastal Water (ACW), characterized by high temperature, low salinity, and low nutrients, flows on the eastern side of the northern Bering and Chukchi Seas. In addition, water masses associated with sea ice dynamics are also known; the Bering Chukchi Winter Water (BCWW) is a cold-water remnant from the previous winter's cooling, ice formation, and brine rejection, and the Melt Water (MW) is relatively cold and fresh which is influenced by sea ice melt. The western Beaufort Sea has a westward Beaufort Gyre offshore, while the ACW is on the landward side (Norton and Weller,

1984; Pickart et al., 2013; Danielson et al., 2017).

1.2.2. Important characteristics of submarine topography and biology in the Pacific Arctic region

The Pacific Arctic region extends from the Bering Sea to the Chukchi, the East Siberian Sea, and Beaufort Seas. There is a broad shelf region, and the total area occupies 3085000 km^2 (East Siberian Sea shelf: 987000 km^2, Chukchi Sea shelf: 620000 km^2, Beaufort Sea shelf: 178000 km^2, and Bering Sea shelf: 1300000 km^2) (Sakshaug, 2004) (Figure 1.1). Within the Pacific Arctic shelves, the northern Bering and the Chukchi Seas display among the highest daily rates of productivity in the Arctic using rich nutrients from the AW (Springer et al., 1996; Hill et al., 2018), leading to the high particulate organic carbon (POC) sinking flux in this region. The POC flux in the Chukchi Sea in 2018 was the highest among literature across the global oceans (O'Daly et al., 2020). Therefore, the shallow depth and high primary productivity in the water column support patchy distributions of high benthic biomass known as "biological hotspots" (Grebmeier et al., 1988, 2006). The high benthic standing stocks in the northern Bering and Chukchi Seas support some higher trophic organisms of benthic feeders, such as Pacific walrus (*Odobenus rosmarus divergens*), gray whales (*Eschrichtius robustus*), and bearded seals (*Erignathus barbatu*) (reviewed in Grebmeier et al., 2006). This strong interaction between the water column and seafloor is called "pelagic-benthic coupling," which expresses one of the critical biogeochemical features in the northern Bering and Chukchi Seas (Grebmeier et al., 1988, 2006). In contrast to the northern Bering and Chukchi Seas, primary productivity in the southwestern Beaufort Sea is low (Frost and Lowry, 1984), and mean daily water column integrated primary productivity in this region is about half of that of the southern Chukchi Sea, even during peak periods in June and July (Hill et al., 2018). The marine food webs in the southwestern Beaufort Sea are relatively simple (Norton and Weller, 1984): Arctic cod, which feed on zooplankton, are consumed by ringed seals, several species of seabirds, and probably also white whales (Frost and Lowry, 1984).

The large microalgal blooms support marine ecosystems in the Pacific Arctic from spring to summer. In the seasonal sea ice area, such as the Pacific Arctic region, where the sea ice extends in winter and retreats in summer, two microalgal blooms are traditionally thought to be formed. In other words, ice algal production occurs in and under the sea ice (ice-associated bloom) and is followed by phytoplankton blooms during the summer retreat of sea ice (open-water bloom)

(Horner and Schrader, 1982; Horner, 1984). During microalgal blooms in this region, diatoms generally dominated (e.g., Sergeeva et al., 2010; Giesbrecht et al., 2019; Suzuki et al., 2021). However, diatom communities have uncertainties against environmental changes, which remain unassessed.

1.2.3. Sea ice loss in the Pacific Arctic – a case during the winter of 2017/2018

The Pacific Arctic region is experiencing the most significant seasonal retreat and thinning of the sea ice in the Arctic (Markus et al., 2009; Grebmeier and Maslowski, 2014; Grebmeier et al., 2015; Frey et al., 2018). In particular, the winter of 2017/2018 experienced the lowest winter-maximum areal sea ice coverage since 1980 in the Bering Sea (Stabeno and Bell, 2019). Sea ice production in the Anadyr polynya, one of the most active polynyas in the Northern Hemisphere (Ohshima et al., 2020), was also the lowest in the past 16 years. The sea ice production was only one-tenth of the high value in the 2015/2016 season (Ohshima et al., 2020). The sea ice decline during the winter of 2017/2018 was due to unusual southerly and relatively warm (> 5ºC) wind during the ice season, which led to the later arrival and earlier retreat of sea ice in the northern Bering Sea (Stabeno and Bell, 2019). South of St. Lawrence Island (SLI) would receive hydrographical effects from low sea ice. That is, the reduced sea ice and, hence, sea ice melt resulted in minimal low-salinity water at the near-surface and, thus, weakening the strength of the vertical stratification (Stabeno and Bell, 2019). This unusually weaker stratification was maintained even until summer (Ueno et al., 2020), and it allowed warming of the bottom south of SLI throughout summer, leading to the loss of cold water known as the “cold pool” and defined as < 2ºC.

The timing of sea ice retreat is thought to influence the microalgal bloom timing and magnitude (Hunt et al., 2002; Fujiwara et al., 2016). When sea ice retreats before sufficient light for algal production, the distinct ice-associated bloom vanishes (Hunt et al., 2002). Still, the open-water bloom is likely to become more prominent (Fujiwara et al., 2016). An unusual sea ice condition during the spring of 2018 also affected microalgal blooms in the northern Bering Sea. Ocean color satellite records and mooring mounted *in situ* fluorescence observation in the northern Bering Sea revealed the higher peak concentrations of chlorophyll *a* and the later bloom onset after the sea ice retreat in 2018 (Hirawake and Hunt, 2020; Kikuchi et al., 2020). The late bloom timing in 2018 led to a delay in large copepod reproduction; thus, smaller copepods

dominated the zooplankton assemblages (Duffy-Anderson et al., 2019; Kimura et al., 2022). These changes in a lower trophic organism affected fish abundance, and thus, states of the higher trophic organisms, for example, seabirds (e.g., Nishizawa et al., 2020) and ice-dependent seals (Boveng et al., 2020) through the marine food webs.

1.3. Diatom resting stages

1.3.1. Brief introduction of diatom resting stages

The high POC sinking flux in the Chukchi Sea (see, section 1.2.2 in this chapter) is mainly composed of viable diatoms (Lalande et al., 2020; O'Daly et al., 2020). Therefore, in sediments of the Chukchi Sea, large amounts of viable diatoms, including diatom resting stages, are accumulated (Tsukazaki et al., 2018).

Diatom resting stages are like "seeds" of higher plants; their photosynthesis and dark respiration rates are lower than those of active vegetative cells (Kuwata et al., 1993). The resting stages of diatoms are classified into "resting spores" and "resting cells," depending on their morphological features. Resting spores usually have quite different morphological features from vegetative cells of the same species, and its frustule is a heavily silicified rounder shape and less elaborate surficial pattern (McQuoid and Hobson, 1996). There are also three types of resting spores, defined depending on where the theca of the resting spore is relative to the original cell (Hargraves and French, 1983) (Figure1.2). On the other hand, resting cells have undergone physiological and cytoplasmic changes but are morphologically very similar to vegetative cells of the species (e.g., Anderson, 1975). The formation of resting spores is more frequent in marine-centric species. In contrast, pennate diatoms and freshwater species may more often form resting cells, and some species use both strategies (reviewed in McQuoid and Hobson, 1996).

Diatom vegetative cells are reproduced by binary fission (Figure1.2), except for the restoring cell-size process that auxospores (a large sphere surrounded by an organic membrane) are formed through sexual acts. Resting stages are generally formed during asexual vegetative cell divisions (Figure 1.2), except for a few species, such as *Leptocylindrus danicus*, forming resting spores in their auxospores (Davis et al., 1980; French III and Hargraves, 1985). Resting spore formation is sometimes thought to occur in specific cell sizes (Drebes, 1966), but actually, some species can form resting spores from variable-size cells (Hargraves and French, 1983;

French III and Hargraves, 1985). Triggers of resting stage formation have been traditionally thought to be some abiotic factors (nutrient, Fe, pH, light, temperature, salinity), and particularly, nitrogen depletion has a strong effect on resting spore formation (Hargraves and French, 1983; McQuoid and Hobson, 1996), while resting cells are reported to be induced even when it places in darkness (Anderson, 1975). In addition, recent studies suggest that some biotic factors, such as virus infection and high cell concentrations, can induce resting spore formation in *Chaetoceros socialis* (Pelusi et al., 2020, 2021).

1.3.2. Physiological features of diatom resting stages

Kuwata et al. (1993) compared ecophysiological characters between resting stages and vegetative cells of *C. pseudocurvisetus*. They revealed that the characteristics of resting spores were significantly different from those of vegetative cells. The net photosynthesis and dark respiration rates per cell in the resting spores were ~67 times and ~9.6 times lower than those in the vegetative cells, respectively (Kuwata et al., 1993). In addition, the carbon content per cell was ~1.7 times higher in the resting spores, although the nitrogen content per cell was ~2.2 times higher in the vegetative cells (Kuwata et al., 1993). As mentioned above, resting spores have heavily silicified frustules, and their sinking rates are generally faster than vegetative cells (McQuoid and Hobson, 1996). Therefore, given all these characteristics of diatom resting spores, they would play a crucial biogeochemical role in sinking carbon and silica fluxes (e.g., Rynearson et al., 2013).

Survival time of resting stages varies depending on literature, even among the same species (reviewed in Hargraves and French, 1983). However, Hargraves and French (1983) pointed out several trends. First, temperature affects the survival time of most resting stages, and they tend to survive longer at colder temperatures. Second, the resting stages of cold-water species do not tolerate higher temperatures than their vegetative cells (Durbin, 1978), while the resting stages of temperate species (e.g., *Leptocylindrus danicus*) can survive relatively long periods even at elevated temperatures. Third, no centric resting stage has survived two years. In addition, another study by Hollibaugh et al. (1981) reported that germination rates of *Chaetoceros diadema*, *C. vanheurckii*, and *C. didymus* decreased over time. Initially, they were 90%, but after 167 days, they declined to 50%. Storage for 392 days reduced the germination rates of these species to 5–20%, and 645 days of storage reduced them by 1–10% (Hollibaugh et al., 1981). However, the

germination of *Chaetoceros* was reported from the sediment core of the Baltic Sea, whose age is estimated to be ~6600 calendar years before the present, with a germination rate of ~12% (Sanyal et al., 2022).

Germination of diatom resting stages is induced by light exposure (Hollibaugh et al., 1981) and blue light is most effective for the germination and subsequent survival of diatoms (Shikata et al., 2009). On the contrary, few studies have investigated the minimum irradiance needed for germination. Hollibaugh et al. (1981) and Shikata et al. (2011) suggested that the irradiance of 1.3 μmol photons m^{-2} s^{-1} did not induce resting spore germination of *C. diadema*, *C. vanheurckii*, and *C. didymus*, and the germination rate of *L. danicus* at 3 μmol photons m^{-2} s^{-1} was the same levels to that in the dark control, respectively. However, these two studies also indicated that relatively low light intensity, such as 30 μmol photons m^{-2} s^{-1} and 10 μmol photons m^{-2} s^{-1}, was adequate to induce germination (Hollibaugh et al., 1981; Shikata et al., 2011). The irradiation time required for germination of *L. danicus* resting spores do not depend on exposed light intensities (Shikata et al., 2011). As a result, some field studies in environments where sufficient light reaches the sea bottom, such as temperate Hakata Bay, Japan, and the coastal shallow Arctic Svalbard, reveal that diatom resting stages contribute to spring diatom blooms (Shikata et al., 2009; Hegseth et al., 2019). In addition, Shiozaki et al. (2022) showed that the light environments near the seafloor during late summer induced bottom-associated blooms related to viable diatoms in the Chukchi Sea sediments.

1.4. Photophysiology of microalgae

1.4.1. Photosynthesis mechanism

Microalgae produce organic compounds through photosynthesis. The sun's energy is captured and stored by a series of events that convert the pure energy of light into the free energy needed to power life (Blankenship, 2014). This process begins with photon absorption and ends with the export of stable carbon products from chloroplast and can be generally described as follows (Falkowski and Raven, 2007):

$$2H_2A + CO_2 + Light \xrightarrow{pigment} (CH_2O) + H_2O + 2A.$$

Except for photosynthetic bacteria other than cyanobacteria and a group of aerobic photoheterotrophs, which can fix carbon only under anaerobic conditions and are incapable of

evolving oxygen, all other photosynthetic organisms (cyanobacteria, prochlorophytes, eukaryotic algae, and higher plants) are oxygenic. The photosynthetic reaction can be written as follows (Falkowski and Raven, 2007):

$$2H_2O + CO_2 + Light \xrightarrow{chl\ a} (CH_2O) + H_2O + O_2$$

where chl *a* denotes the principal photosynthetic pigment chlorophyll *a*.

In eukaryotes, most photosynthesis reactions occur in the chloroplast. The chloroplast has a membrane system known as "thylakoid," while the interior of the chloroplast is called "stroma" (Figure 1.3 a). Photosynthesis can be mainly classified into two processes, "energy conversion" and "biosynthesis," and the former process is associated with the thylakoid, while the latter is conducted in the stroma (Figure 1.3 b). As the first step of energy conversion, light is absorbed by a light-harvesting complex (LHC) which consists of some pigments and associated proteins (e.g., diatom possesses fucoxanthin chlorophyll *a*/*c* proteins as an antenna; Wang et al., 2020). The absorbed light energy is then transferred as excited energy to the reaction center in photosystem II (PSII), leading to the charge separation of a special pair of chlorophyll *a* molecules. Through a reaction in the manganese cluster, not only water (H_2O) is split into an oxygen molecule (O_2) and four protons (H^+), but also electrons are removed. The removed electron is then transferred along the electron transport chain to photosystem I (PSI). In the PSI, after a second electron transfer process driven by light, the electrons reduce an intermediate electron acceptor, $NADP^+$, resulting in NADPH formation. The protons, produced by water splitting or transferred through the cytochrome b_6f complex, accumulate in the thylakoid's lumen side. Therefore, their transportation from the lumen to the stroma, derived by an electrochemical potential gradient, synthesizes the adenosine triphosphate (ATP) from the adenosine diphosphate (ADP) and the inorganic phosphate. Using the generated ATP and reduction power, the biosynthesis step is driven by a cycle known as the "Calvin cycle," and carbon dioxide (CO_2) is assimilated (Figure 1.3 b).

1.4.2. Photoacclimation strategy and its assessment

When microalgae absorb light over the amount available for photochemical reactions of photosynthesis, a plastoquinone (PQ) pool is highly reduced. As a result, it hinders forward electron flow, which triggers charge recombination in PSII and leads to the generation of triplet chlorophyll and highly toxic singlet oxygen molecules (Krieger-Liszkay and Feilke, 2016), which

are one of the reactive oxygen species (ROS). Generated ROS in chloroplast damages the photosystems (Lesser, 2006), resulting in a decrease in the rate of photosynthesis. Therefore, intense light that exceeds the photochemical capability would harm photosynthetic organisms, including microalgae. Furthermore, microalgae experience the fluctuating light environment associated with daylight variations, vertical transportation in the water column, and so on. Therefore, they must quickly acclimate their photochemical capability to be optimal according to the ambient environment, significantly not to suffer damage from the excess light.

Microalgae employs some photoacclimation strategies associated with their pigments. Algal pigments are mainly categorized into two groups based on their functions: light-harvesting and photoprotective (Brunet et al., 2011). The pigments that transfer the absorbed light energy to the reaction center have light-harvesting functions. In contrast, some pigments, which are not involved in photosynthesis and do not transfer the absorbed energy to the reaction center, play a vital role in photoprotection (Brunet et al., 2011). The long-term (hours to days) photoacclimation associated with the pigments results in changes in pigment composition; generally, cells acclimated to high light conditions contain low amounts of light-harvesting pigment and high quantities of photoprotective pigments, while the opposite relationship can be observed for cells acclimated to low light (Brunet et al., 2011). Diatoms have important photoprotective pigments: diadinoxanthin, diatoxanthin, and β-carotene (Kuczynska et al., 2015). β-carotene is the most efficient natural quencher of singlet oxygen and may protect against lipid peroxidation (Stahl and Sies, 2005; Kuczynska et al., 2015), although the pigment is bound exclusively to photosystems I and II and not in the peripheral antenna (Wang et al., 2020; Xu et al., 2020; Buck et al., 2022). The other carotenoids (xanthophylls), diadinoxanthin and diatoxanthin, are involved in the xanthophyll cycle in diatoms, which is believed to play a central role in the non-photochemical fluorescence quenching (NPQ) (Brunet et al., 2011; Yan et al., 2019; Lacour et al., 2020) that is the mechanism by which collected light energy is dissipated as heat. The diadinoxanthin-diatoxanthin cycle involves the de-epoxidation/epoxidation of diadinoxanthin and diatoxanthin (Figure 1.4), responsible for a short-term (minutes to hours) photoacclimation process. This cycle is operated by the two enzymes (diadinoxanthin de-epoxidase and diatoxanthin epoxidase) as a function of pH. Because the optimal pH of diadinoxanthin de-epoxidase localized lumen side of the thylakoid is around 5–7, the irradiance-dependent photosynthetic electron transport rate and subsequent change in pH, allow the enzyme production, leading to de-epoxidation of

diadinoxanthin into diatoxanthin (Brunet et al., 2011). In particular, diadinoxanthin de-epoxidase is active even at pH7 (Jakob et al., 2001) indicates that de-epoxidation of diadinoxanthin already occurs for low light intensities and short illumination times (Brunet et al., 2011). Diatoxanthin epoxidase is also inactivated under excess light conditions (Goss et al., 2006). Therefore, for responding to light exposure, the diadinoxanthin-diatoxanthin cycle would accumulate large amounts of diatoxanthin efficiently and rapidly.

Although the degrees of light acclimation by microalgae to ambient environments can be evaluated using the above pigment indices, it is crucial to assess primary production as the whole photosynthetic process. In other words, we should explore the response of microalgae in terms of carbon assimilation (i.e., primary production) because this is the process by which microalgae affect the ocean carbon cycle. As one of the carbon-based assays, the photosynthesis-energy (P-E) curve experiment, can reveal carbon assimilation rates of microalgae as a function of irradiance, resulting in an understanding of photophysiological characteristics and light acclimation states (Sakshaug et al., 1997). As a fitting curve against the P-E relationship (Figure 1.5), the function suggested by Platt et al. (1980) is commonly used when photoinhibition occurs (see materials and methods in chapter 5 for the equations). This function includes the following three parameters: P_s, α, and β. Because P_s, α, and β indicate the hypothetical maximum photosynthetic rate in the absence of photoinhibition, light utilization efficiency for photosynthesis, and photoinhibition, respectively, we can evaluate the photosynthetic state of a microalgal strain or community from these parameters. In addition, using these three parameters, we can estimate other parameters: P_{max} and E_k (see materials and methods in chapter 5 for the details of the equations) (Figure 1.5). The P_{max} shows the maximum photosynthetic rate, and the E_k is the photoadaptation parameter. Therefore, we can understand the algal photosynthetic capability and the degree of photoadaptation in terms of the whole process of photosynthesis through the carbon-based P-E curve experiment.

1.5. Aims of this study

My PhD work tried to reveal the community dynamics and photophysiological capabilities of diatoms in the water column and sediments of the Pacific Arctic. Diatoms are dominant taxa during the microalgal blooms and can quickly respond to environmental changes. In addition, the surveyed area, the Pacific Arctic region, is experiencing drastic changes in sea ice

dynamics. However, few studies have revealed the relationships between sea ice dynamics and diatom communities, mainly focusing on the intra-community changes in diatoms. Therefore, in chapters 2 and 3, we aimed to understand the diatom community dynamics responding to the interannual sea ice changes as case studies of 2017 and 2018. Chapter 2 approached this objective with the seawater observation during summer. In chapter 3, we used viable diatom communities in sediments to assess the community dynamics in the water column. Chapter 4 focused on the spatial changes in sea ice dynamics over the Pacific Arctic shelves and aimed to reveal the relationships with diatom communities. Also, in this chapter, we used viable diatom communities in the sediments as a proxy for diatom blooms in the water column. The distribution of viable diatom assemblages in sediments is thought to reflect the extent and magnitude of past blooms (Pitcher, 1990; Itakura et al., 1997). However, no one has ever tested this hypothesis on the Pacific Arctic shelf. Therefore, we tried to verify whether the viable diatoms in sediments reflected the primary production in the water column. Through the analyses of chapters 3 and 4, we found many viable diatoms in sediments of the northern Bering and Chukchi shelves. However, regardless of the strong interactions between the water column and seafloor in the northern Bering and Chukchi shelves, responses of viable diatoms in sediments to light exposure are still unknown. Therefore, in chapter 5, we aimed to clarify the photophysiological responses of viable diatoms in sediments of the Chukchi Sea to light exposure. In chapter 6, we tested the possibilities for diatom resting stages in sediments to resuspend to the water column in the Pacific Arctic. In other words, we tried to characterize the autumn diatom community in the Chukchi Sea water column to unravel the source of diatom communities in the water column. Throughout the Ph.D. thesis, we aimed to shed light on the role of diatom communities, including diatom resting stages and viable diatoms in sediments, in the biogeochemical cycle of the Pacific Arctic region.

1.6. Figures

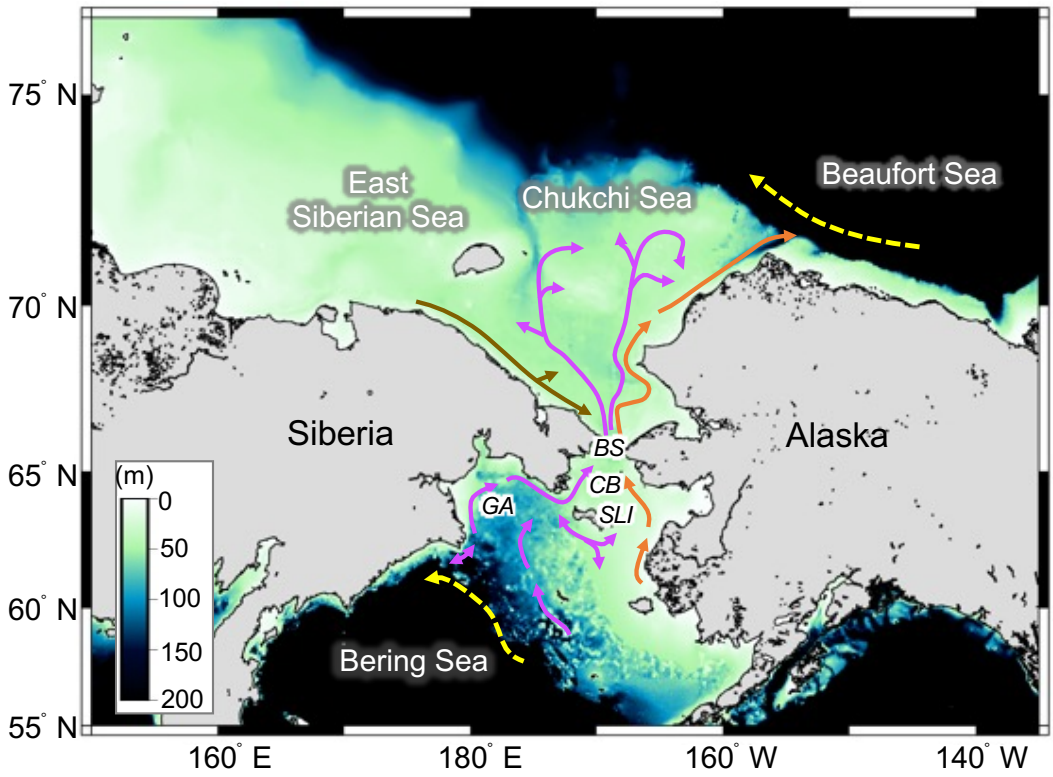

Figure 1.1. The Pacific Arctic region. The contour indicates bottom depth from 0 to 200 m. Mean flow pathways are colored to denote the current systems and/or typical water mass pathways: Yellow=Bering Slope Current and Beaufort Gyre; Orange=Alaskan Coastal Current; Brown=Siberian Coastal Current; Purple=pathways of Bering shelf, Anadyr, and Chukchi shelf waters. Abbreviation: *GA*: Gulf of Anadyr, *SLI*: St. Lawrence Island, *CB*: Chirikov Basin, *BS*: Bering Strait. The figure was made with reference to Danielson et al. (2017).

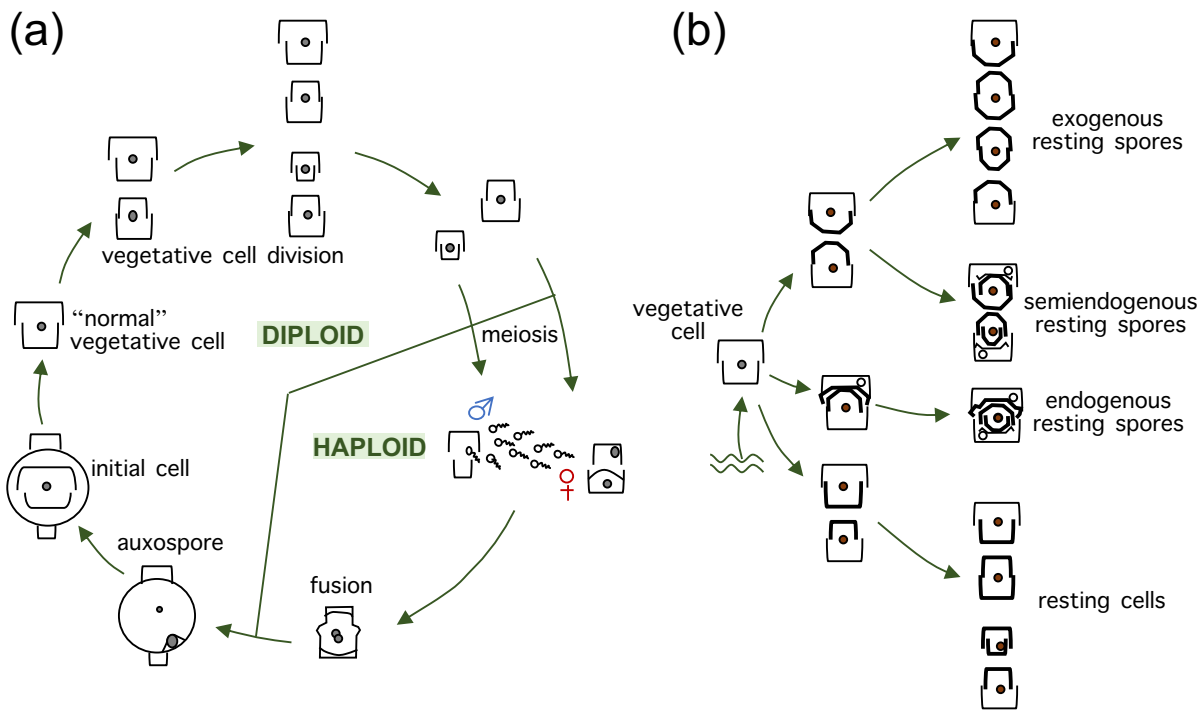

Figure 1.2. (a) Schematics of the diatom life cycle. (b) Formation of diatom resting stages. Resting spores are classified into three types (exogenous, semiendogenous, and endogenous) depending on where the thick frustule is formed. The figures are modified from Hasle and Syvertsen (1997).

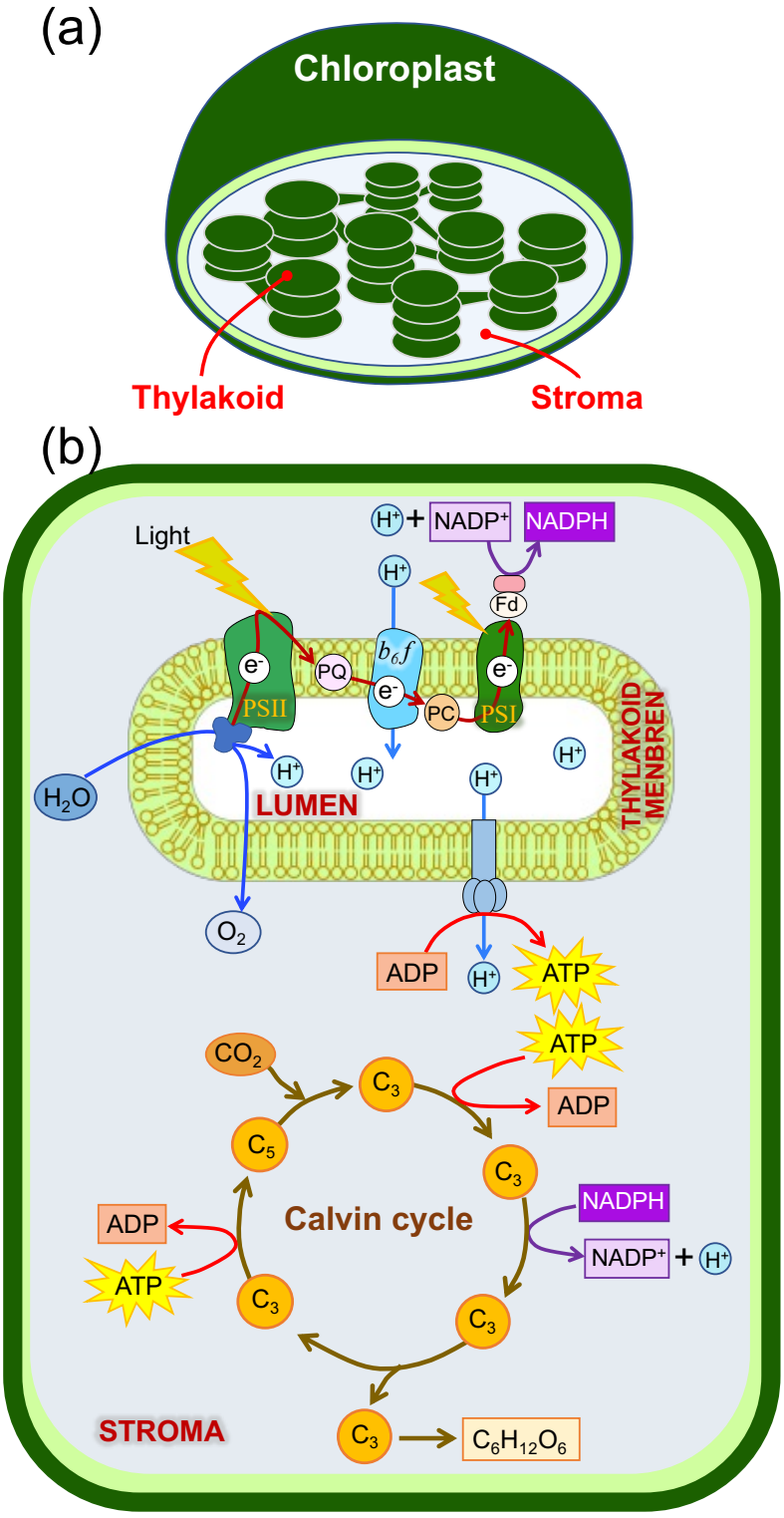

Figure 1.3. Schematics of chloroplast (a) and photosynthesis (b). Abbreviation: PQ: plastoquinone, PC: plastocyanin, b_6f: cytochrome b_6f complex, Fd: ferredoxin.

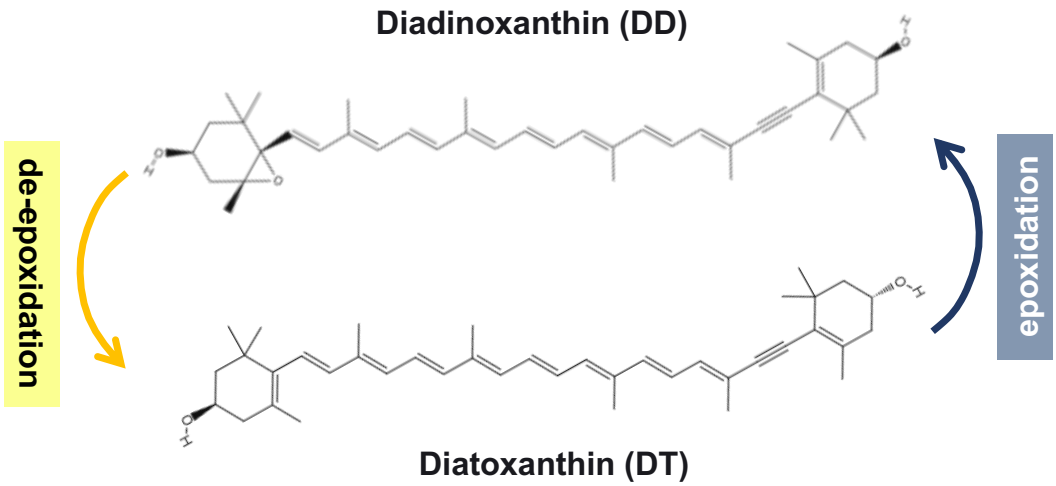

Figure 1.4. A schematic of the diadinoxanthin-diatoxanthin cycle.

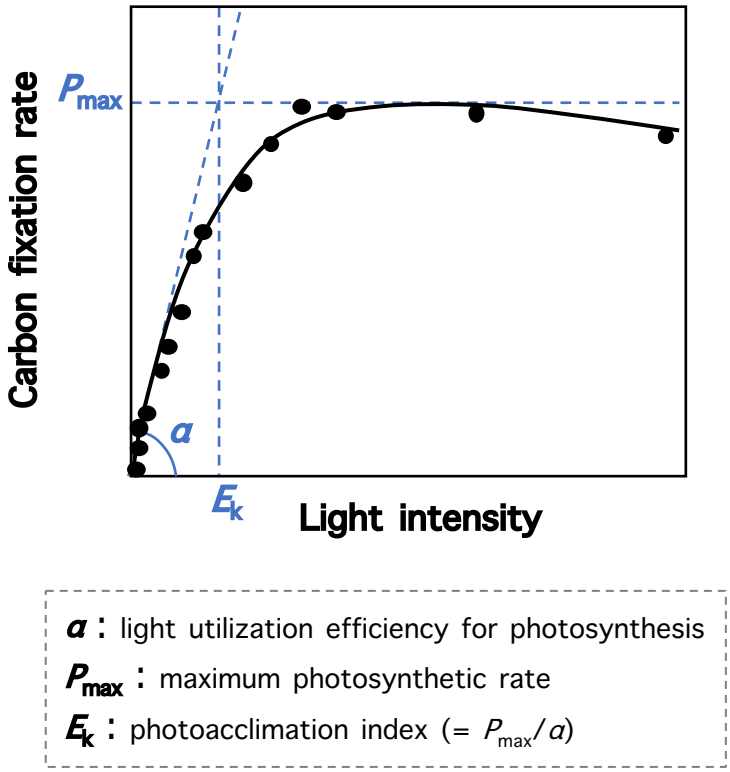

Figure 1.5. A photosynthesis-energy (P-E) curve. The parameters of α, P_{max}, and E_k represent light utilization efficiency for photosynthesis, maximum photosynthetic rate, and photoacclimation index (= P_{max}/α), respectively.

CHAPTER 2 – Summer diatom communities in the northern Bering Sea: the timing of the sea ice retreat affects the diatom composition

2.1. Introduction

The northern Bering Sea is a shallow shelf region and has a complicated hydrographic environment due to the inflow of multiple currents with different hydrographical features (see, general introduction section 1.2.1). Furthermore, mixing of the different water results in complex hydrographic environments that affects the distribution of phytoplankton communities (Giesbrecht et al., 2019). In addition, not only water masses but also the extent of sea ice has been shown to influence regional phytoplankton assemblages (Neeley et al., 2018). As mentioned in the general introduction, the timing of the spring sea ice retreat also affects the magnitude and timing of the phytoplankton bloom (Hunt et al., 2002; Fujiwara et al., 2016).

From late spring to early summer of the northern Bering Sea, when the sea ice is retreating and the light limitation is diminishing, phytoplankton forms large blooms whose chlorophyll *a* concentration sometimes exceeds 8 μg L^{-1} (Springer and McRoy, 1993). Diatoms dominate during the blooms and *Chaetoceros socialis* complex is one of the blooms composing diatoms in the water column during spring and summer (von Quillfeldt, 2000; Sergeeva et al., 2010). The composition of diatom communities is likely to vary depending on the different *in situ* hydrographic environments (Taniguchi et al., 1976; Sergeeva et al., 2010). However, there is little information on how the diatom community responds to changes in sea ice dynamics in the northern Bering Sea despite the importance of diatoms as the bloom composer.

As mentioned in the general introduction, the winter of 2017–2018 had record low sea ice cover in the northern Bering Sea (Hirawake and Hunt, 2020). Because of the sea ice loss in 2018, the magnitudes of the ice edge blooms in early spring were reported to be small (Cornwall, 2019; Kikuchi et al., 2020). Diatom blooms last to early summer but there are few studies to discuss the possibility that sea ice dynamics affect the summer diatom communities.

In this study, we examine the phytoplankton communities, particularly with a focus on the diatom communities, in 2017 and 2018 summer. We conducted the sampling in around the same region (the northern Bering Sea from 62ºN to the Bering Strait) and season (July) in both years and tried to test three hypotheses: 1) that the cell concentrations and species composition of

the diatom community differ by water mass, 2) that the diatom community differed between 2017 and 2018, and 3) that the hydrography, including sea ice condition before sampling, will affect the diatom community.

2.2. Materials and Methods

2.2.1. Study area

Sampling was conducted along the northern Bering Sea shelf from July 9–21, 2017 and July 2–12, 2018 during the 40th and 56th cruises, respectively, of the T/S *Oshoro-Maru* of Hokkaido University (Figure 2.1). The study areas were the waters south of St. Lawrence Island, the Chirikov Basin (from the north of St. Lawrence Island to the south of Bering Strait), and the Bering Strait.

2.2.2. Sea ice

Data on sea ice concentration (SIC) of the Advanced Microwave Scanning Radiometer 2 (AMSR2) was used to evaluate the extent of the sea ice. These AMSR2 data were supplied by the Japan Aerospace Exploration Agency via the Arctic Data archive System (ADS) (https://ads.nipr.ac.jp/), through the cooperation of the National Institute of Polar Research and JAXA. We used a 5-day moving average value of the SIC data. Sea ice covered regions were defined as having a SIC >20%. In addition, the TSR was defined as the last date when the SIC was at 20% before the observed annual sea ice minimum across the study region.

2.2.3. Physical oceanography and water masses

Conductivity-temperature-depth (CTD) casts were conducted at 40 stations in 2017 and 28 stations in 2018 to obtain vertical profiles of the temperature, salinity, and chlorophyll *a* fluorescence (see Figure S2.1). We used a CTD (SBE911, Sea-Bird Electronics, Inc.) calibrated before the cruises. The mixed layer depth was defined as the depth where density was 0.10 kg m^{-3} greater than the value at 5 m depth (Danielson et al., 2011). We identified four water masses that differed in physical characteristics; Bering Chukchi Summer Water (BCSW) ($0 < T < 7$ and $30 < S < 33.5$), Bering Chukchi Winter Water (BCWW) ($-2 < T < 0$ and $30 < S < 33.5$), Alaskan coastal water (ACW) ($7 < T < 12$ and $20 < S < 32$), and Melting Water (MW) ($-2 < T < 7$ and $25 < S <$

30) (Danielson et al., 2017). Note that the water masses (>12ºC in ACW and >7ºC in BCSW) which were unidentified by Danielson et al. (2017) were defined as ACW or BCSW based on their salinity. In addition, to better understand the characteristics of the above water masses defined by Danielson et al. (2017), we classified them according to Danielson et al. (2020) and compared these water masses (Figure S2.2).

2.2.4. Nutrients

At 26 of the CTD stations (14 stations in 2017 and 12 stations in 2018), water samples for nutrient analysis were collected from 4–6 layers every 10 m from the surface to 5 m above the seafloor using a bucket and Niskin bottles (Figure 2.1). The obtained unfiltered nutrient samples (n = 128) in Spitz tubes were frozen on board at –80ºC. In the shore-based laboratory, the major nutrients (NO_2–N + NO_3–N, NH_4–N, PO_4–P, and Si $(OH)_4$) were measured by colorimetric methods using a QuAAtro 2-HR system certified with standard reference materials for nutrient analysis (KANSO, standard Lot BT, BZ, Osaka, Japan) following "The GO-SHIP Repeat Hydrography Manual" (Hydes et al., 2010).

2.2.5. Phytoplankton

Water samples for phytoplankton counts were collected from the same stations and layers as the nutrient samples. A total of 141 phytoplankton samples were collected and preserved as follows: in 2017, 500 mL water samples were concentrated 50-fold using a nucleopore filter (3.0 μm) before being preserved with glutaraldehyde at a final concentration of 1%. Note that the diatoms and dinoflagellates addressed in this study experience little damage from filtering (Dahl and Naustvoll, 2010). In 2018, 1 L of each water sample was preserved on board with glutaraldehyde at a final concentration of 1%. The samples were then settled and concentrated 24- to 33- fold using siphon tubes in the land laboratory. Aliquots (1 mL) of the concentrated samples were transferred to a glass slide to count and identify the diatoms and dinoflagellates with an inverted microscope at 200–600 × magnification. The diatoms and dinoflagellates were counted and identified from approximately 300 cells. When the cell number count was less than 300 cells, the minimum numbers were 18 cells in 2017 and 21 cells in 2018. In addition, the detection limits were 20 cells L^{-1} in 2017 and 30 cells L^{-1} in 2018, suggesting that there was not much difference (ability to detect low numbers of cells in a sample) between the years. Following

Hasle and Syvertsen (1997) and Hoppenrath et al. (2009), the diatoms were identified to the species or genus level and the dinoflagellates were identified to the genus level. Distinguishing *Cylindrotheca closterium* from *Nitzschia longissima* was difficult (Hasle and Syvertsen, 1997), so these species were treated as *Cy. closterium*. In addition, *C. convolutus*, *C. concavicornis,* and *C. borealis* were nearly indistinguishable because they were damaged by current transportation, as mentioned by Taniguchi et al. (1976), so they were collectively counted and identified as *C. convolutus/concavicornis/borealis*. Using the counting data, the diversity of diatoms was evaluated by the Shannon-Wiener index (*H'*).

$$H' = -\sum \frac{n}{N_i} \times ln \frac{n}{N_i}$$

where n is the cell concentrations (cells mL^{-1}) of i th species and N_i is the total diatom cell concentrations (cells mL^{-1}) at each station (Shannon and Weaver, 1949).

2.2.6. Statistical analyses

Differences in phytoplankton cell concentrations among the water masses in the upper mixed layer were tested by the Mann-Whitney *U* test or a one-way analysis of variance (ANOVA). Also, to compare the diatom diversity (*H'*) among the water masses, a one-way ANOVA was used. If the ANOVA identified statistically significant differences ($p < 0.05$), a post hoc Tukey-Kramer test was used to clarify the interactions among the water masses. Differences between the years of the NO_2–N + NO_3–N concentration, which was likely to be a limiting factor among nutrients, were compared by a Mann-Whitney *U* test for each region. Similarly, differences between 2017 and 2018 in the phytoplankton cell concentrations in the Bering Strait, and diatom diversity (*H'*) were tested using a Mann-Whitney *U* test. To compare the diatom community between 2017 and 2018, we first performed a cluster analysis based on the cell concentrations within each water mass (Figure S2.3). Several patterns of the cluster analysis were tested in each year, by water mass, and by depth (cf. Figures S2.3 and S2.4). The results of these tests were uninterpretable, so we used analyses based on all diatom samples from a given year. Thus, this analysis focused on describing year-to-year changes in the diatom community (taxon composition) between 2017 and 2018. To reduce the bias for abundant species, the cell concentration data (X: cells mL^{-1}) for each species were transformed to $\sqrt[4]{X}$ before cluster analysis (Quinn and Keough, 2002). The similarities between samples were examined using the Bray-Curtis index based on the differences

in the species composition. To group the samples, the similarity indices were coupled using hierarchical agglomerative clustering with a complete linkage method (an unweighted pair group method using the arithmetic mean) (Field et al., 1982).

To delineate the sample groups on a two-dimensional map, NMDS ordination was conducted. Thereafter, multiple regression analyses (Y = aX1+ bX2+c, where Y is the environmental variable and X1 and X2 are axes 1 and 2 of NMDS, respectively) were performed to clarify which environmental variables (temperature, salinity, chlorophyll *a* (chl *a*) fluorescence, concentrations of NO_2–N + NO_3–N, NH_4–N, dissolved inorganic nitrogen (DIN), PO_4–P, and $Si(OH)_4$, the ratio of the DIN concentration to that of PO_4–P (N:P ratio), the timing of the sea ice retreat (TSR), observation date, and sampling depth) had significant relationships with the phytoplankton groups. Furthermore, to test intergroup differences in the diatom cell concentrations and hydrographic environments (temperature, salinity, chl *a* fluorescence, concentrations of NO_2–N + NO_3–N, NH_4–N, DIN, PO_4–P, and $Si(OH)_4$, the N:P ratio, and the TSR), a one-way ANOVA and a post hoc Tukey-Kramer test were used. All the analyses were conducted with PRIMER 7 (PRIMER-E Ltd.) or Stat View v5 (SAS Institute Inc.).

2.3. Results

2.3.1. Sea ice

In 2017, the study region south of St. Lawrence Island was first completely ice-covered on January 19, and in 2018, the sea ice cover was not complete until February 5. The sea ice first covered the Bering Strait and the Chirikov Basin, except for the most eastern station, on January 11, 2017, and December 28, 2017. In some stations in 2018 (St. 11 and St. 14, see Figure 2.1), the SIC was repeated over and below 20%. In the most eastern stations in the Chirikov Basin (St. 5 in 2017 and St. 19 in 2018), the SIC exceeded 20% on December 8, 2016 and 2017.

South of St Lawrence Island, in 2017, sea ice disappeared completely by May 3, whereas in 2018, ice left over a month earlier, on March 24. In 2017, the first day when the Chirikov Basin had an ice concentration <20% was on April 5, whereas, in 2018, open water was first detected on March 25, which is 11 days earlier than that in 2017.

2.3.2. Hydrography and nutrient chemistry

We identified four water masses over the study region: BCSW, BCWW, ACW, and MW (Danielson et al., 2017) (Figures 2.2, 2.3, and 2.4). In 2017, the BCWW (< 0ºC) was present at the bottom south of St. Lawrence Island (Figure 2.4). The BCSW was present throughout the water column in the Bering Strait and the northern Chirikov Basin. By contrast, in the eastern coastal area and south of 65ºN in the Chirikov Basin, the ACW was present in the surface layer and the BCSW was observed in the lower layer in 2017 (Figure 2.4). In 2018, the BCWW (< 0ºC) was not present at the bottom in the region South of St. Lawrence Island (Figure 2.4). The BCSW was present throughout the water column in the Bering Strait and the Chirikov Basin, except for the eastern coastal area where the ACW was observed in the surface layer in 2018 (Figure 2.4). However, when compared to the water masses defined by Danielson et al. (2020), warm shelf water was mixed among those divided as the ACW defined by Danielson et al, (2017), especially in 2017 (Figure S2.2). Still, note that ACW, defined by not only Danielson et al. (2017) but also Danielson et al. (2020), extended westward at 65ºN in 2017 (Figure S2.5).

In both years south of St. Lawrence Island, fluorescence above the pycnocline (avg = 0.07 and 0.16 in 2017 and 2018, respectively) was lower than that below the pycnocline (avg = 0.39 and 0.60 in 2017 and 2018, respectively) (Figure 2.2). In Bering Strait, fluorescence was similar in both years (2017, avg = 0.90: 2018, avg = 0.78) (Figure 2.2). In the Chirikov Basin, fluorescence above the pycnocline was higher in 2017 (avg = 0.69) than in 2018 (avg = 0.26), while, below the pycnocline fluorescence was similar in both years (Figure 2.2).

To the south of St. Lawrence Island, NO_2–N + NO_3–N was depleted in the upper mixed layer in both years, but it was high below the pycnocline (Figure 2.5) with no significant differences between the years (*U* test, $p > 0.05$). In the Bering Strait, NO_2–N + NO_3–N did not differ significantly between years (*U* test, $p > 0.05$) (Figure 2.5). In the Chirikov Basin, NO_2–N + NO_3–N were not significantly different between the years (*U* test, $p > 0.05$). In this region, the lowest concentration of nitrate plus nitrite was at the eastern station, whereas the highest concentrations were found in the northern Bering Strait. Concentrations of NO_2–N + NO_3–N and DIN and N:P ratio in the upper mixed layer differed between the water masses, and it was higher in the BCSW than the ACW (*U* test, $p < 0.05$) (Figure 2.6).

Concentrations of the other nutrients were generally similar between years at the same station. In both years in each region, NH_4–N concentrations were similar (Figure 2.5). Likewise,

the PO_4–P concentrations did not vary between years within regions; the highest value detected was in the Bering Strait in 2017 (st.1, 6.62 μM) (Figure 2.5). We found high concentrations of $Si(OH)_4$ over major portions of the study region in both years, except for some stations in 2018 in the eastern Chirikov Basin (st. 11 in 2018) and the south of St. Lawrence Island (sts. 4, 6, 8 in 2018), where this nutrient was not detectable (Figure 2.5). In both years, the N:P ratio was below 16 throughout most of the study area.

2.3.3. Phytoplankton community

2.3.3.1. Cell concentrations

In the upper mixed layer, the cell concentrations of diatoms and dinoflagellates was significantly different in each water mass, and it was higher in BCSW than in ACW (*U* test, $p < 0.05$) (Figure 2.7), whereas cell concentrations below the pycnocline did not differ among water masses (one-way ANOVA, $p > 0.05$). In both 2017 and 2018, the highest cell concentrations were observed in the Bering Strait (2017: 1.6×10^6 cells L^{-1} and in 2018: 3.4×10^5 cells L^{-1}) but diatoms and dinoflagellates in this region were more abundant in 2017 (stations 1–3) than in 2018 (stations 27–30) (*U* test, $p < 0.05$) (Figure 2.8).

2.3.3.2. Phytoplankton species and their diversity

A total of 29 genera and 30 species of diatoms (centric diatoms: 19 genera and 25 species and pennate diatoms: 10 genera and 5 species) and 6 genera and 5 species of dinoflagellate were observed over the two years (Table 2.1). The diversity of the diatoms (*H'*) ranged from 0–3.56 in 2017 and 0.36–2.98 in 2018. The *H'* varied among water masses, with values significantly higher in BCWW and BCSW than in ACW (one-way ANOVA, $p < 0.05$) (Figure 2.7). There were no significant differences in the diversity of diatoms between the years (*U* test, $p > 0.05$) (Figure 2.7).

2.3.3.3. Phytoplankton community by cluster analysis

Phytoplankton communities were classified into four groups (A–D) by a cluster analysis at 27% and 37% similarity levels (Fig. 2.9a). Group A was low concentrations (1.3×10^3–1.3×10^5 cells L^{-1}, avg = 4.6×10^4 cells L^{-1}) and was composed primarily of *C. socialis* complex (Figure 2.9b). Group B had the highest cell density (1.6×10^3–1.6×10^6 cells L^{-1}, avg = 2.5×10^5 cells L^{-1}), and *Hyalochaetae* such as *C. socialis* complex, *C. furcellatus*, and *C. debilis* were dominant

(64%) (Figure 2.9b). The cell concentrations of *C. socialis* complex, *C. diadema*, and *Chaetoceros* spp. in group B was significantly higher than it was in groups C and D. The cell concentration of group C was nearly as low as it was in group A (3.3×10^3–1.2×10^5 cells L^{-1}, avg = 3.4×10^4 cells L^{-1}); however, the community composition was very different. *Phaeoceros* such as *C. convolutus/concavicornis/borealis* had a relatively high concentrations in group C (13%), and the pennate diatoms such as *Thalassionema nitzschioides* and *Cylindrotheca closterium* had a significantly higher concentrations in group C than it did in the other groups (Table 2.2). Group D had the lowest cell concentrations (3.6×10^2–4.4×10^5 cells L^{-1}) and *Leptocylindrus* spp. dominated (85%).

The phytoplankton communities were different in each region (Figure 2.9c). In both years south of St. Lawrence Island, group D was present in the upper layer (0 m or 0–20 m) and groups A, B, and C occurred in the deeper layers. From 65ºN (the Chirikov Basin) to the Bering Strait, the distribution varied across years; group B was observed throughout the area in 2017, but group C was observed in 2018. In these regions (the Chirikov Basin and the Bering Strait), the spatial distribution of water masses and phytoplankton community groups determined by the cluster analysis did not match (Figures 2.4 and 2.9c), thus, the groups were different between years even though BCSW was occupied in both years.

2.3.3.4. Relationships between phytoplankton communities and environmental factors

On the NMDS ordination, phytoplankton plots had significant relationships with various environmental variables ($p < 0.05$), including chl *a* fluorescence ($r^2 = 0.30$), TSR ($r^2 = 0.28$), observation date ($r^2 = 0.16$), sampling depth ($r^2 = 0.13$), salinity ($r^2 = 0.11$), $Si(OH)_4$ ($r^2 = 0.08$) and NO_2+NO_3 ($r^2 = 0.05$) (Figure 2.9d), but the other parameters did not. Especially note that temperature did not have a significant relationship with phytoplankton plots ($p > 0.05$), and that the contribution of TSR to diatom groups was the highest among environmental factors except for chl *a* fluorescence.

In addition, the one-way ANOVA and Tukey-Kramer test indicated that the PO_4–P and DIN concentrations and the N:P ratio did not differ significantly among phytoplankton groups (one-way ANOVA, $p > 0.05$) (Table 2.3). However, the other hydrographic variables differed between groups B and D. Group D had a higher temperature and lower salinity, nutrients

(NO_2+NO_3, PO_4–P, NH_4–N, $Si(OH)_4$), and chlorophyll *a* fluorescence than the other groups. Groups B and C differed only in their salinity, chlorophyll *a* fluorescence and TSR (Table 2.3). Especially note that temperature was not significantly different between Group B and C.

2.4. Discussion

2.4.1. The influence of water masses

Diatom community structure (i.e., species composition and their cell concentration) was not consistently correlated with water mass during summer except for the stations south of St. Lawrence Island. However, there were significant differences among the water masses in the cell concentrations in the upper mixed layer and in diatom diversity. These differences may have been related to differences in the nutrient content of the water masses. Differences in characteristics of water masses are known to influence phytoplankton cell concentrations (Coachman et al., 1975; Danielson et al., 2017; Giesbrecht et al., 2019). The N:P ratio was below 16 throughout the study area, which indicated that the DIN was the limiting nutrient concentration, and differences in DIN concentrations in the various water masses was one of the most important factors for the growth of phytoplankton upper the mixed layer over the study area. Thus, phytoplankton cell concentrations were higher in the upper mixed layer in the BCSW, including the nutrient-rich AW, than in the nutrient-poor ACW (Coachman et al., 1975; Danielson et al., 2017). The diversity of diatoms indicated by *H'* was higher in BCWW and BCSW than in ACW in the same way as the DIN concentration was. We suggest that the differences in the diversity of diatoms between water masses was related to difference in nutrient concentrations between water masses, especially the DIN concentrations. As mentioned above, DIN was the limiting factor in the nutrient concentration and thus, in the water masses with high DIN such as BCWW and BCSW, competition for DIN may have been minimal, thus resulting in many diatom species surviving in these waters.

2.4.2. The phytoplankton community of the south of St. Lawrence Island

In contrast to the Chirikov Basin and the Bering Strait regions, south of St. Lawrence Island year-to-year changes in the phytoplankton community were not observed. In the upper mixed layer south of St. Lawrence Island, nutrient-poor ACW was present in both years, and the

DIN concentrations and, at some stations the Si $(OH)_4$ concentrations, were too low to support diatom growth (Justić et al., 1995). The lack of DIN may have resulted in the dominance of phytoplankton group D, which was predominately non-diatom species that can thrive in low nutrient conditions (Parsons et al., 1978). The timing and magnitude of the spring phytoplankton bloom in the region south of St. Lawrence Island differed in 2017 and 2018, and we hypothesize that this was due to differences in the TSR (Hirawake and Hunt, 2020)(also see, chapter 3). Thus, after the nutrients were depleted from the upper mixed layer, phytoplankton, other than diatoms, dominated. A similar succession may occur in the eastern Bering Sea where coccolithophore blooms during the summer were reported after the diatom bloom (Stockwell et al., 2001; Iida et al., 2002). Coccolithophore blooms were also observed by satellite observation from the eastern Bering Sea to south of St. Lawrence Island after 2000s (Harada et al., 2012). In our study, it is not clear whether the phytoplankton community changed at the species level, because dinoflagellates and phytoplankton other than diatoms were not identified to the species level.

2.4.3. The changes in the summer diatom community in the Chirikov Basin and the Bering Strait, 2017–2018

From 65ºN (the Chirikov Basin) to the Bering Strait, between 2017 and 2018, phytoplankton cell concentrations declined, and community structure changed. In this region in 2017, the highest cell concentrations (1.6×10^6 cells L^{-1}) was nearly the same as that reported by Sergeeva et al. (2010) for July 2003 and by Giesbrecht et al. (2019) (the highest concentrations were approximately 10^6 cells L^{-1}). In 2018, the highest cell concentrations (3.4×10^5 cells L^{-1}) were only 34% of the values observed in 2017.

With respect to the phytoplankton community, in 2017, group B was widely distributed and had high cell concentrations that were dominated (64%) by *Hyalochaetae* such as *C. socialis* complex and *C. furcellatus*. *C. socialis* complex and *C. furcellatus* are common in the Arctic from spring to summer (Hasle and Syvertsen, 1997; Hoppenrath et al., 2009). These species are typically found in the Chukchi Sea adjacent to the study area (von Quillfeldt et al., 2003). In 2018, Group C, which was mostly composed of *Thalassionema nitzschioides*, was widely distributed. The abundance of *Chaetoceros* spp. was low (20%), and *Phaeoceros* such as *C. convolutus/concavicornis/borealis* made up most of the *Chaetoceros* spp.. *T. nitzschioides* and *C. convolutus* are known as cosmopolitan species; the former does not occur in the high Arctic and

the latter is common in temperate waters (Hasle and Syvertsen, 1997; Hoppenrath et al., 2009). *T. nitzschioides* has also been reported in temperate water after the retreating of the sea ice (Neeley et al., 2018), and it is a characteristic species of the Pacific Arctic region in the autumn (Matsuno et al., 2014). These results suggest that between 2017 and 2018, the summer diatom community in the Bering Strait and the Chirikov Basin changed from spring-summer species to cosmopolitan autumn species. Interestingly, the NMDS, the multiple regressions, and the one-way ANOVA did not suggest any significant differences in temperature between 2017 and 2018 in the region north of 65ºN. By contrast, the TSR was the most important contributing factor among the environmental factors for explaining the differences in the diatom communities between the two years. There was also a significant difference in the TSR between group B in 2017 and C in 2018. Because the TSR differed between 2017 and 2018 in the northern Bering Sea (Cornwall, 2019; Grebmeier et al., 2019)(also see chapter 3), the effect of the TSR on the summer diatom community cannot be ignored. The TSR affects the magnitude and timing of the spring bloom in the seasonal sea ice area (Hunt et al., 2002; Fujiwara et al., 2016). The magnitude of the phytoplankton bloom in the open water is usually large when the TSR is early (Hunt et al., 2002; Fujiwara et al., 2016). In 2018, when the TSR was early, large increases in sea surface chlorophyll *a* in the Chirikov Basin were observed with satellite remote sensing from early to late May after the sea ice had completely retreated (see chapter 3). Hence, in 2018, when the TSR was early, the available nutrients may have been consumed by the large open-water bloom during early spring after the sea ice retreat, resulting in the wide distribution of phytoplankton community group C during summer, with low cell concentrations. The results were consistent with the sediment trap data in Lalande et al. (2021). They considered that the low diatom fluxes during July 2018 possibly reflected a rapid depletion of nutrients during the large open water bloom in the northern Bering Sea weeks earlier (Lalande et al., 2021). In summer 2018, the cosmopolitan species composition of group C, some of which, such as *T. nitzschioides*, are species characteristic of the autumn (Matsuno et al., 2014). Nutrient availability would generally drive diatom community succession (e.g., Rousseau et al., 2002; Zhoug et al., 2017), and Andyna and Arrigo (2020) mentioned that environmental factors, such as nutrients and light, could define dominant diatoms in the Arctic. In addition, the water column stratification during summer is relevant to the succession of the dominant diatoms in the northern Bering Sea (Suzuki et al., 2021). However, these previous studies focus only on a few diatom species not completely applicable to this study.

Therefore, we should elucidate the detailed mechanisms by which seasonal succession in diatom communities occurs, from a physiological-ecological perspective.

2.5. Conclusions

This study described and compared northern Bering Sea diatom communities in the summers of 2017 and 2018. The diatom cell concentrations and diatom diversity differed by water mass. However, in 2017, considerably warmer shelf water was present, and the ACW extended unusually far to the west. Therefore, we should monitor the impact of such unusual water mass distribution on the phytoplankton community for future work in the changing Pacific Arctic region. In addition, combined with more detailed water mass classification, such as focusing on the origin of water masses (e.g., Hirawake et al., 2021), we can better understand phytoplankton community differences by water masses.

Year-to-year differences in the diatom community between 2017 and 2018 were found, depending on the region examined. South of St. Lawrence Island, we found no changes in the diatom community between 2017 and 2018. Nitrate and nitrite were depleted in the upper mixed layer in both years, and phytoplankton types other than diatoms dominated this region. Since we focused on only diatoms, it is possible that there were interannual changes in phytoplankton communities other than diatoms that we did not detect. In the Chirikov Basin and Bering Strait, diatom communities in 2017 and 2018 differed, even though the same water masses were present in both years. The TSR was much earlier in 2018 than in 2017, though summer water temperatures were similar in the two years. In 2018, several subarctic or cosmopolitan species were abundant compared to 2017, when arctic species predominated. Since nutrient concentrations were lower in 2018, we hypothesize that the open water bloom in 2018 may have depleted the nutrients, with the result in low diatom concentrations in 2018. However, more detailed mechanisms of diatom community succession need to be examined. It will be important to evaluate the influence of the changing diatom community on the marine ecosystem of the northern Bering and Chukchi Seas. To this end, focus on the entire phytoplankton community, including dinoflagellates, coccolithophores and others, will be required.

2.6. Figures and Tables

Table 2.1. List of phytoplankton species collected from the northern Bering Sea and Bering Strait in July 2017 and 2018.

Class Bacillariophyceae		
Order Centrales		
Actinocyclus spp.	*C. furcellatus*	*Ditylum* spp.
Actinoptychus spp.	*C. socialis* complex	*Eucampia* spp.
Attheya spp.	*C. laciniosus*	*Lauderia annulata*
Bacterosira bathyomphala	*C. lorenzianus*	*Leptocylindrus danicus*
Chaetoceros conturtus	*C. mitra*	*L. minimus*
C. convolutus/concavicornis/borealis	*C. subtilis*	*Odontella aurita*
C. curvicetus	*C. teres*	*Paralia sulcata*
C. danicus	*Chaetoceros* spp.	*Rhizosolenia* spp.
C. debilis	*Corethron hystrix*	*Skeletonema* spp.
C. decipiens	*Coscinodiscus* spp.	*Stephanopyxis turris*
C. diadema	*Detonula pumuila*	*Thalassiosira* spp.
C. didymus	*Dactyliosolen fragilissimus*	Other centric diatoms
Order Pennales		
Asteroplanus karianus	*Pauelia taeniata*	*Navicula* spp.
Asterionellopsis glacialis	*Pleurosigma* spp.	*Nitzschia* spp.
Cylindrotheca closterium	*Pseudo-nitzschia* spp.	Other pennate diatoms
Thalassionema nitzschioides	*Fragilariopsis* spp.	
Class Dinophyceae		
Alexandrium spp.	*Protoperidinium* spp.	*Dinophysis norvegica*
Ceratium spp.	*Heterocapsa triquetra*	*Dinophysis rudgei*
Prorocentrum triestinum	*Dinophysis acuta*	Other dinofalagellates

Table 2.2. Comparison of phytoplankton species in the phytoplankton community groups (A–D). The values are given as the mean cell density (× 10^3 cells L^{-1}) and standard deviation in each group. The numbers in parentheses indicate the number of stations. The differences among the phytoplankton communities were evaluated by a one-way ANOVA and a Tukey-Kramer test. Any groups not connected by the underlines are significantly different (*: $p < 0.05$, **: $p < 0.01$, and ***: $p < 0.005$).

Species	Group name				one-way ANOVA	Tukey-Kramer test
	A (5)	B (74)	C (41)	D (21)		
C. convolutus/concavicornis/borealis	4.49 ± 6.47	3.56 ± 7.79	4.37 ± 9.50	0.26 ± 1.01	NS	
C. debilis	–	16.45 ± 42.68	0.20 ± 1.05	–	*	Not detected
C. diadema	0.65 ± 1.29	3.35 ± 4.73	0.06 ± 0.20	0.01 ± 0.02	***	D C A B
C. furcellatus	–	49.95 ± 118.66	–	–	**	Not detected
C. socialis complex	31.28 ± 44.80	65.46 ± 114.33	0.02 ± 0.06	0.12 ± 0.33	***	C D A B
Chaetoceros spp.	2.22 ± 2.81	13.94 ± 20.48	0.84 ± 2.91	0.50 ± 1.36	***	D C A B
Leptocylindrus danicus	–	15.43 ± 30.69	3.08 ± 10.43	21.01 ± 89.63	NS	
Cylindrotheca closterium	0.05 ± 0.05	1.09 ± 1.03	1.79 ± 1.60	0.15 ± 0.27	***	A D B C
Thalassionema nitzschioides	0.21 ± 0.28	0.68 ± 1.05	7.51 ± 15.35	0.47 ± 0.95	***	A D B C
Pseudo-nitzschia spp.	–	5.23 ± 12.90	1.45 ± 4.94	0.08 ± 0.34	NS	
Fragilariopsis spp.	0.02 ± 0.04	2.92 ± 10.65	0.41 ± 1.09	0.05 ± 0.21	NS	

Table 2.3. Hydrographic environmental factors among the phytoplankton communities (A–D). The values are given as the average and standard deviation of each factor. The numbers in parentheses indicate the number of stations. The differences among the phytoplankton communities were evaluated by a one-way ANOVA and a Tukey-Kramer test. Any groups not connected by the underlines are significantly different (*: $p < 0.05$, **: $p < 0.01$, and ***: $p < 0.005$).

Factors	Group name				one-way ANOVA	Tukey-Kramer test
	A (5)	B (74)	C (41)	D (21)		
Temperature	1.97 ± 3.29	3.56 ± 1.66	2.89 ± 2.49	6.21 ± 2.78	**	A C B D
Fluorescence	0.54 ± 0.56	0.75 ± 0.53	0.44 ± 0.17	0.20 ± 0.13	***	D C A B
Salinity	32.00 ± 0.32	32.49 ± 0.41	32.10 ± 0.87	31.58 ± 0.36	***	D A C B
NO_2+NO_3	5.68 ± 6.55	9.34 ± 6.38	7.88 ± 6.29	0.96 ± 1.01	**	D A C B
PO_4-P	1.18 ± 0.65	1.35 ± 0.83	1.42 ± 0.39	0.80 ± 0.32	NS	
NH_4-N	1.11 ± 1.43	0.78 ± 0.48	0.84 ± 0.61	0.18 ± 0.13	*	D B C A
$Si(OH)_4$	29.48 ± 40.68	25.01 ± 13.25	19.10 ± 12.29	8.60 ± 7.69	*	D C B A
DIN	6.79 ± 7.95	10.41 ± 6.76	10.59 ± 13.33	1.13 ± 1.11	NS	
N/P	4.30 ± 3.34	7.24 ± 3.46	6.94 ± 9.78	1.28 ± 1.02	NS	
TSR	91.00 ± 8.22	115.28 ± 14.44	107.78 ± 11.67	99.38 ± 15.44	***	A D C B

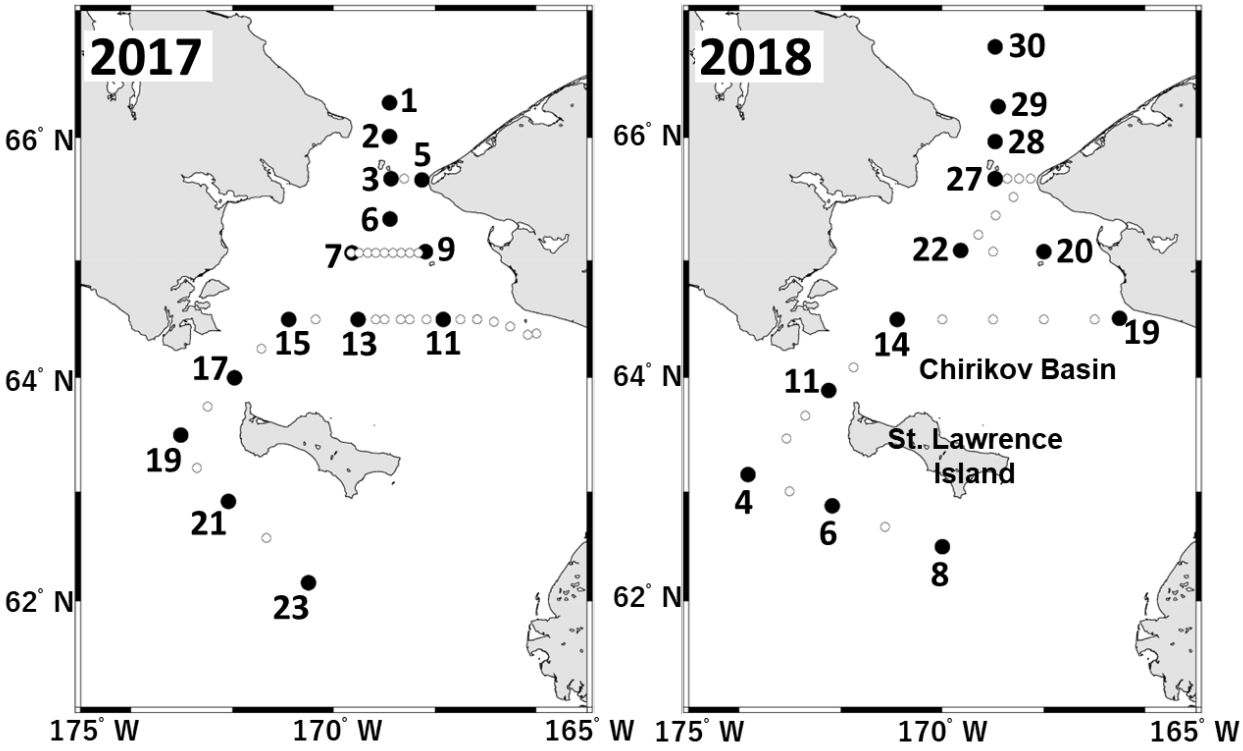

Figure 2.1. Location of stations in the northern Bering Sea from July 9–21, 2017 and July 2–12, 2018. The numbers indicate the station ID. The open and solid circles indicate stations with hydrographic observations only taken by CTD and those with water sampling and hydrographic observations, respectively.

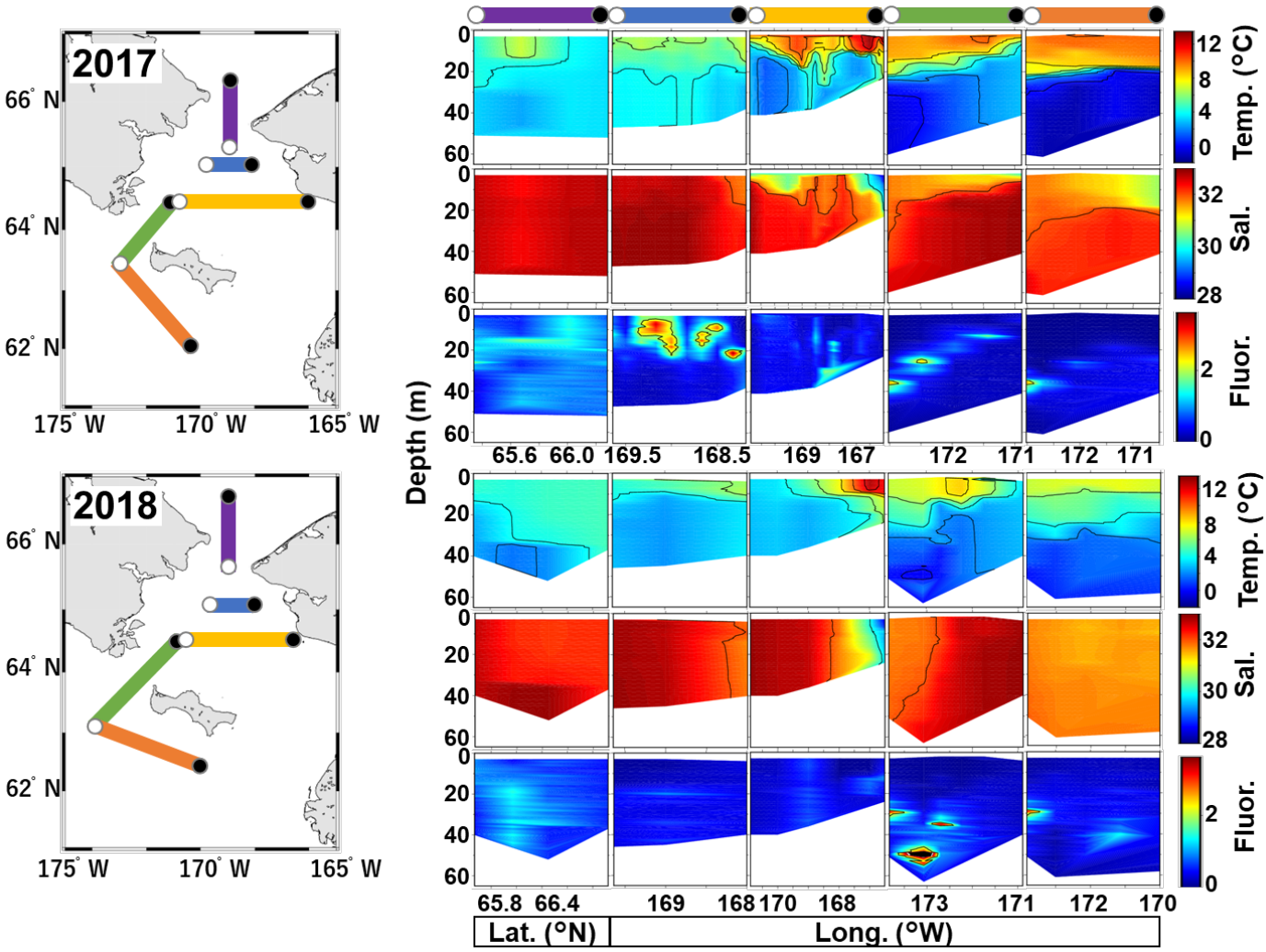

Figure 2.2. Cross-sectional distributions of the temperature, salinity, and fluorescence in the northern Bering Sea in 2017 (upper) and 2018 (lower).

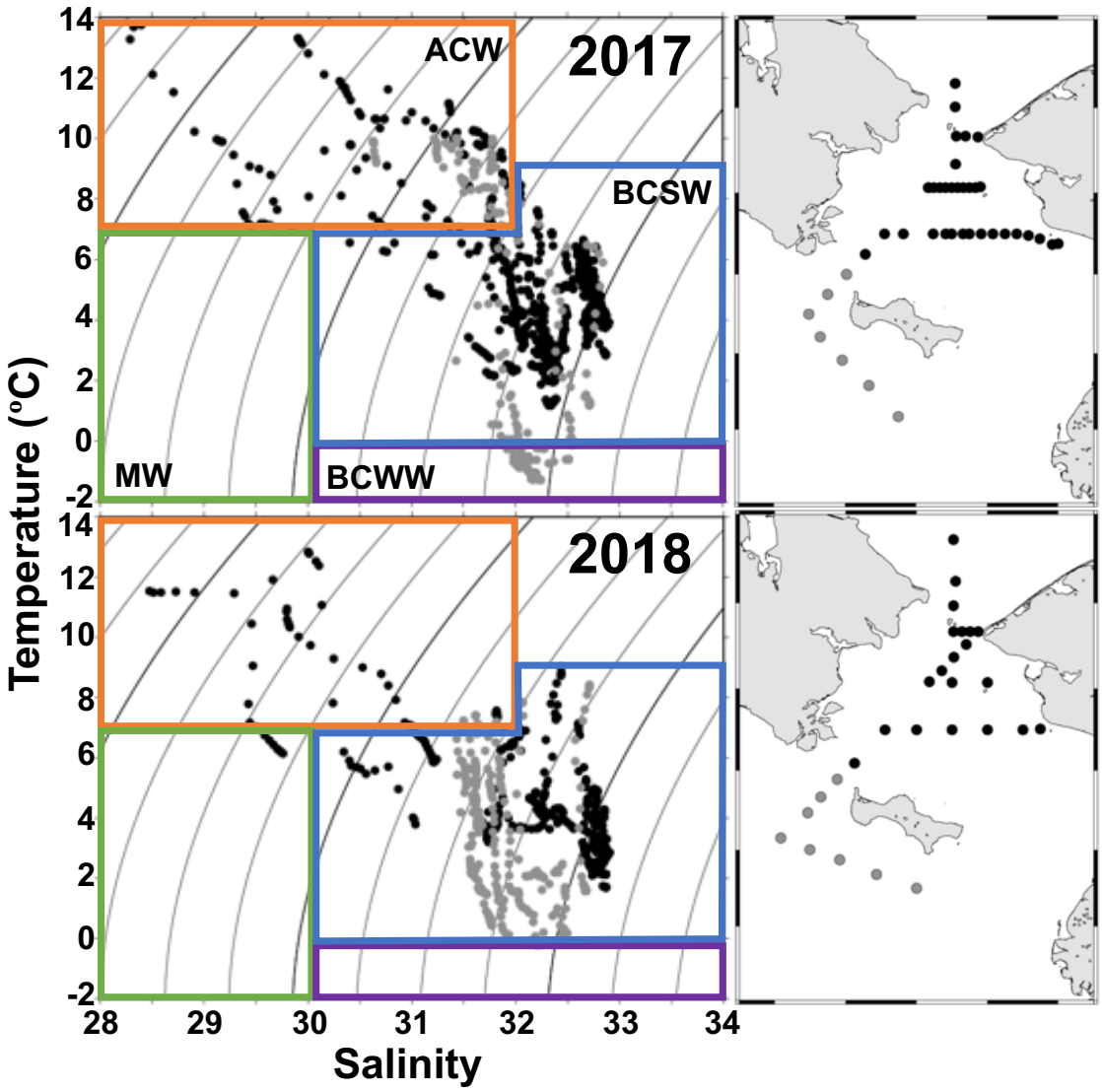

Figure 2.3. T-S diagrams of all the stations in 2017 (upper) and 2018 (lower). Note that the symbols of the stations vary with the geographical location.

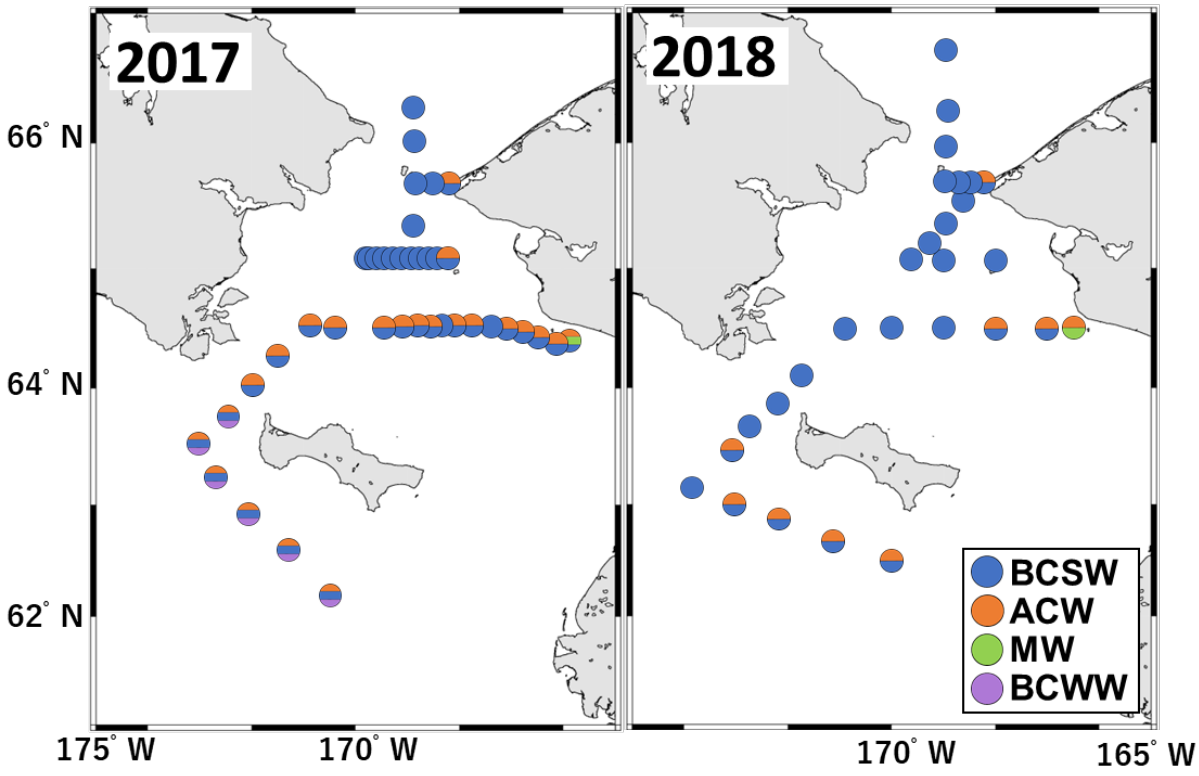

Figure 2.4. Spatial distribution of water masses as defined by Danielson et al. (2017). Colored circles indicate differences in water masses with depth in the water column. Abbreviation: BCSW: Bering-Chukchi Summer Water, ACW: Alaskan Coastal Water, MW: Melting Water, and BCWW: Bering-Chukchi Winter Water.

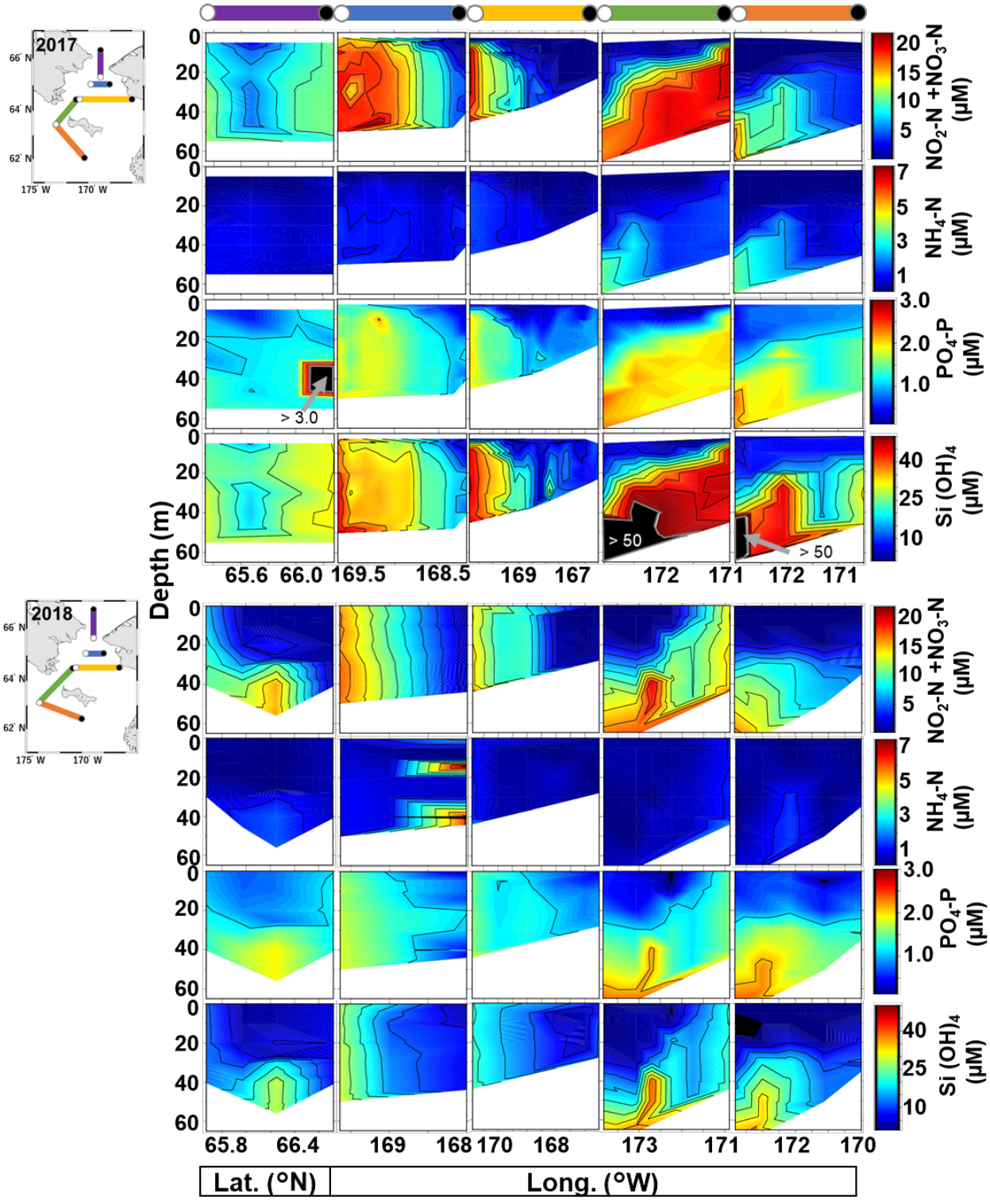

Figure 2.5. Cross-sectional distributions of nutrient (NO_2-N + NO_3-N, NH_4-N, PO_4-P, and Si $(OH)_4$) concentrations in the northern Bering Sea in 2017 (upper) and 2018 (lower).

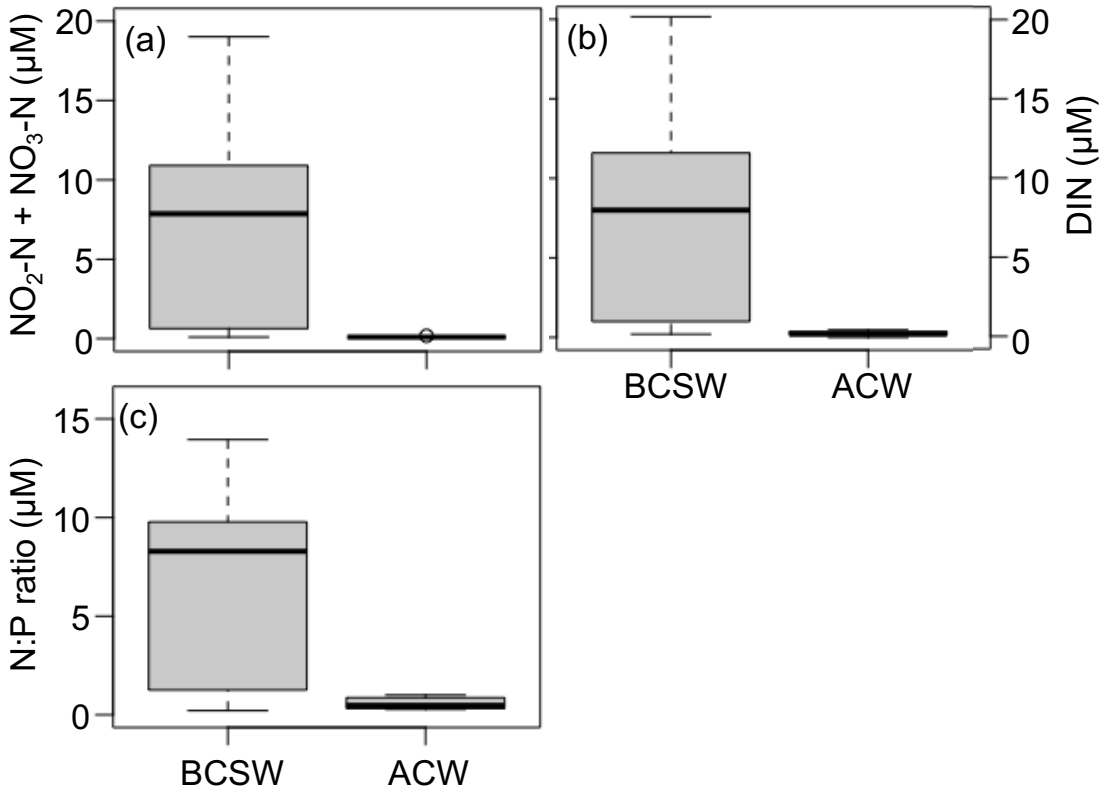

Figure 2.6. Comparison of (a) NO_2–N + NO_3–N and (b) DIN concentrations and (c) N:P ratio between the water masses in the upper mixed layer. Abbreviation: BCSW: Bering Chukchi Summer Water, ACW: Alaskan Coastal Water.

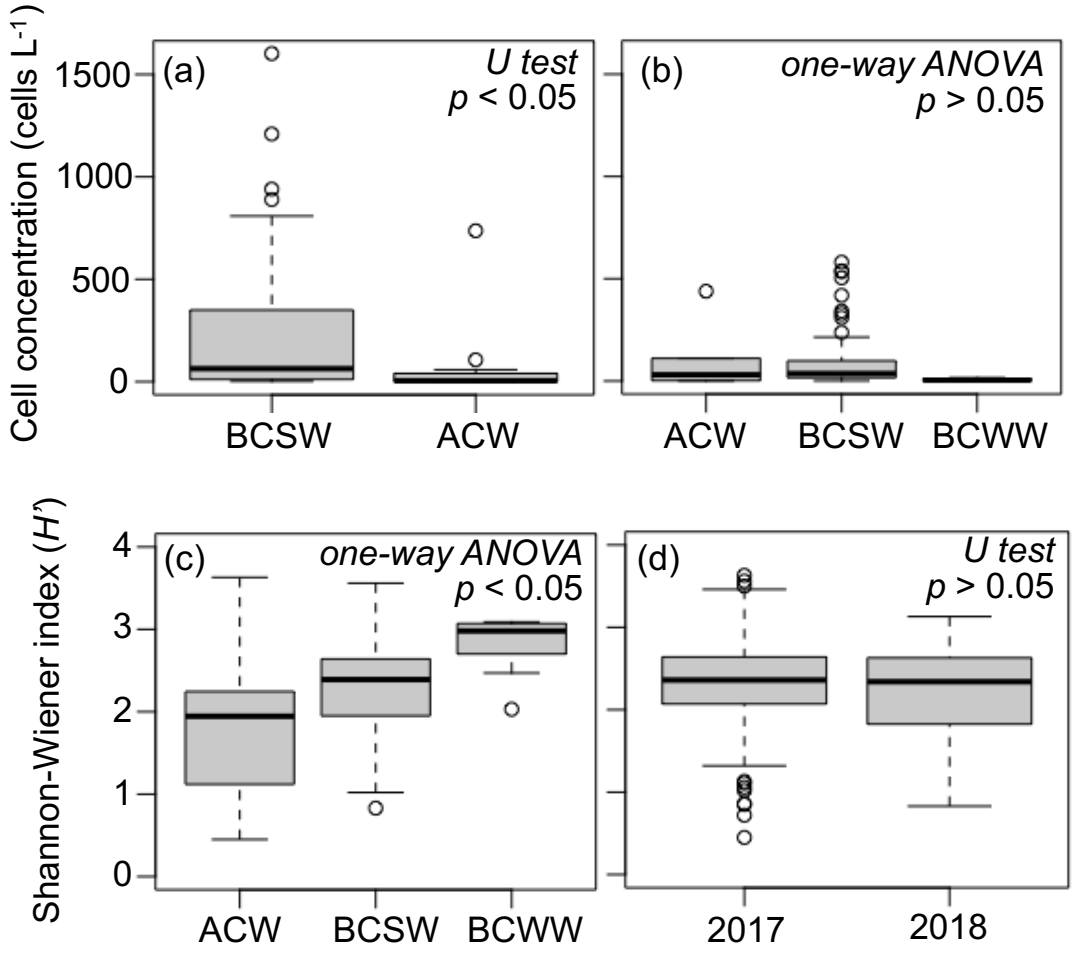

Figure 2.7. Comparison of cell concentrations between the water masses in the (a) upper and (b) lower mixed layer. Differences in the Shannon-Wiener index (*H'*) between (c) the water masses and (d) the observation years. Abbreviation: BCSW: Bering Chukchi Summer Water, ACW: Alaskan Coastal Water, BCWW: Bering Chukchi Winter Water.

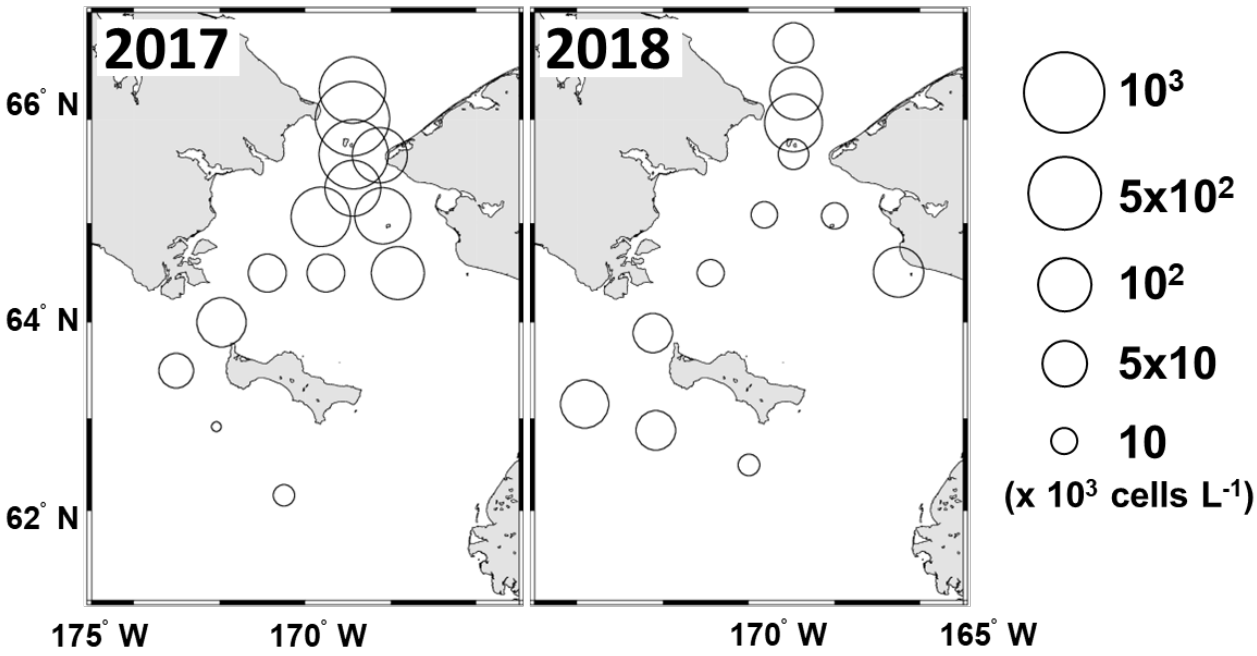

Figure 2.8. Horizontal distribution of the average phytoplankton cell density in 2017 (left) and 2018 (right). The circles indicate the mean cell density in the water column.

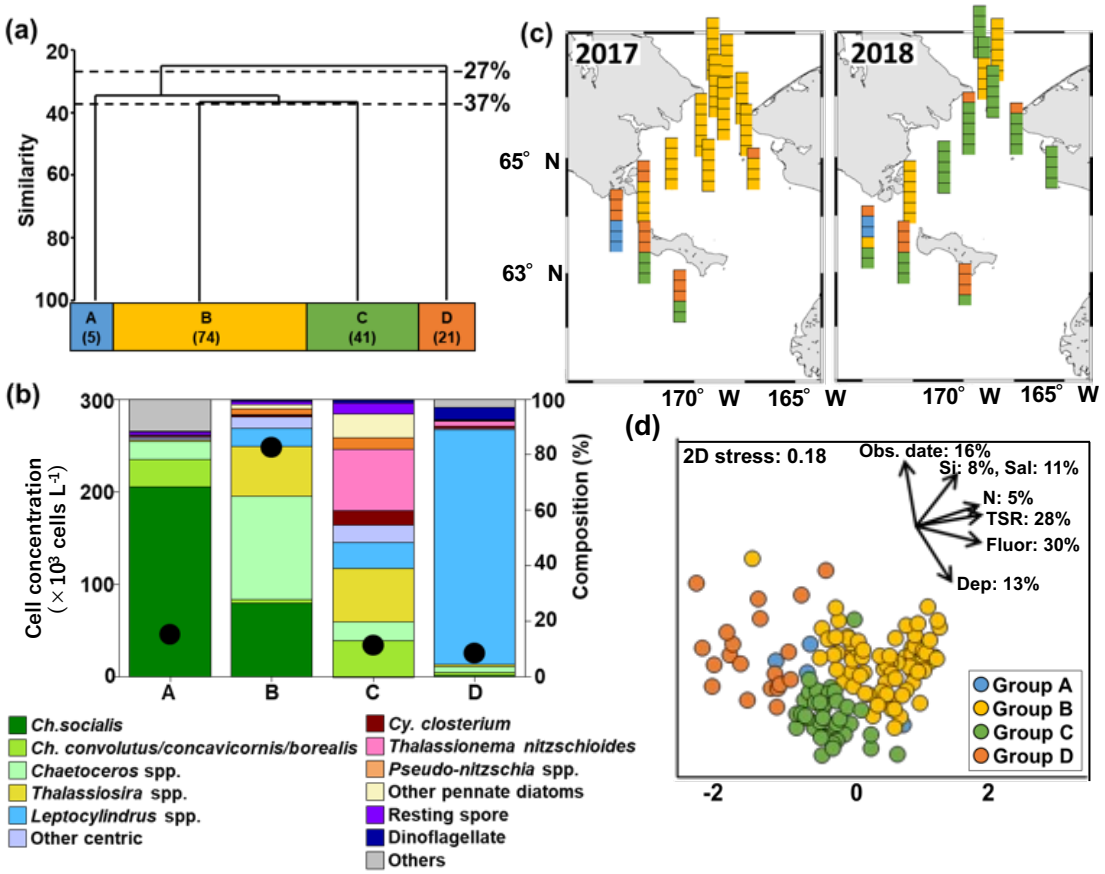

Figure 2.9. (a) Results of the cluster analysis based on the phytoplankton cell density found by Bray-Curtis similarity. (b) Species composition and cell concentrations of each group. (c) Spatial distribution of the phytoplankton community in the northern Bering Sea during the summers of 2017 (left) and 2018 (right). (d) Nonmetric multidimensional scaling plots of the four groups, with *arrows* and *percentages* indicating the directions of the environmental parameters and the coefficient of determination (r^2), respectively. *Obs. date*: observation date, *Si*: silicate, *Sal*: salinity, *N*: nitrate and nitrite, *TSR*: the timing of sea ice retreat, *Fluor*: fluorescence, and *Dep*: sampling depth.

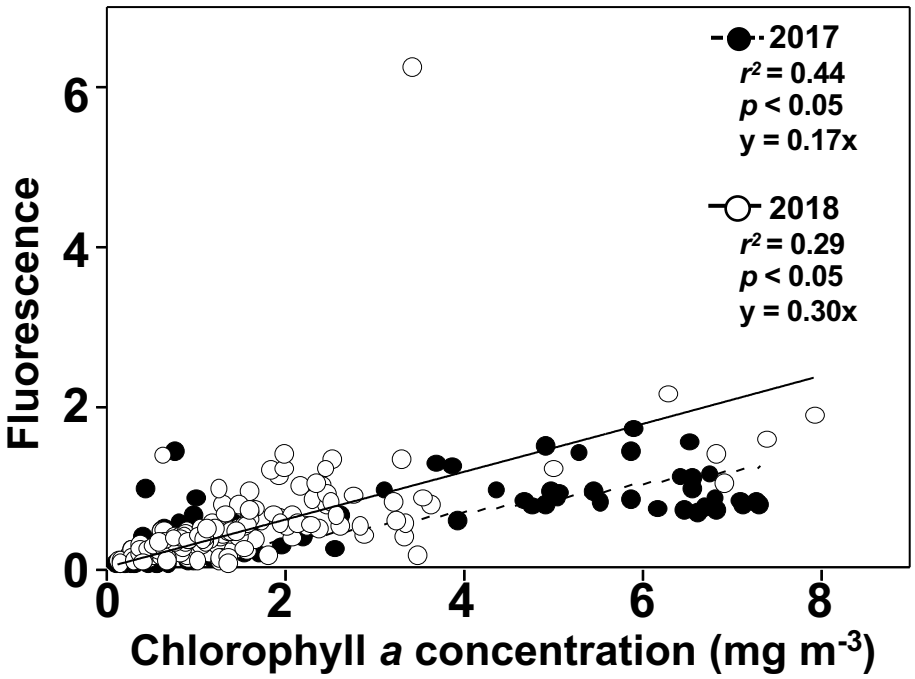

Figure S2.1. Relationship between the chlorophyll *a* concentration and the fluorescence.

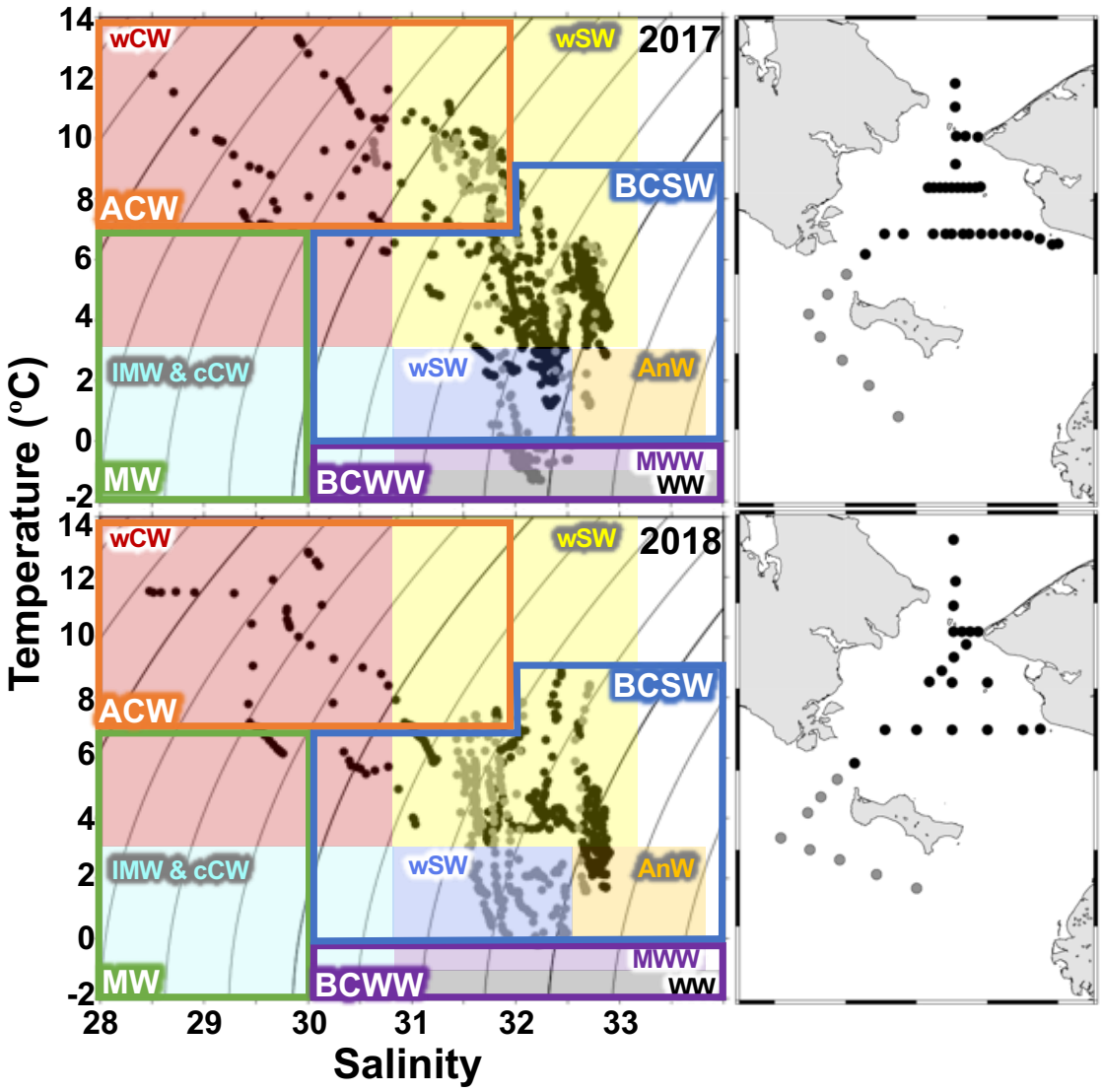

Figure S2.2. Comparison of water masses defined by Danielson et al. (2017) and Danielson et al. (2020). The background color and the box border are the definitions of Danielson et al. (2017) and Danielson et al. (2020), respectively.

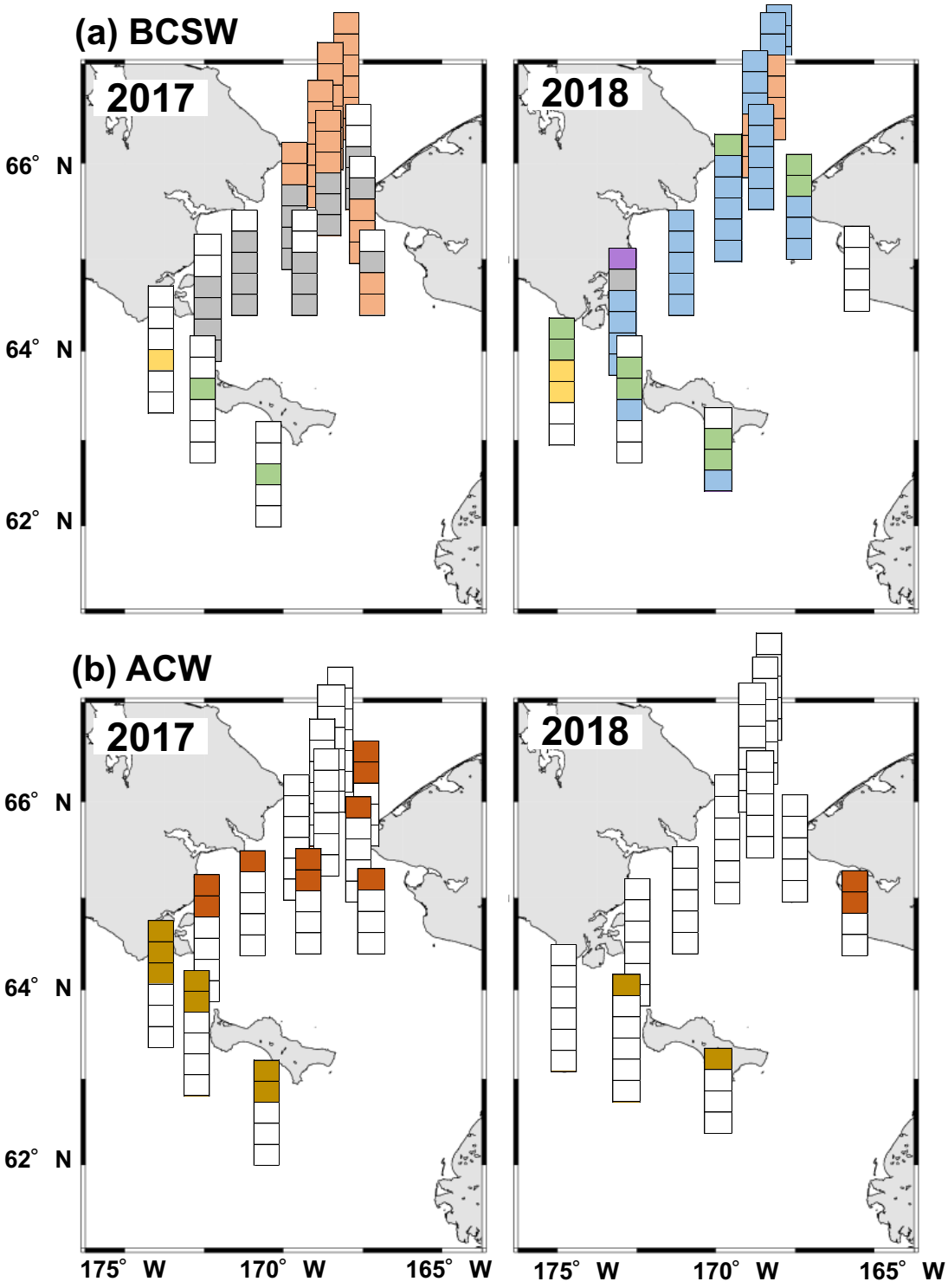

Figure S2.3. Spatial distribution of the phytoplankton communities in each water mass (the BCSW (a) and the ACW (b)) by cluster analyses. Stacked boxes indicate water depth. The cluster analyses were conducted in each water mass independently. White boxes indicated water masses that were not the focus of this analysis. Color codes for the communities were shown different groups analyzed by the cluster analysis.

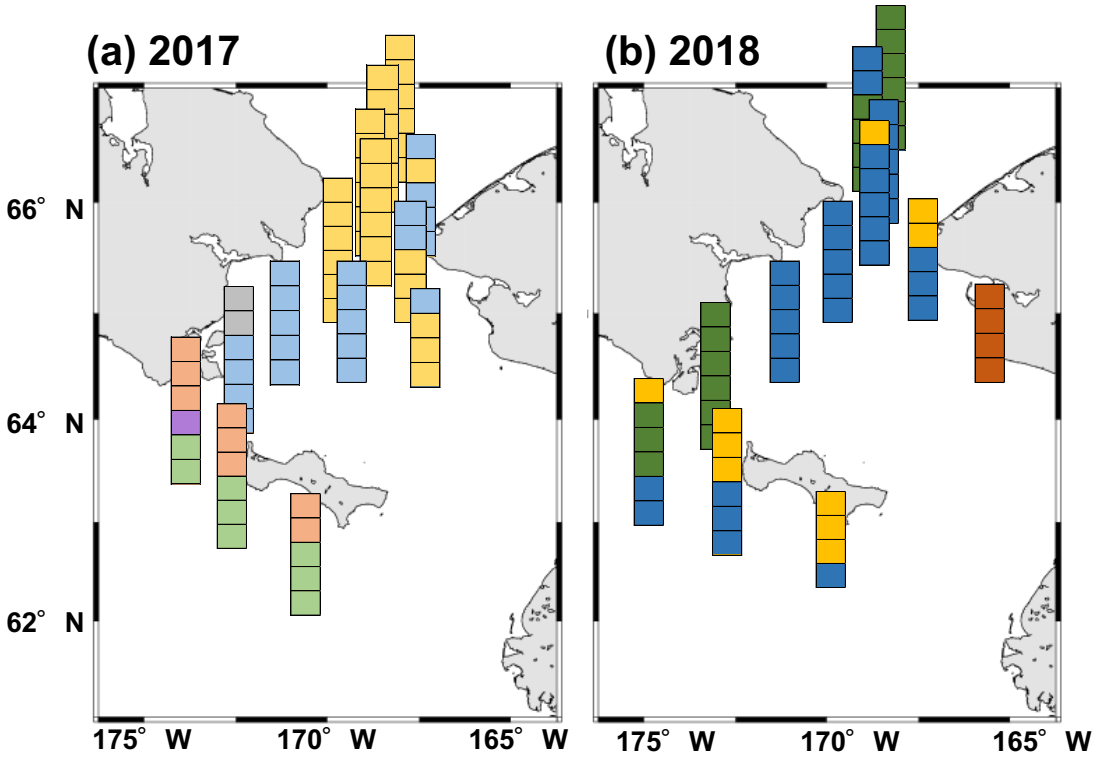

Figure S2.4. Spatial distribution of the phytoplankton communities in each year. Stacked boxes indicate water depth. Cluster analyses were conducted in each year independently. Color codes for the communities were shown different groups analyzed by the cluster analysis.

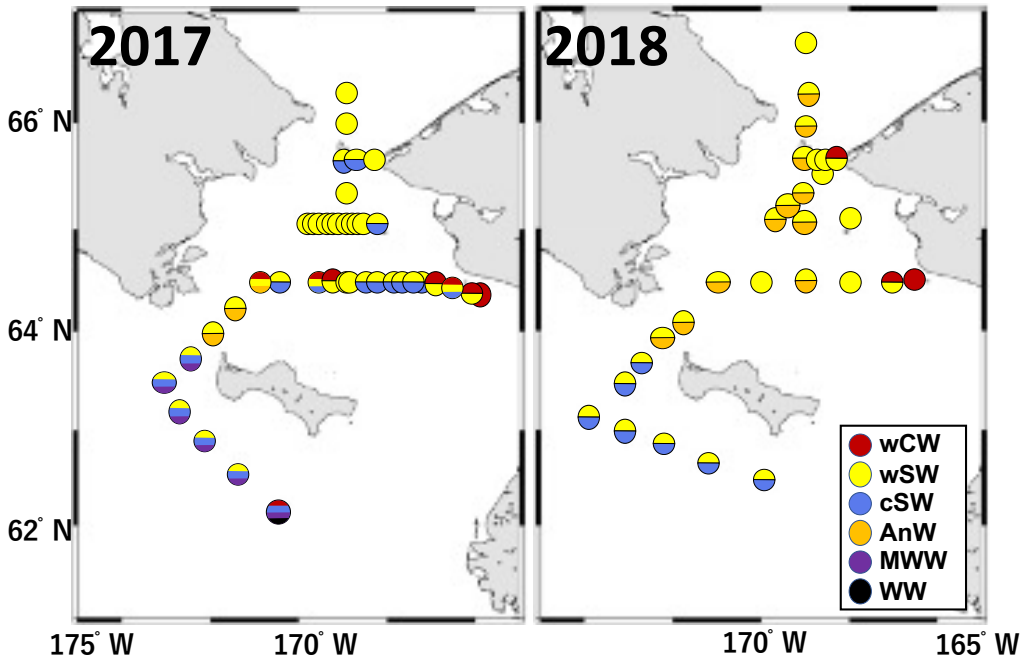

Figure S2.5. Spatial distribution of water masses as defined by Danielson et al. (2020). Colored circles indicate differences in water masses with depth in the water column. Abbreviation: wCW: warm Coastal Water, wSW: warm Shelf Water, cSW: cool Shelf Water, and AnW: Anadyr Water, MWW: Modified Winter Water, WW: Winter Water.

CHAPTER 3 – Timing of sea ice retreat affects the composition of viable diatoms in sediments of the northern Bering Sea

3.1. Introduction

Chapter 2 suggested that the changes in timing of sea ice retreat had affected diatom community composition during summer. However, because the microalgal community in the water column shows a rapid seasonal succession, the obtained data from seawater is a snapshot result. On the other hand, abundant viable diatoms, including diatom resting stages, are accumulated in bottom sediments of the Chukchi and eastern Bering Seas (Tsukazaki et al., 2013, 2018). The distribution of viable diatoms in the sediment may reflect the past blooms that have occurred in the water column (Pitcher, 1990; Itakura et al., 1997). In the Arctic of seasonal sea ice zones, ice algae production occurs in and under the sea ice, and is followed by phytoplankton blooms after the retreat of sea-ice (Horner, 1984; Horner & Schrader, 1982). Therefore, the investigation of viable diatom community could give us further understanding of the diatom community dynamics during two types of blooms from a relatively long-term perspective.

As mentioned in the general introduction, the northern Bering Sea shelf is a shallow seasonal sea ice zone with a water depth of approximately 50 m. The majority of microalgae settles to the seafloor due to the low grazing pressure of zooplankton in the water column, supporting the benthic community in the Bering Sea and the Chukchi Sea (Grebmeier et al., 1988, 2006).

Ice algae is ice-associated microalgae and can grow even under the dim light conditions such as < 1 μmol photons s^{-1} m^{-2} (Cota and Smith, 1991; Mock and Gradinger, 1999). The timing of ice algae growth is controlled by the light environment (Smith et al., 1988; Cota and Home, 1989; Gosselin et al., 1990), and their blooms in the Bering and Chukchi Sea generally occur during March–May (Leu et al., 2015). Because peak of ice algal production precedes peak of the water column production by 1–4 months (e.g., Arrigo, 2017), they are an important food source for various zooplankton and benthic species especially in the early spring (Brown and Belt, 2012; Wang et al., 2015), although ice algae contribute only ~2–10% of total primary production in the Arctic waters (Arrigo, 2017). In the Bering Sea, since the annual variation of sea ice extent is large, the distribution of ice algae can be considered to have large annual fluctuation, but details

are unknown.

In this study, to estimate the diatom communities during spring blooms and analyze relationships with sea ice dynamics, we investigated viable diatoms in the northern Bering Sea sediments during the summer of 2017 and 2018, when the sea ice retreat timing varied greatly. Through this analysis, we aimed to evaluate the influence of changes in sea ice retreat timing on the viable diatom assemblage: *Fragilariopsis/Fossula* spp., ice algae species, were abundant in 2017, but *Thalassiosira* spp. dominated in 2018.

3.2. Materials and Methods

3.2.1. Sampling

Sampling was conducted in the northern Bering Sea shelf on 9–21 July 2017 and 2–12 July 2018 during the 40th and 56th cruises of the T/S *Oshoro-Maru* of Hokkaido University (Figure 3.1). Sediment samples were collected by a multiple corer or Smith-Mclntyre bottom sampler at each station. The top 1 cm or 3 cm of sediment core was extruded and stored in darkness at 5˚C for more than one month in order to eliminate vegetative cells.

3.2.2. Quantification of viable diatoms in sediments

Sediment samples were analyzed following the procedure of the most probable number (MPN) method and the abundance of viable diatoms in the sediments was estimated (Imai et al., 1984, 1990). Homogenized wet sediment samples were suspended in filtered sea water at a concentration of 0.1 g mL^{-1} (=10^0 dilution), and serial tenfold dilutions (10^{-1} to 10^{-6}) were made with modified SWM-3 medium. Then 1 mL aliquots of diluted suspensions were inoculated into five replicate wells of disposable tissue culture plates (48 wells). Incubation was carried out at 5°C and under the white fluorescent light of 50 µmol photons m^{-2} s^{-1} with a 14 h light:10 h dark photocycle (Tsukazaki et al., 2018) for 10–14 days. The appearance of vegetative cells of planktonic diatoms in each well was examined using an inverted epifluorescence microscope. The most probable number (MPN for a series of 5 tenfold dilutions) of diatoms in the sediment sample (MPN cells g^{-1} wet sediment) was then estimated according to the statistical table by Throndsen (Throndsen, 1978).

3.2.3. Satellite data

To evaluate the sea ice extent in each year, the AMSR2 (Advanced Microwave Scanning Radiometer 2) standard sea ice concentration (SIC) product at a 10-km resolution was obtained from the JAXA (Japan Aerospace Exploration Agency) web portal (https://gportal.jaxa.jp/gpr/). We used a 5-day moving average value of the SIC data. The ice-covered pixel was defined as SIC > 20% and then the number of ice-covered days during the cold season prior to the field samplings was counted for each pixel. We also calculated the timing of sea ice retreat (TSR). The TSR was defined as the last date when the SIC fell below 20%, prior to observed annual sea ice minimum across the study region during summer. We also acquired Aqua-MODIS daily L3-binned sea surface chlorophyll *a* (chl *a*) concentration at a 9-km resolution from NASA/ GSFC/DAAC website (https://oceancolor.gsfc.nasa.gov/). Daily surface chl *a* concentration was computed using the algorithm of Cota et al. (2004). Daylength at each station were calculated referred to Brock (1981). We defined the growing periods of the ice-associated diatoms as the days between the date when the daylight hours exceed 12 hours day^{-1} and the TSR, because the chl *a* in the Bering sea ice would begin to increase from that season (Leu et al., 2015).

3.3. Results

In the bottom sediments, the viable diatom cell concentrations estimated by the MPN method ranged from 3.0×10^4 to 1.9×10^6 MPN cells g^{-1} wet sediments in 2017 and 2.8×10^5 to 6.1×10^7 MPN cells g^{-1} wet sediments in 2018 (Table 3.1, Figure 3.2). In 2017, the cell concentration was very high (>10^6 MPN cells g^{-1} wet sediments) south of the Bering Strait (St. 6) and in the easternmost station of the study area (St. 11). On the other hand, it was lowest (3.0×10^4 MPN cells g^{-1} wet sediments) at a nearshore station in the Bering Strait (St. 5). In 2018, viable diatom concentration was very high (>10^6 MPN cells g^{-1} wet sediments) south of the St. Lawrence Island (Sts. 4, 6, 8) and in the central station of the study area (St. 22). Twenty taxa and twenty-two species (centric diatom: 12 taxa and 17 species, pennate diatom: 8 taxa and 5 species) were observed over the two years. In 2017, centric diatoms, especially *Chaetocero*s spp., *C. socialis* complex, and *Thalassiosira* spp. dominated (67–98%) the study area (Figure 3.2). Even in 2018, centric diatoms were dominant (85.5–99.8%), but the dominant species varied within the region. Thus, *Thalassiosira* spp. dominated (48.9–96.4%) south of St. Lawrence Island, while *C. socialis*

complex dominated (30.9–75.1%) other areas. The pennate diatom *Fragilariopsis/Fossula* spp., a known ice alga, were numerous (5.9×10^4–2.6×10^5 MPN cells g^{-1} wet sediments) at St.11 and south of St. Lawrence Island in 2017. Particularly south of St. Lawrence Island, they account for a large percentage of the abundance (24–35%). On the other hand, *Fragilariopsis/Fossula* spp. were rarely (0–6.7%) noted throughout the study area in 2018 (Figure 3.2).

From satellite data, the sea ice concentration was varied greatly between 2017 and 2018. In 2017, sea ice existed south of St. Lawrence Island even in mid-April whereas in April 2018, the sea ice had completely retreated to the north of St. Lawrence Island in 2018 (Figure 3.3). The TSR at each station was evaluated for 6 April to 10 May in 2017 and 22 March to 8 May in 2018. When comparing the sea surface chl *a* (the median value from the TSR to the observation day) at each station, there was no significant difference for all stations between 2017 and 2018 (*U*-test, $p > 0.36$). However, south of St. Lawrence Island, the chl *a* concentration was significantly different between years (*U*-test, $p < 0.05$), which was 3.6–11 times higher in 2018 (1.81–3.15 mg m^{-3}; Sts. 4, 6, 8) than in 2017 (0.27–0.53 mg m^{-3}; Sts. 19, 21, 23) (Table 3.1). In the study area, the date when the daylength exceeds 12 hours day^{-1} is 22 March. (Table 3.1). The growing periods of the ice-associated diatoms, which was indexed by the number of days between the date when the daylength exceeds 12 hours day^{-1} and the TSR, ranged from 0 to 49 days throughout the study area. South of St. Lawrence Island, the growing periods of the ice-associated diatoms was 15–40 days in 2017, while only 0–2 days in 2018 (Table 3.1). Thus, it in 2017 was substantially longer than in 2018.

3.4. Discussion

In the Pacific Arctic, *C. socialis* complex and *Thalassiosira* spp. generally dominate in microalgal blooms in the open-water (von Quillfeldt, 2000; Sukhanova et al., 2009; Sergeeva et al., 2010). Distribution of viable diatoms in sediment is greatly affected by the distribution of diatoms in the water column (Pitcher, 1990). This is considered to be the reason that the viable diatoms of *C. socialis* complex and *Thalassiosira* spp. were dominant in the sediments of this study. The viable diatom concentration observed in this study is comparable to eutrophic coastal areas (Itakura et al., 1997). This study area, the northern Bering Sea shelf, is known to have high primary productivity (Springer and McRoy, 1993). Therefore, the results of this study are considered to reflect high primary productivity in the water column. In the northern Bering Sea,

the viable diatoms, including resting stages, would settle and accumulate on the seafloor after the microalgal blooms. However, we need to consider further the relationships between diatom concentrations in sediments and primary productivity in the water column (see chapter 4) because various horizontal processes exist in the northern Bering Sea.

In the Pacific-side of the Arctic Ocean, the nutrient-rich Anadyr Water flows west, while the nutrient-limited Alaskan Coastal Water flows east. East-west differences also exist in the species composition, biomass, and productivity of the microalgal community in these waters (Giesbrecht et al., 2019). On the other hand, the viable diatom population in the sediment showed similar community structure throughout the study area (similarity: >51.3%). While microalgae respond rapidly to environmental changes such as current and nutrient conditions, viable diatoms accumulating on the bottom are suitable for evaluating the microalgal community on a relatively long-time scale. In addition, uncertainty due to horizontal transport and differences in flow velocity would result in the high similarity of diatom communities, with no involvement of water masses with different productivity.

In the study area, flow velocity varies greatly depending on location and the resulting particle size deposited on the ocean floor also varies greatly with location (Grebmeier et al., 2006). Because the flow velocity in the Bering Strait is very fast (the annual mean: 0.8 Sv) (Woodgate et al., 2010), sediments are mainly sand, pebbles, and rock. Sediment in the Chirikov Basin north of St. Lawrence Island is sandy under the influence of fast flow velocity (Grebmeier et al., 2006). The viable diatoms in the sediments are also considered to be influenced by ocean currents during the sedimentation process (Tsukazaki et al., 2018). Therefore, it may not be appropriate to compare the viable diatom community in sediments over different years across regions with vastly different physical environments. Meanwhile, sediments south of St. Lawrence Island have been reported to be fine-grained sand with particle size $\varphi>3$ or silt and clay (Grebmeier and Cooper, 1995). In this less dynamic area, viable diatoms in sediments are considered to relatively reflect the productivity of diatoms in the water column.

South of St. Lawrence Island, the concentration of viable diatoms in the sediment in 2018 were 10–100 times higher than in 2017. In particular, *Thalassiosira* spp. in 2018 was 27–522 times higher than in 2017. Median value of chl *a* from the TSR to observation date based on satellite data was 3.6–11 times higher in 2018 than in 2017. This high chlorophyll is presumed to be a result of much earlier sea ice retreat in 2018. The limited sea ice and ice melt in spring 2018

resulted in minimal low-salinity water in the near surface and, thus, halving the strength of the vertical stratification (Stabeno and Bell, 2019). In addition, the continuous southerly wind blew until early spring (Stabeno and Bell, 2019), which would lead to nutrient mixing into the surface layer (Duffy-Anderson et al., 2019). Furthermore, nutrient level of lower-layer in the Gulf of Anadyr, from which nutrients are supplied to the northern Bering, would be higher in low sea ice production years because of enhanced transportation of Pacific originated water, which known as subarctic intermediate nutrient pooled water (Nishioka et al., 2020; Abe et al., 2021). Therefore, the nutrient condition before the open-water bloom could be better in 2018 than in 2017, and planktonic microalgae could form dense blooms under the open-water condition shown by satellite chl *a* (Table 1). Indeed, the proportion of *Thalassiosira* spp. in sediment was larger in 2018 than in 2017 (Figure 3.4a), suggesting that *Thalassiosira* spp. would contribute to the enhanced open-water bloom.

South of St. Lawrence Island, ice algae *Fragilariopsis/Fossula* spp. were found at relatively high concentrations in 2017, whereas they were extremely rare in 2018 (Figure 3.2). The growth rate of ice algae is known to increase even when the daylength exceed 10 hours day^{-1} (Gilstad and Sakshaug, 1990) and massive ice algae blooms are reported to occur when the timing of daylength exceeds 15 hours day^{-1} (Cota et al., 1991). In the Bering Strait, chl *a* in the sea ice has been reported to reach an annual maximum in April–May (Leu et al., 2015). South of St. Lawrence Island, the growing periods of the ice-associated diatoms in 2017 was much longer than in 2018 (15–40 days vs 0–2 days), although no significance (Figure 3.4b and Table 3.1). Thus, in 2017, sea ice existed until April–May under favorable conditions, while in 2018, it seems that ice algae production was much less because sea ice retreated on 22–24 March before light conditions were favorable for the growth of ice algae (Table 3.1). Therefore, the annual variation of ice algae in the sediments seems to reflect the annual differences in the sea ice extent.

3.5. Conclusions

This study estimated the two-year differences in spring diatom communities in the northern Bering Sea by investigating viable diatoms in sediments. South of St. Lawrence Island, the composition and concentrations of viable diatom communities differed between 2017 and

2018 when the sea ice retreat timing varied greatly. In 2017, *Fragilariopsis/Fossula* spp., which are ice algae species, were abundant, but *Thalassiosira* spp. dominated in 2018. Therefore, it became clear that ice algae populations decline when sea ice retreat is earlier, allowing open water bloom of *Thalassiosira* spp. to dominate in the south of St. Lawrence Island, which is one of the famous biological hot spots in the Bering Sea and the Chukchi Sea (Grebmeier et al., 2006, 2015).

Ice algae have an important role as food for higher trophic level organisms such as zooplankton and benthos in early spring because they can grow under the limited light condition and may sink to the seafloor (Gradinger, 2009; Leu et al., 2015; Wang et al., 2015). Thus, the results of this study suggest that changes in sea ice retreat timing could alter the food supply condition to higher trophic level organisms in early spring in the region. Furthermore, the resulting change in algal production is thought to have the potential to alter the material cycle and flux in the marine ecosystem of the northern Bering Sea, characterized by pelagic-benthic coupling (Grebmeier et al., 2006).

3.6. Figures and Tables

Table 3.1. Information on the sediment sampling, and environmental data from satellite observations and the most probable number (MPN) of diatoms in the sediment samples. Stations with underlines indicate that their location is south of the St. Lawrence Island where prominent inter-annual changes were detected. The median value of chlorophyll *a* (chl. *a*) is that from the timing of sea ice retreat (TSR) to the observation day. The growing periods of the ice-associated diatoms was calculated by TSR-date when the daylength exceeded 12 hours day^{-1}.

Year	Station No.	Latitude (N)	Longitude (W)	Date	Bottom depth (m)	(a) Date when the daylight hours exceed 12 h d^{-1}	Median value of chl. *a*	(b) Timing of sea ice retreat (TSR)	Duration of ice algae growth (day) (=b-a)	Total MPN (cells g-1 wet sediments)
2017	1	66°16'	168°54'	9-Jul	57	22-Mar	6.11	10-May	49	62,770
	5	65°39'	168°15'	11-Jul	41	22-Mar	2.44	4-May	43	30,180
	6	65°21'	168°53'	12-Jul	56	22-Mar	5.65	30-Apr	39	1,303,520
	7	65°04'	169°38'	12-Jul	51	22-Mar	2.18	29-Apr	38	73,200
	9	65°04'	168°12'	13-Jul	43	22-Mar	1.86	5-May	44	251,250
	11	64°31'	167°52'	17-Jul	35	22-Mar	0.57	7-May	46	1,911,790
	13	64°31'	169°31'	17-Jul	43	22-Mar	3.46	17-Apr	26	223,240
	15	64°30'	170°53'	18-Jul	46	22-Mar	1.47	11-Apr	20	288,250
	19	63°31'	173°02'	19-Jul	67	22-Mar	0.53	6-Apr	15	255,940
	21	62°55'	172°06'	20-Jul	56	22-Mar	0.34	7-Apr	16	246,290
	23	62°10'	170°31'	21-Jul	47	22-Mar	0.27	1-May	40	313,860
2018	4	63°09'	173°50'	2-Jul	75	22-Mar	1.95	22-Mar	0	10,732,620
	6	62°53'	172°10'	3-Jul	55	22-Mar	1.81	23-Mar	1	60,897,100
	8	62°29'	169°60'	3-Jul	37	22-Mar	3.15	24-Mar	2	3,440,190
	14	64°31'	170°52'	5-Jul	46	22-Mar	2.17	16-Apr	25	282,990
	19	64°30'	166°31'	6-Jul	28	22-Mar	5.77	30-Apr	39	515,070
	20	65°05'	167°60'	6-Jul	46	22-Mar	1.38	18-Apr	27	722,420
	22	65°05'	169°42'	7-Jul	51	22-Mar	2.67	17-Apr	26	2,092,930
	30	66°44'	168°58'	11-Jul	42	22-Mar	2.62	8-May	47	436,070

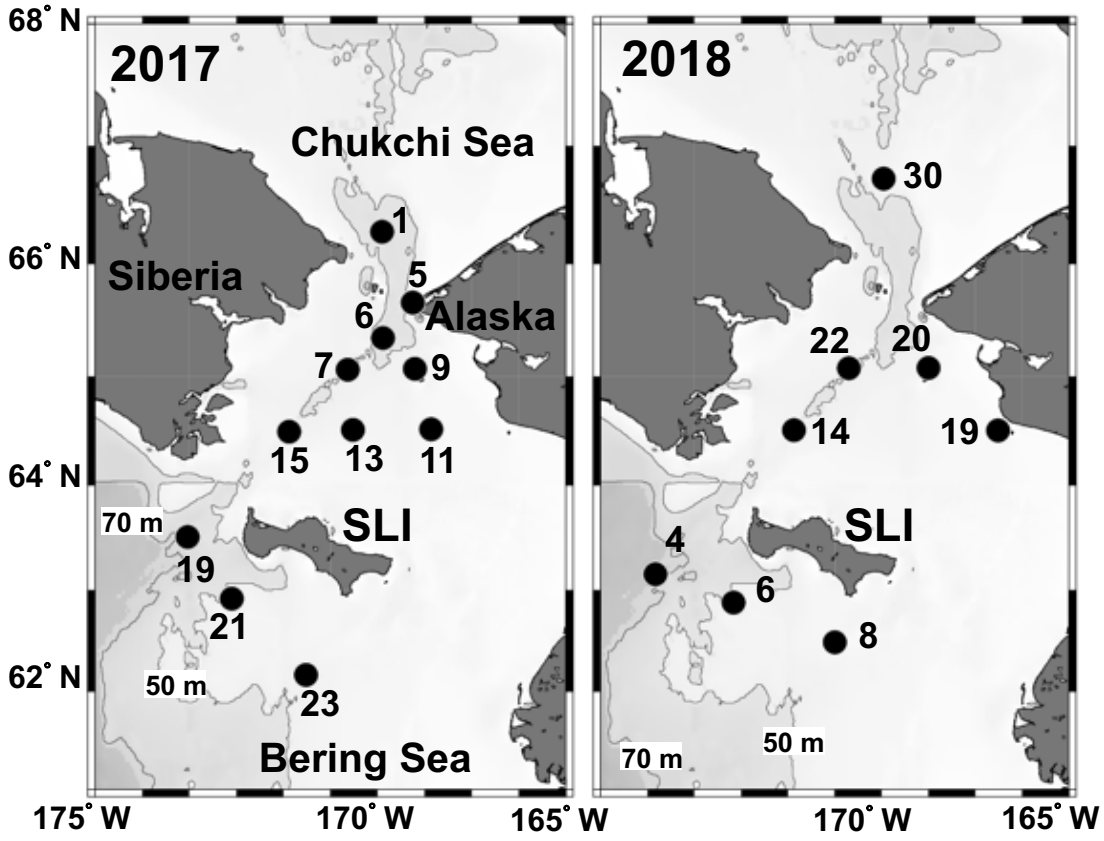

Figure 3.1. Location of the sediment samplings in the northern Bering Sea during the summers of 2017 and 2018. The numbers indicate the station ID. SLI: St. Lawrence Island.

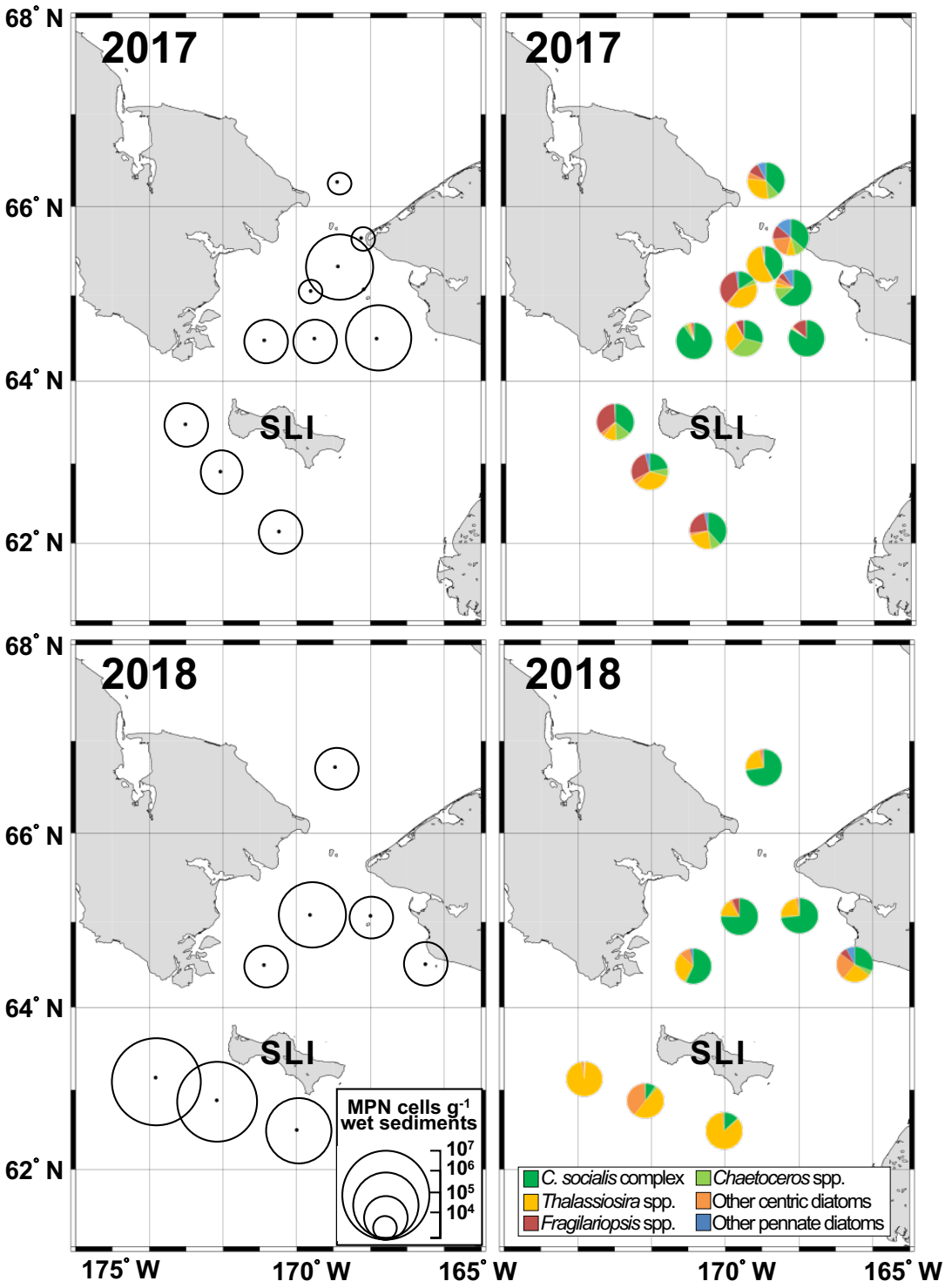

Figure 3.2. Horizontal distribution of the abundance (left panels) and species composition (right panels) of viable diatom resting stages from the bottom sediments in the northern Bering Sea during the summers of 2017 and 2018. SLI: St. Lawrence Island.

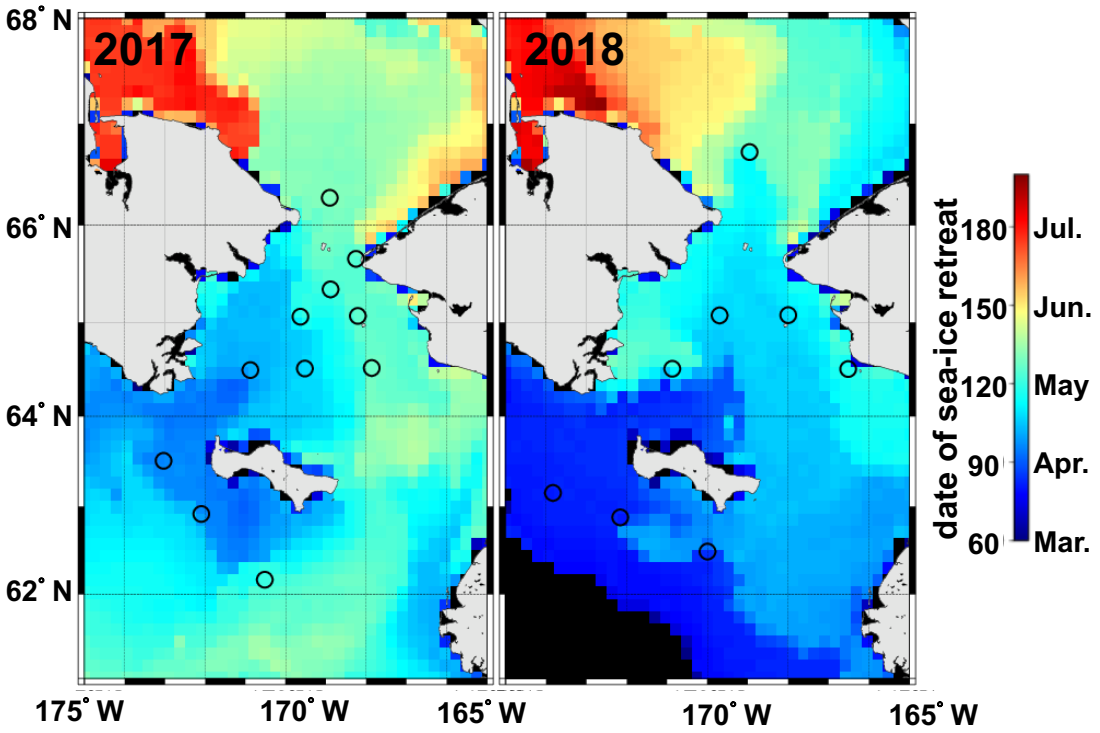

Figure 3.3. Horizontal distribution of the sea ice retreat date derived from AMSR2 SIC data in the northern Bering Sea during 2017 (left panel) and 2018 (right panel). Open circles indicate the sampling station in each year.

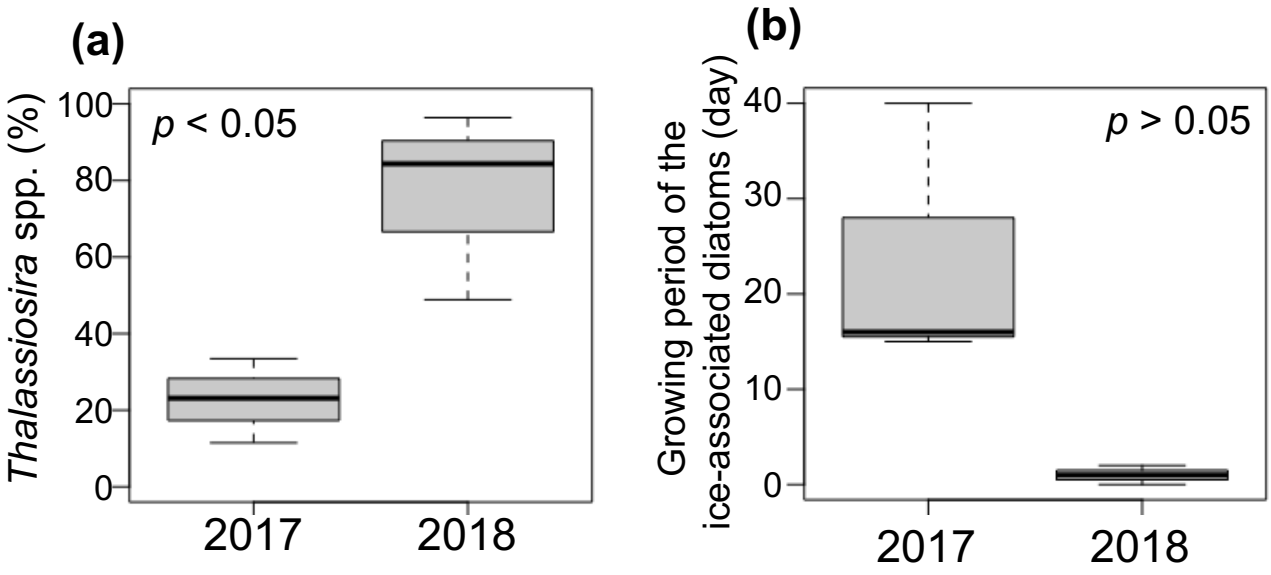

Figure 3.4. Comparison of the proportion of *Thalassiosira* spp. to total MPN (a) and the growing periods of the ice-associated diatoms (b) in 2017 and 2018.

CHAPTER 4 – Impact of the sea ice dynamics on the spatial distribution of viable diatoms in sediments of the Pacific Arctic region

4.1. Introduction

As mentioned in the general introduction, the characteristics of primary productivity in the Pacific Arctic is regional dependent. The northern Bering and Chukchi Seas display among the highest daily rates of productivity in the Arctic (Springer et al., 1996). As a consequences, the sinking POC flux measured in 2018 in the northern Bering and Chukchi Seas was the among highest ever documented across global oceans (O'Daly et al., 2020). In contrast, primary productivity in the southwestern Beaufort Sea is low (Frost and Lowry, 1984).

Diatoms support primary productivity during spring and summer blooms in the Pacific Arctic region (von Quillfeldt, 2000; Sergeeva et al., 2010), which drive sinking POC flux (Lalande et al., 2020). Some diatom genera, *Chaetoceros* spp. and *Thalassiosira* spp., are known to form dense blooms in this region (von Quillfeldt, 2000; Sergeeva et al., 2010). In particular, *C. socialis* complex can constitute more than 90% of phytoplankton assemblages during blooms in the northern Bering and Chukchi Seas (Sergeeva et al., 2010). The centric diatoms *Attheya* spp. are reported to be present in the sea ice of the Arctic (Campbell et al., 2018; Melnikov et al., 2002; von Quillfeldt et al., 2003; Szymanski & Gradinger, 2016; Werner et al., 2007) and can comprise over 60% of diatom abundance in the sea ice during spring (Campbell et al., 2018). Pennate diatoms are also known to constitute a large proportion of the sea ice algal community (von Quillfeldt et al., 2003; Szymanski and Gradinger, 2016).

Chapter 3 showed that temporal changes in the timing of the sea ice retreat affected the diatom composition during early spring. It was suggested through the investigations of diatom community in sediments. On the other hand, the sea ice dynamics in the Pacific Arctic is also spatially various and the extent and duration of sea ice presence are considerably different. The extent of sea ice has been shown to influence regional microalgal assemblages (Neeley et al., 2018), but this relationship is not fully understood. Sea ice decline has been reported in the region (Markus et al., 2009; Grebmeier et al., 2015; Frey et al., 2018), and Arrigo et al. (2008) used satellite observations to show that this decline was associated with increasing annual primary production. However, changes in microalgal assemblages and particularly in ice-associated

assemblages, cannot be evaluated by satellite observations only, necessitating field-based studies to examine the structure of these communities in more detail and broader area.

In this study, we enumerated viable diatoms in sediments collected in a broad area across the Pacific Arctic region, from the northern Bering Sea to the Chukchi Sea and the southwestern Beaufort Sea. We describe the features of viable diatom assemblages in sediments over these regions, and discuss two hypotheses: 1) the concentrations of viable diatoms in sediments are correlated with primary production in the water column, and 2) the extent and duration of sea ice during the previous winter and spring determines community structure of viable diatom assemblages in sediments. In addition, we discuss how observed variations in diatom assemblages may impact organisms at higher trophic levels that rely on diatoms as an important food source.

4.2. Materials and Methods

4.2.1. Sea ice, primary production and daylength

To evaluate the sea ice extent in each region, the TSR was defined using the SIC data as mentioned chapter 3. Here, we used a 5-day moving average value of the SIC data.

To obtain a continuous primary production time-series, we used Level-3 standard mapped image (9-km resolution) of Aqua-MODIS data downloaded as spectral remote sensing reflectance (R_{rs}, sr^{-1}) and daily photosynthetically available radiation (PAR, mol photons m^{-2} day^{-1}) from the Goddard Space Flight Centre/Distributed Active Archive Centre, NASA. The absorption coefficient for 443 nm ($a_{ph}(443)$) and euphotic zone depth (Z_{eu}, m) were computed from $R_{rs}(\lambda)$ using Quasi-Analytical Algorithm (QAA) version 5 (Lee et al., 2007, 2009) and daylength (DL, hours day^{-1}) for the study area calculated according to Brock (1981). We then computed the daily euphotic-depth-integrated primary production (PP_{eu}, mg C m^{-2} day^{-1}) using $a_{ph}(443)$, Z_{eu}, PAR, and DL as inputs to an absorption-based productivity model (ABPM; Hirawake et al., 2012). Missing values in $a_{ph}(443)$ and Z_{eu} due to cloud cover were interpolated using their annual medians and hence PP_{eu} was derived for the cloud-covered pixels. From these values we calculated cumulative PP_{eu} (IP_{eu}, mg C m^{-2}) from TSR to the date when the *in situ* sediment sampling was conducted for each shipboard observation site.

4.2.2. Sampling

Sediment sampling was conducted in the shallow Pacific Arctic region at stations ranging from 24–194 m bottom depths (the northern Bering Sea, Chukchi Sea and the southwestern Beaufort Sea; Figure 4.1, Table 4. 1) from 2–12 July 2018 aboard T/S *Oshoro-Maru* of Hokkaido University, and from 9–23 August 2018 and 30 October to 15 November 2018 aboard the U.S. Coast Guard icebreaker *Healy* (*HLY 1801* and *HLY 1803*, respectively) (Figure 4.2 (a)). Sediment samples were collected using a multiple corer (*Oshoro-Maru* cruise), a Van Veen Grab sampler, or a HAPS core sampler (*Healy* cruises) at each station. A portion of the 0–1 cm of each sediment core was extruded and stored in darkness at 5˚C for *Oshoro-Maru* samples, and for *Healy* samples, a portion of the 0–3 cm layer was collected from the grab or the core and stored in air-tight amber jars at 1–4˚C. The sediment samples were stored for more than one month in order to eliminate vegetative cells.

4.2.3. Quantification of viable diatoms in sediments

The abundance of viable diatoms in the sediment samples was analyzed using the most probable number (MPN) method (Imai et al., 1984, 1990) as the same procedure to the method in chapter 3 expect for the incubation conditions. Incubation was carried out at a temperature of 5°C and under white fluorescent light of 50 or 116 μmol photons m^{-2} s^{-1} with a 14 h light:10 h dark photocycle for 10 days. Since we observed wells with 10^{-2}–10^{-6} dilutions, the detectable cell numbers by the MPN method were from 1.8×10^2 to 2.4×10^7 MPN cells g^{-1} for each species. Note that we used the dataset of chapter 3 for the *Oshoro-Maru* expedition.

4.2.4. Statistical analyses

The viable diatom communities in sediments were distinguished by cluster analysis. To reduce the bias for abundant species, the cell concentration data (X: MPN cells g^{-1} wet sediment) for each species were transformed to $\sqrt[4]{X}$ prior to cluster analysis (Quinn and Keough, 2002). Dissimilarities between samples were examined using the Bray-Curtis index based on the differences in the species composition. To group the samples, the dissimilarity indices were coupled using hierarchical agglomerative clustering with a complete linkage method (an unweighted pair group method using the arithmetic mean). A Mann-Whitney *U*-test was conducted to evaluate environmental factors (the TSR, IP_{eu}, and the growth period of ice-

associated assemblages (GP)) between the distinguished groups. The GP was defined as the integrated daylength during the periods with SIC > 20% after the daylength exceeded 10 hours, as Gilstad and Sakshaug (1990) indicated that ice-associated assemblages could increase their growth rate when daylength exceeded 10 h.

We conveniently classified diatoms into two groups based on previous studies. In other words, we defined the open-water assemblages as the community with centric diatoms, excluding *Attheya* spp., and the ice-associated assemblages as the community with pennate diatoms and *Attheya* spp., since *Attheya* spp. and pennate diatoms are often reported to be present in the sea ice (e.g. Campbell et al., 2018; Melnikov et al., 2002; von Quillfeldt et al., 2003; Szymanski & Gradinger, 2016; Werner et al., 2007). Based on this definition, we analyzed the relationships of ice-associated assemblages with the TSR and the GP using Spearman's rank correlation coefficient.

All statistical analyses were conducted using R software (version 3.6.1, R Development Core Team, 2019).

4.3. Results

4.3.1 Sea ice and primary production

The TSR was different among regions (Table 4. 1). The sea ice retreated from south to north in the northern Bering and the Chukchi Seas, and from west to east in the southwestern Beaufort Sea (Figure 4.1). The IP_{eu} had a regional feature in which high values were observed in the southern Chukchi Sea and low values in the southwestern Beaufort Sea (Table 4.1, Figure 4.2b).

4.3.2 Diatom concentrations and species composition

The viable diatoms in sediments determined by the MPN method ranged over four orders of magnitude, from 1.2×10^3 to 6.1×10^7 MPN cells g^{-1} wet sediment (Figure 4.3). Highest concentrations were found to the south of St. Lawrence Island (3.4×10^6–6.1×10^7 MPN cells g^{-1} wet sediment). In the Chirikov Basin, which extends northwards from St. Lawrence Island to the Bering Strait (DBO2-1, DBO2-4, OS14, OS19, OS20, OS22), diatom concentrations were relatively high (2.8×10^5–3.0×10^6 MPN cells g^{-1} wet sediments). Diatom concentrations near

Utqiagvik (DBO5-10) were also relatively high (1.2×10^6 MPN cells g^{-1} wet sediments). In contrast, cell concentrations were lower in samples from the coastal region of the southwestern Beaufort Sea (DBO6-5, PRW-7, PRB-4, PRB-7, KTO-5, MCK-1, MCK-2, MCK-3, MCK-4) (1.2×10^3–7.8×10^3 MPN cells g^{-1} wet sediments). Nineteen genera and twenty species were observed over the study region – 12 genera and 14 species of centric diatoms and 7 genera and 6 species of pennate diatoms. Centric diatoms were dominant at almost all stations, although dominant species varied geographically; proportional abundance of *Chaetoceros* spp. and *Thalassiosira* spp. were found in samples collected from the northern Bering Sea and Chukchi Sea, whereas *Attheya* spp. were highest in the southwestern Beaufort Sea (Figure 4.4). Pennate diatoms comprised over 50% of the diatom assemblages at some stations (DBO4-4, MCK-1, MCK-2, MCK-3), with highest proportional abundance found in samples from the southwestern Beaufort coastal region (Figure 4.4). Total cell concentration in sediments were positively correlated with the cell concentrations of *Chaetoceros* spp. and *Thalassiosira* spp. (Spearman, $\rho = 0.97$, $p < 0.05$) (Figure 4.5).

In order to test for seasonal effects, diatom assemblages were compared over time in stations in the northern Bering Sea and Southern Chukchi Sea, which included locations from each sampling period (OS14, 19, 20, 22, 30 by *Oshoro-Maru*, DBO2-1, 2-4, 3-6, 3-8 in *HLY 1801*, and DBO 3-1, 3-5, 3-7 in *HLY 1803)*. There were no significant differences in species or genera among these samples (one-way ANOVA, $p > 0.05$), with the exception of *Attheya* spp. and *C. debilis* (one-way ANOVA, $p < 0.05$).

4.3.3. Diatom assemblages by cluster analysis

Cluster analysis based on concentrations of viable diatoms classified the diatom assemblages into two groups (A, B) and four outgroups at 52% and 64% dissimilarity levels. Group A was distributed from the northern Bering Sea to the Chukchi Sea near Utqiagvik (Figure 4.6a). Cell concentrations in group A were very high (7.9×10^4–1.1×10^7 MPN cells g^{-1} wet sediments, avg = 1.2×10^6 MPN cells g^{-1} wet sediment), and samples in this group with dominated by *Chaetoceros* spp. and *Thalassiosira* spp. (35% and 51%, respectively) (Figure 4.6b). Group B included stations from the southwestern Beaufort Sea, where cell concentrations ranged from 3.2×10^3 to 2.1×10^5 MPN cells g^{-1} wet sediment (avg = 5.8×10^4 MPN cells g^{-1} wet sediment) and *Attheya* spp. were dominant (47%) (Figure 4.6b). All stations from the easternmost transect in the study region (MCK) were classified as outgroups (Figure 4.6a).

4.3.4. Relationships with environmental factors

Environmental factors differed between samples comprising diatom groups A and B. The TSR was significantly later at the group B locations compared to group A (*U*-test, $p < 0.05$) (Figure 4.7a), and the GP was significantly longer at group B locations than group A (*U*-test, $p < 0.05$) (Figure 4.7b). The switching between the two diatom groups occurred around 200 Julian day of the TSR and approximately 2500 hours of the GP (Figures 4.7a, 4.7b, and 4.8). By contrast, the IP_{eu} and the sampling depth were not significantly different between groups (*U*-test, $p > 0.05$) (Figures 4.7c and 4.7d).

In addition, the TSR and the GP were significantly positively correlated with the proportion of pennate diatoms and *Attheya* spp., which are defined as the ice-associated assemblages ($\rho = 0.63$ and 0.29, respectively, $p < 0.05$) (Figure 4.8).

4.4. Discussion

Examination of the distribution and abundance of viable diatoms in Pacific Arctic sediments demonstrated a strong correlation with the timing of sea ice retreat and the growth period of ice-associated assemblages. Details regarding spatial community dynamics and relationships between diatom assemblages and TSR, GP, and environmental parameters are discussed below.

4.4.1. Distribution of viable diatoms in sediments and the relationships with primary production in the Pacific Arctic Region

Cell concentrations of viable diatoms in sediments exhibited geographic variability that roughly corresponded with levels of primary production previously reported in the region. However, primary production values (IP_{eu}) estimated by satellite remote sensing in this study did not have any statistically significant relationships with viable diatom assemblages in sediments.

This study found high concentrations of viable diatoms in the northern Bering and the Chukchi Sea sediments (avg = 3.1×10^6 MPN cells g^{-1} wet sediments), but low concentrations (avg = 6.2×10^4 MPN cells g^{-1} wet sediments) in the southwestern Beaufort Sea sediments. This is consistent with prior studies of primary productivity that documented high annual water-

column integrated primary production in the northern Bering and Chukchi Seas and low productivity in the western Beaufort Sea (Grebmeier et al., 2006; Hill et al., 2018). However, we did not find a significant relationship between viable diatom assemblages in sediments and primary production values estimated by satellite. O'Daly et al. (2020) presented similar findings; that higher rates of primary productivity were correlated with higher rates of POC flux, including viable diatoms, but that there is variability in the export efficiency. One reason why there was no significant relationship between the diatom community in sediments and primary productivity in the water column may be horizontal advection. Generally, when diatom sinking rates range from 3.9–17.5 m day^{-1} (Miklasz and Denny, 2010), it takes 3–13 days for diatom to fall to the seafloor as the bottom depth is about 50 m in this region. Considering that time-mean and depth-averaged flow vectors in the study area ranged from about 5–20 cm s^{-1} (Anderson et al., 2021), the horizontal flow distance of diatoms is about 13–225 km. On the other hand, satellite data resolution used to estimate primary productivity was 9 km. Therefore, this difference in scale may be uncertain for comparison between the diatom community in sediments and primary productivity in the water column. Comparisons on a broader spatial scale would need because of the effects of horizontal transport by various processes in the ocean. Another reason for the disproportion between primary production and sediment diatom concentrations would relate to the size structure of microalgal communities. For example, the smaller microalgae than diatoms sometimes contribute to 2.3¬–87.9% of primary production in the Chukchi water column (Lee et al., 2023). In addition, Waga et al. (2019) suggested that sediment chl *a* concentrations were strongly related to surface microalgal size structure. Therefore, while the hypothesis that viable diatom concentrations in sediments reflect primary productivity in the water column (Imai et al., 1990; Pitcher, 1990; Itakura et al., 1997) holds up over broad features of the Pacific Arctic region, additional data are needed to justify this using viable diatom assemblages in sediments as a strict proxy for productivity.

Another cause of high concentrations of viable diatoms in sediments observed in the northern Bering and Chukchi Seas is related to the high sinking flux in this region (O'Daly et al., 2020). Lalande et al. (2020) used a time series of sediment trap observations at single station in the Chukchi Sea to show that diatoms make up a high proportion of POC flux. The characteristically high sinking flux in the northern Bering and Chukchi Seas could drive high concentrations of sediment diatom assemblages reported here, though diatom losses by

zooplankton grazing also need to be considered (Campbell et al., 2009; Sherr et al., 2009).

We considered the impact that variable sampling times may have had upon the assemblages observed in this study. The sediments were obtained over several different time periods (2–12 July 2018, 9–23 August 2018, and 30 October to 15 November 2018), and it is possible that the community structure changed from summer to fall. However, there were no significant differences in species or genera except for *Attheya* spp. and *C. debilis* between samples at replicated stations in the northern Bering Sea and Southern Chukchi Sea, where sampling was conducted over multiple time periods. Dissimilarity among almost all the samples was less than 40%, and they were also grouped in the cluster analysis. Water temperature is known to influence survival time of resting stages, one of the forms of viable diatoms in sediments, with colder water increasing survival time length (McQuoid and Hobson, 1996). Hargraves and French (1983) reported that *Chaetoceros diadema*, *Detonula confervacea*, *Leptocylindrus danicus* and *Thalassiosira nordenskioeldii*, which sometimes appear in the Pacific Arctic sediments, survived for 291, 220, 400, and 220 days, respectively, at temperatures between 5−6°C. These periods are sufficiently longer than the difference in sampling periods (the longest difference is 136 days). Given that temperatures at the seafloor of the Pacific Arctic are lower than 5−6°C, we do not believe that the survival time of viable diatoms impacted our results. For these reasons, differences over sampling periods appeared to be almost negligible in this study.

4.4.2. The relationship of viable diatom assemblages in sediments with the TSR and the GP

Prior investigators have shown that the magnitude and composition of diatom assemblages in the Arctic spring bloom are influenced by the presence of the sea ice and the timing of the sea ice retreat (Fujiwara et al., 2016; Neeley et al., 2018) (also see chapter 3). In this study, the distribution of viable diatom assemblages in sediments were clearly related to spatial differences in the TSR. In locations where the ice retreat was early, such as the northern Bering and the Chukchi Seas, *Chaetoceros* spp. including *C. socialis* complex and *Thalassiosira* spp. were dominant in sediments (*C. socialis* complex: 0.36–93.1%, *Chaetoceros* spp.: 0.76–93.6%, *Thalassiosira* spp.: 2.0–96.4%). Because they are known to form dense spring blooms in these regions (von Quillfeldt, 2000; Sergeeva et al., 2010), these data suggest that viable diatoms were settled to the seafloor after spring blooms of *Chaetoceros* spp. and *Thalassiosira* spp. in the

northern Bering Sea and the Chukchi Sea. In addition, the positive correlation between *Chaetoceros* spp. and *Thalassiosira* spp. cell concentrations with total cell concentrations indicates that where the TSR was early and the open-water period was long, large diatom blooms of *Chaetoceros* spp. and *Thalassiosira* spp. produced high quantities of viable diatom cells.

The TSR had also an effect on the diatom community composition, especially the proportion of ice-associated diatoms in diatom assemblages. In the southwestern Beaufort Sea, where the TSR was late, diatom assemblages were dominated by ice-associated species (Groups B and outgroups in the transect MCK), again demonstrating that sea ice is a driver of benthic community structure among the exported diatoms. In addition, the prevalence of ice-associated species was positively correlated with the TSR, suggesting that the proportion of ice algae in diatom assemblages is higher when sea ice persists. This is likely due in part to their ability to sustain growth under low light levels (< 1 μmol photon s^{-1} m^{-2}) (Cota and Smith, 1991; Mock and Gradinger, 1999); notably, Tsukazaki et al. (2018) demonstrated that the centric genus *Attheya* spp. could survive in dark for more than six months, and thus can withstand low light conditions in the Arctic. It is possible that this study underestimated the concentrations of pennate diatoms in sediments compared with *Attheya* spp. and other centric diatoms, as few marine pennate diatoms are known to form resting stages, while many centric diatoms do (McQuoid and Hobson, 1996), and the fate of the pennate diatoms in sediment is largely unknown. Despite this potential bias, these data indicate that the proportion of ice-associated species was higher where the TSR occurred later. Interestingly, a spatial change from the assemblage dominated by open-water species to that with high proportion of ice-associated diatoms occurred at stations where the TSR was around the 200th Julian day (mid-July). This indicates a potential threshold between dominant diatom groups based on the TSR parameter.

For ice-associated assemblages in the surface sediments, the length of the growth period during which algae receive sufficient light before the TSR is important (chapter 3). The proportional abundance of ice-associated diatoms was significantly higher when GP was longer, suggesting that photoperiod during sea ice presence is another important driver of diatom community structure (Smith et al., 1988; Cota and Home, 1989; Gosselin et al., 1990). In addition, a GP boundary of 2500 hours may be an important parameter for the distribution of ice-associated assemblages due to corresponding changes that were observed. Future efforts to evaluate and predict diatom assemblages should consider both the TSR and the GP.

4.4.3 Connecting diatom distribution to higher trophic levels

The diatom assemblages had clear relationships with the TSR and the GP. In the northern Bering Sea, the early timing of the sea ice retreat and subsequent changes in diatom assemblages in the water column and the sediment was reported in 2018 (chapters 2 and 3). This indicates that the recent drastic reduction of sea ice in the Pacific Arctic region may induce a shift in diatom assemblages from relative dominance of ice-associated species to open-water species.

The distribution and composition of diatom species in this study were associated with the zooplankton feeding environment in the Pacific Arctic region. As diatoms comprise the largest portion of the mesozooplankton diet, especially in spring (Campbell et al., 2016), changes in diatom species composition will perturb prey environments of higher trophic-level organisms. The spatial trend of viable diatom concentrations in sediments exhibited a similar gradient to zooplankton $\delta^{13}C$ values showed by Pomerleau et al. (2014), which reported values that were more enriched in the western Bering Strait and less enriched on the Beaufort shelf. Nakatsuka et al. (1992) reported an increase in $\delta^{13}C$ of POC during a diatom bloom in a mesocosm experiment in Saanich Inlet, Canada. Additionally, they showed that the main factor influencing the variation of $\delta^{13}C$ of POC during a phytoplankton bloom in a mesocosm experiment was the specific production rate of POC, which can be proportional to the specific growth rate of phytoplankton, rather than carbon dioxide system or community composition (Nakatsuka et al., 1992). Typically, fast-growing diatoms (e.g. *Chaetoceros* spp. and *Thalassiosira* spp.) and zooplankton that feed on these diatoms are enriched with ^{13}C (Fry and Wainright, 1991). The inflow of nutrient rich Anadyr waters from the western Bering Strait is known to fuel huge blooms of *Chaetoceros* spp. and *Thalassiosira* spp. (Sergeeva et al., 2010; Danielson et al., 2017), explaining the high concentrations of these species in sediments of the northern Bering and the Chukchi Seas reported here. In addition, regions of high viable diatom concentrations in sediments roughly corresponded to benthic hotspots, which include waters to the south of St. Lawrence Island, the Chirikov Basin, the southeastern Chukchi Sea and the northeastern Chukchi Sea (Grebmeier et al., 2015). In these regions with mean depths from 43 to 65 m, benthic primary production can be lower than pelagic production due to light limitation, and accumulation of microalgae in sediments are the main food source for benthic communities (Grebmeier et al., 2015). In particular, diatoms are valuable taxa because they are rich in polyunsaturated fatty acids (PUFAs) (Brown et al., 1997). Furthermore,

Wang et al. (2016) analyzed the blubber fatty acid composition and stable carbon isotope ratios of ice seals, who feed on pelagic and benthic fishes, in the northern Bering and the southern Chukchi Seas to show that ice algae production contributed up to 80% of ice seal diets through trophic transfer. Therefore, changes in diatom assemblages caused by sea ice dynamics will directly influence zooplankton and benthos production, with indirect effects upon higher trophic levels.

4.5. Conclusions

This study demonstrated that the distribution and community composition of viable diatoms in the Pacific Arctic sediments were significantly influenced by the presence of sea ice and the light environment. Viable diatoms in sediments appear to follow broad spatial patterns of primary productivity across the region, suggesting the potential use of viable diatoms in sediments as one of the proxies for productivity, despite the fact that there was not a significant relationship between diatom assemblages and primary productivity estimated by satellite observations. The TSR and the GP were important drivers of diatom assemblages, and significantly influenced the composition of diatoms in sediments. In particular, diatom assemblages changed spatially from composition dominated by open-water species to a high proportion of ice-associated diatoms in the region where the TSR occurred after mid-July (around the 200th Julian day) and the GP was over 2500 hours. This result may indicate that a shift to earlier TSR under future climate conditions could induce not only delayed bloom timing (Hirawake and Hunt, 2020; Kikuchi et al., 2020) but also a change in the composition of diatom assemblages forming the spring bloom. The distribution of viable diatoms in sediments is a valuable approach for investigating the diatom community, particularly on the Arctic shelves where it is logistically challenging to characterize the rapid seasonal succession in community composition that occurs across this remote and dynamic geographic region. Moreover, this approach provides species-level resolution lacking in satellite observations, providing a more robust assessment of the ecosystem implications of community changes. On the ecosystem level, it is interesting that the distribution of viable diatoms in sediments corresponded spatially with benthic hot spots and the feeding environment of zooplankton. Based on this research, it is clear that future changes in sea ice extent and duration could impact diatom communities, and that resulting fluctuations in primary productivity and community structure could affect other components of Arctic marine ecosystems.

4.6. Figures and Tables

Table 4.1. Locations of sediment sampling stations in the Bering, Chukchi, and Beaufort Seas from July to November in 2018. In sample type column, "core" and "Van Veen" indicate that the samples were collected by multiple corer and Van Veen grab sampler, respectively. The timing of sea ice retreat (TSR) indicates the last date when the sea ice concentration falls below 20%, prior to observed annual sea ice minimum across the study region during summer. IP_{eu} indicates daily integrated values of primary production from TSR to the date of the *in situ* sediment sampling was conducted. The growth period of the ice-associated assemblages (GP) indicates the integrated daylength during the periods with SIC > 20% after the daylength exceeds 10 hours.

Cruise	Station	Date (Julian day)	Latitude (°N)	Longitude (°W)	Bottom depth (m)	Sample Type	TSR (Julian day)	IP_{eu} (mg C m^{-2})	GP (hours)
Oshoro-maru C056	OS4	2018/7/2 (183)	63.15	173.83	75	Core	2018/3/23 (82)	80254	103
	OS6	2018/7/3 (184)	62.88	172.16	55	Core	2018/3/23 (82)	56306	158
	OS8	2018/7/3 (184)	62.49	170	37	Core	2018/3/24 (83)	77753	234
	OS14	2018/7/5 (186)	64.51	170.87	46	Core	2018/3/25 (84)	66312	415
	OS19	2018/7/6 (187)	64.51	166.51	28	Core	2018/4/24 (114)	39181	755
	OS20	2018/7/6 (187)	65.08	168	46	Core	2018/4/18 (108)	32002	581
	OS22	2018/7/7 (188)	65.07	169.7	51	Core	2018/4/17 (107)	106377	469
	OS30	2018/7/11 (192)	66.73	168.96	42	Core	2018/4/24 (114)	59460	1033
Healy 1801	DBO2-1	2018/8/9 (221)	64.67	169.93	48	Van Veen	2018/4/16 (106)	104869	427
	DBO2-4	2018/8/9 (221)	64.96	169.9	49	Van Veen	2018/4/17 (107)	143194	469
	DBO3-6	2018/8/10 (222)	67.9	168.25	59	Core	2018/5/20 (140)	95858	936
	DBO3-7	2018/8/11 (223)	67.79	168.6	51	Core	2018/5/21 (141)	104109	935
	IC-3	2018/8/13 (225)	71.6	165.3	43	Van Veen	2018/6/26 (177)	32305	1830
	IC-8	2018/8/14 (226)	70.97	163.56	46	Van Veen	2018/6/29 (180)	48395	1391
	DBO4-2	2018/8/15 (227)	71.22	161.29	50	Core	2018/7/14 (195)	17824	1891
	DBO4-4	2018/8/15 (227)	71.48	161.5	49	Core	2018/7/15 (196)	15406	2378
	DBO4-5	2018/8/15 (227)	71.61	161.62	47	Core	2018/7/16 (197)	19747	2478
	DBO5-9	2018/8/17 (229)	71.58	157.82	66	Van Veen	2018/7/27 (208)	2915	2668
	DBO5-10	2018/8/17 (229)	71.63	157.9	64	Core	2018/7/26 (207)	2813	2670
	LB-11	2018/8/22 (234)	70.06	167.66	50	Van Veen	2018/5/13 (133)	95614	974
	LB-9	2018/8/23 (235)	69.88	166.82	47	Van Veen	2018/5/12 (132)	105276	877
	LB-7	2018/8/23 (235)	69.68	166.09	42	Van Veen	2018/5/12 (132)	96511	801

Table 4.1. Continued

Cruise	Station	Date (Julian day)	Latitude (°N)	Longitude (°W)	Bottom depth (m)	Sample Type	TSR (Julian day)	IP_{eu} (mg C m^{-2})	GP (hours)
Healy 1803	DBO6-1	2018/10/30 (303)	71.16	152.26	32	Van Veen	2018/8/9 (221)	42214	2825
	DBO6-3	2018/10/30 (303)	71.25	152.17	48	Van Veen	2018/8/8 (220)	55327	2829
	DBO6-5	2018/10/30 (303)	71.34	152.1	71	Van Veen	2018/8/27 (239)	63070	2899
	DBO6-7	2018/10/31 (304)	71.42	152.04	194	Van Veen	2018/8/28 (240)	52154	2902
	PRB-1	2018/11/2 (306)	70.69	148.44	26	Van Veen	2018/8/21 (233)	—	3347
	PRB-2	2018/11/2 (306)	70.77	148.33	35	Van Veen	2018/8/24 (236)	17622	3465
	PRB-4	2018/11/2 (306)	70.9	148.14	45	Van Veen	2018/9/3 (246)	16083	3406
	PRB-7	2018/11/2 (306)	71.02	147.98	58	Van Veen	2018/9/4 (247)	19897	3490
	MCK-1	2018/11/4 (308)	69.82	139.61	38	Van Veen	2018/8/22 (234)	40557	2240
	MCK-2	2018/11/4 (308)	69.9	139.49	44	Van Veen	2018/8/4 (216)	47210	2111
	MCK-3	2018/11/4 (308)	69.94	139.39	55	Van Veen	2018/8/1 (213)	47343	2114
	MCK-4	2018/11/4 (308)	69.97	139.3	60	Van Veen	2018/7/30 (211)	46783	2114
	KTO-2	2018/11/5 (309)	70.28	143.93	38	Van Veen	2018/8/22 (234)	30871	3192
	KTO-3	2018/11/5 (309)	70.37	143.79	48	Van Veen	2018/8/22 (234)	14101	3248
	KTO-5	2018/11/5 (309)	70.56	143.61	110	Van Veen	2018/8/18 (230)	13958	3222
	PRW-1	2018/11/7 (311)	70.68	148.91	24	Van Veen	2018/8/12 (224)	115526	3369
	PRW-4	2018/11/7 (311)	70.82	148.84	33	Van Veen	2018/8/25 (237)	76571	3373
	PRW-7	2018/11/7 (311)	70.95	148.78	38	Van Veen	2018/9/1 (244)	26141	3474
	DBO5-1	2018/11/14 (318)	71.25	157.13	47	Van Veen	2018/7/19 (200)	79118	2661
	DBO5-3	2018/11/41 (318)	71.33	157.31	91	Van Veen	2018/7/20 (201)	59408	2637
	DBO5-5	2018/11/14 (318)	71.41	157.49	128	Van Veen	2018/7/25 (206)	44094	2639
	DBO5-7	2018/11/14 (318)	71.5	157.66	85	Van Veen	2018/7/29 (210)	35765	2668
	DBO5-9	2018/11/14 (318)	71.58	157.83	66	Van Veen	2018/7/27 (208)	35857	2668
	DBO3-1	2018/11/15 (319)	68.31	166.92	35	Van Veen	2018/4/26 (116)	196801	812
	DBO3-5	2018/11/15 (319)	68.01	167.88	54	Van Veen	2018/5/5 (125)	212879	829
	DBO3-8	2018/11/15 (319)	67.67	168.95	50	Van Veen	2018/5/31 (151)	179195	1125

Table 4.2. Components of the modified SWM-3 medium. Solvent is natural filtered sea water. Medium pH is 7.7−7.8.

Component	Concentrations in final medium / Amounts per litter	Component	Concentrations / Amounts
$NaNO_3$	2 mM	P-1 metal in10 mL	
$NaH_2PO_4 \cdot 2H_2O$	0.1 mM	H_3BO_3	1.0 mM
$Na_2SiO_3 \cdot 9H_2O$	0.2 mM	$MnCl_2 \cdot 4H_2O$	3.5×10^{-2} mM
Na_2EDTA	30 μM	$ZnCl_2$	4.0×10^{-3} mM
Fe-EDTA	2 μM	$CoCl_2 \cdot 6H_2O$	1.0×10^{-4} mM
Na_2SeO_3	2 nM	$CuCl_2 \cdot 2H_2O$	1.0×10^{-6} mM
$Na_2MoO_4 \cdot 2H_2O$	100 nM	S-3 Vitamin in 2mL	
TRIS	500 mg	B_1-HCl	0.5 mg
P1-metals	10 mL	Ca-Pantothenate	0.1 mg
S-3 Vitamins	2 mL	Nicotinic acid	0.1 mg
		P-Aminobenzoic acid	10 μg
		Biotin	1.0 μg
		Inositol	5.0 mg
		Folic acid	2.0 μg
		Thymine	3.0 mg
		Vitamin B_{12}	1.0 μg

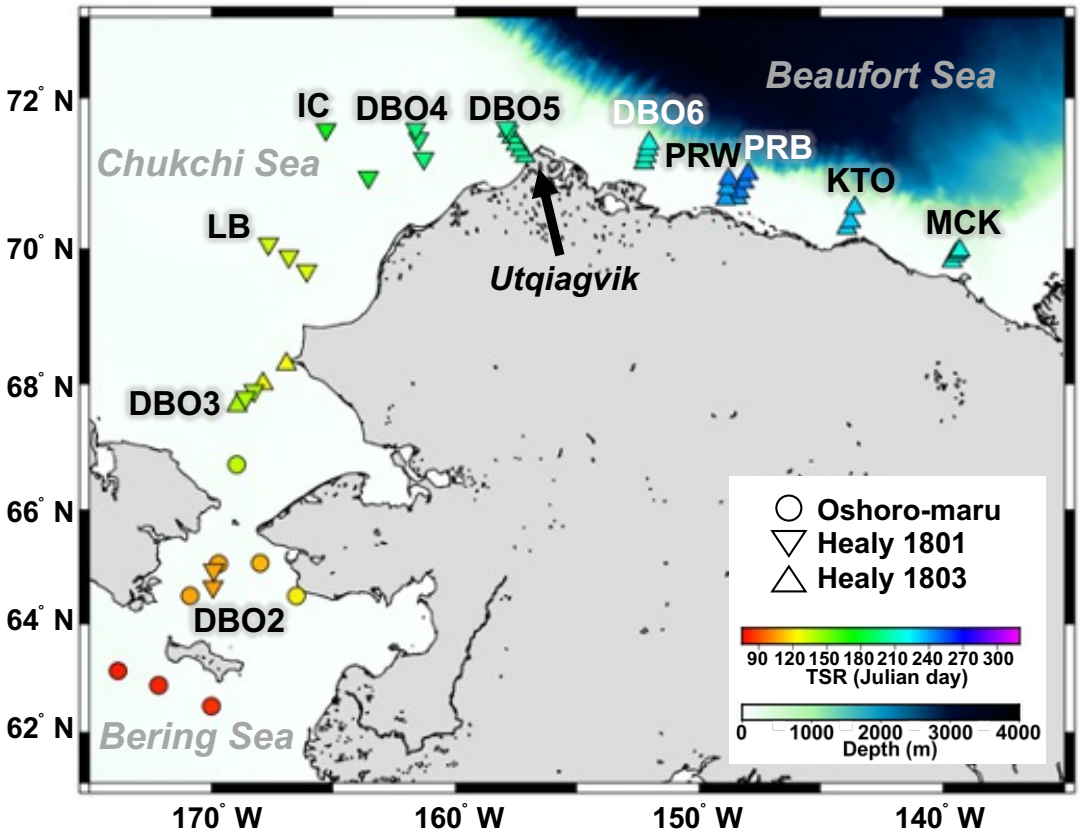

Figure 4.1. Sediment sampling locations in the northern Bering Sea, Chukchi Sea, and Beaufort Sea in 2018. Color contours indicate the timing of the sea ice retreat (rainbow contour) and the bottom depth (blue contour). Abbreviations indicate the transect names during Healy cruises 1801 and 1803. *SLI*: St. Lawrence Island

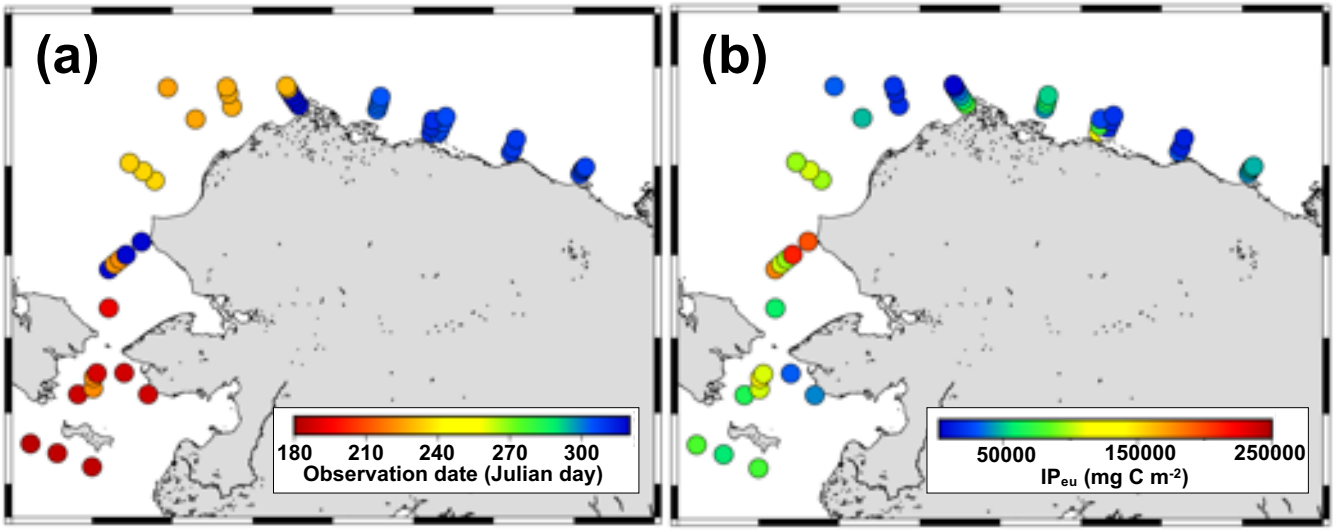

Figure 4.2. Horizontal values of the observation date (a) and the daily cumulative euphotic-depth-integrated primary production from the TSR to the observation date (IP_{eu}) (b).

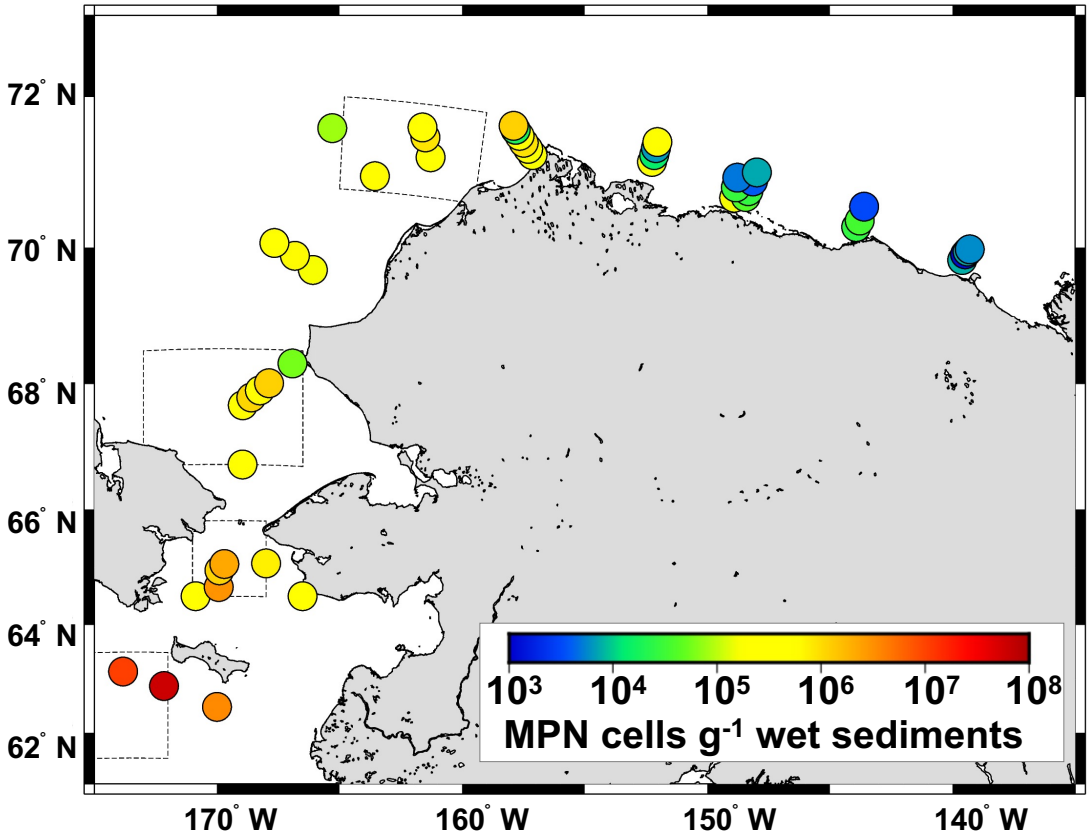

Figure 4.3. Horizontal distribution of diatom resting stages in the north Bering, Chukchi and Beaufort Seas in 2018. Squares indicate benthic hot spots indicated by Grebmeier et al. (2015).

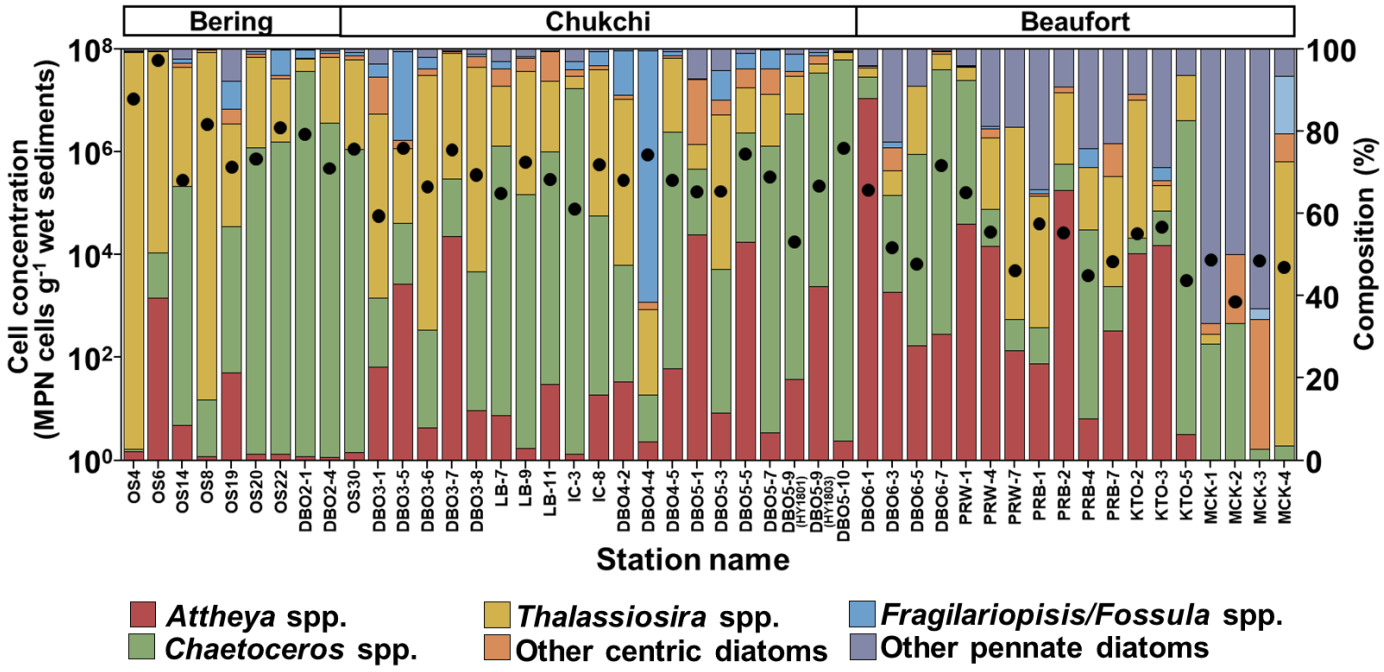

Figure 4.4. Cell concentrations and species composition of viable diatoms in sediments of the northern Bering, Chukchi and Beaufort Seas in 2018.

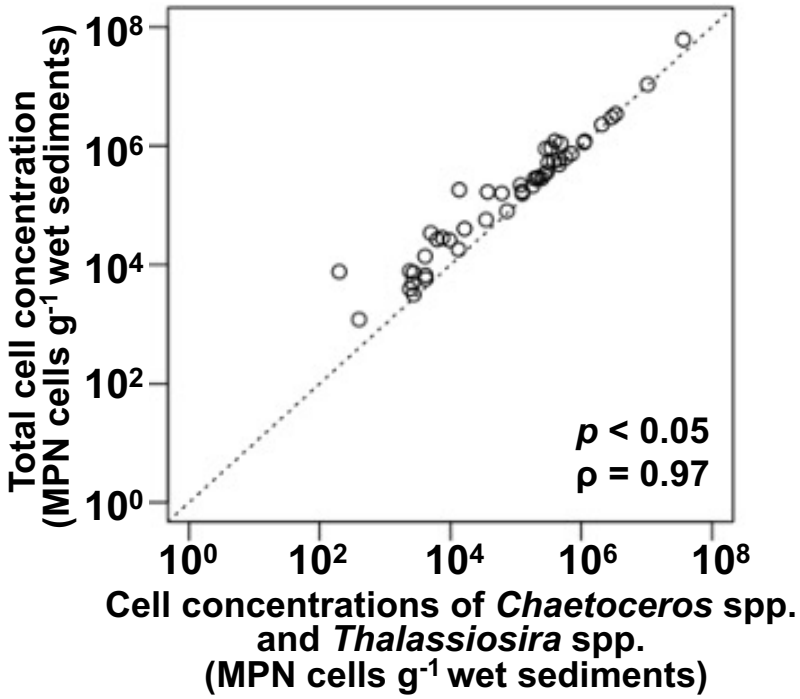

Figure 4.5. The relationship between the abundances of *Chaetoceros* spp. and *Thalassiosira* spp. and total cell concentrations in MPN.

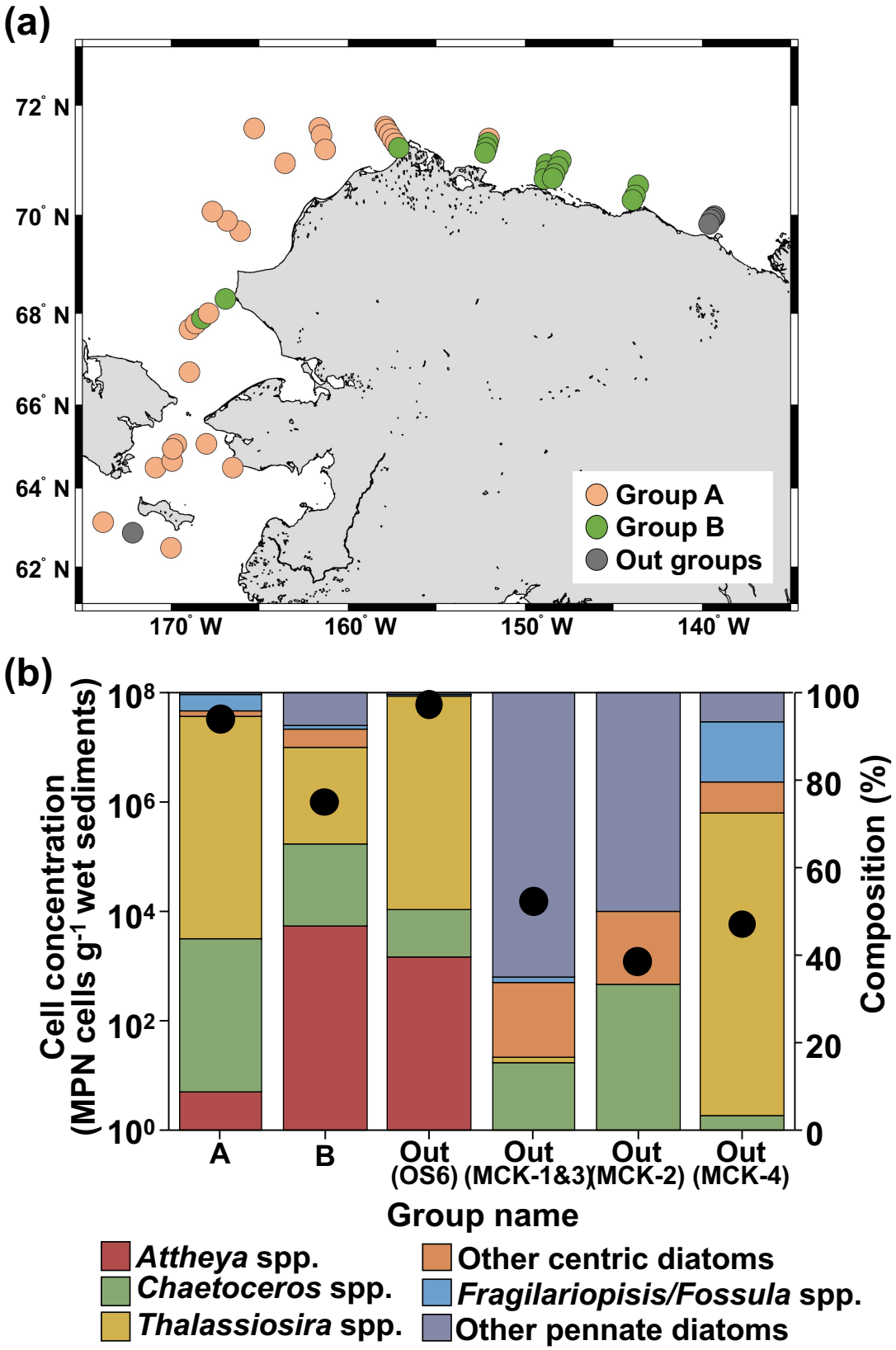

Figure 4.6. (a) Spatial distribution of viable diatom communities in sediments by group. (b) Species composition and cell concentrations in each group.

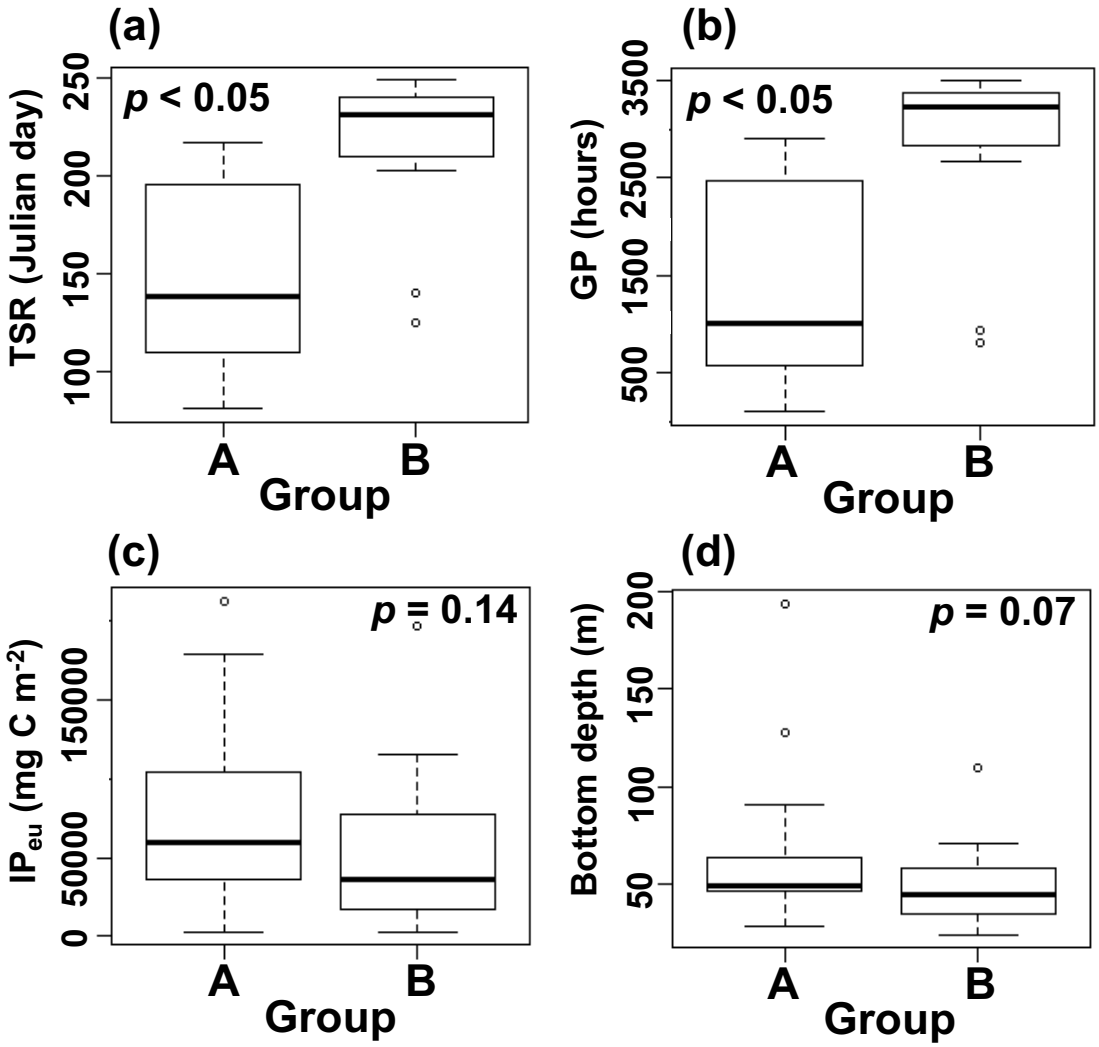

Figure 4.7. Comparison of environmental factors between sediment diatom groups. (a) the timing of the sea ice retreat (TSR). (b) the growth period of ice-associated assemblages (GP). (c) the daily cumulative euphotic-depth-integrated primary production from the TSR to the observation date (IP_{eu}). (d) the bottom depth of sampling station.

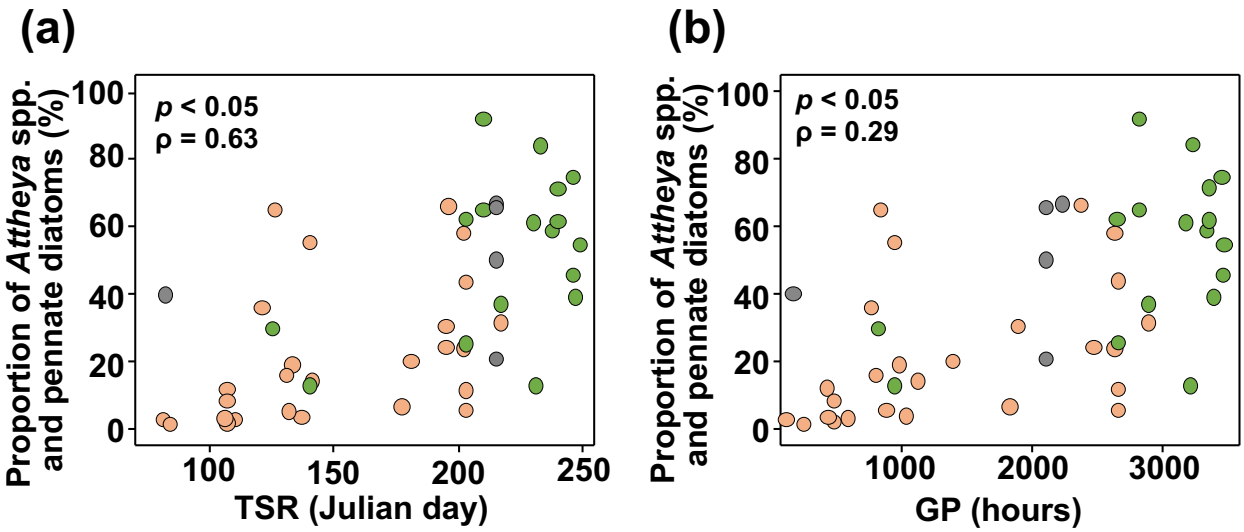

Figure 4.8. Relationships between the proportion of the ice-associated species (*Attheya* spp. and pennate diatoms) in MPN and the TSR (a), and the GP (b). Each color indicates the diatom groups (pink: group A, green: group B, and gray: out groups).

CHAPTER 5 – Photophysiological response of diatoms in surface sediments to light exposure: A laboratory experiment on a diatom community in sediments from the Chukchi Sea

5.1. Introduction

Microalgae in the Arctic need to survive for proliferation in the prolonged darkness (up to several months annually) during winter using various strategies (McMinn and Martin, 2013). As chapters 3 and 4 showed, diatom cells settled on the seafloor support the high concentration of viable diatoms in sediments of the northern Bering and Chukchi Seas. The open-water bloom-forming diatom species such as *Chaetoceros* spp. and *Thalassiosira* spp. observed in the water column (e.g., von Quillfeldt, 2000; Sergeeva et al., 2010; Suzuki et al., 2021) are mainly dominated in the viable diatom community in the sediments of the northern Bering and Chukchi Seas (chapter 4).

Viable diatoms, including diatom resting stages, sinking to and accumulated on the seafloor can germinate and resume cell growth when they assimilate sufficient light (Hollibaugh et al., 1981) (see, general introduction section 1.3.2). Therefore, the high contributions of viable diatoms in sediments to spring diatom blooms have been reported in a bay (Shikata et al., 2009) and a coastal shallow area (Hegseth et al., 2019) (see, general introduction section 1.3.2). Previous studies observed increases in cell abundance, biomass, and pigment concentration in seawater from the sediments (e.g., Shikata et al., 2009), but there is little evidence of how algal assemblages respond to light regimes when they germinate and resume photosynthesis. It is critical to pile up the physiological knowledge about the carbon fixation by diatoms in sediments because they can play a significant role in primary production in the Arctic Ocean after a long dark period (Hegseth et al., 2019; Johnsen et al., 2020). In the Pacific Arctic shelves, sediments can be re-suspended during autumn by the fast flow in the Bering Strait (Abe et al., 2019) and strong wind events (Uchimiya et al., 2016). In addition, irradiance reaching the shallow seafloor of the Pacific Arctic may increase because of the future thinner sea ice and earlier sea ice retreat (Nicolaus et al., 2012; Horvat et al., 2017). Therefore, our understanding of photophysiological responses by microalgae in sediments to light exposure would provide valuable insights into the primary production

processes in the Pacific Arctic shelves.

Natural diatoms face considerable variation in irradiance, which is especially prominent in the Arctic (Cohen et al., 2020). For acclimating to the light variation, diatoms possess photophysiological strategies. Short-term (minutes to hours) acclimation in diatoms mainly includes the diadinoxanthin-diatoxanthin cycle (i.e., de-epoxidation of diadinoxanthin to diatoxanthin) and non-photochemical quenching (NPQ) that dissipate excess excitation energy and quench chlorophyll fluorescence (Goss and Lepetit, 2015; Yan et al., 2019). Additionally, changes in the structure and composition of the photosystems in diatoms support the hourly to daily photoacclimation (Brunet et al., 2011)(see, general introduction section 1.4.2). To explore the photosynthetic response of microalgae, including diatoms, to light exposure, the photosynthesis-energy (P-E) curve experiment has been conducted (e.g., Isada et al., 2019; Yoshida et al., 2020b) (see, general introduction section 1.4.2). Although photophysiological parameters, including P-E parameters, were assessed in many studies for microalgal communities (e.g., Isada et al., 2019; Yoshida et al., 2020b), there have been few studies focused on photophysiological responses by microalgae in sediments.

In this chapter, we aimed to unravel the responses of diatoms that survived in the prolonged darkness of ca. 9 months after sampling from surface Chukchi shelf sediments to different levels of light exposure with particular reference to their photosynthetic physiology in terms of pigment composition, the maximum quantum yield of photochemistry (F_v/F_m) in photosystem II, and the P-E parameters.

5.2. Materials and Methods

5.2.1. Spatial distribution of viable diatom assemblages in sediments

5.2.1.1. Sampling of sediments

Sampling was conducted on the shallow shelves in the southern Chukchi Sea (Figure 5.1) from October 7–20, 2020, during the R/V *Mirai* MR20-05C expedition (Japan Agency for Marine-Earth Science and Technology). Sediment samples were collected using a Smith-McIntyre bottom sampler, and then the surface sediments (0–3 cm) were divided using an acrylic tube and a spatula. Subsamples of the surface sediments were stored in darkness at 3°C for about three months until further experimental procedures on land. Note that the near bottom temperature

at station 35, where sediments were collected for the further experiment (see session 5.2.2), was 3.2°C.

5.2.1.2. Quantification of viable diatom cells in sediments

The concentrations of viable diatom cells in the sediment samples were analyzed by the most probable number (MPN) method (Imai et al., 1984, 1990) as the same procedures to that in chapter 3, except for kinds of medium and incubation conditions. We used f/2 medium (Guillard and Ryther, 1962) and incubation was carried out at a temperature of 5°C and under the white light-emitting diode (LED) light (LXHL-BW02, Lumileds, Netherlands) with about 50 μmol photons m^{-2} s^{-1} and a 12 h light:12 h dark photocycle for 10 days.

5.2.2. Laboratory experiment for investigating benthic algal photophysiology

5.2.2.1. Viable diatom cells in sediments

To accurately determine the concentrations and composition of viable diatom cells in sediments used in the laboratory experiment, the MPN method was conducted again immediately before the laboratory experiment (Imai et al., 1984, 1990) because the experiment was implemented after 5 months from the estimation of the spatial distribution of viable diatoms (see section 5.2.1.2). The procedures were the same, except that the incubation was carried out at 3°C and under the white fluorescent light of about 60 μmol photons m^{-2} s^{-1} with a 12 h light:12 h dark photocycle for 9 days.

5.2.2.2. Experimental set-up

Sediments and the near-bottom seawater collected at station 35 (bottom depth: 53.9 m) and a site (69.03°N, 168.83°W) (bottom depth: 51.3 m) near station 7, respectively, were used for the experiment. Because cell concentrations of viable diatoms were the highest, we used the sediments from this station (see sections 5.3.1 and 5.4.1). Sediments were sampled as described above. Subsamples of the surface sediments were stored in darkness at 3°C for about 9 months until the experiment was started. The near-bottom (about 5 m above the bottom) seawater was collected with a Niskin water sampler, filtered immediately using a Merck Sterivex filter (pore size 0.22 μm), and sterilized by an autoclave (121°C, 20 minutes). The sterilized filtered seawater was stored at 3°C until use.

For the sediment incubation, a sediment subsample (1.1 g) was suspended into the 4.4 L sterilized filtered seawater. Then, the sediment suspended seawater was stored in darkness at 3°C for about 16 hours to acclimate to the experiment temperature. After the acclimation, samplings and sample analyses (see below for details) on day 0 were conducted before the sediment suspended seawater was divided into two 2 L bottles. Then, the sediment suspended seawater in the two bottles was moved into the experimental incubator at 3°C with white fluorescent light (LMGA1WG21K50A410F, Prince Industry Inc., Japan) of 300 μmol photons m^{-2} s^{-1} (High Light; HL) or 30 μmol photons m^{-2} s^{-1} (Low Light; LL), respectively. The two irradiance levels were set to simulate different light regimes in the water column. A square-shaped illumination cycle was set at 12 h light: 12 h dark for 7 days in both light conditions. The experiments were conducted three times to test the repeatability of the results.

In this study, the following parameters were determined: the concentrations of viable diatom cells, including resting stages, in sediments, the composition and concentrations of microalgal pigments, the maximum photochemical quantum yield (F_v/F_m) of photosystem II for microalgae, the concentrations of diatom cells, and ^{13}C based P-E parameters. Samples for these parameters, except for the concentrations of viable diatom cells in sediments, were obtained from HL and LL bottles according to the procedures detailed below.

5.2.2.3. Microalgal pigments

Samplings for microalgal pigments were conducted every day (i.e., from day 0 to day 7). Samples of 10 or 20 mL were filtered onto Whatman GF/F filters under a gentle vacuum (<0.013Mpa). The filter was immediately frozen in the deep freezer at −80°C until further analysis. Microalgal pigments were extracted using the *N*, *N*-dimethylformamide (DMF) bead-beating technique and analyzed by Ultra-High Performance Liquid Chromatography (UHPLC) following Suzuki et al. (2015).

The chlorophyll *a* (chl *a*) specific growth rate ($\mu_{chl\,a}$, day^{-1}) was calculated as the slope of the regression line plotting the natural log-transformed chl *a* concentration against the incubation time. The concentrations of light-harvesting photosynthetic pigments (LHP) were estimated with the sum of chl *a*, chl *c,* and fucoxanthin, whereas the sum of diadinoxanthin (DD) and diatoxanthin (DT) was treated as an indicator of photoprotective pigments. The size of xanthophyll pool (DD-DT pool) was assessed as the sum of DD and DT normalized by chl *a* (i.e.,

([DD] + [DT])/[chl *a*]) (Yoshida et al., 2020a), where [DD], [DT], and [chl *a*] indicate the concentrations of diadinoxanthin, diatoxanthin, and chl *a*, respectively. In addition, the pool size of carotenes was estimated from the concentration of carotenes normalized by chl *a* (i.e., [carotenes]/[chl *a*]), where [carotenes] denotes the concentration of carotenes.

The de-epoxidation state index (DES; Ruban et al., 2004) in the diadinoxanthin-diatoxanthin cycle was calculated as follows:

$$DES = [DT]/([DD] + [DT]).$$

When the concentrations of DD and DT were null, the data were excluded from the calculation.

5.2.2.4. Maximum photochemical quantum yield of photosystem II

The maximum quantum yield of photochemistry in photosystem II (i.e., F_v/F_m) for microalgae was measured every day using a pulse amplitude modulated fluorometer (Water-PAM, Walz, Germany). Samples were acclimated in darkness at 3°C for about 1 hour before the measurement and then put into a quartz cuvette. The minimum fluorescence (F_o) after the dark acclimation and the maximum fluorescence under the saturation pulse (F_m) were determined. The saturating pulse was provided by red light-emitting diodes (LEDs), which had a peak illumination at 660 nm of 4000 μmol photons m^{-2} s^{-1} and lasted for 600 ms. The F_v/F_m was calculated as follows:

$$F_v/F_m = (F_m - F_o)/F_m.$$

The fluorescence measurements were conducted twice per sample.

5.2.2.5. Diatom cell counting

Samples for diatom cell counting were obtained every day. The sample of 9 mL was fixed by neutral formalin at a final concentration of 2%. If necessary, the samples were then settled and concentrated by 2.0- to 3.3- fold. Aliquots (1 mL) of the sub-samples were transferred to a glass slide to count and identify the diatoms under an inverted microscope (Olympus BH2 BHS system, Olympus, Tokyo, Japan; 10 × oculars and 40 × objective lenses). The diatoms were counted and identified from more than 150 cells, including the sufficient counting (more than 50 cells) of the dominant species (Edler and Elbrächter, 2010). It was difficult to distinguish the resting stages of the genus *Thalassiosira* from their vegetative cells; therefore, the total cell numbers were estimated in this study. The cell-specific growth rate (μ_{cell}, day^{-1}) was calculated as the slope of

the regression line plotting the natural log-transformed cell concentrations against the incubation time.

5.2.2.6. ^{13}C-based Photosynthesis-Energy (P-E) curve experiment

The Photosynthesis-Energy (P-E) curve experiments were conducted on day 0, 1, 4, and 7. The culture samples were dispensed into eleven 30 mL acid-cleaned polycarbonate bottles. As an initial sample, a bottle of a sample without any isotope addition was filtered onto a Whatman GF/F glass fiber filter pre-combusted over 5 hours at 450°C. The other ten sample bottles were inoculated with a known amount of $NaH^{13}CO_3$ solution (99 atom% ^{13}C, Shoko Co., Ltd.), equivalent to ca. 10% of dissolved inorganic carbon (DIC) in the medium. These ^{13}C-enriched samples were set on an incubator by Babin et al. (1994) and kept at 3°C under ten different light intensities from 1.47 to 1770 μmol photons m^{-2} s^{-1} using a PCS-UMX250 light source (Nippon PI Co., Ltd.) for 2 hours. After incubation, the samples were filtered on pre-combusted GF/F glass fiber filters. All filters were stored in a deep freezer at −80°C until further analysis. The duplicate samples of DIC in the medium without $NaH^{13}CO_3$ enrichment were obtained in 120 mL glass bottles. The DIC concentrations were determined using a Total Alkalinity Titrator ATT-05 (Kimoto Electric Co., Ltd) with authentic standards (KANSO Technos).

The filters were thawed, exposed to the fumes of HCl to remove inorganic carbon, and entirely dried in a desiccator under a vacuum. The amount of particulate organic carbon (POC) and the atom percent of ^{13}C in each sample were determined by an online element analyzer (FlashEA1112, Thermo Finnigan)/isotope ratio mass spectrometer (Delta-V, Thermo Finnigan).

The chl *a* concentration normalized photosynthetic carbon fixation rates were calculated following Hama et al. (1983) based on the ^{13}C technique and chl *a* concentration measured by UHPLC. The P-E curve fitting and parameters were obtained from the photoinhibition model of Platt et al. (1980) with the "phytotools" package (Silsbe and Malkin, 2015) of R software (version 4.0.4, R Development Core Team, 2021).

$$P^B = P_s^* \left[1 - exp\left(\frac{-\alpha_{PAR}^B \cdot E_{PAR\ inc}}{P_s^B}\right)\right] \cdot exp\left(\frac{-\beta_{PAR}^B \cdot E_{PAR\ inc}}{P_s^B}\right)$$

where the superscript B denotes the normalization by chl *a* concentration, and P is the photosynthetic rate, $E_{\mathrm{PAR\ inc}}$ is the irradiance at each position of the incubator, P_s is the hypothetical

maximum photosynthetic rate in the absence of photoinhibition, α is the initial slope of the P-E curve, and β is the photoinhibition parameter. The maximum photosynthetic rate, P^{B}_{max}, is calculated as follows:

$$P^{B}_{max} = P^{*}_{s} \cdot \left(\frac{\alpha^{B}}{\alpha^{B}+\beta^{B}}\right) \cdot \left(\frac{\beta^{B}}{\alpha^{B}+\beta^{B}}\right)^{\beta^{B}/\alpha^{B}}.$$

The photoacclimation index, E_k, was derived from the following equation.

$$E_k = P^{B}_{max}/\alpha^{B}$$

To estimate the maximum quantum yield of carbon fixation, microalgal absorption coefficient values under the HL and LL conditions were measured on day 7. The duplicate water samples (10 or 20 mL) were filtered onto Whatman GF/F filters. The filters were covered with aluminum foil and stored in a deep freezer (−80°C) until further analyses. A spectrophotometer (MPS-2450, Shimadzu) equipped with an end-on-type photomultiplier tube was used to measure the absorbance spectra of the total particles on the filters at every 1 nm in the wavelength (λ) range of 350 to 750 nm. Then, the algal pigments on the filters were extracted by soaking in methanol, and the absorption spectra of detritus on the filter were measured in the same manner. The measured absorption spectra of the total particles and the detritus were corrected for the path-length amplification effect following the equation of Stramski et al. (2015) after offsetting at the wavelength of 750 nm.

$$OD_s(\lambda) = 0.679 \cdot \{OD_f(\lambda)\}^{1.2804}$$

where OD_s (λ) and OD_f (λ) are the absorption spectra of suspension and filter, respectively. Then, the absorption coefficient (a_p (λ)) values were calculated for the total particles and the detritus, respectively, following (Kishino et al., 1985):

$$a_p(\lambda) = 2.3 \cdot OD_s(\lambda) \cdot s/v.$$

where s is the filtered area (m^2) and v is the filtered volume (m^3) of the samples. The absorption coefficient of microalgae (a_{ph}) was obtained by subtracting the absorption coefficient of the detritus from that of the total particles.

The P-E parameters for light absorbed by microalgae (α^{B}_{PUR} and β^{B}_{PUR}) were derived from the equations described above using the photosynthetic absorbed radiation at each position of the incubator ($E_{PUR\ inc}$). The subscript PUR indicates the light absorbed by microalgae, and the $E_{PUR\ inc}$ was calculated as follows (Dubinsky, 1980):

$$E_{PUR\ inc} = \int_{\lambda=400}^{700} E_{PAR\ inc}(\lambda) \cdot a_{ph}(\lambda)\, d\lambda$$

where

$$E_{PAR\ inc}(\lambda) = \frac{E_L(\lambda)}{\int_{400}^{700} E_L(\lambda)d\lambda} \cdot E_{PAR\ inc}$$

where E_L (λ) is the incubator lamp spectrum. The maximum quantum yield of carbon fixation ($\Phi_{c\ max}$, mol C (mol photon)$^{-1}$) was calculated by the following equation:

$$\phi_{c\ max} = 0.0231 \cdot [chl\ a] \cdot \alpha_{PUR}^{B}$$

where [chl *a*] is the chl *a* concentration (mg m^{-3}) and 0.0231 is a factor to convert milligrams of carbon to moles, μmol photons to mol photons, and hours to seconds (Isada et al., 2009).

5.2.3. Statistical analyses

Differences among treatments and incubation time or period were tested using one-way analysis of variance (ANOVA) and post hoc Tukey-Kramer test. To compare differences in the values between day 0 and day 1 in HL or between HL and LL, *t*-test was conducted for each treatment. Also, the differences in the concentration of viable diatom cells in the sediment at station 35 were estimated twice using the MPN method with *t*-test. All statistical analyses were performed using R software (version 4.0.4, R Development Core Team, 2021).

5.3. Results

5.3.1. Spatial distribution of viable diatom cells in sediments of the Chukchi Sea shelf

The viable diatom cells determined by the MPN method ranged from 1.90 × 10^5 to 1.91 × 10^6 MPN cells g^{-1} wet sediment (Figure 5.1). The concentrations reached 10^6 MPN cells g^{-1} wet sediment only at station 35. Centric diatoms were predominant throughout the region, and the relatively high contributions of *Chaetoceros socialis* complex to the total viable diatom cells were found at almost all stations (40–89%), except stations 9 and 29 (31% and 18%, respectively). At stations 9 and 29, *Attheya* spp. were dominant in the viable diatoms, while the genus comprised only 0.30–21% at the other stations. Other genera showed a locally high proportion. For example, *Thalassiosira* spp. accounted for 24% of the diatom assemblage at station 30 and *Chaetoceros* spp. contributed 23% and 29% of the diatoms at stations 30 and 31, respectively. The other centric diatoms, including *Actinoptychus* sp., *Paralia sulcata*, *Skeletonema* spp., *Leptocylindrus* spp., and *Odontella* spp., appeared from the sediments but little contributed to the diatom communities.

Pennate diatoms, such as *Asteroplanus karianus*, *Fragilariopsis* spp., *Navicula* spp., and *Cylindrotheca closterium*, emerged from the sediments at all stations, but the proportion was relatively low over the study region (0.47–13%).

5.3.2. Incubation experiment

5.3.2.1. Viable diatoms in sediments

The concentrations of viable diatoms in sediments at station 35, estimated immediately before the onset of the experiment, were $6.0 \times 10^5 \pm 4.7 \times 10^5$ MPN cells g^{-1} wet sediment. The total concentrations decreased from that of the former estimation of viable diatom cells at station 35 (t-test, $p < 0.05$), while the diatom composition and the appearing diatom species were not different from each other (Figures 5.1 and 5.2). Centric diatoms accounted for 97%, and the genera of *Chaetoceros* and *Thalassiosira* contributed to 93% of the community. *Chaetoceros socialis* complex was primarily dominated (79%). The other centric diatoms, including *Attheya* spp., *Detonula pumila*, *Odontella* spp., *P. sulcata*, *Skeletonema* spp., *L. danicus*, and *Melosira* sp., sometimes appeared from the sediment but little contributed to the community. Pennate diatoms, such as *A. karianus*, *Fragilariopsis* spp., and *Navicula* spp., also appeared, but the relative abundance was very low. Note that the most dominant species, *C. socialis* complex, remained consistent, although some taxa changed slightly in percentage, such as *Attheya* spp. and pennate diatoms.

5.3.2.2. Microalgal pigments

The sum of chl *a* and chl *c* concentration increased in both HL and LL and became more than double the initial level in HL on day 5 and in LL on day 4 (Figures 5.3a and 5.3b). Similarly, fucoxanthin concentrations increased in both treatments (Figures 5.3a and 5.3b). In HL on day 4 and LL on day 3, the concentrations of fucoxanthin reached double the initial levels.

The trends of the concentration of diadinoxanthin and diatoxanthin (i.e., [DD] + [DT]) were also distinct between HL and LL (Figures 5.3c and 5.3d). In HL, the [DD] + [DT] initially decreased, reduced by 22% of initial on day 1, and thereafter increased after day 3 (Figure 5.3c). On the other hand, the [DD] + [DT] gradually increased with time under LL (Figure 5.3d). The LHP concentrations under HL and LL increased from day 3 and day 2, respectively, and reached about 10 times on day 7 from the initial value (Figures 5.3c and 5.3d). In HL, the DD-DT pool

size estimated from [DD] + [DT])/[chl *a*] (Figure 5.3e) decreased on day 1 due to the decrease in [DD] + [DT], although the decline was not significant (t-test, p =0.05). After day 1, the DD-DT pool size under HL returned to the initial level by day 3, whereas the ratio in LL decreased to almost half the initial pool size. The carotene pool size (i.e., [carotene]/[chl *a*]) decreased over incubation (Figure 5.3f).

The DES value was the highest on day 0 and initially decreased in HL and LL. After that, there were an increasing trend and a decreasing trend in HL and LL, respectively (Figure 5.3g).

5.3.2.3. Diatom cell abundance

The diatom cell abundance increased during incubation (Figure 5.4). The chl *a*-specific and the cell-specific growth rates were significantly different between the periods from day 0 to day 4 and from day 4 to day 7 in both HL and LL (one-way ANOVA and Tukey-Kramer test, $p < 0.05$). Both of the growth rates were larger in the second half (i.e., exponential growth phase) than in the first half (i.e., lag phase; Figure 5.5).

The HL and the LL microscopy data showed that centric diatoms dominated the microalgal communities, and *Chaetoceros* and *Thalassiosira* were the main genera (26–79% and 14–54% during the experiment, respectively) (Figure 5.4). On day 0, all *Chaetoceros* cells were in resting stages (data not shown). Early to the middle of the experiment, the diatom composition counted directly under light microscopy differed from that estimated with the MPN method, in which *Thalassiosira* spp. accounted for a high percentage of the community. The proportion of *C. socialis* complex rapidly increased in the exponential growth phase from day 4 to day 7 under HL and LL. The other centric diatoms, mainly including *D. pumila*, *Odontella* spp., and *P. sulcata*, sometimes emerged, but their contributions were low (1.8–7.6%) in terms of abundance. Pennate diatoms appeared from all samples, but the contributions to the diatom communities kept relatively low in HL and LL (3.6–20% and 5.4–19%, respectively). The difference in the cell concentrations of diatoms between HL and LL on day 7 was not statistically significant (*t*-test, $p > 0.05$).

5.3.2.4. F_v/F_m

Distinct changes over time in F_v/F_m were observed between HL and LL (Figure 5.6).

Although F_v/F_m under LL increased from 0.14 ± 0.02 on day 0 until the end of incubation, the ratio in HL significantly decreased from day 0 to day 1 (*t*-test, $p < 0.05$) and then improved with time. The maximum values of F_v/F_m reached 0.50 ± 0.03 and 0.61 ± 0.01 on day 7 in HL and the LL, respectively.

5.3.2.5. P-E parameters

The P-E curve experiments revealed that relationships between algal carbon fixation rate normalized by chl *a* concentration and incubation light intensity significantly changed during the experiment (Figures 5.7 and 5.8). The initial slope α^B decreased dramatically from day 0 to day 1 in both light conditions (one-way ANOVA and Tukey-Kramer test, $p < 0.05$) (Figure 5.8a), but changed only slightly thereafter. The maximum carbon fixation rate normalized by chl *a* concentration (P^B_{max}) increased until day 4 under HL and LL (Figure 5.8b). On day 1, P^B_{max} in the HL condition became lower than in the LL. The photoacclimation index, E_k, had an increasing trend from day 0 to day 7 and reached 130 and 109 μmol photons m^{-2} s^{-1} in HL and LL, respectively (Figure 5.8c). The E_k was slightly higher in HL than in LL throughout the incubation period. The maximum quantum yield of carbon fixation ($\Phi_{c\ max}$) was relatively high on day 0 (0.018 mol C (mol photon)$^{-1}$) but sharply declined on day 1 (one-way ANOVA and Tukey-Kramer test, $p < 0.05$) and then increased with time (Figure 5.8d). Differences in the values of $\Phi_{c\ max}$ between HL and LL were relatively small after day 1, but the value of LL was slightly higher than that of HL throughout incubation.

5.4. Discussion

5.4.1. Critical seeds community of diatoms in sediments of the Chukchi Sea shelf

The viable diatom cells containing resting stages are accumulated with high abundance in sediments of the northern Bering and the Chukchi Sea shelves (Tsukazaki et al., 2018; chapters 3 and 4). In this study, the concentrations of viable diatom cells in sediments obtained by the MPN were similar to those previously reported over the Pacific Arctic shelves (chapter 4). In particular, the region around station 35, showing the highest concentration of viable diatom cells in this study, is the so-called biological hot spots (Grebmeier et al., 2015). Thus, the abundant viable diatom cells may reflect the increased productivity in the water column (chapter 4). It is also known that

lateral advection can enhance particle export in the biological hot spots of the northern Bering Strait (Cooper et al., 2015). Common diatoms in the water column of the Pacific Arctic have been observed in the sediments (Matsuno et al., 2014; chapter 2). The dominant *C. socialis* complex found at all stations in this study is known to form dense blooms in the Chukchi Sea from July to August (Sergeeva et al., 2010). Suzuki et al. (2021) revealed that *C. socialis* complex became predominant in the microalgal communities in terms of abundance with an increase in the water column stratification in the northern Bering and Chukchi Seas during summer. O'Daly et al. (2020) showed that the sinking POC flux in the Chukchi Sea was among the highest ever documented across the global oceans, and sinking particles consisting of aggregated diatoms and viable diatom cells were observed. Indeed, *Chaetoceros* spp., including *C. socialis* complex, dominated viable diatom communities in sediments of the northern Bering and southern Chukchi shelves (chapter 4). Therefore, *C. socialis* complex, which is capable of resting stages and settled on the seafloor, can contribute to their proliferation in the water column once they are brought into sun-lit surface waters by physical mixing processes. According to Lalande et al. (2020), high sinking flux by pennate diatoms of *Cy. closterium* and *Nitzschia frigida* was observed in the Chukchi Sea. However, the two species were little observed from the sediments in this study. Tsukazaki et al. (2018) reported that some diatoms such as *Pseudo-nitzschia delicatissima*, *Cy. closterium*, *Proboscia alata*, and *Thalassionema* spp. dominated in the autumn water column in the Chukchi Sea cannot survive in the dark for more than 6 months. Also, few marine pennate diatoms are known to form resting stages in contrast to centric diatoms (McQuoid and Hobson, 1996). Therefore, not all diatoms growing in the water column can survive in the dark for a long time. However, it is also critical that many "seeds" of diatoms exist in the sediments of the Pacific Arctic shelf, and they can resume even after prolonged dark conditions.

5.4.2. Quick responses for light exposure and high photophysiological plasticity of viable diatom cells in sediments

The diatom composition on day 0 as counted directly under light microscopy differed from that estimated with the MPN method, especially in *Thalassiosira* spp. and *C. socialis* complex. Although the MPN technique can detect viable diatom cells (Imai et al., 1984), the abundance of *Thalassiosira* spp. determined by direct cell counting could include their dead cells. In contrast, we could have underestimated the abundance of *C. socialis* complex because they have small cell

sizes (the apical axis is 2 μm at the minimum; Hasle and Syvertsen, (1997)). Thus, although there were some uncertainties in cell counting, the enhanced growth of *C. socialis* complex contributed to the increased diatom abundance after light exposure.

Light availability is the main trigger for germinating and resuming cell growth from resting stages (Hollibaugh et al., 1981). However, drastic changes in light availability may be stressful for diatom cells because they need to acclimate to the light variability. Although β-carotene functions an antioxidant, the pigment is bound exclusively to photosystems I and II and not in the peripheral antenna (Wang et al., 2020; Xu et al., 2020; Buck et al., 2022). Thus, β-carotene can be used as a proxy for the amount of photosystems (Buck et al., 2022). The cellular contents of β-carotene in diatoms are reported to be relatively constant or increase after light exposure (e.g., Kuczynska et al., 2015; Telussa et al., 2019). In the present study, although the carotene pool size (i.e., [carotenes]/[chl *a*]) and cellular contents of carotenes decreased in LL and HL, the underlying mechanisms are unclear and need to be investigated further. To protect the photosynthetic apparatus in diatoms from high light, the organisms can also utilize the diadinoxanthin-diatoxanthin cycle (Goss and Lepetit, 2015). Diatom resting stages are reported to have a sufficient xanthophyll pool to support the xanthophyll cycle (Oku and Kamatani, 1998). In addition, diatoms can alter cellular pigment composition on long time scales of hours to days to acclimate to the higher light by increasing photoprotective pigments (PPP) and decreasing light-harvesting pigments (LHP) (Brunet et al., 2011). This study showed temporal changes in DD-DT pool size between HL and LL. From day 0 to day 1, the DD-DT pool showed increasing and decreasing trends in LL and HL, respectively, although both trends were statistically insignificant. These results suggest that the algal community in HL suffered from excess light energy for photosynthesis. This speculation was supported by the results of F_v/F_m that dramatically decreased in HL and increased in LL on day 1. It is noteworthy that even under HL, resting-stages-containing viable diatom cells can actively resume growing with high F_v/F_m within a few days. Additionally, the DES showed intriguing behavior – it was the highest on day 0 before light exposure and then decreased. Diatoms in prolonged darkness can synthesize and accumulate diatoxanthin (i.e., the so-called dark NPQ), allowing them to take a low risk of reactive oxygen-dependent damage (Lacour et al., 2019; Lepetit et al., 2022). This capability could be important for diatoms in prolonged darkness because even a low photon flux might exceed their photosynthetic capacity. The dark NPQ could provide immediate photoprotection during re-

illumination (Lacour et al., 2019; Lepetit et al., 2022). In HL, as the F_v/F_m increased and the DD-DT pool recovered, the increases in DES were observed, and the diadinoxanthin-diatoxanthin cycle might work well, allowing the cells to grow actively.

The quick physiological response to irradiance was also observed in the carbon fixation, which was similar to the results of Kvernvik et al. (2018) showing that the high photosynthetic capacity of microalgae was established within 24 hours of reillumination during the polar night. In this study, all P-E parameters remarkably changed from day 0 and day 1. Especially, the drastic decrease in α^B and increase in E_k indicated that the resting-stages-containing viable diatom cells could respond to light exposure within 24 hours and acclimate to higher light conditions for carbon fixation. Since α^B can be biophysically expressed by the functional absorption cross-section of photosystem II (σ_{PSII}) and the numbers (n) of photosynthetic units in photosystem II (i.e., $\alpha^B = \sigma_{PSII} \cdot n$) (Sakshaug et al., 1997), the viable diatom cells could decrease σ_{PSII} and/or the number of photosynthetic units immediately after light exposure. The optimum light intensities for carbon fixation in the vegetative cells under HL and LL during day 4 and day 7 were about 110–130 μmol photons m^{-2} s^{-1} as estimated by E_k. This value could be almost equivalent to those of Arctic microalgal communities in the euphotic layer (117 and 112 μmol photons m^{-2} s^{-1} in 50% and 1% light level, respectively; using the results of Platt et al. (1982) with the conversion factor of 4.66 μmol photons s^{-1} per watt used in Cota (1985)). In the Chukchi shelf, the bottom depths are shallow (ca. 50 m) and euphotic layers sometimes reaches deeper than 30 m during summer (Suzuki et al., 2021). Therefore, surface sediments, which contain abundant diatom resting stages (chapter 4), can easily resuspend into the sunlit layer of the water column by wind events (Uchimiya et al., 2016).

It has been reported that cellular chl *a* concentrations in diatom resting stages are relatively high compared with vegetative cells (Hargraves and French, 1983), which would help diatom resting stages to survive under low light conditions. In this study, E_k on day 0 was only 4.11 ± 0.28 μmol photons m^{-2} s^{-1}, indicating their dim-light acclimation. The E_k value was almost identical to those in Arctic ice algae (2.5 ± 1.7 μmol photons m^{-2} s^{-1}; Cota, 1985). Interestingly, the maximum quantum yield of carbon fixation ($\Phi_{c\,max}$) was relatively high on day 0 (Figure 5.8d), suggesting that the resting-stages-containing viable diatom cells in sediments can utilize photons efficiently for carbon fixation.

The maximum carbon fixation rate normalized by chl *a* concentration (P^B_{max}) became more than

double under LL from day 0 to day 1 and reached the maximum by day 4 in both light conditions. The maximum values (4.47 ± 0.740 mg C [mg chl *a*]$^{-1}$ h^{-1} and 4.13 ± 0.213 mg C [mg chl *a*]$^{-1}$ h^{-1} in HL and LL, respectively) were slightly higher than those from natural Arctic microalgal assemblages (1.32 ± 0.19 mg C [mg chl *a*]$^{-1}$ h^{-1} and 1.29 ± 0.51 mg C [mg chl *a*]$^{-1}$ h^{-1} in 50% and 1% light level, respectively; Platt et al., 1982) and ice algae (0.052 ± 0.027 mg C [mg chl *a*]$^{-1}$ h^{-1}; Cota, 1985) and the P^{B}_{max} values of polar diatoms (0.2–2.46 mg C [mg chl *a*]$^{-1}$ h^{-1}; Lacour et al., 2017). The quick increase in P^{B}_{max} contrasted with the response of cell abundance and chl *a* concentration which increased sharply in the second half of the incubation. Although P^{B}_{max} generally increases with increasing temperature (e.g., Yoshida et al., 2018), the trend may not apply for polar diatoms at −1.6–4.0°C (Lacour et al., 2017). The P^{B}_{max} is biophysically determined by the number of photosynthetic units (n) and the maximum turnover rate of a photosynthetic unit (τ^{-1}) (Sakshaug et al., 1997). Therefore, the dramatic increase in P^{B}_{max} observed in this study could be attributed to changes in these parameters. Further study would be required to understand the behavior of P^{B}_{max} in Arctic diatoms.

5.5. Conclusions

Changes in the sea ice environment in the Pacific Arctic region can affect light penetration in the water column (Nicholaus et al., 2012; Horvat et al., 2017), resulting in changes in the composition of microalgae (Ardyna and Arrigo, 2020) and viable diatom resting stages in sediments (chapter 4). However, few studies have focused on photophysiological responses of viable diatom in sediments to light exposure. Previous studies showed the potential seeding effects of diatom resting stage germination (Shikata et al., 2009; Hegseth et al., 2019) based on increases in cell and pigment concentrations. In the present study, we revealed that viable diatom cells containing resting stages were abundant, and these of *Chaetoceros socialis* complex were dominated in sediments of the Chukchi Sea shelf, and they can resume growing even after the 9 months of darkness. There was no difference in the cell concentration of diatoms between LL and HL on day 7, suggesting that the microalgae were well acclimated to both light conditions. In the higher latitude region of the Pacific Arctic, there were different viable diatom communities dominated by *Attheya* spp., which could be associated with sea ice (chapter 4). Therefore, further studies are needed to elucidate the photophysiological responses of various diatom communities to light availability. In this study, the responses of resting-stages-containing viable diatom cells

to light exposure were more quickly in photosynthetic physiology (i.e., F_v/F_m, some of the P-E parameters and DD-DT pool size, and DES) than in abundance (i.e., cell concentration and chl *a* concentration). In particular, we found a swift decrease in α^B and a gradual increase in E_k (Figure 5.8), indicating that the resting-stages-containing viable diatom cells responded to light exposure within 24 hours and acclimated gradually to higher light conditions for carbon fixation, respectively. Although the excess light exposure suppressed the photosynthetic activity in the microalgal cells at the onset of the experiment, which was evident by a decreased F_v/F_m of HL on day 0, they recovered quickly, indicating the high photophysiological plasticity to dynamic light changes (Kvernvik et al., 2018). We also revealed that the optimum light intensities for carbon fixation in the microalgal cells reactivated from sediments were about 110–130 μmol photons m^{-2} s^{-1}, as estimated by E_k between day 4 and day 7. The highest daily maximum intensity of photosynthetically active radiation (PAR) on deck during the study period in October was about 606 μmol photons m^{-2} s^{-1}; on average, it was 217 μmol photons m^{-2} s^{-1}. Therefore, given the light attenuation in the sea surface during autumn (Shiozaki et al., 2022), the transportation of diatoms in sediments to the surface or subsurface layer during autumn would reactivate their photosynthesis. In the shallow Chukchi shelf, diatom resting stages in surface sediments may easily resuspend into the euphotic layer (Uchimiya et al., 2016). The photosynthetic capability of the viable diatom cells in sediments that quickly respond to light exposure even after long darkness would indicate their high seeding potential for blooms in the shallow Pacific Arctic shelf, which has historically acted as an effective carbon sink, characterized by tight pelagic-benthic coupling (O'Daly et al., 2020), and is called the "benthic biological hotspots" (Grebmeier et al., 2015).

5.6. Figures

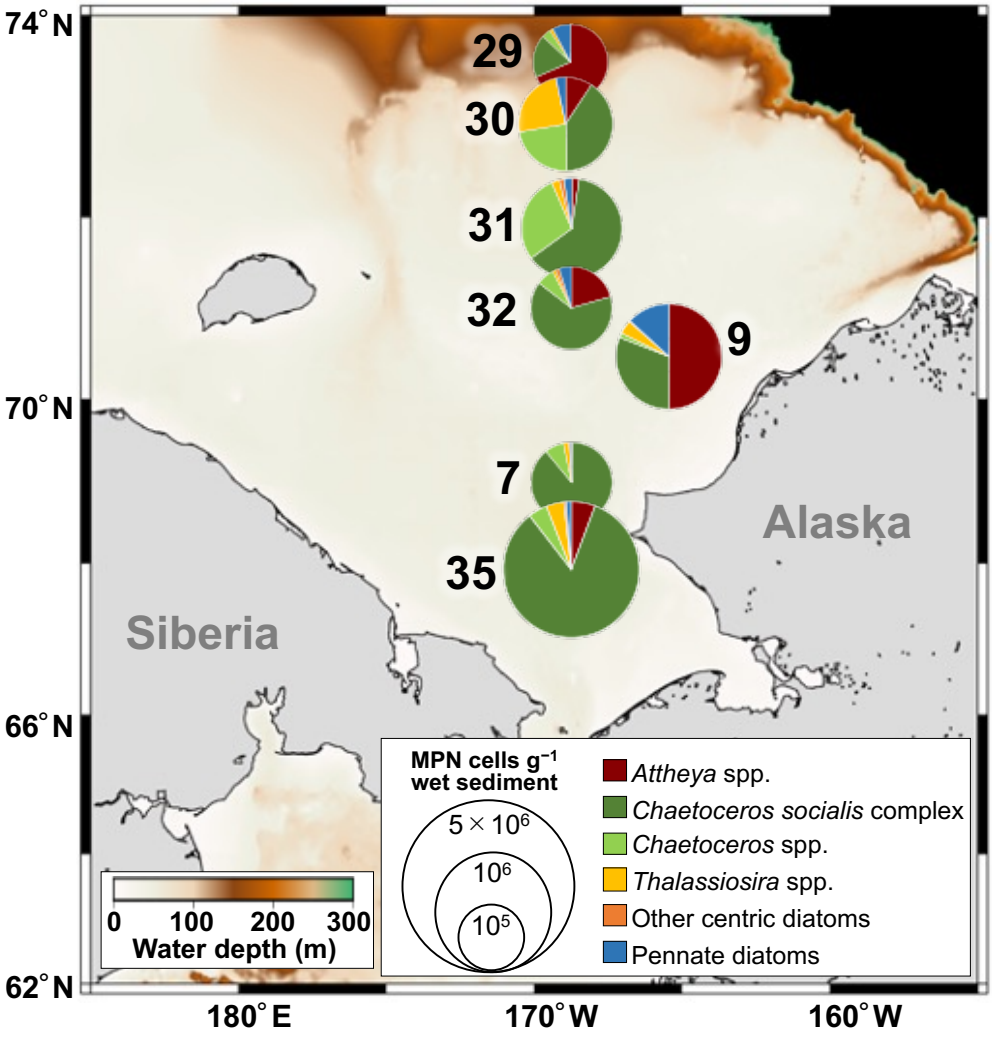

Figure 5.1. Locations of the sediment sampling in October 2020 and the horizontal distribution and composition of viable diatom cells in the Chukchi Sea sediments as estimated by the MPN method. Color contours and numbers indicate the bottom depth and station name, respectively.

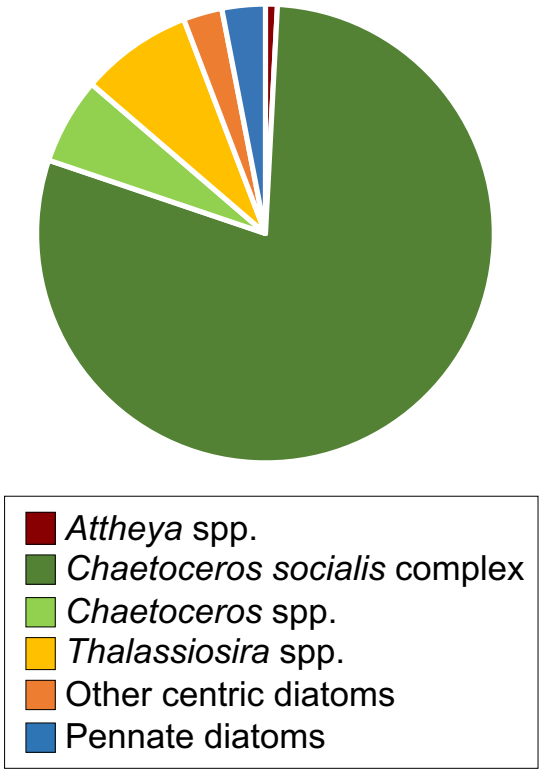

Figure 5.2. The composition of viable diatom cells at station 35 by the MPN method, which was assessed just before the incubation experiment.

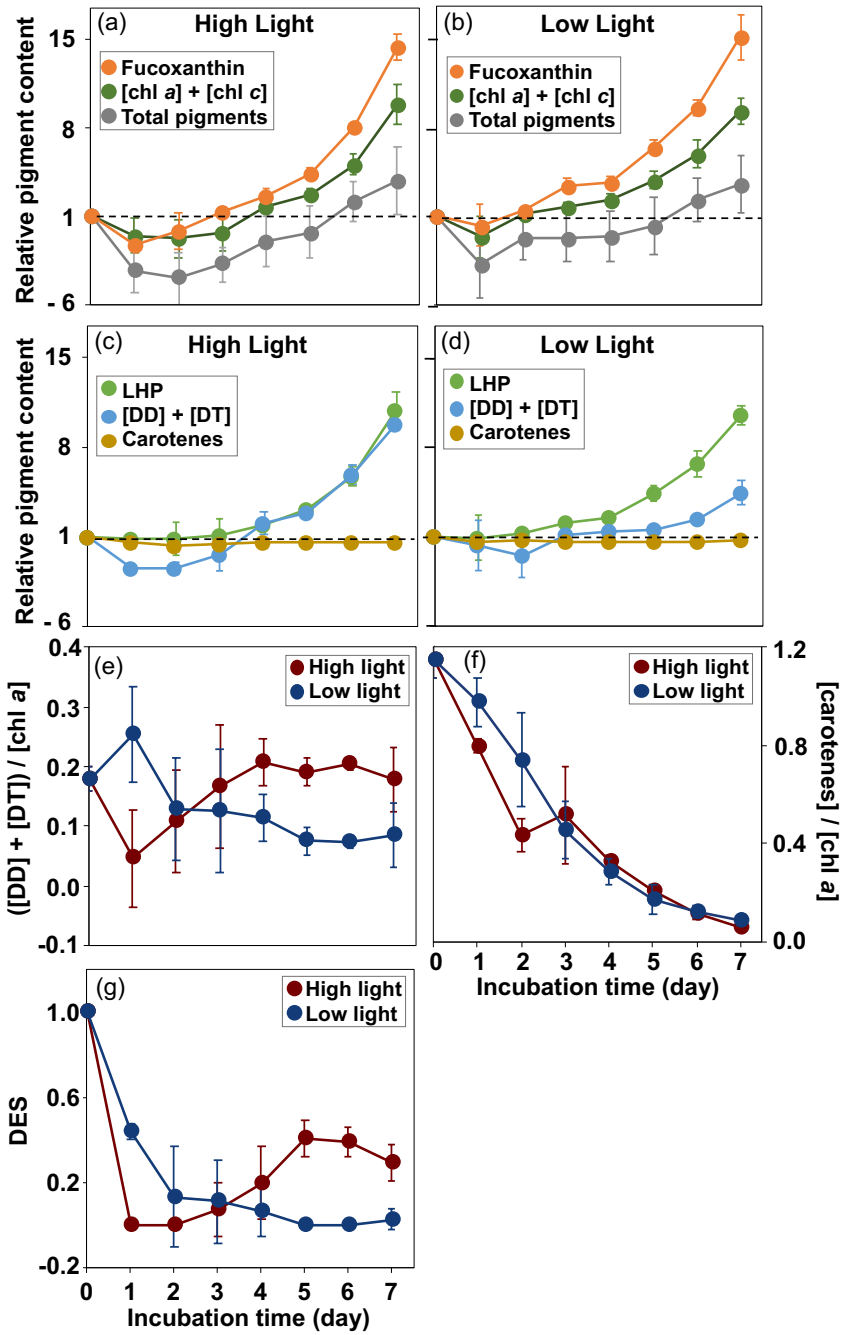

Figure 5.3. (a)–(d) The wight-based relative pigment concentration to that on day 0 during the incubation. Fucoxanthin, the sum of chl *a* and chl *c* ([chl *a*] + [chl *c*]), and total concentrations of measured pigments (chlorophyll *a*, chlorophyll *b*, chlorophyll *c*, chlorophyllide *a*, 19'-butanoyloxyfucoxanthin, fucoxanthin, neoxanthin, diadinoxanthin, diatoxanthin, carotenes) in the high (300 µmol photons m^{-2} s^{-1}; a) and low light (30 µmol photons m^{-2} s^{-1};b) conditions. Light-harvesting pigments (chl *a*, chl *c*, plus fucoxanthin; LHP), diadinoxanthin plus diatoxanthin ([DD]+[DT]), and carotenes in the high (300 µmol photons m^{-2} s^{-1}; c) and low (30 µmol photons m^{-2} s^{-1}; d) light conditions. Note that the value below 1.0 are showed as the reciprocal value. (e)–(f) Variations of ([DD] + [DT])/[chl *a*] (i.e., DD-DT pool size) and [carotenes]/[chl *a*] (i.e., carotene pool size). (g) The de-epoxidation state index (DES; [DT]/([DD]+[DT])) during incubation. Mean values (±SD) indicate the average of three independent measurements.

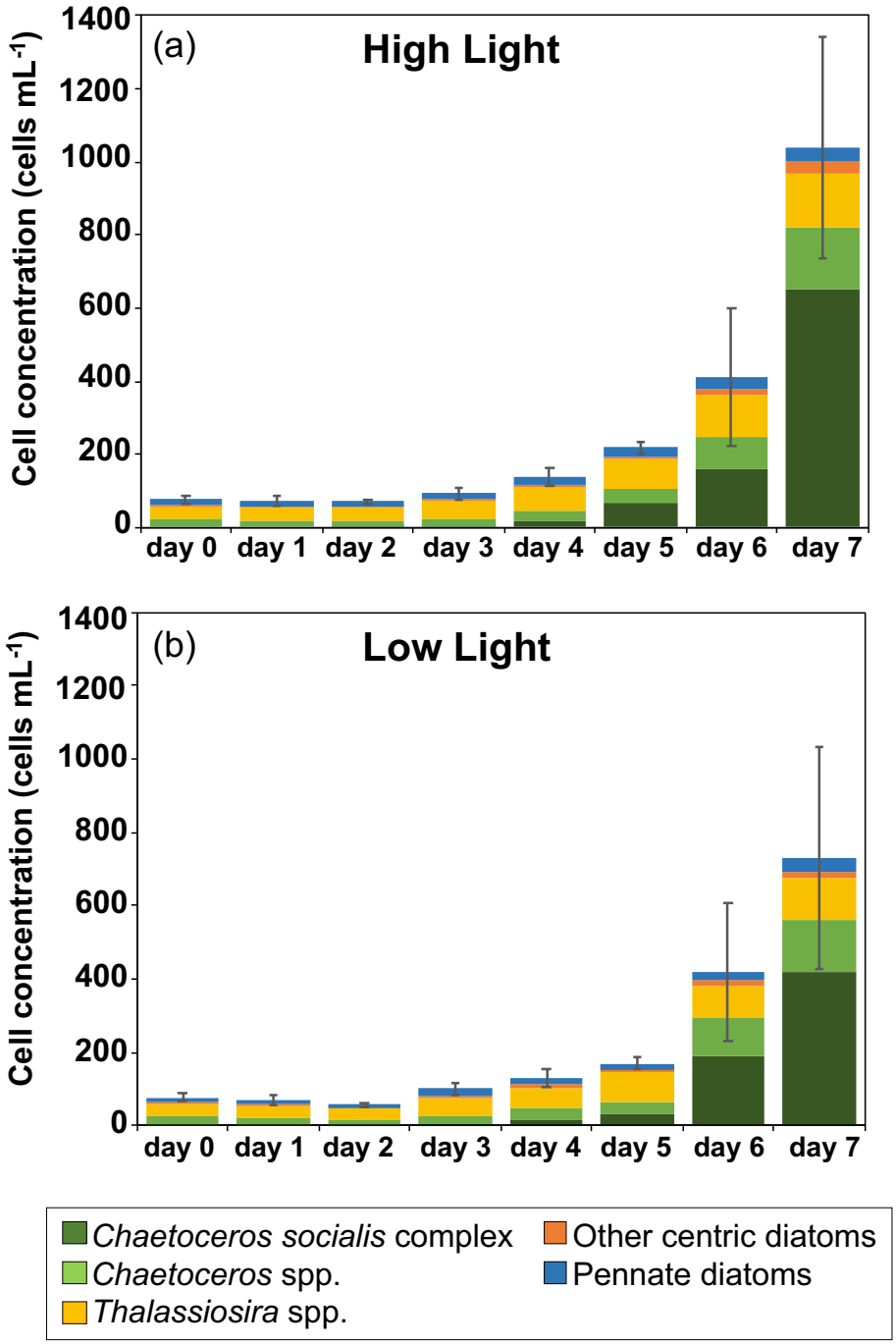

Figure 5.4. Cell concentration and composition of diatoms, which were identified and counted using an inverted light microscope, during incubation under the (a) high (300 µmol photons m^{-2} s^{-1}) and (b) low (30 µmol photons m^{-2} s^{-1}) light conditions. Mean values (±SD) indicate the average of three independent measurements.

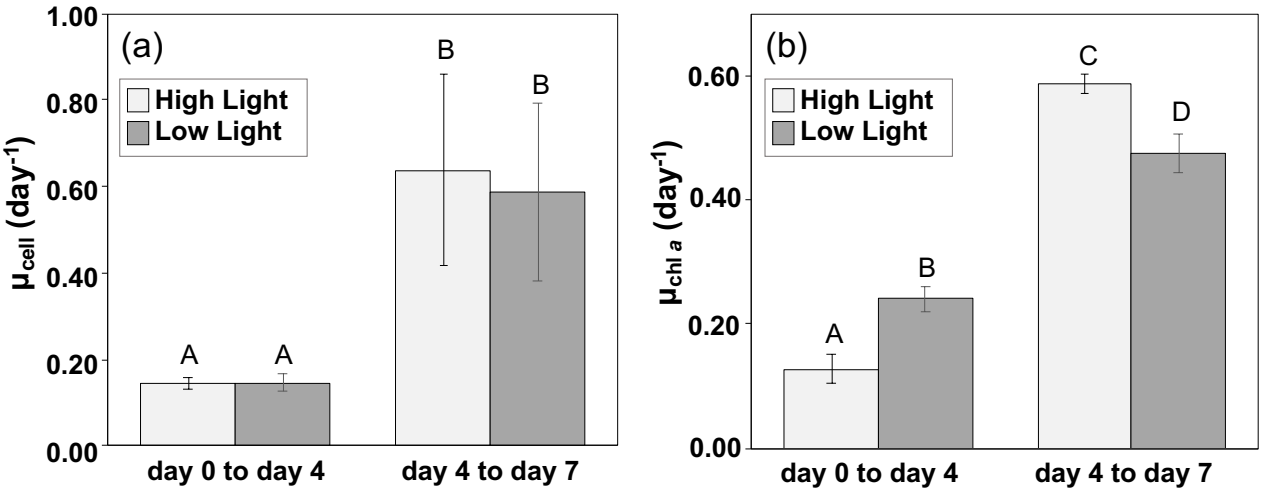

Figure 5.5. (a) Cell-specific and (b) chl *a*-specific growth rate during the incubation of two periods (day 0 to day 4 and day 4 to day 7). Light gray and gray represent the high (300 µmol photons m^{-2} s^{-1}) and low (30 µmol photons m^{-2} s^{-1}) light conditions, respectively. The uppercase alphabetic characters indicate significant differences among groups (one-way ANOVA and Tukey-Kramer test, $p < 0.05$). Mean values (±SD) indicate the average of three independent measurements.

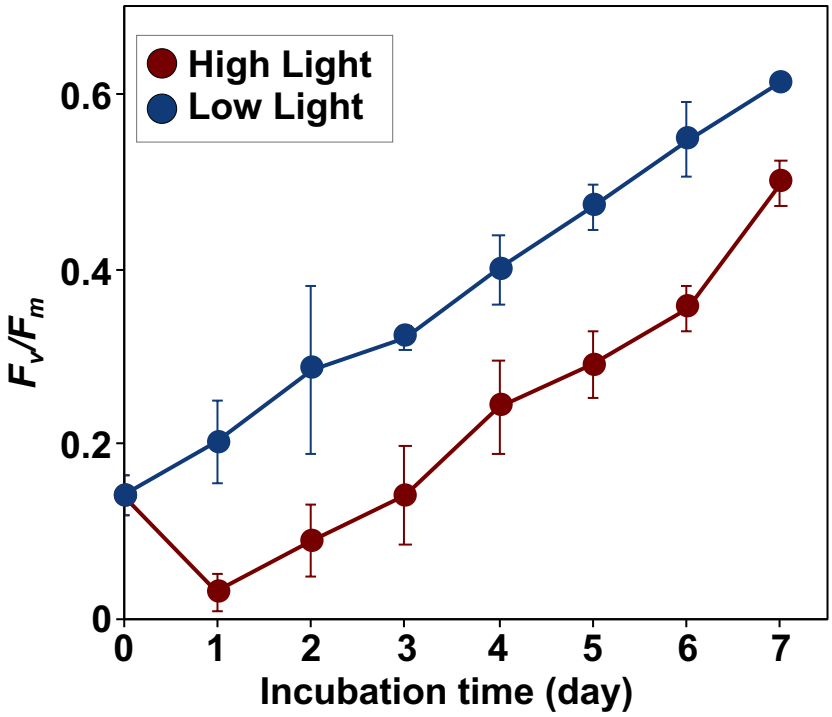

Figure 5.6. Variations in the maximum photochemical efficiency of PSII (F_v/F_m) during incubation. Mean values (±SD) indicate the average of three independent measurements.

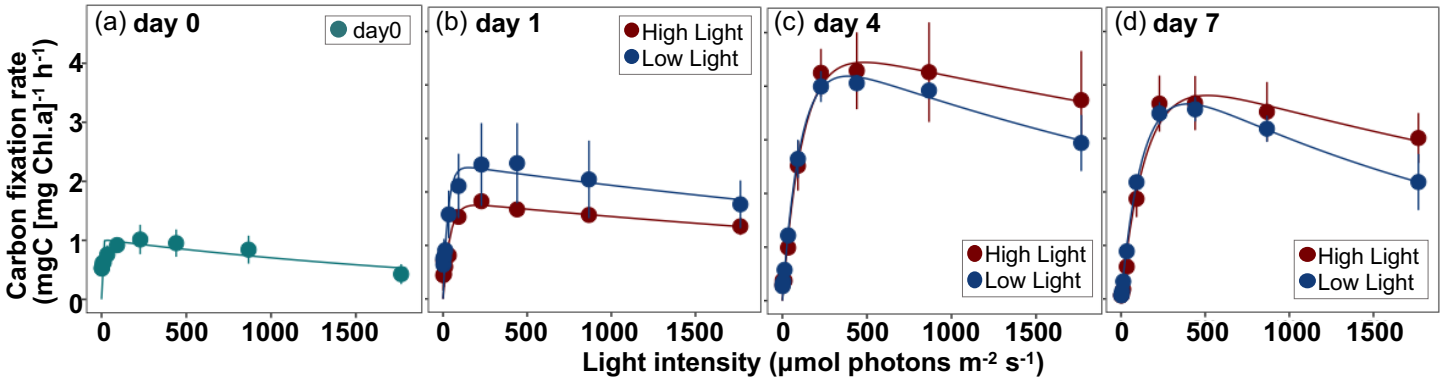

Figure 5.7. Photosynthesis-Energy (P-E) curves during incubation on (a) day 0, (b) day 1, (c) day 4, and (d) day 7 fitted by the photoinhibition model of Platt et al. (1980). The vertical axis indicates the carbon fixation rate normalized by chl *a* concentration (mg C [chl *a*]$^{-1}$ h^{-1}), and the horizontal one indicates the light intensity (µmol photons m^{-2} s^{-1}) during incubation. The red and blue colors represent the high (300 µmol photons m^{-2} s^{-1}) and low (30 µmol photons m^{-2} s^{-1}) light conditions, respectively. Mean values (±SD) indicate the average of three independent measurements.

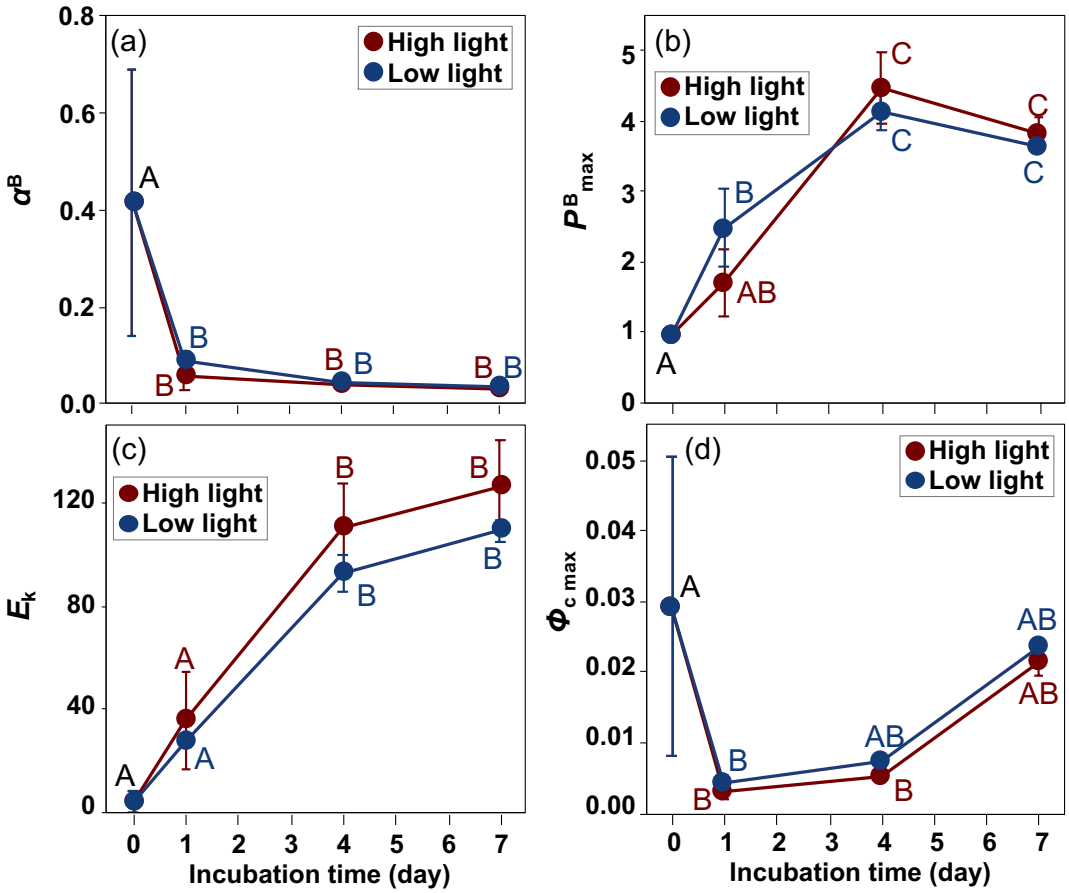

Figure 5.8. Variations in photosynthetic parameters during incubation. (a) the initial slope of the P-E curve normalized by chl *a* concentrations, α^B ((mg C [chl *a*]$^{-1}$ h^{-1}) (µmol photons m^{-2} s^{-1})$^{-1}$), (b) the maximum photosynthetic rate normalized by chl *a* concentration, P^B_{max} (mg C [chl *a*]$^{-1}$ h^{-1}), (c) the photoacclimation index, E_k (µmol photons m^{-2} s^{-1}), and (d) the maximum quantum yield of carbon fixation, $\Phi_{c\,max}$ (mol C (mol photon)$^{-1}$). The red and blue colors represent the high (300 µmol photons m^{-2} s^{-1}) and low (30 µmol photons m^{-2} s^{-1}) light conditions, respectively. The uppercase alphabetic characters indicate significant differences among groups (one-way ANOVA and Tukey-Kramer test, $p < 0.05$). Mean values (±SD) represent the average of three independent measurements.

CHAPTER 6 – Characteristics of autumn diatom communities in the Chukchi Sea unraveled by combined DNA metabarcoding and scanning electron microscope techniques

6.1. Introduction

The Pacific Arctic region has a broad, shallow shelf in the Chukchi Sea and known as one of the most daily productive regions during spring and summer in the Arctic (Springer et al., 1996; Hill et al., 2018) as described in the general introduction. Diatoms highly contribute to the primary production (e.g., Sergeeva et al., 2010; Giesbrecht et al., 2019; Suzuki et al., 2021) and POC sinking flux (Lalande et al., 2020) in this area. Therefore, many studies focus on the spring and summer community in the Chukchi Sea, while only a few research on the late summer and autumn diatom community. Because the predominance of diatoms from September to October in the Chukchi shelf is suggested by microscopy and chemotaxonomic algal pigments (Fujiwara et al., 2014; Matsuno et al., 2014), we should investigate the diatom community in more depth. A strong wind event during autumn of the Chukchi Sea supplied nutrients to the surface and enhanced primary productivity and microalgal biomass, particularly by large phytoplankton such as diatoms (Nishino et al., 2015). In addition, some diatoms, such as *Dactyliosolen fragilissimus*, *Rhizosolenia* spp., *Cylindrotheca closterium*, *Navicula* spp. and resting spores of *Chaetoceros furcellatus*, significantly increased after the events (Yokoi et al., 2016).

Diatoms have been traditionally investigated using microscopy due to their large cell size (~5 μm and up to 2 mm; Hoppenrath et al., 2009). In particular, this technique can distinguish diatom life stages based on their morphological features. Classification of their stages is important because diatoms can form resting stages when triggered by unfavorable conditions, e.g., nutrient depletion (Hargraves and French, 1983; McQuoid and Hobson, 1996). Since their carbon and silicate contents are generally higher than vegetative cells (Kuwata et al., 1993), diatom resting stages play a critical role in the ocean carbon and silica cycles (e.g., Rynearson et al., 2013) (see, general introduction section 1.3.2). However, analysis using microscopy is time-consuming and requires mastery skills to identify diatoms at the genus or species levels.

In contrast, the molecular approach has been recently used to investigate the diversity of eukaryotic organisms, including microalgae. One of the approaches, metabarcoding, consists

of amplifying a marker gene and sequencing the amplicon, and studies using this technique have been increasing, particularly in aquatic ecosystems (Lopes dos Santos et al., 2022). Although several marker genes have been suggested, the 18S rRNA gene is the most commonly used in eukaryotic plankton studies (Lopes dos Santos et al., 2022). The DNA metabarcoding technique eventually allows us to objectively estimate the relative abundance of each algal group based on nucleic acid databases. Since reference database for the sequence annotation are vital and sometimes significantly affects the final outputs, reliable databases for protists (i.e., eukaryotic microorganisms), such as PR^2, have been developed (Guillou et al., 2013). However, data derived from the two analytical methods (i.e., microscopy and DNA metabarcoding techniques) have seldom been compared and validated reciprocally in the Arctic. This comparison would pave the way for easier examination of eukaryotic communities while maintaining validity with previous microscopic studies. We, therefore, investigated the autumn diatom communities in the Chukchi Sea using scanning electron microscopy (SEM) and DNA metabarcoding techniques and tried to characterize their community composition in detail with environmental conditions.

6.2. Materials and Methods

6.2.1. Sampling and environmental parameters

Seawater sampling for phytoplankton pigments, the maximum quantum yield of photochemistry in photosystem II (i.e., F_v/F_m) scanning electron microscopy (SEM) analyses, and DNA metabarcoding were conducted at 19 stations (bottom depth: 39–1983 m) in the Pacific Arctic region (Figure 6.1) from October 8–21, 2020 during the Research Vessel *Mirai* (Japan Agency for Marine-Earth Science and Technology) MR20-05C expedition. Seawater was collected from the surface and the sub-surface chlorophyll *a* maximum (SCM) layers using a bucket and a Niskin water sampler for pigment and diatom analyses (Table 6.1). Although the SCM layers were decided based on *in situ* data of chlorophyll *a* fluorescence by conductivity-temperature-depth (CTD) observations, samples were taken from arbitrary sub-surface layers (ASL) at some stations because sometimes there was no distinct chlorophyll *a* maximum in the sub-surface. In the following, both SCM and ASL are denoted as the sub-surface layers (SSL).

The hydrographic parameters (temperature, salinity, chlorophyll *a,* fluorescence, and beam transmission) were measured by a CTD profiler and amounted sensors at 27 stations over

the Pacific Arctic region (Figure 6.1). The parameters in the 5 m layer were used as the values in the surface layer. Measured chlorophyll *a* fluorescence was converted to chlorophyll *a* (chl *a*) concentrations using a relationship between chl *a* concentrations measured by a fluorometer (10-AU-015-CE, TURNER DESIGNS, USA) and chl *a* fluorescence (Figure S6.1). The mixed layer depth (MLD) was defined as the depth where the density was 0.10 kg m^{-3} greater than the value at 5 m depth (Danielson et al., 2011). When the data at 5 m was absent, the data of the shallowest depth was used as the reference value. As a stratification index of the water column, the 3-m moving average of the square of the Brunt-Väisälä frequency (N^2_{3m}) was determined from vertical CTD profiles at 1 m intervals (Vallis, 2017; Suzuki et al., 2021). The calculation of N^2_{3m} was followed by Suzuki et al. (2021).

For nutrient analysis, seawater was collected from 7–23 layers of 27 stations with 0–1993 m depth. Nitrate, nitrite, ammonium, phosphate, and silicic acid were measured on board by colorimetric methods using a QuAAtro 2-HR system (BL-Tec co.) certified with standard reference materials (KANSO, standard lot symbols of CE, CL, CO, and CG, Osaka, Japan) for nutrient analysis.

6.2.2. Phytoplankton pigments

The seawater samples of 1200 mL were filtered onto Whatman GF/F filters under a gentle vacuum (< 0.013mPa), and the filters were immediately frozen in the deep freezer at −80°C until further analysis. In the shore-based laboratory, phytoplankton pigments were extracted using the *N*,*N*-dimethylformamide (DMF) bead-beating technique and analyzed by Ultra-High Performance Liquid Chromatography (UHPLC Nexera X2, Shimazu, Japan) following Suzuki et al. (2015). Class-level phytoplankton composition was estimated by multiple linear regression based on major diagnostic pigment signatures and chl *a* (Suzuki et al., 1997; Yoshida et al., 2018). The total diagnostic pigment concentrations [Total DP] are defined as the sum of the following chemotaxonomic levels (Vidussi et al., 2001):

[Total DP] = [Fuco] + [Peri] + [19'-BF] + [19'-HF]+ [Allo] + [Zea] + [Chl *b*]

where [Fuco], [Peri], [19'-BF], [19'-HF], [Allo], [Zea], and [Chl *b*] are the concentrations of fucoxanthin, peridinin, 19'-butanoyloxyfucoxanthin, 19′-hexanoyloxyfucoxanthin, alloxanthin, zeaxanthin, and chlorophyll *b*, respectively. These pigments were used as signatures for diatoms, dinoflagellates, pelagophytes, prymnesiophytes, cryptophytes, cyanophytes, and chlorophytes,

respectively (Garibotti et al., 2003). The multiple linear regression analysis was performed using the least squares method by LINEST function in Microsoft Excel, and its validation was conducted with *F*-test and *t*-test. When the *p*-value of the *t*-test was larger than 0.05, the diagnostic pigments were excluded, and the multiple linear regression analysis was performed again. The concentrations of each pigment were converted to chl *a* based concentration by multiplication of a partial regression coefficient and the pigment concentration. Thereafter, the contributions of each pigment to chl *a* concentrations (%) were calculated as follows:

$$Contribiutions\ to\ chl\ a\ (\%) = 100 \times \frac{Chl\ a\ based\ concentrations\ of\ a\ pigment}{Chl\ a\ concentrations}$$

6.2.3. The maximum quantum yield of photochemistry in photosystem II

The maximum quantum yield of photochemistry in photosystem II (i.e., F_v/F_m) for phytoplankton was measured using a pulse-amplitude-modulated (PAM) fluorometer (Water-PAM, Walz, Germany). Samples from the surface and SSL layers were acclimated in darkness at the sea-surface temperature for more than 30 minutes before the measurement and then put into a quartz cuvette. The F_v/F_m was obtained following the same procedure in chapter 5. The fluorescence measurements were conducted 3–5 times per sample.

6.2.4. Scanning electron microscopy (SEM)

The seawater samples of 107–120 mL were collected into dark bottles fixed with 10% paraformaldehyde at a final concentration of ca. 0.2% and stored at 4°C until further analysis. For the preparation of SEM analyses, 5–61 mL of the fixed seawater was filtered onto polycarbonate filters (pore size 2.0μm, 25 mm, Whatman, UK) using a glass funnel with a diameter of 3 mm under a gentle vacuum (<0.013 mPa), and then the filters were rinsed with Milli-Q water to remove salts. These filters were secured with conductive carbon tape on a microscope stage before coating with Pt-Pb alloy by vapor deposition using an MSP-1S magnetron spatter device (Vacuum device Inc. Japan). The Pt-Pb alloy-coated samples were transferred to a scanning electron microscope (SEM; VE-8800, KEYENCE Corp. Japan), and diatoms in the samples were counted and identified following Hasle and Syvertsen (1997). The volume (μm^3) of counted diatoms was estimated following Hillebrand et al. (1999).

6.2.5. DNA metabarcoding

The seawater of 290–1200 mL was filtered onto a polycarbonate membrane (pore size 2.0 μm, diameter 25 mm, Merck) under a gentle vacuum (<0.013 mPa). The filters were immediately frozen at –80°C until DNA extraction. In the shore-based laboratory, DNA was extracted using the bead-beating method following Endo et al. (2013). The V4 region of the 18S rRNA gene was targeted and amplified by the two-step PCR method. In the first PCR step, the targeted region was amplified by primers (Piredda et al., 2017b) (forward: 5'-CCAGCASCYGCGGTAATTCC-3', reverse: 5'-ACTTTCGTTCTTGATYRATGA-3') with adaptor sequences (forward: 5'-ACACTCTTTCCCTACACGACGCTCTTCCGATCT-3', reverse: 5'-GTGACTGGAGTTCAGACGTGTGCTCTTCCGATCT-3'). The thermal cycling condition for the first PCR was that 94°C hold for 2 min, followed by 30 cycles at 94°C for 30 sec, at 50°C for 30 sec, and at 72°C for 30 sec, and then a 72°C hold for 5 min. Then, after the PCR products were refined using AMPure XP beads (Beckman Coulter), sequence adaptors and index sequences were added in the second PCR step. The thermal cycling condition was that 94°C hold for 2 min, followed by ten cycles at 94°C for 30 sec, at 60°C for 30 sec, and at 72 °C for 30 sec, and then a 72°C hold for 5 min. The amplicon libraries were purified using AMPure beads (Beckman Coulter) and quantified by Fragment Analyzer (Advanced Analytical Technologies) using the dsDNA 915 Reagent Kit. The amplicon libraries were sequenced by a MiSeq system (Illumina) using a MiSeq Reagent Kit v3 according to the manufacturer's protocol.

The obtained sequence data were analyzed through QIIME2 (Bolyen et al., 2019) with the DADA2 plugin (Callahan et al., 2016). After quality-controlled reads were obtained using the "dada2 denoise-paird" command, the Amplicon Sequence Variants (ASVs) were estimated. The ASVs were annotated by BLAST using the Protist Ribosomal Reference (PR^2) database (Guillou et al., 2013) version 4.14.0 to convert taxonomy data.

6.2.6. qPCR

Copy numbers of 18S rDNA from diatoms were quantified by a real-time PCR system (CFX Connect, Bio-Rad, USA) using the diatom-specific primer set designed by Endo et al. (2018):

Forward primer: 5'-AACTACTGCGAAAGCATTTA-3'

Reverse primer: 5'-GACTACGATGGTATCTRATCAT-3'.

The standard curve for the 18S rDNA fragment was generated using liner plasmids containing artificial gene fragments (88 bp in size) of *Thalassiosira weissflogii* (Endo et al., 2018). The thermal cycling condition for the qPCR was that 95°C hold for 1 min, followed by 40 cycles at 95°C for 5 sec and 55°C for 60 sec.

6.2.7. Microalgal data combining

The absolute abundance (copy L^{-1}) of each ASV was calculated by multiplying the diatom-specific 18S rDNA abundance estimated by qPCR and the relative contribution of the ASVs obtained from the DNA metabarcoding. In addition, data from the SEM analysis and DNA metabarcoding were combined to improve the ASV-based diatom data set (see discussion section 6.4.1). Because of a significant correlation between biovolume and 18S rDNA copy number in diatoms (Godhe et al., 2008), the copy number of genus *Chaetoceros* was separated for vegetative cells and resting spores as follows:

$$Chaetoceros\ VC_{(copy\ number)} = Chaetoceros\ total_{(copy\ number)} \times \frac{Chaetoceros\ VC_{(biovolume)}}{Chaetoceros\ total_{(biovolume)}}$$

$$Chaetoceros\ RS_{(copy\ number)} = Chaetoceros\ total_{(copy\ number)} - Chaetoceros\ VC_{(copy\ number)}$$

where VC and RS indicate vegetative cells and resting spores, respectively.

6.2.8. Diatom community diversity

Diversity in diatom communities was assessed using Pielou's evenness (*J*) index. The index was calculated based on the absolute abundance (copy L^{-1}) of ASVs annotated at the species level. Note that the ASV data used for the calculation was not modified by *Chaetoceros* RS biovolume.

6.2.9. Statistical analyses

Correlation-based network analysis was conducted to assess co-occurring patterns of the diatom ASVs (Endo et al., 2022). The absolute abundance of ASVs (see section 6.2.7) was

used for the examination. The ASVs which emerged in less than five samples were not used for further analysis to avoid potentially unreliable correlations. Ultimately, 21 of 30 ASVs were retained for subsequent analysis. The absolute abundance of each ASV (X: copy L^{-1}) was transformed to log (X+1) before building Spearman's correlation coefficient matrix. At the same time, the p-values adjusted by the Bonferroni method were estimated, and the data with p-values larger than 0.05 were removed from the correlation coefficient matrix. The "tidygraph" package (version 1.2.2) in R software (version 4.2.1, R Development Core Team, 2022) was used to build a correlation-based network. Co-occurrence modules of ASVs in the network were determined by a fast greedy algorithm in the "igraph" package (version 1.3.4) (https://cran.ism.ac.jp/web/packages/igraph) in the R software .

The diatom community was distinguished by a cluster analysis based on the copy number of each ASV in the combined data. To reduce the bias for abundant ASVs, the copy number data (X: copy L^{-1}) for each ASV were transformed to $\sqrt[4]{X}$ before the cluster analysis (Quinn and Keough, 2002). Dissimilarities between samples were examined using the Bray-Curtis index based on the differences in the ASV composition. The dissimilarity indices were coupled to group the samples using hierarchical agglomerative clustering with a complete linkage method (an unweighted pair group method using the arithmetic mean).

To test intergroup differences in the environmental factors, diatom physiological status, and community diversity, a Kruskal-Wallis test and a post hoc Steel-Dwass test were conducted. All statistical analyses were performed using R software.

6.3. Results

6.3.1. Hydrography and nutrient chemistry

The temperature and the salinity values ranged from -1.74–4.49˚C and 25.2–34.9 over the study area, respectively (Figure S2). Three water masses with different features were identified in the two sampling layers (0 m and SSL) over the study area: Bering Chukchi Summer Water (BCSW) (intermediate temperature and salinity water), Bering Chukchi Winter Water (BCWW) (cold water remnant from the previous winter's cooling) and Melt Water (MW) (relatively cool and fresh water influenced by sea ice melt) (Danielson et al., 2017). The water masses were distributed regionally (Figure 6.2). The MW was present over the northern and

eastern regions, while the BCSW was southern of the study area. The BCWW was distributed only in the SSL at two stations.

The MLD ranged from 11 to 55 m (Table 6.1). The sampling depths of the SSL were deeper than the MLD at ten stations (Table 6.1).

Nutrient concentrations varied over the study area. The concentrations were relatively high in the southern region but lower in the northern and eastern parts of the study area (see section 6.3.5) (Table 6.1).

6.3.2. The maximum quantum yield of photochemistry in photosystem II

The F_v/F_m ranged from 0.225–0.627 during the cruise (Table 6.1). Relatively high values of F_v/F_m were detected in the northern and northeastern parts of the study area with lower nutrient concentrations (Table 6.1). On the other hand, the values were relatively low at the stations along 168.8˚W. The regional trend was similar between the surface and SSL.

6.3.3. Phytoplankton pigments

Relatively low chl *a* concentrations (0.11–1.06 mg m^{-3}) were observed throughout the study area (Figures 6.3 and S6.1). The chl *a* concentrations were calculated by a multiple linear regression as follows:

$$[\text{Chl } a] = 2.05[19'\text{-BF}] + 1.27\,[\text{Fuco}] + 4.90\,[\text{Allo}] + 1.44[\text{Chl } b]$$

where the R^2 was 0.999 and partial regression coefficients were statistically significant ($p < 0.05$ by *F*-test and $p < 0.05$ by *t*-test). Reciprocals of each partial coefficient were within the range of the previously reported pigment/chl *a* ratios (Mackey et al., 1996; Suzuki et al., 2002). The contributions of fucoxanthin to chl *a* concentrations were more significant than the other diagnostic pigments in all samples, except the sea surface samples at stations 10, 11, 12, 25, 34 and 35 and the SSL samples at stations 11 and 12, where alloxanthin or chl *b* were predominant (Figure 6.3).

6.3.4. Composition, abundance, and biovolume of diatoms

We identified 14 genera of diatoms under the SEM. *Chaetoceros* spp. accounted for the highest percentage (34–99%) in abundance in 25 samples, 14 of which were dominated by *Chaetoceros* resting spores (Figure 6.4a). Centric diatoms of *Attheya* spp. and *Thalassiosira* spp.

or the pennate diatom, *Thalassionema nitzschioides*, were often dominated in other samples (Figure 6.4a). *Proboscia* spp. was rarely found in the SEM analysis. From the DNA metabarcoding, 21 genera of diatom were identified. *Proboscia* spp. or *Chaetoceros* spp. was dominated in most samples in read, while in stations 11 and 12, centric diatoms which belong to Coscinodiscophyceae accounted for high percentages (Figure 6.4b). Although 8 genera of pennate diatoms were identified, *Thalassionema* spp., which often appeared from SEM samples, was not verified. Only nine genera (i.e., *Attheya*, *Chaetoceros*, *Coscinodiscus*, *Ditylum*, *Proboscia*, *Rhizosolenia*, *Thalassiosira*, *Cylindrotheca*, *Fragilariopsis*) were commonly identified in the SEM and DNA metabarcoding analyses.

The copy number of diatom-specific 18S rDNA fragment ranged from 7.05×10^5–1.49×10^9 copies L^{-1} and it was significantly correlated with the concentrations of fucoxanthin (mg m^{-3}) (Pearson, $p < 0.05$) (Figure 6.5 a). On the contrary, the total biovolume of diatoms (μm^3 mL^{-1}) did not have any significant correlations with the fucoxanthin concentrations (mg m^{-3}) (Figure 6.5 b) or the copy number of diatom-specific 18S rDNA fragment (copy L^{-1}) (Pearson, $p > 0.05$) (Figure 6.5 c). At the genus level, the biovolume of *Fragilariopsis*, *Thalassiosira, Chaetoceros* and *Ditylum* was significantly correlated with the copy number of 18S rDNA fragment estimated by multiplying the diatom-specific 18S rDNA abundance and the relative contribution of each ASV (Pearson, $p < 0.05$, respectively). However, the other common genera between the SEM and the metabarcoding analyses did not have such a significant relationship between biovolume and 18S rDNA abundance.

6.3.5. Diatom community and relationships with environmental parameters

The correlation-based network analysis revealed three co-occurrence modules. Some correlations between modules 1and 3 existed, while module 2 was relatively independent (Figure 6.6 a). Contributions of each module to the diatom-specific 18S rDNA fragments differed among stations, but either modules 1 or 2 were dominated (Figure 6.6 b).

The cluster analysis, which is based on the copy number of each ASV in the combined data, classified the diatom community over the study area into three groups (A, B and C). The distinguished group was not different between the sampling layers at all stations, but the spatial distribution of the groups was regionally dependent (Figure 6.7 a). Group B was distributed in the northern and eastern regions of the study area, while group C was along the 168.8°W and station

20. Group A was only spread at station 9. The dominated module differed between groups B and C, and the contribution of module 2 was the highest in group B, although that of module 1 showed the highest in group C (Figure 6.7b). A detailed view of the dominant modules revealed that *Proboscia* and *Chaetoceros* RS contributed to the diatom community in groups B and C, respectively (Figure 6.7c). The community diversity of diatoms (i.e., *J* index) differed between groups, and it was significantly lower in group B compared with groups A and C (Figure 6.7d and Table 6.2).

Differences in some environmental and physiological factors (i.e., latitude, sampling date, temperature, salinity, beam transmission, N^2_{3m}, bottom depth, F_v/F_m, NO_2 + NO_3, NH_4, $Si(OH)_4$, PO_4) among groups were detected by a Kruskal-Wallis test and a post hoc Steel-Dwass test (Figure 6.8 and Table 6.2). Group B was distributed in colder, fresher, and larger N^2_{3m} (i.e., more stable) region, and it contained microalgae with higher F_v/F_m than group C. All nutrients were higher in group C distributed shallower with lower beam-transmission (i.e., turbid) regions.

6.4. Discussion

6.4.1. Comparison of results between scanning electron microscopy (SEM) and DNA metabarcoding – diatoms

Biovolume can be correlated with the copy number of 18S rDNA in diatoms (Godhe et al., 2008). However, in the present study, diatom biovolume did not have a significant relationship with the copy number of diatom-specific 18S rDNA fragments. Although the results indicated either an overestimation of the 18S rDNA copy number or an underestimation of the diatom biovolume, we considered that the diatom biovolume was probably estimated less than the actual because the copy number of diatom-specific 18S rDNA fragments significantly correlated with the fucoxanthin concentration. Therefore, in the present study, we concluded that the data of DNA metabarcoding was more reliable than that of SEM in assessing the diatom community. Furthermore, because the biovolume of *Fragilariopsis*, *Thalassiosira, Chaetoceros,* and *Ditylum* was significantly correlated with the 18S rDNA copy number, they would not be the reason for underestimation.

On the contrary, the abundance of *Proboscia*, which is often dominated in the Pacific Arctic shelf during autumn (Matsuno et al., 2014), was very different between the DNA metabarcoding and the SEM. Although *Proboscia* was rarely detected in all SEM samples, they

were often dominated in the DNA metabarcoding samples. Since *Proboscia* is a large and long diatom whose cell length is more extensive than 220 μm (Hasle and Syvertsen, 1997; Kulk et al., 2019) and the silicate frustule is thin (Sukhanova et al., 2006), the filtration to prepare for the SEM analysis would damage the long cells of *Proboscia*. Many unidentified and uncounted fragments in some samples might be broken *Proboscia* cells. However, the SEM analysis has the advantage of detecting diatom resting spores depending on morphology differences because distinguishing vegetative cells and resting spores based on the 18S rDNA sequence is impossible. In the Chukchi Sea, especially in the shelf region, there were many diatom resting spores in sediments (chapter 4). Because diatom forms a thick frustule when resting spores and the sinking rate is faster than vegetative cells (Sugie and Kuma, 2008), sinking diatom resting spores play an essential role in POC flux (Rynearson et al., 2013). Thus, it is crucial to assess vegetative cells and resting spores separately. Therefore, we tried to modify ASV data by combining *Chaetoceros* resting spore data (see section 6.2.7).

As a result of using the improved data set, the correlation-based network analysis allocated vegetative cells and resting spores of *Chaetoceros* in the different modules. In addition, the advantages of the DNA metabarcoding and SEM analyses were well pictured with the quantification of *Proboscia* by the DNA metabarcoding and the detection of resting spores by the SEM. The widely distributed groups B and C were dominated by *Proboscia* and *Chaetoceros* resting spore, respectively. Therefore, in the present study, we suggest the usefulness of a resting-spore-combined ASV data set, especially for the shallow shelf regions with abundant resting spores in sediments.

6.4.2. Diatom community – composition, distribution, and relationships with environmental factors

Diatoms are dominant groups during blooms from spring to summer in the Pacific Arctic region (e.g., von Quillfeldt, 2000; Sergeeva et al., 2010; Suzuki et al., 2021). In addition, a previous study showed that the microalgal communities with high fucoxanthin contribution were dominant during the late summer (primarily in September) of the Chukchi shelf (Fujiwara et al., 2014). The results of this study in October were consistent with Fujiwara et al. (2014), and the contributions of fucoxanthin to chl *a* concentrations were the highest in most samples. Furthermore, the fucoxanthin concentrations significantly correlated with the copy numbers of

the diatom-specific 18S rDNA fragments, suggesting that it's highly associated with diatoms, although prymnesiophytes, chrysophytes, and raphidophytes also contain fucoxanthin (Jeffrey et al., 1997).

A traditional view of spring bloom in the Arctic is that ice algal production occurs in and under the sea ice, followed by an increase in phytoplankton after sea ice retreat (Horner and Schrader, 1982; Horner, 1984). Pennate diatoms, including *Fragilariopsis* and *Navicula*, and the centric diatoms *Attheya* are known as ice-associated diatoms (Melnikov et al., 2002; von Quillfeldt et al., 2003; Werner et al., 2007; Szymanski and Gradinger, 2016; Campbell et al., 2018). In addition, they are often detected in sediments with *Chaetoceros* resting spores (chapter 4). After the sea ice retreat in early spring, *Thalassiosira* often appears before *Chaetoceros* (von Quillfeldt, 2000). Furthermore, *Chaetoceros socialis* complex is characterized as a late spring or summer species (Sergeeva et al., 2010; Suzuki et al., 2021). Therefore, diatoms assigned for modules 1 and 3 included diatoms that appear in early spring and from sediments. Module 1 was dominant in the diatom community group C, which was distributed in the southern Chukchi Sea, and especially *Chaetoceros* resting spores occupied with high proportions. Since group C was spread in the shallower, lower beam transmission (i.e., higher turbidity), and less stable regions with higher nutrient levels, diatoms in this group, including *Chaetoceros* resting spores, would be transported from the seafloor. The abundant viable diatoms are in the sediments of the southern Chukchi Sea (chapter 4), and they have high photophysiological plasticity to grow actively after light exposure (chapter 5). Therefore, the resuspension of the diatom community with many *Chaetoceros* resting spores from the seafloor to the surface layer of the water column may provide opportunities for viable diatoms in sediments to initiate the primary production during the autumn in the southern Chukchi Sea. Although the average daily maximum intensity of photosynthetically active radiation (PAR) on deck during the study period in October was 217 μmol photons m^{-2} s^{-1}, which was high enough to reactivate diatoms in sediments (chapter 5), we considered that the bloom did not occur because F_v/F_m values were low. Thus, further study about autumn blooms related to sediments resuspension will be needed. The high community diversity (i.e., *J* index) in group C also indicated the coexistence of various species without the dominance of any specific species. They could be partly derived from the benthic algal community.

The other module, module 2, which had little correlation with the other modules, was composed of diatoms from late spring to autumn of the Pacific Arctic, such as *Chaetoceros*,

Proboscia, and *Cylindrotheca* (Matsuno et al., 2014). This module was dominant in group B, which was distributed in the northern and eastern study areas. The regional distribution pattern of the diatom community was similar to those of the water masses. The diatom community group B occurred in the Melting Water (MW). This feature was statistically shown: the region where group B was present was colder, fresher, and more stable than the places where group C occurred. Therefore, group B might be attributed to the sea ice melt. However, diatoms in group B little contained ice-associated diatoms such as *Proboscia*, which was characteristically found in the Pacific Arctic during autumn (Matsuno et al., 2014). *Proboscia* cannot survive for a long time in darkness (Tsukazaki et al., 2018), suggesting that group B would not be derived from sea ice. Annual observation in the eastern Bering Sea by sediment traps indicated the preference for high temperature and irradiance by *Proboscia alata* (Takahashi et al., 1994). In addition, Sukhanova et al. (2006) suggested that *P. alata* bloomed during the late summer of the eastern Bering Sea with temperature of about 10°C. However, *Proboscia* was abundant in the MW with low temperature (0.29°C on average for group B), which indicated that irradiance might be a more critical factor than the high temperature for the growth of *Proboscia*. Previous studies also reported that *P. alata* dominated even in the upper mixing layer with depletion of nutrients, and the abundance and biomass sometimes reached typical spring bloom levels (Goering and Iverson, 1981; Sukhanova et al., 2006). In the present study, *P. alata* was also dominated in the nitrogen-limited region (i.e., the average concentration in group B of $NO_2 + NO_3$ and NH_4 were 0.37 μmol L^{-1} and 0.43 μmol L^{-1}, respectively). Furthermore, F_v/F_m in the *P. alata* dominated the group B community was relatively high. Although Goering and Iverson (1981) suggested the capability of *P. alata* to utilize urea as a nitrogen source, the reason why the photosynthetic competence of large-sized *Proboscia* was relatively high under nutrient-depleted conditions is still unclear.

6.5. Conclusions

This study tried to characterize the diatom community during the autumn of the Chukchi Sea using the improved diatom data set and the correlation-based network analysis. The improved diatom data set, constructed from the DNA metabarcoding and SEM analyses, made up for the underestimation of *Proboscia* by SEM analysis and the challenge of the DNA metabarcoding not distinguishing vegetative diatom cells from resting stages. Since *Chaetoceros* resting spores and *Proboscia* were important diatoms to characterize the alga assemblages over the study area,

combining the DNA metabarcoding and SEM data was beneficial for our analysis. The diatom community distributed in the southern Chukchi Sea would be transported from the seafloor because of the statistical relationships with environmental factors. In addition, the evidence that module 1, which was dominant in the southern Chukchi Sea, involved the spring centric diatoms, pennate diatoms, and resting spores of *Chaetoceros* supported our speculation. These results indicated a possibility that viable diatoms in sediments resuspended to the surface layer of the water column during the autumn of the southern Chukchi Sea. Such resuspended diatoms could contribute to primary production in the sunlit surface layer because they can proliferate after light exposure (chapter 5). However, species that are abundant in the Arctic sea ice (e.g., genera *Fragilariopsis*, *Navicula*, and *Attheya*; Campbell et al., 2018; Melnikov) were not necessarily dominant in abundance in module 1. Therefore, it may be necessary to clarify the dynamics of sediment-derived diatoms, such as how they resuspend, are taken up by sea ice, spend the lightless winter, and may be selected as ice algae.

6.6. Figures and Tables

Table 6.1. Locations of water sampling stations, the subsurface layer (SSL) depth, the mixing layer depth (MLD), F_v/F_m, and the nutrient concentrations (μmol L^{-1}) in the Chukchi Sea from October 8 to 21, 2020.

Station name	Sampling date	Latitude (°N)	Longitude (°W)	SSL depth (m)	MLD (m)	F_v/F_m		NO_3+NO_2 (μmol L^{-1})		NH_4 (μmol L^{-1})		Si $(OH)_4$ (μmol L^{-1})		PO_4 (μmol L^{-1})	
						surface	SSL	surface	SSL	surface	SSL	surface	SSL	surface	SSL
St. 9	2020/10/8	70.50	165.50	11	32	0.545	0.607	0.37	0.11	0.47	0.40	4.00	3.92	0.68	0.66
St. 10	2020/10/10	74.55	161.88	33	23	0.408	0.443	0.11	0.44	0.13	0.46	3.07	5.31	0.42	0.67
St. 11	2020/10/11	74.98	158.13	15	18	0.574	0.583	0.25	0.00	0.07	0.03	4.01	3.75	0.43	0.43
St. 12	2020/10/12	75.18	160.01	15	14	0.570	0.574	0.33	0.01	0.12	0.09	4.14	3.84	0.46	0.43
St. 13	2020/10/13	73.29	160.01	32	11	0.612	0.439	0.10	0.79	0.15	0.75	2.05	5.45	0.41	0.68
St. 15	2020/10/14	72.79	158.02	15	18	0.581	0.615	0.10	0.06	0.26	0.27	1.84	1.83	0.44	0.43
St. 17	2020/10/15	71.32	158.44	22	18	0.570	0.627	0.44	2.01	0.53	1.05	2.97	7.05	0.50	0.80
St. 20	2020/10/15	71.97	153.99	15	23	0.467	0.460	2.48	2.52	1.56	1.58	10.66	10.95	0.97	0.97
St. 22	2020/10/17	75.01	164.96	26	26	0.553	0.555	0.08	0.03	0.17	0.09	2.50	2.58	0.48	0.49
St. 23	2020/10/18	75.00	167.24	16	24	0.609	0.524	0.25	0.04	0.27	0.21	2.24	2.25	0.42	0.40
St. 24	2020/10/18	75.00	169.64	34	31	0.507	0.505	0.18	0.15	0.45	0.26	4.63	7.58	0.51	0.77
St. 25	2020/10/18	75.00	175.00	27	26	0.532	0.504	0.15	0.11	0.24	0.19	4.40	6.59	0.52	0.75
St. 26	2020/10/19	75.00	172.02	27	26	0.483	0.475	0.11	0.05	0.23	0.12	3.01	4.16	0.51	0.58
St. 27	2020/10/19	74.60	170.21	25	13	0.374	0.277	0.15	0.20	0.55	0.49	4.48	4.94	0.48	0.53
St. 29	2020/10/19	73.50	168.81	18	55	0.284	0.261	1.80	1.70	1.99	1.98	7.57	7.62	0.87	0.86
St. 31	2020/10/20	72.00	168.83	12	44	0.377	0.369	4.08	4.06	3.70	3.67	19.68	19.65	1.24	1.23
St. 33	2020/10/20	70.00	168.81	15	26	0.330	0.225	3.55	3.34	4.32	4.16	17.96	17.75	1.28	1.25
St. 34	2020/10/20	69.03	168.83	16	22	0.413	0.402	14.29	14.91	3.48	3.63	24.50	26.04	1.75	1.81
St. 35	2020/10/21	68.01	168.83	26	15	0.416	0.403	14.58	17.64	6.19	3.81	36.77	37.47	2.17	2.08

Table 6.2. Hydrographic environmental factors and Pielou's Evenness (*J*) among the diatom communities (A, B and C). The values are given as the average and standard deviation of each factor. The numbers in parentheses indicate the number of samples. The differences among the diatom communities were evaluated by Kruskal-Wallis and a post hoc Steel-Dwass tests. Groups unconnected underlines denote that diatom assemblages significantly differed among groups (*: $p < 0.05$, **: $p < 0.01$, and ***: $p < 0.005$).

Factors	Group name			Kruskal-Wallis	Steel-Dwass		
	A (2)	B (26)	C (10)				
Latitude (°N)	70.5	74.2	70.2	***	B	A	C
Longitude (°W)	165.5	165.0	165.9	NS			
Sampling depth (m)	5.5	11.6	8.3	NS			
Sampling date (Julian day)	282	290	293	***	C	B	A
Temprature (°C)	4.48	0.29	2.59	***	A	C	B
Salinity	30.6	29.0	31.8	***	C	A	B
Beam transmission (%)	95.2	98.8	77.0	***	B	A	C
$N^2_{3m\ max}$	0.00004	0.00311	0.00098	*	B	C	A
Bottom depth (m)	44.4	661.6	187.6	***	B	C	A
Mixing layer depth (m)	32.0	23.3	26.0	NS			
Chl *a* (mg m^{-3})	1.02	0.28	0.26	NS			
F_v/F_m	0.58	0.50	0.39	**	A	B	C
NO_3+NO_2 (µmol L^{-1})	0.24	0.37	8.14	***	C	B	A
NH_4 (µmol L^{-1})	0.43	0.43	3.61	***	C	A	B
SiO_2 (µmol L^{-1})	3.96	4.22	22.1	***	C	B	A
PO_4 (µmol L^{-1})	0.67	0.55	1.47	***	C	A	B
Pielou's evenness index (*J*)	0.64	0.41	0.59	*	A	C	B

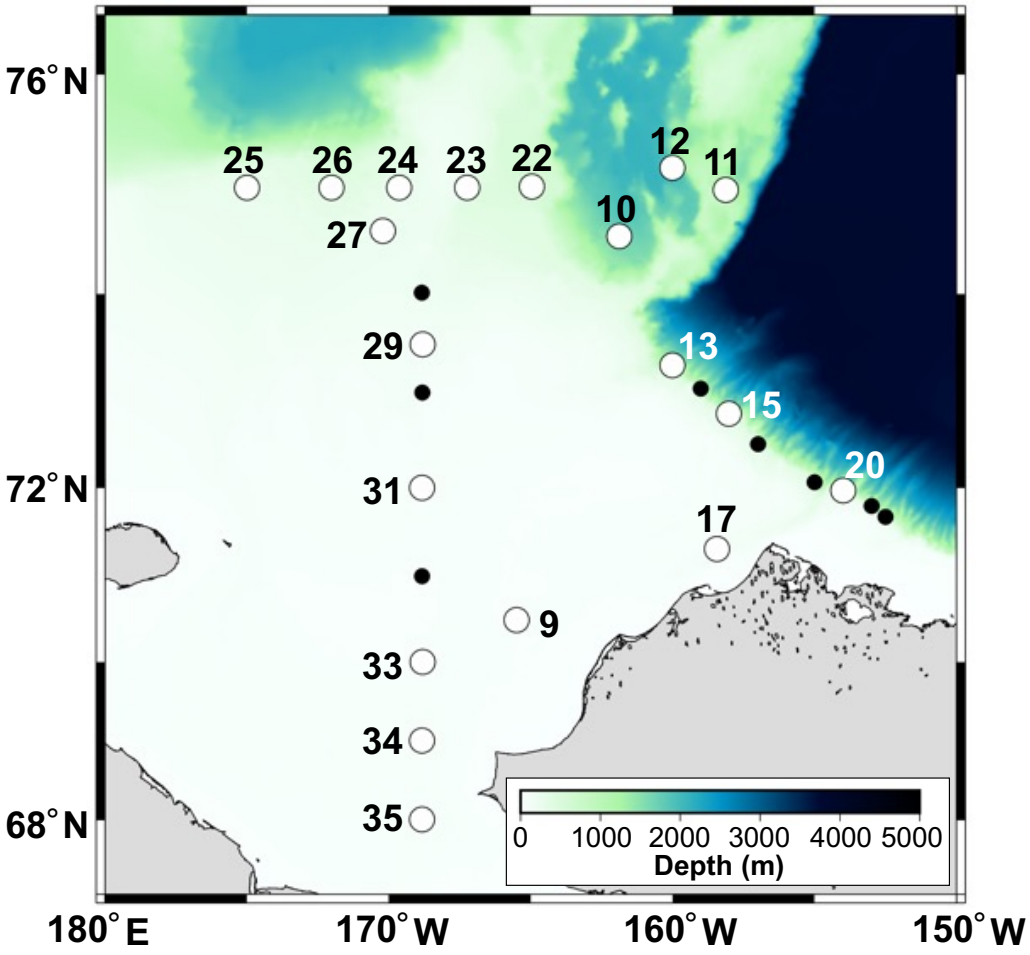

Figure 6.1. Location of stations in the Pacific Arctic region. The numbers indicate the station ID. The solid and open circles represents the stations with water sampling only for nutrients plus hydrographic CTD observations, and those with water sampling for all parameters plus hydrographic CTD observations, respectively.

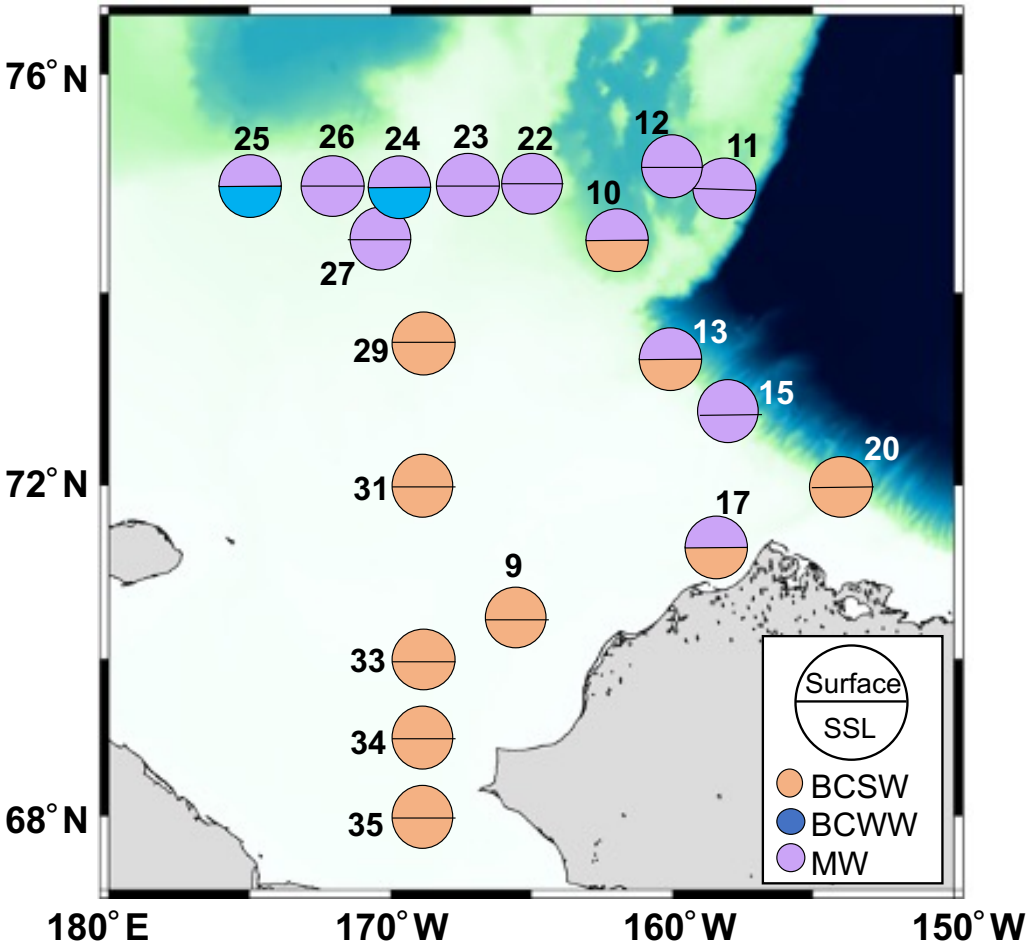

Figure 6.2. Spatial distribution of water masses in the surface and the sub-surface layers (SSL). Water masses were defined following Danielson et al. (2017). BCSW: Bering-Chukchi Summer Water, BCWW: Bering-Chukchi Winter Water, and MW: Melting Water.

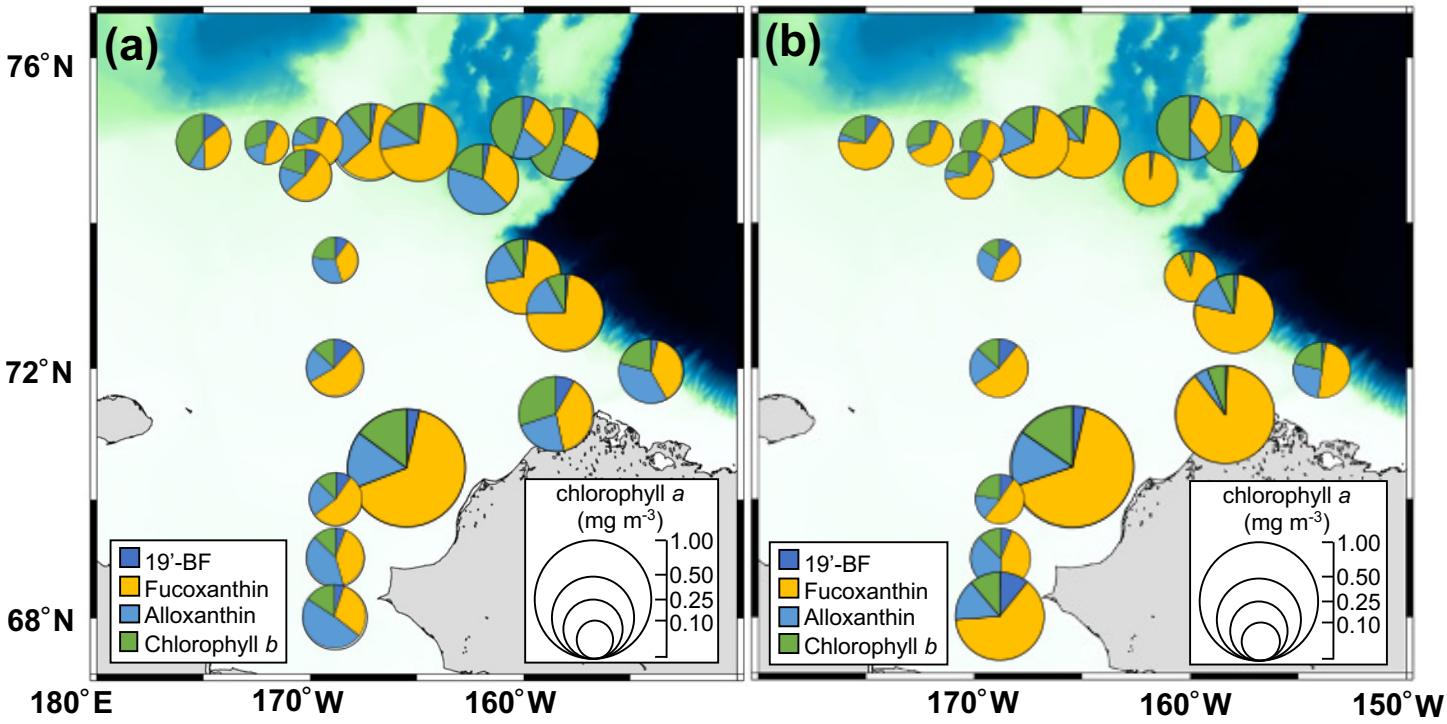

Figure 6.3. Chlorophyll *a* concentration and the contributions of major algal diagnostic pigments to the chlorophyll *a* biomass in the (a) surface and (b) sub-surface layers (SSL) over the study area.

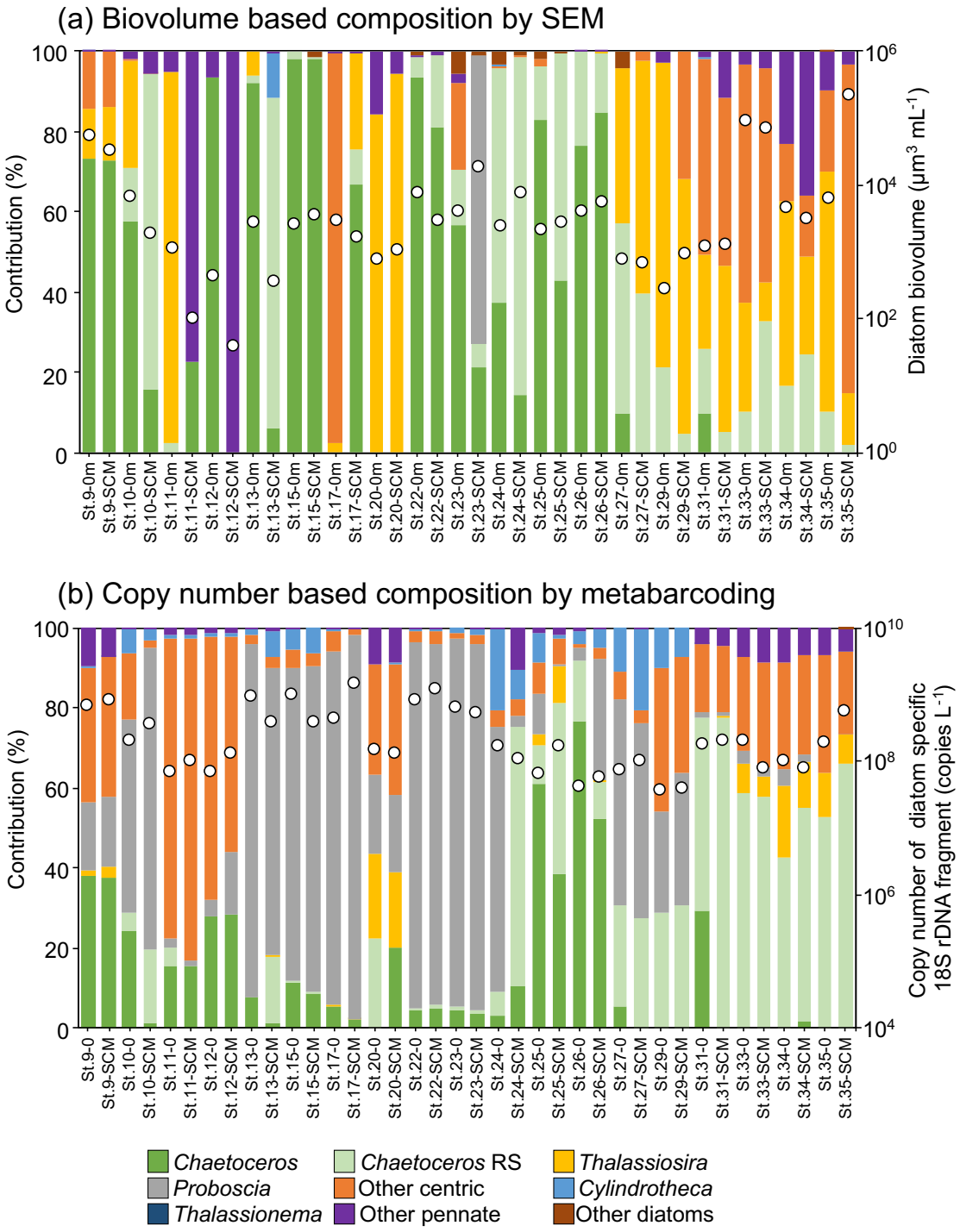

Figure 6.4. (a) Diatom biovolume (μm^3 mL^{-1}) and genus composition estimated by SEM analysis. (b) Copy number of diatom specific 18S rDNA fragment (copies L^{-1}) and the diatom composition at the genus level estimated by DNA metabarcoding. Note that *Chaetoceros* resting spores (RS) were estimated using the biovolume data by SEM analysis (see the text).

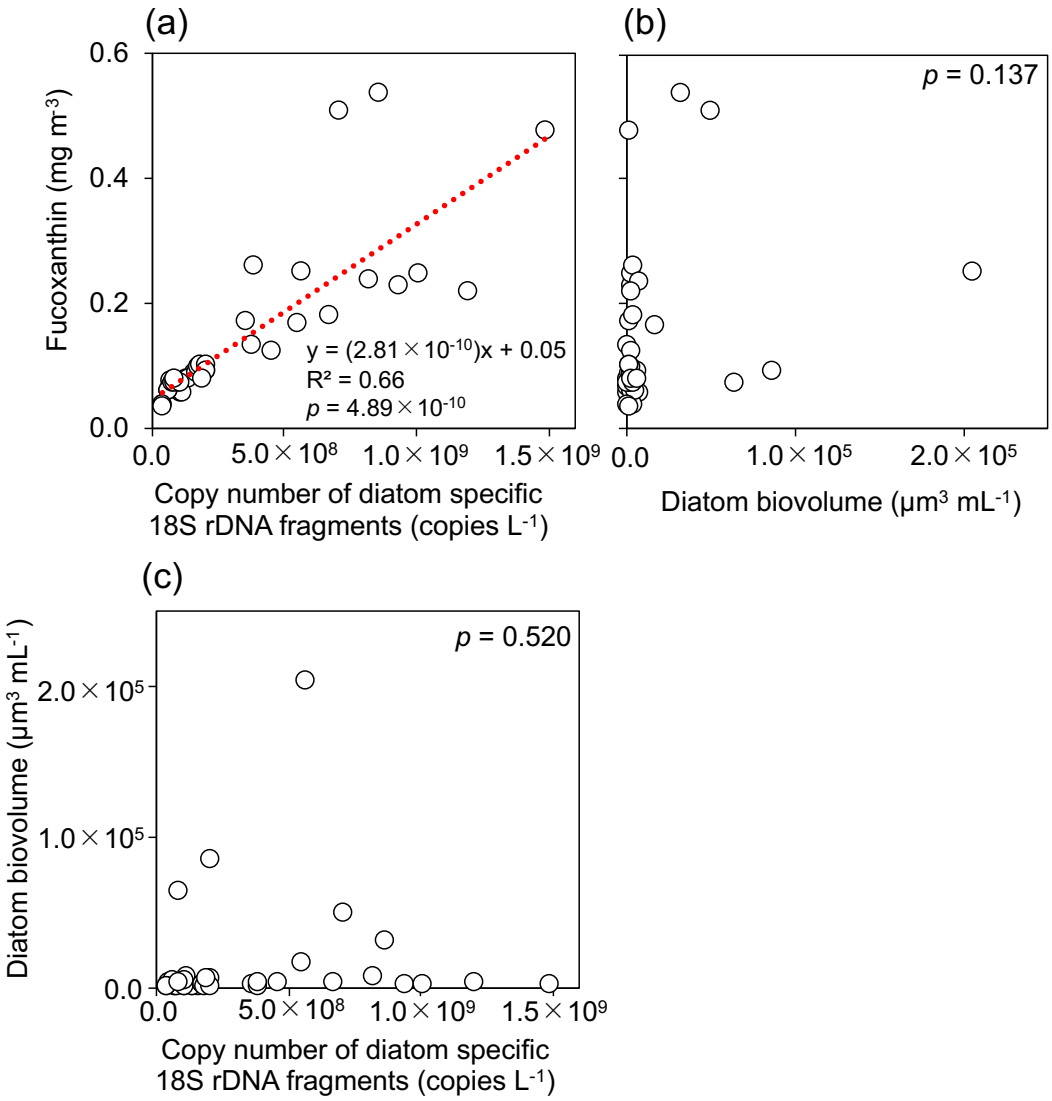

Figure 6.5. Relationship between the copy number of diatom specific 18S rDNA fragments (copies L^{-1}) and fucoxanthin concentration (mg m^{-3}) (a), diatom biovolume (μm^3 mL^{-1}) and fucoxanthin concentration (mg m^{-3}) (b), and the copy number of diatom specific 18S rDNA fragments (copies L^{-1}) and diatom biovolume (μm^3 mL^{-1}) (c).

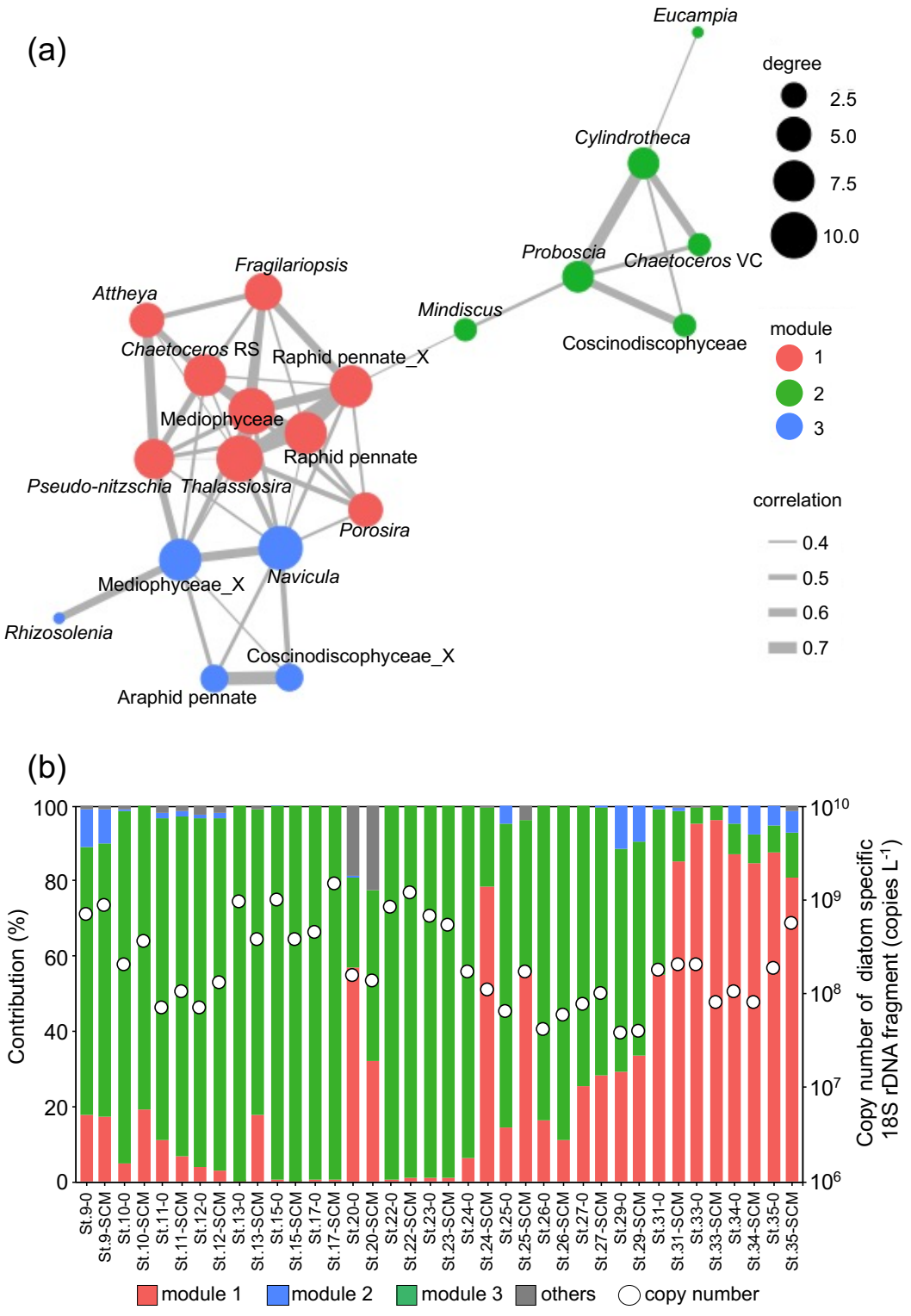

Figure 6.6. (a) The results of correlation-network analysis. Colors indicate each module members. Edge width and node size represent the correlation coefficient and the number of connections (i.e., degrees), respectively. (b) Copy number of diatom specific 18S rDNA fragments (copies L^{-1}) and module composition at the surveyed stations.

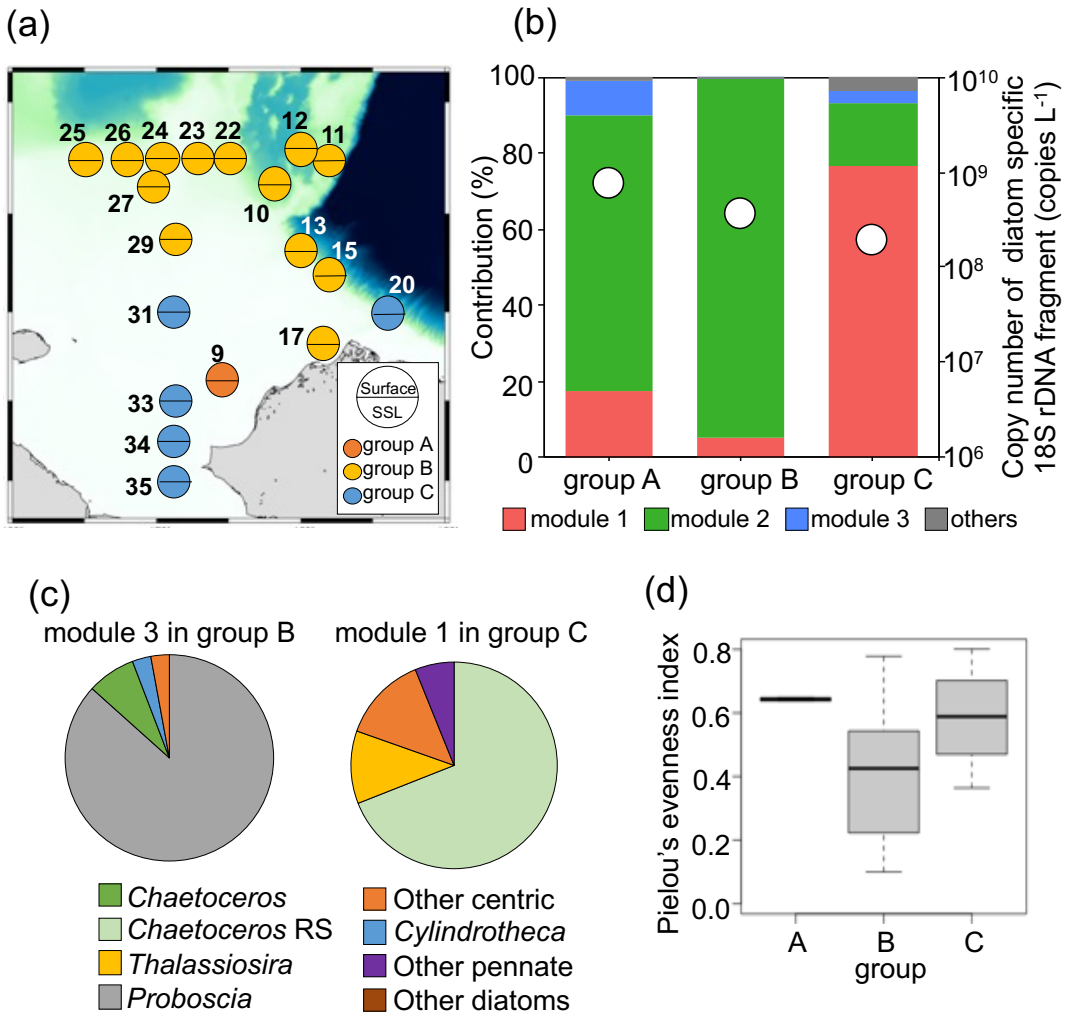

Figure 6.7. (a) Distribution of diatom groups (groups A–C) classified by a cluster analysis. (b) Copy number of diatom specific 18S rDNA fragments (copies L^{-1}) and module composition in each diatom group. (c) Detailed composition of diatoms in the dominant modules for each group (i.e., module 3 and 1 in group B and C, respectively). (d) Pielou's evenness (*J*) index of each group. The differences were evaluated by Kruskal-Wallis and post hoc Steel-Dwass tests, and *J* index was lower in group B than groups A and C ($p < 0.05$).

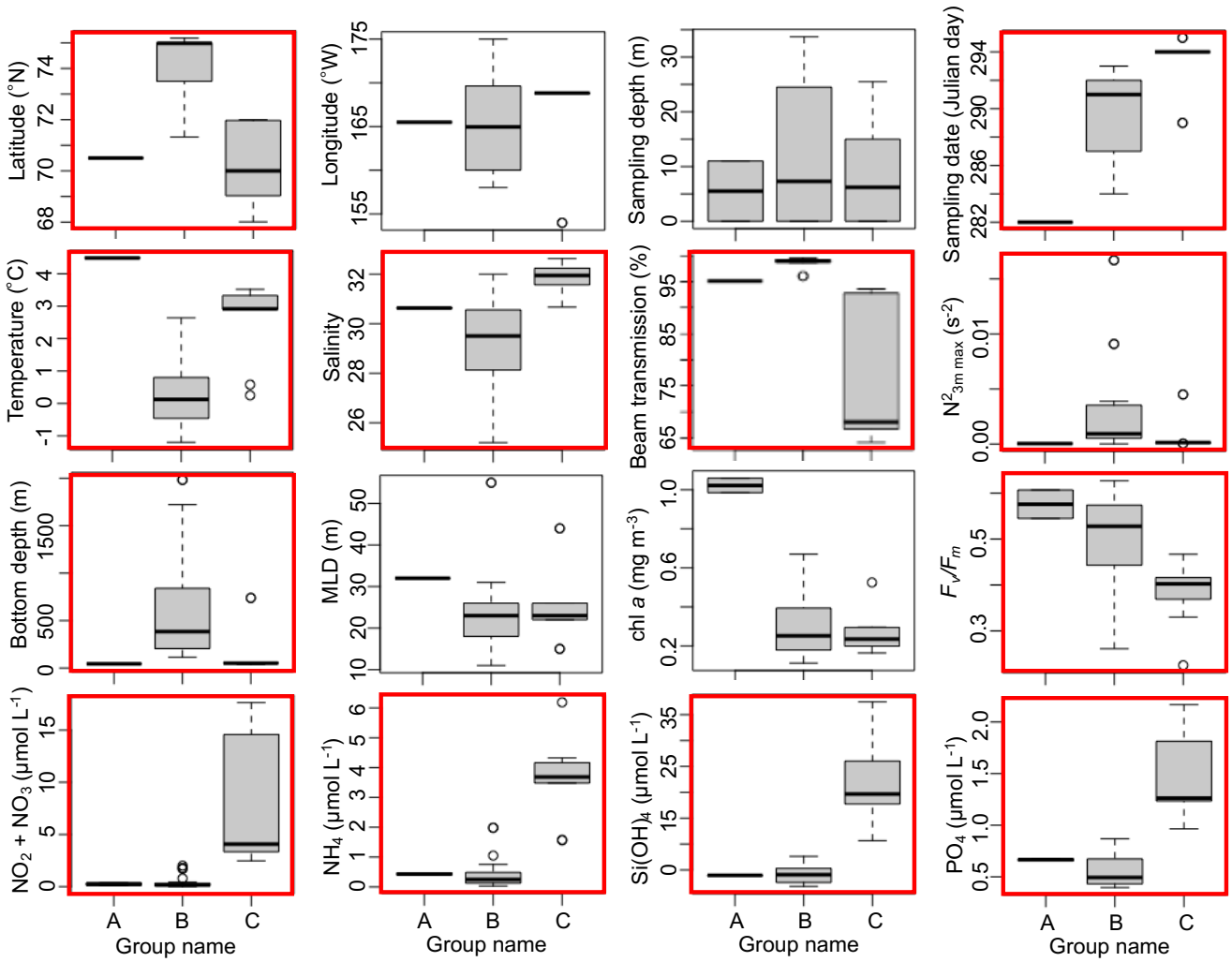

Figure 6.8. Environmental and physiological parameters of each group. The differences were evaluated by Kruskal-Wallis test and post hoc Steel-Dwass tests. Red boxes indicated significant differences among groups. See Table 2 for the detail results of the differences.

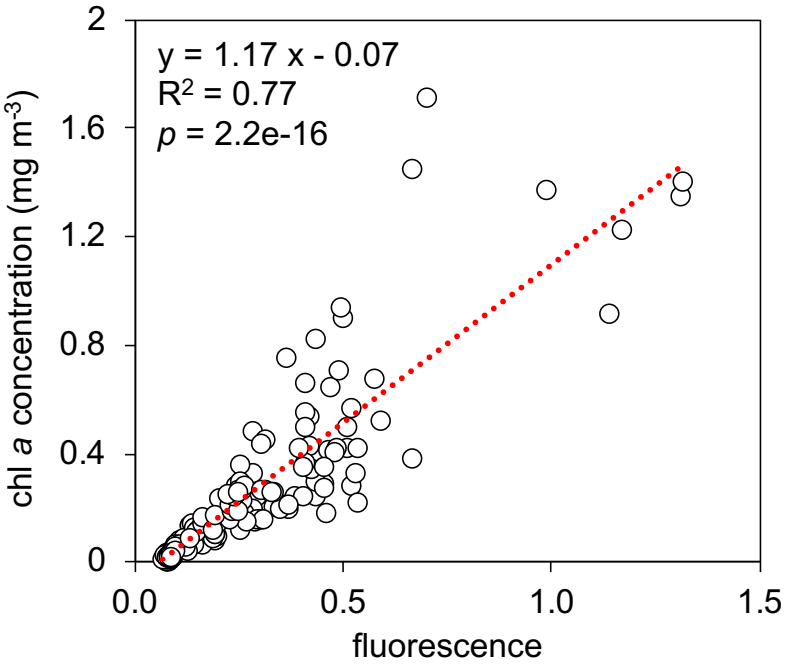

Figure S6.1. Relationship between the chlorophyll *a* (chl *a*) concentration and the *in vivo* fluorescence. For the measurement of chl *a* concentration, seawater of 250 mL was filtered onto ADVANTEC GF-75 glass-fiber filters under a gentle vacuum (< 0.02MPa) and chl *a* was immediately extracted in *N,N*-dimethylformamide (DMF) at -20 °C over 24 hours. When prompt chl *a* analyses was infeasible, the filters were immediately stored at −80°C until extraction. Chl *a* concentrations were determined using a fluorometer (10-AU-015-CE, TURNER DESIGNS, USA).

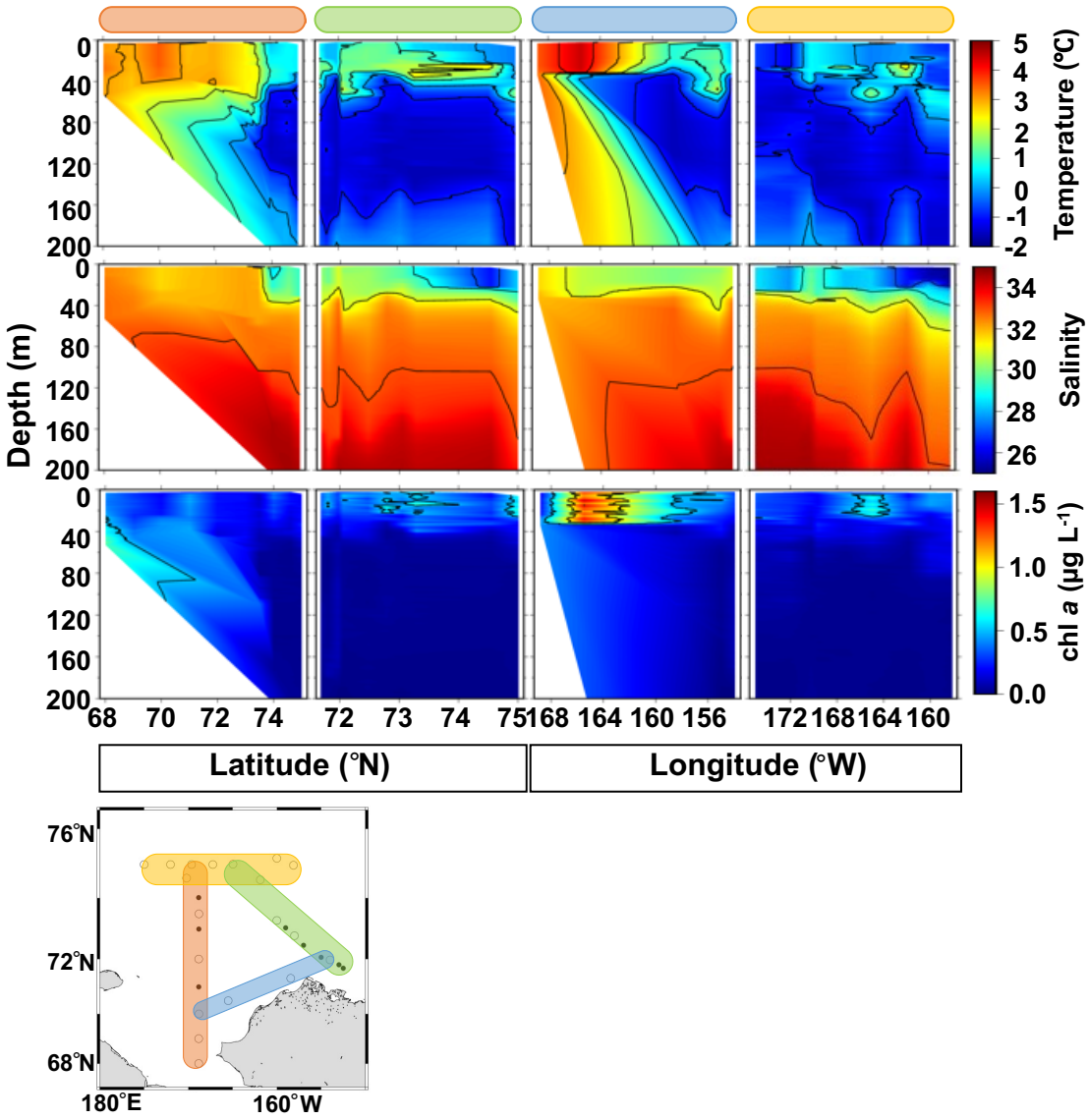

Figure S6.2. Cross-sectional distribution patterns of the temperature, salinity, and chlorophyll *a* (chl *a*) concentrations. Note that chl *a* concentrations were estimated from the *in vivo* fluorescence using the relationship found in Figure S6.1.

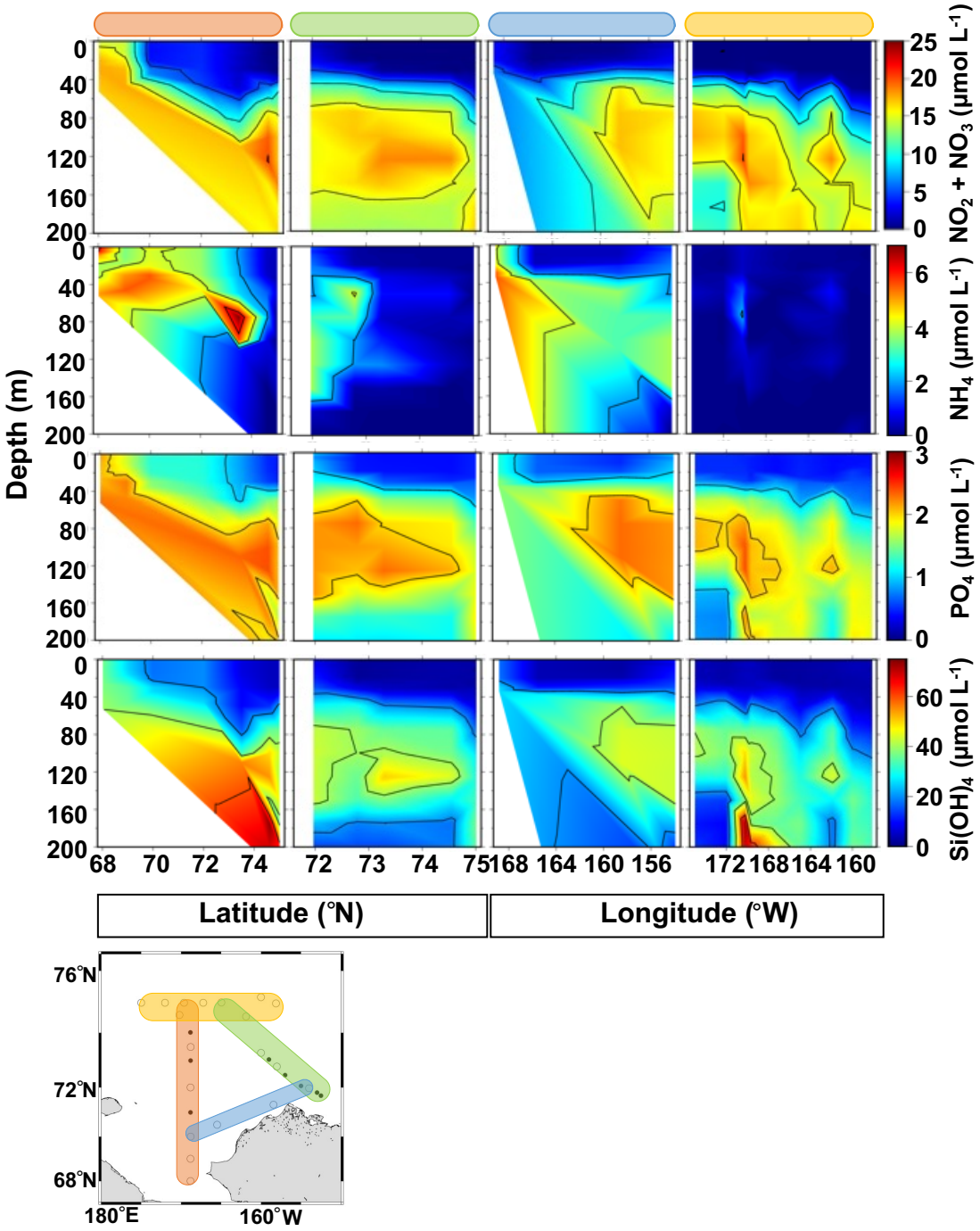

Figure S6.3. Cross-sectional distribution patterns of nutrient (NO_2 + NO_3, NH_4, PO_4, and Si $(OH)_4$) concentrations.

CHAPTER 7 – General conclusions and perspectives

The Pacific Arctic region has faced changes in sea ice dynamics (e.g., Markus et al., 2009; Grebmeier et al., 2015; Frey et al., 2018). Although previous studies suggested that the timing of sea ice retreat affected the timing and magnitude of phytoplankton bloom (Hunt et al., 2002; Fujiwara et al., 2016), we proposed that its timing could impact the bloom-forming diatom communities at the species or genus levels from early spring to summer. (Chapters 2, 3, and 4). In particular, the relative abundance of ice algal diatoms during the spring bloom would decrease when sea ice retreats earlier. According to Wang et al. (2015), zooplankton in the Bering Sea relied on ice algae as the primary food source for up 72% of organic matter when water column phytoplankton were unavailable, whereas predicted increases in the water column phytoplankton production may help offset the expected reduction in ice algal production. Abe et al. (2013) showed that carbon assimilation efficiencies by copepods varied with diatom species in the subarctic Pacific. Therefore, as a future study, we should consider the influence of changes in diatom species composition on energy transfer efficiency in marine ecosystems quantitatively.

One of the key outcomes of the present study was the unraveling of dominant primary producers in the broad Pacific Arctic shelf region, including the northern Bering, Chukchi, and Beaufort Seas (chapter 4). The analysis of sediment diatom communities indicated that the dominant bloom-forming diatoms changed spatiotemporally from ice-associated species to open-water ones. In addition, due to the unique characteristics of the Pacific Arctic region with a shallow shelf, high productivity, and the high POC sinking flux, viable diatoms in sediments would become a proxy for the blooms and primary production in the water column. However, several uncertainties remain in the results. Firstly, some diatom species, especially pennate diatoms, have not been reported to form resting stages (McQuoid and Hobson, 1996), and their lifetime is still unknown. Indeed, sediment trap data by Lalande et al. (2020) in the Chukchi Sea suggest that the abundant *Nitzschia frigida* highly contributes to POC sinking fluxes. Still, we did not detect this species from the sediments. The sinking diatom composition in the sediment samples is generally analyzed using light microscopy, and whether the diatoms are viable has seldom been considered. In addition, the diatom resting stages are sometimes present as a tiny single cell, which could be underestimated when many particles are present in the samples. These uncertainties would make a difference between the sediment trap data and our results. Therefore,

as future work, we should attempt to estimate the percentages of viable diatoms sinking particles, especially after the bloom, and differences in lifetime among diatom species or genera. A marine snow catcher, an instrument to collect sinking particles, is also helpful during the spring bloom (Giering et al., 2016). In addition, DNA metabarcoding used in chapter 6, would become a powerful technique to investigate the diatom communities in sediments comprehensively (Piredda et al., 2017a). Secondly, the validity of assessing the year-to-year changes using the surface sediments should be improved. Our study in chapter 3 showed the two-year viable diatom shift in composition, thanks to the facts that the southern St. Lawrence Island region is a polynya, where open water is surrounded by sea ice, and the succession of viable diatom community in the surface sediments can be made after the sea ice retreat. Although the other shallow Pacific Arctic regions, such as the Chukchi Sea, could also experience vertical mixing by strong winds and cooling from autumn to early winter, there was no evidence that the diatom community in sediments was reset during winter by the physical process. A method to confirm it may be an investigation of sediment diatom communities during winter, although there are many challenges because of the seasonal sea ice areas. Furthermore, based on *in situ* observations, we need to pile up evidence of the significant relationship between sea ice and diatom community dynamics in sediments. Therefore, we should continue samplings and assessing viable diatom communities in sediments over the Pacific Arctic shelf for many years. Suppose we establish more reliability by using viable diatoms in sediments when assessing the diatom community dynamics. In that case, it becomes a more valuable method to comprehensively evaluate the experienced blooms in the Pacific Arctic, where the investigation period is limited.

The present study also emphasizes the ability of diatoms accumulated in sediments of the Chukchi Sea. Viable diatoms distributed in sediments with high abundance in the productive Pacific Arctic region could quickly respond to light exposure within 24 hours, and their photophysiology was acclimated to a higher light condition quickly (chapter 5). A recent study shows that the bottom-associated microalgal bloom occurred in the Chukchi Sea because sufficient light reached the seafloor underlying nutrient-rich bottom during late summer (Shiozaki et al., 2022). Although the maximum light intensity that could reach the sea bottom with 7.5 μmol photons m^{-2} s^{-1} during summer (Shiozaki et al., 2022) was lower than that of our experiments (30 μmol photons m^{-2} s^{-1}), their results were consistent with ours. In addition, sediment-laden sea ice is spread in this region (Waga et al., 2022). Thus, viable diatoms in the sediment-laden sea ice

could obtain sufficient light for photosynthesis during the sea ice melt. Another opportunity for viable diatoms in sediments to resume growing is the resuspension of sediments. The number of extreme wind events during September and October has been increasing in the Arctic (Ardyna et al., 2014). As a result, wind-driven mixing and following autumn bloom dominated by diatoms were reported in the Chukchi Sea (Nishino et al., 2015; Yokoi et al., 2016). We also suggested that diatoms, including abundant resting stages, would be resuspended from the seafloor to the surface in the southern Chukchi Sea during October (chapter 6). Because the maximum intensity of photosynthetically active radiation (PAR) measured on deck during the cruise was ca. 600 μmol photons m^{-2} s^{-1}, our results suggest that diatoms in sediments would resume growing in the sunlit surface layer through the resuspension process. Viable diatoms in sediments with high photophysiological plasticity would potentially initiate blooms in the Pacific Arctic. We, however, have not obtained evidence of how significant the impact of viable diatoms in sediments is on primary production. In addition, underwater optical properties in the Pacific Arctic region are also still scarce. Thus, as one of our future studies, we should aim to quantify how critically viable diatoms in sediments contribute to primary production in the Pacific Arctic region, along with environmental data.

Regarding seasonal diatom dynamics in the Pacific Arctic region, we found that the spring and summer communities were sensitive to the sea ice dynamics, and the diatoms in sediments could be transported to the surface and subsurface layers during autumn (Figure 7.1). However, little is known about how diatoms survive in winter when their photosynthetic capability is limited. In addition, the fate of autumn diatoms is unclear – some of them would overwinter and become seeds for the spring bloom. Therefore, we need to investigate the algal community under the sea ice and the incorporation processes of algae into the sea ice to uncover the diatom community dynamics throughout the year. For future field-based process studies, continued observations under and within sea ice would be mandatory to elucidate the seasonal variability of algal communities in the changing Arctic.

In conclusion, the Pacific Arctic, especially the northern Bering and Chukchi Seas, shows high productivity, followed by enhanced POC sinking fluxes. This downward process is known as the pelagic-benthic coupling and supports the marine ecosystems in this region (Grebmeier et al., 1988, 2006). Our results supported the previous studies: abundant diatoms, as major primary producers, sink to the bottom, and accumulate on the seafloor, especially in the

productive regions. On the other hand, this study emphasized that the diatom communities were probably affected by sea ice dynamics. Additionally, the accumulated diatoms in the seafloor could be resuspended to the euphotic layers during autumn. We revealed that diatoms in surface sediments quickly respond to light exposure and have high photophysiological plasticity even after a long darkness, suggesting that they can contribute to primary production in the Pacific Arctic shelf, as discussed above. Therefore, the present study has, for the first time, shed light on the importance of the upward biogeochemical process of sedimentary diatoms in the Pacific Arctic.

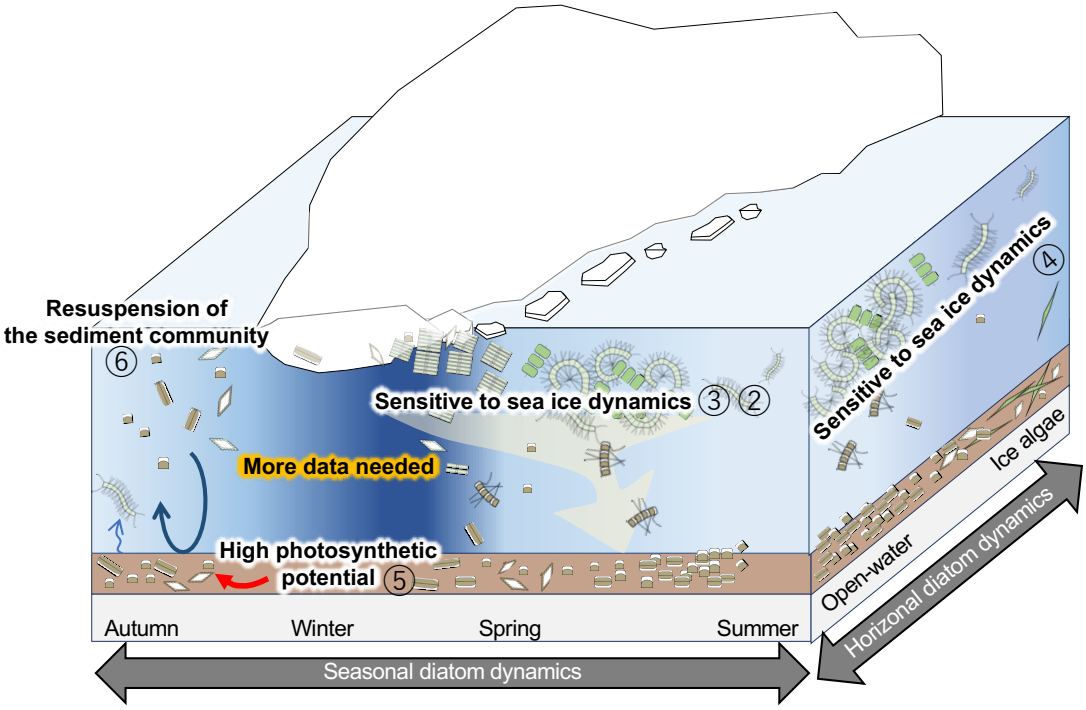

Figure 7.1. A schematic of diatom community dynamics in the Pacific Arctic region, revealed by the present study. The circled numbers in this figure refer to the chapter numeral(s) illustrating each topic in the thesis.

Acknowledgments

I would like to express my sincere thanks to my supervisor Prof. Koji Suzuki for his continuous support and numerous suggestions. I have learned the importance of having physiological and biogeochemical views when studying the ocean. His support and discussion with him made it possible for me to continue my research for three years amid the COVID-19 pandemic. My sincere thanks also go to my master's supervisor Dr. Kohei Matsuno for his kind support even after entering a Ph.D. course at the Graduate School of Environmental Science. The Arctic cruise in 2020 using the R/V *Mirai*, in which he gave me a chance to be on board, took my Ph.D. research forward. I am also grateful to my undergraduate supervisor Prof. Ichiro Imai for allowing me to start studying diatoms and their resting stages. I would also like to thank Prof. Atsushi Yamaguchi for allowing me to participate in the T/S *Oshoro-maru* cruises and for suggesting staying at the Woods Hole Oceanographic Institution (WHOI). My sincere appreciation goes to Prof. Donald M. Anderson and the members of Anderson Laboratory for allowing me to study at WHOI and for every kind of support during my stay. All my experiences at Woods Hole were wonderful, driving me to the Ph.D. course. I would also like to thank Dr. Amane Fujiwara for supporting my research by analyzing satellite data and giving many valuable comments. I would like to express my gratitude to Prof. Jun Nishioka, Prof. Sohiko Kameyama, and Prof. Tomohisa Irino for their insightful comments and helpful suggestions for my Ph.D. dissertation. In particular, I would appreciate valuable advice and useful comments on my master's and Ph.D. dissertations from Prof. Toru Hirawake. I am deeply grateful to Ms. Akiko Kamimura for analyzing my pigment samples, helping with many laboratory experiments, and always looking out for me. I thank officers, crews, and researchers on board the T/S *Oshoro-maru*, the U.S. Coast Guard icebreaker *Healy*, and R/V *Mirai* for their tremendous efforts during the field sampling. Thanks are extended to everyone in the Marine and Atmospheric Geochemistry (MAG) group, especially people at the Suzuki Laboratory. Finally, I would like to express the deepest thanks to my parents, brother, and sisters for their unlimited support and encouragement.

References

Abe, H., Nomura, D., and Hirawake, T. (2021). Salinity regime of the northwestern Bering Sea shelf. *Prog. Oceanogr.* 198, 102675. doi: 10.1016/j.pocean.2021.102675.

Abe, H., Sampei, M., Hirawake, T., Waga, H., Nishino, S., and Ooki, A. (2019). Sediment-associated phytoplankton release from the seafloor in response to wind-induced barotropic currents in the Bering Strait. *Front. Mar. Sci.* 6, 97. doi: 10.3389/fmars.2019.00097.

Abe, Y., Natsuike, M., Matsuno, K., Terui, T., Yamaguchi, A., and Imai, I. (2013). Variation in assimilation efficiencies of dominant Neocalanus and Eucalanus copepods in the subarctic Pacific: Consequences for population structure models. *J. Exp. Mar. Biol. Ecol.* 449, 321–329. doi: 10.1016/j.jembe.2013.10.023.

Anderson, D. M., Fachon, E., Pickart, R. S., Lin, P., Fischer, A. D., Richlen, M. L., et al. (2021). Evidence for massive and recurrent toxic blooms of *Alexandrium catenella* in the Alaskan Arctic. *Proc. Natl. Acad. Sci.* 118, e2107387118. doi: 10.1073/pnas.2107387118.

Anderson, O. R. (1975). The ultrastructure and cytochemistry of resting cell formation in *Amphora coffaeformis* (bacillariophyceae)1. *J. Phycol.* 11, 272–281. doi: 10.1111/j.1529-8817.1975.tb02778.x.

Ardyna, M., and Arrigo, K. R. (2020). Phytoplankton dynamics in a changing Arctic Ocean. *Nat. Clim. Change* 10, 892–903. doi: 10.1038/s41558-020-0905-y.

Ardyna, M., Babin, M., Gosselin, M., Devred, E., Rainville, L., and Tremblay, J.-É. (2014). Recent Arctic Ocean sea ice loss triggers novel fall phytoplankton blooms. *Geophys. Res. Lett.* 41, 6207–6212. doi: 10.1002/2014GL061047.

Arrigo, K. R. (2017). "Sea ice as a habitat for primary producers," in *Sea Ice*, ed. D. N. Thomas (John Wiley & Sons, Ltd), 352–369. doi: 10.1002/9781118778371.ch14.

Arrigo, K. R., van Dijken, G., and Pabi, S. (2008). Impact of a shrinking Arctic ice cover on marine primary production. *Geophys. Res. Lett.* 35, L19603. doi: 10.1029/2008GL035028.

Babin, M., Morel, A., and Gagnon, R. (1994). An incubator designed for extensive and sensitive measurements of phytoplankton photosynthetic parameters. *Limnol. Oceanogr.* 39, 694–702. doi: 10.4319/lo.1994.39.3.0694.

Bar-On, Y. M., Phillips, R., and Milo, R. (2018). The biomass distribution on Earth. *Proc. Natl. Acad. Sci.* 115, 6506–6511. doi: 10.1073/pnas.1711842115.

Blankenship, E. R. (2014). *Molecular mechanisms of photosynthesis.* 2nd edition. New Jersey: John Wiley & Sons, Inc.

Bolyen, E., Rideout, J. R., Dillon, M. R., Bokulich, N. A., Abnet, C. C., Al-Ghalith, G. A., et al. (2019). Reproducible, interactive, scalable and extensible microbiome data science using QIIME 2. *Nat. Biotechnol.* 37, 852–857. doi: 10.1038/s41587-019-0209-9.

Boveng, P. L., Ziel, H. L., McClintock, B. T., and Cameron, M. F. (2020). Body condition of phocid seals during a period of rapid environmental change in the Bering Sea and Aleutian Islands, Alaska. *Deep Sea Res. Part II Top. Stud. Oceanogr.* 181–182, 104904. doi: 10.1016/j.dsr2.2020.104904.

Brock, T. D. (1981). Calculating solar radiation for ecological studies. *Ecol. Model.* 14, 1–19. doi: 10.1016/0304-3800(81)90011-9.

Brown, M. R., Jeffrey, S. W., Volkman, J. K., and Dunstan, G. A. (1997). Nutritional properties of microalgae for mariculture. *Aquaculture* 151, 315–331. doi: 10.1016/S0044-8486(96)01501-3.

Brown, T. A., and Belt, S. T. (2012). Identification of the sea ice diatom biomarker IP25 in Arctic benthic macrofauna: direct evidence for a sea ice diatom diet in Arctic heterotrophs. *Polar Biol.* 35, 131–137. doi: 10.1007/s00300-011-1045-7.

Brunet, C., Johnsen, G., Lavaud, J., and Roy, S. (2011). "Pigments and photoacclimation processes," in *Phytoplankton pigments: characterization, chemotaxnomy and applications in oceanography*, eds. S. Roy, C. A. Llewellyn, E. S. Egeland, and G. Johnsen (New York: Cambridge University Press), 445–471.

Buck, J. M., Wünsch, M., Schober, A. F., Kroth, P. G., and Lepetit, B. (2022). Impact of Lhcx2 on acclimation to low iron conditions in the diatom *Phaeodactylum tricornutum*. *Front. Plant Sci.* 13, 841058.

Callahan, B. J., McMurdie, P. J., Rosen, M. J., Han, A. W., Johnson, A. J. A., and Holmes, S. P. (2016). DADA2: High-resolution sample inference from Illumina amplicon data. *Nat. Methods* 13, 581–583. doi: 10.1038/nmeth.3869.

Campbell, K., Mundy, C. J., Belzile, C., Delaforge, A., and Rysgaard, S. (2018). Seasonal dynamics of algal and bacterial communities in Arctic sea ice under variable snow cover. *Polar Biol.* 41, 41–58. doi: 10.1007/s00300-017-2168-2.

Campbell, R. G., Ashjian, C. J., Sherr, E. B., Sherr, B. F., Lomas, M. W., Ross, C., et al. (2016). Mesozooplankton grazing during spring sea-ice conditions in the eastern Bering Sea. *Deep Sea Res. Part II Top. Stud. Oceanogr.* 134, 157–172. doi: 10.1016/j.dsr2.2015.11.003.

Campbell, R. G., Sherr, E. B., Ashjian, C. J., Plourde, S., Sherr, B. F., Hill, V., et al. (2009). Mesozooplankton prey preference and grazing impact in the western Arctic Ocean. *Deep Sea Res. Part II Top. Stud. Oceanogr.* 56, 1274–1289. doi: 10.1016/j.dsr2.2008.10.027.

Coachman, L. K., Coachman, L. K., Aagaard, K., and Tripp, R. B. (1975). *Bering Strait: The Regional Physical Oceanography.* University of Washington Press.

Cohen, J. H., Berge, J., Moline, M. A., Johnsen, G., and Zolich, A. P. (2020). "Light in the polar night," in *POLAR NIGHT Marine Ecology*, eds. J. Berge, G. Johnsen, and J. H. Cohen (Switzerland: Springer, Cham), 37–66.

Cooper, L. W., Savvichev, A. S., and Grebmeier, J. M. (2015). Abundance and production rates of heterotrophic bacterioplankton in the context of sediment and water column processes in the Chukchi Sea. *Oceanography* 28, 84–99.

Cornwall, W. (2019). Vanishing Bering Sea ice poses climate puzzle. *Science* 364, 616–617. doi: 10.1126/science.364.6441.616.

Cota, G. F. (1985). Photoadaptation of high Arctic ice algae. *Nature* 315, 219–222. doi: 10.1038/315219a0.

Cota, G. F., and Home, E. (1989). Physical control of arctic ice algal production. *Mar. Ecol. Prog. Ser.* 52, 111–121. doi: 10.3354/meps052111.

Cota, G. F., Legendre, L., Gosselin, M., and Ingram, R. G. (1991). Ecology of bottom ice algae: I. Environmental controls and variability. *J. Mar. Syst.* 2, 257–277. doi: 10.1016/0924-7963(91)90036-T.

Cota, G. F., and Smith, R. E. H. (1991). Ecology of bottom ice algae: II. Dynamics, distributions and productivity. *J. Mar. Syst.* 2, 279–295. doi: 10.1016/0924-7963(91)90037-U.

Cota, G. F., Wang, J., and Comiso, J. C. (2004). Transformation of global satellite chlorophyll retrievals with a regionally tuned algorithm. *Remote Sens. Environ.* 90, 373–377. doi: 10.1016/j.rse.2004.01.005.

Dahl, E., and Naustvoll, L. J. (2010). "Filtering – semitransparent filters for quantitative phytoplankton analysis," in *Microscopic and molecular methods for quantitative phytoplankton analysis.*, eds. B. Karlson, C. Cusack, and E. Bresnan (Paris: UNESCO), 37–39. doi: 10.25607/OBP-1371.

Danielson, S., Eisner, L., Weingartner, T., and Aagaard, K. (2011). Thermal and haline variability over the central Bering Sea shelf: Seasonal and interannual perspectives. *Cont. Shelf Res.* 31, 539–554. doi: 10.1016/j.csr.2010.12.010.

Danielson, S. L., Ahkinga, O., Ashjian, C., Basyuk, E., Cooper, L. W., Eisner, L., et al. (2020). Manifestation and consequences of warming and altered heat fluxes over the Bering and Chukchi Sea continental shelves. *Deep Sea Res. Part II Top. Stud. Oceanogr.* 177, 104781. doi: 10.1016/j.dsr2.2020.104781.

Danielson, S. L., Eisner, L., Ladd, C., Mordy, C., Sousa, L., and Weingartner, T. J. (2017). A comparison between late summer 2012 and 2013 water masses, macronutrients, and

phytoplankton standing crops in the northern Bering and Chukchi Seas. *Deep Sea Res. Part II Top. Stud. Oceanogr.* 135, 7–26. doi: 10.1016/j.dsr2.2016.05.024.

Davis, C. O., Hollibaugh, J. T., Seibert, D. L. R., Thomas, W. H., and Harrison, P. J. (1980). Formation of resting spores by *Leptocylindrus danicus* (bacillariophyceae) in a controlled experimental ecosystem. *J. Phycol.* 16, 296–302. doi: 10.1111/j.1529-8817.1980.tb03034.x.

de Vargas, C., Audic, S., Henry, N., Decelle, J., Mahé, F., Logares, R., et al. (2015). Eukaryotic plankton diversity in the sunlit ocean. *Science* 348, 1261605. doi: 10.1126/science.1261605.

Drebes, G. (1966). On the life history of the marine plankton diatom *Stephanopyxis palmeriana*. *Helgoländer Wiss. Meeresunters*. 13, 101–114. doi: 10.1007/BF01612659.

Dubinsky, Z. (1980). "Light utilization efficiency in natural marine phytoplankton communities," in *Primary Productivity in the Sea*, ed. P. G. Falkowski (New York: Plenum Press), 83–89.

Duffy-Anderson, J. T., Stabeno, P., Andrews III, A. G., Cieciel, K., Deary, A., Farley, E., et al. (2019). Responses of the Northern Bering Sea and Southeastern Bering Sea pelagic ecosystems following record-breaking low winter sea ice. *Geophys. Res. Lett.* 46, 9833–9842. doi: 10.1029/2019GL083396.

Durbin, E. G. (1978). Aspects of the biology of resting spores of *Thalassiosira nordenskioeldii* and *Detonula confervacea*. *Mar. Biol.* 45, 31–37. doi: 10.1007/BF00388975.

Edler, L., and Elbrächter, M. (2010). "The Utermöhl method for quantitative phytoplankton analysis," in *Microscopic and Molecular Methods for Quantitative Phytoplankton Analysis*, eds. B. Karlson, C. Cusack, and E. Bresnan (Paris: UNESCO), 13–20.

Edwards, K. F., Thomas, M. K., Klausmeier, C. A., and Litchman, E. (2015). Light and growth in marine phytoplankton: allometric, taxonomic, and environmental variation. *Limnol. Oceanogr.* 60, 540–552. doi: 10.1002/lno.10033.

Endo, H., Ogata, H., and Suzuki, K. (2018). Contrasting biogeography and diversity patterns between diatoms and haptophytes in the central Pacific Ocean. *Sci. Rep.* 8, 10916. doi: 10.1038/s41598-018-29039-9.

Endo, H., Umezawa, Y., Takeda, S., and Suzuki, K. (2022). Haptophyte communities along the Kuroshio Current reveal their geographical sources and ecological traits. *Mol. Ecol.* doi: 10.1111/mec.16734.

Endo, H., Yoshimura, T., Kataoka, T., and Suzuki, K. (2013). Effects of CO_2 and iron availability on phytoplankton and eubacterial community compositions in the northwest subarctic Pacific. *J. Exp. Mar. Biol. Ecol.* 439, 160–175. doi: 10.1016/j.jembe.2012.11.003.

Falkowski, P. G., and Raven, J. A. (2007). *Aquatic Photosynthesis*. Second edition. Princeton University Press.

Field, C. B., Behrenfeld, M. J., Randerson, J. T., and Falkowski, P. (1998). Primary production of the biosphere: integrating terrestrial and oceanic components. *Science* 281, 237–240. doi: 10.1126/science.281.5374.237.

Field, J., Clarke, K., and Warwick, R. (1982). A practical strategy for analysing multispecies distribution patterns. *Mar. Ecol. Prog. Ser.* 8, 37–52. doi: 10.3354/meps008037.

French III, F. W., and Hargraves, P. E. (1985). Spore formation in the life cycles of the diatoms *Chaetoceros diadema* and *Leptocylindrus danicus*. *J. Phycol.* 21, 477–483. doi: 10.1111/j.0022-3646.1985.00477.x.

Frey, K. E., Comiso, J. C., Cooper, L. W., Grebmeier, J. M., and Stock, L. V. (2018). "Arctic Ocean primary productivity: The response of marine algae to climate warming and sea ice decline", in *Arctic Report Card. Arctic Region 2018*. Available at: http://www.arctic.noaa.gov/ reportcard

Frost, K. J., and Lowry, L. F. (1984). "Trophic relationships of vertebrate consumers in the Alaskan Beaufort Sea," in *The Alaskan Beaufort Sea*: Ecosystems and Environments (Florida: Academic Press), 381–401.

Fry, B., and Wainright, S. C. (1991). Diatom sources of 13 C-rich carbon in marine food webs. *Mar. Ecol. Prog. Ser.* 76, 149–157.

Fujiwara, A., Hirawake, T., Suzuki, K., Eisner, L., Imai, I., Nishino, S., et al. (2016). Influence of timing of sea ice retreat on phytoplankton size during marginal ice zone bloom period on the Chukchi and Bering shelves. *Biogeosciences* 13, 115–131. doi: 10.5194/bg-13-115-2016.

Fujiwara, A., Hirawake, T., Suzuki, K., Imai, I., and Saitoh, S.-I. (2014). Timing of sea ice retreat can alter phytoplankton community structure in the western Arctic Ocean. *Biogeosciences* 11, 1705–1716. doi: 10.5194/bg-11-1705-2014.

Garibotti, I. A., Vernet, M., Kozlowski, W. A., and Ferrario, M. E. (2003). Composition and biomass of phytoplankton assemblages in coastal Antarctic waters: a comparison of chemotaxonomic and microscopic analyses. *Mar. Ecol. Prog. Ser.* 247, 27–42. doi: 10.3354/meps247027.

Giering, S. L. C., Sanders, R., Martin, A. P., Lindemann, C., Möller, K. O., Daniels, C. J., et al. (2016). High export via small particles before the onset of the North Atlantic spring bloom. *J. Geophys. Res. Oceans* 121, 6929–6945. doi: 10.1002/2016JC012048.

Giesbrecht, K. E., Varela, D. E., Wiktor, J., Grebmeier, J. M., Kelly, B., and Long, J. E. (2019). A decade of summertime measurements of phytoplankton biomass, productivity and assemblage composition in the Pacific Arctic Region from 2006 to 2016. *Deep*

Sea Res. Part II Top. Stud. Oceanogr. 162, 93–113. doi: 10.1016/j.dsr2.2018.06.010.

Gilstad, M., and Sakshaug, E. (1990). Growth rates of ten diatom species from the Barents Sea at different irradiances and day lengths. *Mar. Ecol. Prog. Ser.* 64, 169–173. doi: 10.3354/meps064169.

Godhe, A., Asplund, M. E., Härnström, K., Saravanan, V., Tyagi, A., and Karunasagar, I. (2008). Quantification of diatom and dinoflagellate biomasses in coastal marine seawater samples by real-time PCR. *Appl. Environ. Microbiol.* 74, 7174–7182. doi: 10.1128/AEM.01298-08.

Goering, J. J., and Iverson, R. L. (1981). "Phytoplankton distribution on the Southeastern Bering Sea Shelf," in *The Eastern Bering Sea Shelf : oceanography and resources*, eds. D. W. Hood and J. A. Calder (Seattle: University of Washington), 933–946.

Goldman, J. C. (1993). Potential role of large oceanic diatoms in new primary production. *Deep Sea Res. Part Oceanogr. Res. Pap.* 40, 159–168. doi: 10.1016/0967-0637(93)90059-C.

Goss, R., Ann Pinto, E., Wilhelm, C., and Richter, M. (2006). The importance of a highly active and ΔpH-regulated diatoxanthin epoxidase for the regulation of the PS II antenna function in diadinoxanthin cycle containing algae. *J. Plant Physiol.* 163, 1008–1021. doi: 10.1016/j.jplph.2005.09.008.

Goss, R., and Lepetit, B. (2015). Biodiversity of NPQ. *J. Plant Physiol.* 172, 13–32. doi: 10.1016/j.jplph.2014.03.004.

Gosselin, M., Legendre, L., Therriault, J.-C., and Demers, S. (1990). Light and nutrient limitation of sea-ice microalgae (Hudson Bay, Canadian Arctic). *J. Phycol.* 26, 220–232. doi: https://doi.org/10.1111/j.0022-3646.1990.00220.x.

Gradinger, R. (2009). Sea-ice algae: Major contributors to primary production and algal biomass in the Chukchi and Beaufort Seas during May/June 2002. *Deep Sea Res. Part II Top. Stud. Oceanogr.* 56, 1201–1212. doi: 10.1016/j.dsr2.2008.10.016.

Grebmeier, J. M., Bluhm, B. A., Cooper, L. W., Danielson, S. L., Arrigo, K. R., Blanchard, A. L., et al. (2015). Ecosystem characteristics and processes facilitating persistent macrobenthic biomass hotspots and associated benthivory in the Pacific Arctic. *Prog. Oceanogr.* 136, 92–114. doi: 10.1016/j.pocean.2015.05.006.

Grebmeier, J. M., and Cooper, L. W. (1995). Influence of the St. Lawrence Island Polynya upon the Bering Sea benthos. *J. Geophys. Res. Oceans* 100, 4439–4460. doi: 10.1029/94JC02198.

Grebmeier, J. M., Cooper, L. W., Feder, H. M., and Sirenko, B. I. (2006). Ecosystem dynamics of the Pacific-influenced Northern Bering and Chukchi Seas in the Amerasian Arctic. *Prog. Oceanogr.* 71, 331–361. doi: 10.1016/j.pocean.2006.10.001.

Grebmeier, J. M., and Maslowski, W. (2014). "The Pacific Arctic Region: An Introduction," in *The Pacific Arctic Region: Ecosystem Status and Trends in a Rapidly Changing Environment*, eds. J. M. Grebmeier and W. Maslowski (Dordrecht: Springer Netherlands), 1–15. doi: 10.1007/978-94-017-8863-2_1.

Grebmeier, J. M., Moore, S. E., Cooper, L. W., and Frey, K. E. (2019). The Distributed Biological Observatory: A change detection array in the Pacific Arctic – An introduction. *Deep Sea Res. Part II Top. Stud. Oceanogr.* 162, 1–7. doi: 10.1016/j.dsr2.2019.05.005.

Grebmeier, J., McRoy, C., and Feder, H. (1988). Pelagic-benthic coupling on the shelf of the northern Bering and Chukchi Seas. I. Food supply source and benthic bio-mass. *Mar. Ecol. Prog. Ser.* 48, 57–67. doi: 10.3354/meps048057.

Guillard, R. R. L., and Ryther, J. H. (1962). Studies of marine planktonic diatoms. I. *Cyclotella nana* Hustedt, and *Detonula confervacea* (cleve) Gran. *Can. J. Microbiol.* 8, 229–239. doi: 10.1139/m62-029.

Guillou, L., Bachar, D., Audic, S., Bass, D., Berney, C., Bittner, L., et al. (2013). The Protist Ribosomal Reference database (PR2): a catalog of unicellular eukaryote Small Sub-Unit rRNA sequences with curated taxonomy. *Nucleic Acids Res.* 41, D597–D604. doi: 10.1093/nar/gks1160.

Hama, T., Miyazaki, T., Ogawa, Y., Iwakuma, T., Takahashi, M., Otsuki, A., et al. (1983). Measurement of photosynthetic production of a marine phytoplankton population using a stable ^{13}C isotope. *Mar. Biol.* 73, 31–36. doi: 10.1007/BF00396282.

Harada, N., Sato, M., Oguri, K., Hagino, K., Okazaki, Y., Katsuki, K., et al. (2012). Enhancement of coccolithophorid blooms in the Bering Sea by recent environmental changes. *Glob. Biogeochem. Cycles* 26. doi: 10.1029/2011GB004177.

Hargraves, P. E., and French, F. W. (1983). "Diatom resting spore: significance and strategies," in *Survival Strategies of the Algae* (New York: Cambridge University Press), 49–68.

Hasle, G. R., and Syvertsen, E. E. (1997). "Marine diatoms," in *Identifying Marine Phytoplankton*, ed. C. R. Tomas (San Diego: Academic Press), 5–385.

Hegseth, E. N., Assmy, P., Wiktor, J. M., Wiktor Jr, J., Kristiansen, S., Leu, E., et al. (2019). "Phytoplankton seasonal dynamics in kongsfjorden, svalbard and the adjacent

shelf," in *Ecosystem of Kongsfjorden, Svalbard*, eds. H. Hop and C. Wiencke (Springer International Publishing), 173–227.

Hill, V., Ardyna, M., Lee, S. H., and Varela, D. E. (2018). Decadal trends in phytoplankton production in the Pacific Arctic Region from 1950 to 2012. *Deep Sea Res. Part II Top. Stud. Oceanogr.* 152, 82–94. doi: 10.1016/j.dsr2.2016.12.015.

Hillebrand, H., Dürselen, C.-D., Kirschtel, D., Pollingher, U., and Zohary, T. (1999). Biovolume Calculation for Pelagic and Benthic Microalgae. *J. Phycol.* 35, 403–424. doi: 10.1046/j.1529-8817.1999.3520403.x.

Hirawake, T., and Hunt, G. L. (2020). Impacts of unusually light sea-ice cover in winter 2017-2018 on the northern Bering Sea marine ecosystem – An introduction. *Deep Sea Res. Part II Top. Stud. Oceanogr.* 181–182, 104908. doi: 10.1016/j.dsr2.2020.104908.

Hirawake, T., Oida, J., Yamashita, Y., Waga, H., Abe, H., Nishioka, J., et al. (2021). Water mass distribution in the northern Bering and southern Chukchi seas using light absorption of chromophoric dissolved organic matter. *Prog. Oceanogr.* 197, 102641. doi: 10.1016/j.pocean.2021.102641.

Hirawake, T., Shinmyo, K., Fujiwara, A., and Saitoh, S. (2012). Satellite remote sensing of primary productivity in the Bering and Chukchi Seas using an absorption-based approach. *ICES J. Mar. Sci.* 69, 1194–1204. doi: 10.1093/icesjms/fss111.

Hollibaugh, J. T., Seibert, D. L. R., and Thomas, W. H. (1981). Observations on the Survival and Germination of Resting Spores of Three *Chaetoceros* (bacillariophyceae) Species. *J. Phycol.* 17, 1–9. doi: https://doi.org/10.1111/j.1529-8817.1981.tb00812.x.

Hoppenrath, M., Elbrächter, M., and Drebes, G. (2009). *Marine phytoplankton: selected microphytoplankton species from the North Sea around Helgoland and Sylt*. Frankfurt, Germany: Schweizerbart Science Publishers.

Horner, R. (1984). "Phytoplankton abundance, chlorophyll a, and primary production in the western Beaufort Sea," in *The Alaskan Beaufort Sea: Ecosystems and Environments* (Florida: Academic Press), 295–310.

Horner, R., and Schrader, G. C. (1982). Relative contributions of ice algae, phytoplankton, and benthic microalgae to primary production in nearshore regions of the Beaufort Sea. *ARCTIC* 35, 485–503. doi: 10.14430/arctic2356.

Horvat, C., Jones, D. R., Iams, S., Schroeder, D., Flocco, D., and Feltham, D. (2017). The frequency and extent of sub-ice phytoplankton blooms in the Arctic Ocean. *Sci. Adv.* 3, e1601191. doi: 10.1126/sciadv.1601191.

Hunt Jr, G. L., Stabeno, P., Walters, G., Sinclair, E., Brodeur, R. D., Napp, J. M., et al. (2002). Climate change and control of the southeastern Bering Sea pelagic ecosystem. *Deep Sea Res. Part II Top. Stud. Oceanogr.* 49, 5821–5853. doi: 10.1016/S0967-0645(02)00321-1.

Hydes, D. J., Aoyama, M., Aminot, A., Bakker, K., Becker, S., Coverly, S., et al. (2010). "Determination of dissolved nutrients (N, P, SI) in seawater with high precision and inter-comparability using gas-segmented continuous flow analysers", in *The GOSHIP Repeat Hydrography Manual: A Collection of Expert Reports and Guidelines*, Version 1, eds. E. M. Hood, C. L. Sabine, B. M. Sloyan, B.M., IOCCP Report Number 14, ICPO Publication Series Number 134. doi: 10.25607/OBP-15. Available at: http://www.go-ship.org/HydroMan.html [Accessed November 2022]

Iida, T., Saitoh, S. I., Miyamura, T., Toratani, M., Fukushima, H., and Shiga, N. (2002). Temporal and spatial variability of coccolithophore blooms in the eastern Bering Sea, 1998-2001. *Prog. Oceanogr.* 55, 165–175. doi: 10.1016/S0079-6611(02)00076-9.

Imai, I., Itakura, S., and Itoh, K. (1990). Distribution of diatom resting cells in sediments of Harima-Nada and northern Hiroshima Bay, the Seto Island Sea, Japan. *Bull. Coast. Oceanogr.* 28, 75–84. doi: 10.32142/engankaiyo.28.1_75.

Imai, I., Itoh, K., and Anraku, M. (1984). Extinction dilution method for enumeration of dormant cells of red tide organisms in marine sediments. *Bull. Plankton Soc. Jpn.* 312, 123–124.

Isada, T., Hattori-Saito, A., Saito, H., Kondo, Y., Nishioka, J., Kuma, K., et al. (2019). Responses of phytoplankton assemblages to iron availability and mixing water masses during the spring bloom in the Oyashio region, NW Pacific. *Limnol. Oceanogr.* 64, 197–216. doi: 10.1002/lno.11031.

Isada, T., Kuwata, A., Saito, H., Ono, T., Ishii, M., Yoshikawa-Inoue, H., et al. (2009). Photosynthetic features and primary productivity of phytoplankton in the Oyashio and Kuroshio–Oyashio transition regions of the northwest Pacific. *J. Plankton Res.* 31, 1009–1025. doi: 10.1093/plankt/fbp050.

Itakura, S., Imai, I., and Itoh, K. (1997). "Seed bank" of coastal planktonic diatoms in bottom sediments of Hiroshima Bay, Seto Inland Sea, Japan. *Mar. Biol.* 128, 497–508. doi: 10.1007/s002270050116.

Jakob, T., Goss, R., and Wilhelm, C. (2001). Unusual pH-dependence of diadinoxanthin de-epoxidase activation causes chlororespiratory induced accumulation of diatoxanthin in the diatom *Phaeodactylum tricornutum*. *J. Plant Physiol.* 158, 383–390. doi: 10.1078/0176-1617-00288.

Jeffrey, S. W., Mantoura, R. F. C., and Wright, S. W. eds. (1997). *Phytoplankton pigments in oceanography: Guidelines to modern methods*. Paris: UNESCO.

Jin, X., Gruber, N., Dunne, J. P., Sarmiento, J. L., and Armstrong, R. A. (2006). Diagnosing the contribution of phytoplankton functional groups to the production and export of particulate organic carbon, $CaCO_3$, and opal from global nutrient and alkalinity distributions. *Glob. Biogeochem. Cycles* 20. doi: 10.1029/2005GB002532.

Johnsen, G., Leu, E., and Gradinger, R. (2020). "Marine Micro- and Macroalgae in the Polar Night," in *POLAR NIGHT Marine Ecology: Life and Light in the Dead of Night Advances in Polar Ecology*, eds. J. Berge, G. Johnsen, and J. H. Cohen (Cham: Springer International Publishing), 67–112. doi: 10.1007/978-3-030-33208-2_4.

Justić, D., Rabalais, N. N., Turner, R. E., and Dortch, Q. (1995). Changes in nutrient structure of river-dominated coastal waters: stoichiometric nutrient balance and its consequences. *Estuar. Coast. Shelf Sci.* 40, 339–356. doi: 10.1016/S0272-7714(05)80014-9.

Kikuchi, G., Abe, H., Hirawake, T., and Sampei, M. (2020). Distinctive spring phytoplankton bloom in the Bering Strait in 2018: A year of historically minimum sea ice extent. *Deep Sea Res. Part II Top. Stud. Oceanogr.* 181–182, 104905. doi: 10.1016/j.dsr2.2020.104905.

Kimura, F., Matsuno, K., Abe, Y., and Yamaguchi, A. (2022). Effects of early sea-ice reduction on zooplankton and copepod population structure in the Northern Bering Sea during the summers of 2017 and 2018. *Front. Mar. Sci.* 9, 808910.

Kishino, M., Takahashi, M., Okami, N., and Ichimura, S. (1985). Estimation of the spectral absorption coefficients of phytoplankton in the sea. *Bull. Mar. Sci.* 37, 9.

Krieger-Liszkay, A., and Feilke, K. (2016). The dual role of the plastid terminal oxidase PTOX: Between a protective and a pro-oxidant function. *Front. Plant Sci.* 6, 1147.

Kuczynska, P., Jemiola-Rzeminska, M., and Strzalka, K. (2015). Photosynthetic pigments in diatoms. *Mar. Drugs* 13, 5847–5881. doi: 10.3390/md13095847.

Kulk, G., Buist, A., van de Poll, W. H., Rozema, P. D., and Buma, A. G. J. (2019). Size scaling of photophysiology and growth in four freshly isolated diatom species from Ryder Bay, western Antarctic peninsula. *J. Phycol.* 55, 314–328. doi: 10.1111/jpy.12813.

Kuwata, A., Hama, T., and Takahashi, M. (1993). Ecophysiological characterization of two life-forms, resting spores and resting cells of a marine planktonic diatom, *Chaetoceros pseudocurvisetus* formed under nutrient depletion. *Mar. Ecol. Prog. Ser.* 102, 245–255.

Kvernvik, A. C., Hoppe, C. J. M., Lawrenz, E., Prášil, O., Greenacre, M., Wiktor, J. M., et al. (2018). Fast reactivation of photosynthesis in arctic phytoplankton during the polar night. *J. Phycol.* 54, 461–470. doi: 10.1111/jpy.12750.

Lacour, T., Babin, M., and Lavaud, J. (2020). Diversity in xanthophyll cycle pigments content and related nonphotochemical quenching (NPQ) among microalgae: Implications for growth strategy and ecology. *J. Phycol.* 56, 245–263. doi: 10.1111/jpy.12944.

Lacour, T., Larivière, J., and Babin, M. (2017). Growth, Chl *a* content, photosynthesis, and elemental composition in polar and temperate microalgae. *Limnol. Oceanogr.* 62, 43–58. doi: 10.1002/lno.10369.

Lacour, T., Morin, P.-I., Sciandra, T., Donaher, N., Campbell, D. A., Ferland, J., et al. (2019). Decoupling light harvesting, electron transport and carbon fixation during prolonged darkness supports rapid recovery upon re-illumination in the Arctic diatom *Chaetoceros neogracilis. Polar Biol.* 42, 1787–1799. doi: 10.1007/s00300-019-02507-2.

Lalande, C., Grebmeier, J. M., Hopcroft, R. R., and Danielson, S. L. (2020). Annual cycle of export fluxes of biogenic matter near Hanna Shoal in the northeast Chukchi Sea. *Deep Sea Res. Part II Top. Stud. Oceanogr.* 177, 104730. doi: 10.1016/j.dsr2.2020.104730.

Lalande, C., Grebmeier, J. M., McDonnell, A. M. P., Hopcroft, R. R., O'Daly, S., and Danielson, S. L. (2021). Impact of a warm anomaly in the Pacific Arctic region derived from time-series export fluxes. *PLOS ONE* 16, e0255837. doi: 10.1371/journal.pone.0255837.

Lee, S. H., Yun, M. S., Jang, H. K., Kang, J. J., Kim, K., Lee, D., et al. (2023). Size-differential photosynthetic traits of phytoplankton in the Chukchi Sea. *Cont. Shelf Res.* 255, 104933. doi: 10.1016/j.csr.2023.104933.

Lee, Z., Lubac, B., Werdell, J., and Arnone, R. (2009). *An update of the Quasi-Analytical Algorithm (QAA_v5)*. Available at: http://www.ioccg.org/groups/software.html [Accessed January 6, 2021].

Lee, Z., Weidemann, A., Kindle, J., Arnone, R., Carder, K. L., and Davis, C. (2007). Euphotic zone depth: Its derivation and implication to ocean-color remote sensing. *J. Geophys. Res. Oceans* 112. doi: https://doi.org/10.1029/2006JC003802.

Lesser, M. P. (2006). Oxidative stress in Marine environments: Biochemistry and Physiological *Ecology. Annu. Rev. Physiol.* 68, 253–278. doi: 10.1146/annurev.physiol.68.040104.110001.

Leu, E., Mundy, C. J., Assmy, P., Campbell, K., Gabrielsen, T. M., Gosselin, M., et al. (2015). Arctic spring awakening – Steering principles behind the phenology of vernal ice algal blooms. *Prog. Oceanogr.* 139, 151–170. doi: 10.1016/j.pocean.2015.07.012.

Lopes dos Santos, A., Gérikas Ribeiro, C., Ong, D., Garczarek, L., Shi, X. L., Nodder, S. D., et al. (2022). "Chapter 11 - Phytoplankton diversity and ecology through the lens of high throughput sequencing technologies," in *Advances in Phytoplankton Ecology*, eds. L. A. Clementson, R. S. Eriksen, and A. Willis (Elsevier), 353–413. doi: 10.1016/B978-0-12-822861-6.00020-0.

Mackey, M., Mackey, D., Higgins, H., and Wright, S. (1996). CHEMTAX - a program for estimating class abundances from chemical markers: application to HPLC measurements of phytoplankton. *Mar. Ecol. Prog. Ser.* 144, 265–283. doi: 10.3354/meps144265.

Malviya, S., Scalco, E., Audic, S., Vincent, F., Veluchamy, A., Poulain, J., et al. (2016). Insights into global diatom distribution and diversity in the world's ocean. *Proc. Natl. Acad. Sci.* 113, E1516–E1525. doi: 10.1073/pnas.1509523113.

Markus, T., Stroeve, J. C., and Miller, J. (2009). Recent changes in Arctic sea ice melt onset, freezeup, and melt season length. *J. Geophys. Res. Oceans* 114. doi: 10.1029/2009JC005436.

Matsuno, K., Ichinomiya, M., Yamaguchi, A., Imai, I., and Kikuchi, T. (2014). Horizontal distribution of microprotist community structure in the western Arctic Ocean during late summer and early fall of 2010. *Polar Biol.* 37, 1185–1195. doi: 10.1007/s00300-014-1512-z.

McMinn, A., and Martin, A. (2013). Dark survival in a warming world. *Proc. R. Soc. B Biol. Sci.* 280, 20122909. doi: 10.1098/rspb.2012.2909.

McQuoid, M. R., and Hobson, L. A. (1996). Diatom resting stages. *J. Phycol.* 32, 889–902. doi: 10.1111/j.0022-3646.1996.00889.x.

Melnikov, I. A., Kolosova, E. G., Welch, H. E., and Zhitina, L. S. (2002). Sea ice biological communities and nutrient dynamics in the Canada Basin of the Arctic Ocean. *Deep Sea Res. Part Oceanogr. Res. Pap.* 49, 1623–1649. doi: 10.1016/S0967-0637(02)00042-0.

Miklasz, K. A., and Denny, M. W. (2010). Diatom sinkings speeds: Improved predictions and insight from a modified Stokes' law. *Limnol. Oceanogr.* 55, 2513–2525. doi: 10.4319/lo.2010.55.6.2513.

Mock, T., and Gradinger, R. (1999). Determination of Arctic ice algal production with a new in situ incubation technique. *Mar. Ecol. Prog. Ser.* 177, 15–26. doi: 10.3354/meps177015.

Nakatsuka, T., Handa, N., Wada, E., and Wong, C. S. (1992). The dynamic changes of stable isotopic ratios of carbon and nitrogen in suspended and sedimented particulate organic matter during a phytoplankton bloom. *J. Mar. Res.* 50, 267–296. doi: 10.1357/002224092784797692.

Neeley, A. R., Harris, L. A., and Frey, K. E. (2018). Unraveling Phytoplankton Community Dynamics in the Northern Chukchi Sea Under Sea-Ice-Covered and Sea-Ice-Free Conditions. *Geophys. Res. Lett.* 45, 7663–7671. doi: 10.1029/2018GL077684.

Nelson, D. M., Tréguer, P., Brzezinski, M. A., Leynaert, A., and Quéguiner, B. (1995). Production and dissolution of biogenic silica in the ocean: Revised global estimates, comparison with regional data and relationship to biogenic sedimentation. *Glob. Biogeochem. Cycles* 9, 359–372. doi: 10.1029/95GB01070.

Nicolaus, M., Katlein, C., Maslanik, J., and Hendricks, S. (2012). Changes in Arctic sea ice result in increasing light transmittance and absorption. *Geophys. Res. Lett.* 39. doi: 10.1029/2012GL053738.

Nishino, S., Kawaguchi, Y., Inoue, J., Hirawake, T., Fujiwara, A., Futsuki, R., et al. (2015). Nutrient supply and biological response to wind-induced mixing, inertial motion, internal waves, and currents in the northern Chukchi Sea. *J. Geophys. Res. Oceans* 120, 1975–1992. doi: 10.1002/2014JC010407.

Nishioka, J., Obata, H., Ogawa, H., Ono, K., Yamashita, Y., Lee, K., et al. (2020). Subpolar marginal seas fuel the North Pacific through the intermediate water at the termination of the global ocean circulation. *Proc. Natl. Acad. Sci. U. S. A.* 117, 12665–12673. doi: 10.1073/pnas.2000658117.

Nishizawa, B., Yamada, N., Hayashi, H., Wright, C., Kuletz, K., Ueno, H., et al. (2020). Timing of spring sea-ice retreat and summer seabird-prey associations in the northern Bering Sea. *Deep Sea Res. Part II Top. Stud. Oceanogr.* 181–182, 104898. doi: 10.1016/j.dsr2.2020.104898.

Norton, D., and Weller, G. (1984). "The Beaufort Sea: background, history and perspective," in *The Alaskan Beaufort Sea*, eds. P. W. Barnes, D. M. Schell, and E. Reimnitz (Academic Press), 3–19. doi: 10.1016/B978-0-12-079030-2.50007-1.

O'Daly, S. H., Danielson, S. L., Hardy, S. M., Hopcroft, R. R., Lalande, C., Stockwell, D. A., et al. (2020). Extraordinary Carbon Fluxes on the Shallow Pacific Arctic Shelf During a Remarkably Warm and Low Sea Ice Period. *Front. Mar. Sci.* 7, 986. doi: 10.3389/fmars.2020.548931.

Ohshima, K. I., Tamaru, N., Kashiwase, H., Nihashi, S., Nakata, K., and Iwamoto, K. (2020). Estimation of sea ice production in the Bering Sea from AMSR-E and AMSR2

data, with special emphasis on the Anadyr polynya. *J. Geophys. Res. Oceans* 125, e2019JC016023. doi: 10.1029/2019JC016023.

Oku, O., and Kamatani, A. (1998). Resting spore formation and xanthophyl pigments of the marine planktonic diatom *Chaetoceros pseudocurvisetus*. *Bull. Plankton Soc. Jpn.* 45, 123–132.

Parsons, T. R., Harrison, P. J., and Waters, R. (1978). An experimental simulation of changes in diatom and flagellate blooms. *J. Exp. Mar. Biol. Ecol.* 32, 285–294. doi: 10.1016/0022-0981(78)90122-3.

Pelusi, A., Luca, P. D., Manfellotto, F., Thamatrakoln, K., Bidle, K. D., and Montresor, M. (2021). Virus-induced spore formation as a defense mechanism in marine diatoms. *New Phytol.* 229, 2251–2259. doi: 10.1111/nph.16951.

Pelusi, A., Margiotta, F., Passarelli, A., Ferrante, M. I., d'Alcalà, M. R., and Montresor, M. (2020). Density-dependent mechanisms regulate spore formation in the diatom *Chaetoceros socialis*. *Limnol. Oceanogr. Lett.* 5, 371–378. doi: 10.1002/lol2.10159.

Pickart, R. S., Schulze, L. M., Moore, G. W. K., Charette, M. A., Arrigo, K. R., van Dijken, G., et al. (2013). Long-term trends of upwelling and impacts on primary productivity in the Alaskan Beaufort Sea. *Deep Sea Res. Part Oceanogr. Res. Pap.* 79, 106–121. doi: 10.1016/j.dsr.2013.05.003.

Piredda, R., Sarno, D., Lange, C. B., Tomasino, M. P., Zingone, A., and Montresor, M. (2017a). Diatom Resting Stages in Surface Sediments: A Pilot Study Comparing Next Generation Sequencing and Serial Dilution Cultures. *Cryptogam. Algol.* 38, 31–46. doi: 10.7872/crya/v38.iss1.2017.31.

Piredda, R., Tomasino, M. P., D'Erchia, A. M., Manzari, C., Pesole, G., Montresor, M., et al. (2017b). Diversity and temporal patterns of planktonic protist assemblages at a Mediterranean Long Term Ecological Research site. *FEMS Microbiol. Ecol.* 93, fiw200. doi: 10.1093/femsec/fiw200.

Pitcher, G. C. (1990). Phytoplankton seed populations of the Cape Peninsula upwelling plume, with particular reference to resting spores of *Chaetoceros* (bacillariophyceae) and their role in seeding upwelling waters. *Estuar. Coast. Shelf Sci.* 31, 283–301. doi: 10.1016/0272-7714(90)90105-Z.

Platt, T., Gallegos, C. L., and Harrison, W. G. (1980). Photoinhibition and photosynthesis in natural assemblages of marine phytoplankton. *J. Mar. Res.* 38, 687–701.

Platt, T., Harrison, W. G., Irwin, B., Horne, E. P., and Gallegos, C. L. (1982). Photosynthesisand photoadaptation of marine phytoplankton in the Arctic. *Deep-Sea Res.* 29, 1159–1170.

Pomerleau, C., Nelson, R. J., Hunt, B. P. V., Sastri, A. R., and Williams, W. J. (2014). Spatial patterns in zooplankton communities and stable isotope ratios ($\delta^{13}C$ and $\delta^{15}N$) in relation to oceanographic conditions in the sub-Arctic Pacific and western Arctic regions during the summer of 2008. *J. Plankton Res.* 36, 757–775. doi: 10.1093/plankt/fbt129.

Quinn, G. P., and Keough, M. J. (2002). *Experimental Design and Data Analysis for Biologists*. New York: Cambridge University Press.

Rousseau, V., Leynaert, A., Daoud, N., and Lancelot, C. (2002). Diatom succession, silicification and silicic acid availability in Belgian coastal waters (Southern North Sea). *Mar. Ecol. Prog. Ser.* 236, 61–73. doi: 10.3354/meps236061.

Ruban, A., Lavaud, J., Rousseau, B., Guglielmi, G., Horton, P., and Etienne, A.-L. (2004). The super-excess energy dissipation in diatom algae: comparative analysis with higher plants. *Photosynth. Res.* 82, 165. doi: 10.1007/s11120-004-1456-1.

Rynearson, T. A., Richardson, K., Lampitt, R. S., Sieracki, M. E., Poulton, A. J., Lyngsgaard, M. M., et al. (2013). Major contribution of diatom resting spores to vertical flux in the sub-polar North Atlantic. *Deep Sea Res. Part Oceanogr. Res. Pap.* 82, 60–71. doi: 10.1016/j.dsr.2013.07.013.

Sakshaug, E. (2004). "Primary and Secondary Production in the Arctic Seas," in *The Organic Carbon Cycle in the Arctic Ocean*, eds. R. Stein and R. W. MacDonald (Berlin, Heidelberg: Springer), 57–81. doi: 10.1007/978-3-642-18912-8_3.

Sakshaug, E., Bricaud, A., Dandonneau, Y., Falkowski, P. G., Kiefer, D. A., Legendre, L., et al. (1997). Parameters of photosynthesis: definitions, theory and interpretation of results. *J. Plankton Res.* 19, 1637–1670. doi: 10.1093/plankt/19.11.1637.

Sanyal, A., Larsson, J., van Wirdum, F., Andrén, T., Moros, M., Lönn, M., et al. (2022). Not dead yet: Diatom resting spores can survive in nature for several millennia. *Am. J. Bot.* 109, 67–82. doi: 10.1002/ajb2.1780.

Sergeeva, V. M., Sukhanova, I. N., Flint, M. V., Pautova, L. A., Grebmeier, J. M., and Cooper, L. W. (2010). Phytoplankton community in the Western Arctic in July–August 2003. *Oceanology* 50, 184–197. doi: 10.1134/S0001437010020049.

Shannon, C. E., and Weaver, W. (1949). *The Mathematical Theory of Communication*. Urbana: The University of Illinois Press.

Sherr, E. B., Sherr, B. F., and Hartz, A. J. (2009). Microzooplankton grazing impact in the Western Arctic Ocean. *Deep Sea Res. Part II Top. Stud. Oceanogr.* 56, 1264–1273. doi: 10.1016/j.dsr2.2008.10.036.

Shikata, T., Iseki, M., Matsunaga, S., Higashi, S., Kamei, Y., and Watanabe, M. (2011). Blue and red light-induced germination of resting spores in the red-tide diatom

Leptocylindrus danicus. *Photochem. Photobiol.* 87, 590–597. doi: 10.1111/j.1751-1097.2011.00914.x.

Shikata, T., Nukata, A., Yoshikawa, S., Matsubara, T., Yamasaki, Y., Shimasaki, Y., et al. (2009). Effects of light quality on initiation and development of meroplanktonic diatom blooms in a eutrophic shallow sea. *Mar. Biol.* 156, 875–889. doi: 10.1007/s00227-009-1131-3.

Shiozaki, T., Fujiwara, A., Sugie, K., Nishino, S., Makabe, A., and Harada, N. (2022). Bottom-associated phytoplankton bloom and its expansion in the Arctic Ocean. *Glob. Change Biol.* 28, 7286–7295. doi: 10.1111/gcb.16421.

Silsbe, G. M., and Malkin, S. Y. (2015). *CRAN - Package phytotools*. Available at: https://mran.microsoft.com/snapshot/2017-06-23/web/packages/phytotools/index.html [Accessed August 14, 2022].

Smetacek, V. (1999). Diatoms and the ocean carbon cycle. *Protist* 150, 25–32. doi: 10.1016/S1434-4610(99)70006-4.

Smith, W. O., Keene, N. K., and Comiso, J. C. (1988). "Interannual Variability in Estimated Primary Productivity of the Antarctic Marginal Ice Zone," in *Antarctic Ocean and Resources Variability*, ed. D. Sahrhage (Berlin, Heidelberg: Springer), 131–139.

Sournia, A., Chrdtiennot-Dinet, M.-J., and Ricard, M. (1991). Marine phytoplankton: how many species in the world ocean? *J. Plankton Res.* 13, 1093–1099. doi: 10.1093/plankt/13.5.1093.

Springer, A. M., and McRoy, C. P. (1993). The paradox of pelagic food webs in the northern Bering Sea—III. Patterns of primary production. *Cont. Shelf Res.* 13, 575–599. doi: 10.1016/0278-4343(93)90095-F.

Springer, A. M., McROY, C. P., and Flint, M. V. (1996). The Bering Sea Green Belt: shelf-edge processes and ecosystem production. *Fish. Oceanogr.* 5, 205–223. doi: 10.1111/j.1365-2419.1996.tb00118.x.

Stabeno, P. J., and Bell, S. W. (2019). Extreme Conditions in the Bering Sea (2017–2018): Record-Breaking Low Sea-Ice Extent. *Geophys. Res. Lett.* 46, 8952–8959. doi: 10.1029/2019GL083816.

Stahl, W., and Sies, H. (2005). Bioactivity and protective effects of natural carotenoids. *Biochim. Biophys. Acta BBA - Mol. Basis Dis.* 1740, 101–107. doi: 10.1016/j.bbadis.2004.12.006.

Stockwell, D. A., Whitledge, T. E., Zeeman, S. I., Coyle, K. O., Napp, J. M., Brodeur, R. D., et al. (2001). Anomalous conditions in the south-eastern Bering Sea, 1997: nutrients, phytoplankton and zooplankton. *Fish. Oceanogr.* 10, 99–116. doi: 10.1046/j.1365-2419.2001.00158.x.

Stramski, D., Reynolds, R., Kaczmarek, S., Uitz, J., and Zheng, G. (2015). Correction of pathlength amplification in the filter-pad technique for measurements of particulate absorption coefficient in the visible spectral region. *Appl. Opt.* 54, 6763–6782. doi: 10.1364/AO.54.006763.

Sugie, K., and Kuma, K. (2008). Resting spore formation in the marine diatom *Thalassiosira nordenskioeldii* under iron- and nitrogen-limited conditions. *J. Plankton Res.* 30, 1245–1255. doi: 10.1093/plankt/fbn080.

Sukhanova, I. N., Flint, M. V., Pautova, L. A., Stockwell, D. A., Grebmeier, J. M., and Sergeeva, V. M. (2009). Phytoplankton of the western Arctic in the spring and summer of 2002: Structure and seasonal changes. *Deep Sea Res. Part II Top. Stud. Oceanogr.* 56, 1223–1236. doi: 10.1016/j.dsr2.2008.12.030.

Sukhanova, I. N., Flint, M. V., Whitledge, T. E., Stockwell, D. A., and Rho, T. K. (2006). Mass development of the planktonic diatom *Proboscia alata* over the Bering sea shelf in the summer season. *Oceanology* 46, 200–216. doi: 10.1134/S000143700602007X.

Suzuki, K., Handa, N., Nishida, T., and Wong, C. S. (1997). Estimation of phytoplankton succession in a fertilized mesocosm during summer using high-performance liquid chromatographic analysis of pigments. *J. Exp. Mar. Biol. Ecol.* 214, 1–17. doi: 10.1016/S0022-0981(97)00003-8.

Suzuki, K., Kamimura, A., and Hooker, S. B. (2015). Rapid and highly sensitive analysis of chlorophylls and carotenoids from marine phytoplankton using ultra-high performance liquid chromatography (UHPLC) with the first derivative spectrum chromatogram (FDSC) technique. *Mar. Chem.* 176, 96–109. doi: 10.1016/j.marchem.2015.07.010.

Suzuki, K., Minami, C., Liu, H., and Saino, T. (2002). Temporal and spatial patterns of chemotaxonomic algal pigments in the subarctic Pacific and the Bering Sea during the early summer of 1999. *Deep Sea Res. Part II Top. Stud. Oceanogr.* 49, 5685–5704. doi: 10.1016/S0967-0645(02)00218-7.

Suzuki, K., Yoshino, Y., Nosaka, Y., Nishioka, J., Hooker, S. B., and Hirawake, T. (2021). Diatoms contributing to new production in surface waters of the northern Bering and Chukchi Seas during summer with reference to water column stratification. *Prog. Oceanogr.* 199, 102692. doi: 10.1016/j.pocean.2021.102692.

Szymanski, A., and Gradinger, R. (2016). The diversity, abundance and fate of ice algae and phytoplankton in the Bering Sea. *Polar Biol.* 39, 309–325. doi: 10.1007/s00300-015-1783-z.

Takahashi, K., Jordan, R., and Priddle, J. (1994). The diatom genus *Proboscia* in subarctic waters. *Diatom Res.* 9, 411–428.

Taniguchi, A., Saito, K., Koyama, A., and Fukuchi, M. (1976). Phytoplankton communities in the Bering Sea and adjacent seas. *J. Oceanogr. Soc. Jpn.* 32, 99–106. doi: 10.1007/BF02107038.

Telussa, I., Rusnadi, and Zeily Nurachman (2019). Dynamics of β-carotene and fucoxanthin of tropical marine *Navicula* sp. as a response to light stress conditions. *Algal Res.* 41, 101530. doi: 10.1016/j.algal.2019.101530.

Throndsen, J. (1978). "The dilution-culture method," in *Phytoplankton Manual* (Paris: Unesco), 218–224.

Tréguer, P., Bowler, C., Moriceau, B., Dutkiewicz, S., Gehlen, M., Aumont, O., et al. (2018). Influence of diatom diversity on the ocean biological carbon pump. *Nat. Geosci.* 11, 27–37. doi: 10.1038/s41561-017-0028-x.

Tréguer, P. J., and De La Rocha, C. L. (2013). The World Ocean Silica Cycle. *Annu. Rev. Mar. Sci.* 5, 477–501. doi: 10.1146/annurev-marine-121211-172346.

Tsukazaki, C., Ishii, K.-I., Matsuno, K., Yamaguchi, A., and Imai, I. (2018). Distribution of viable resting stage cells of diatoms in sediments and water columns of the Chukchi Sea, Arctic Ocean. *Phycologia* 57, 440–452. doi: 10.2216/16-108.1.

Tsukazaki, C., Ishii, K.-I., Saito, R., Matsuno, K., Yamaguchi, A., and Imai, I. (2013). Distribution of viable diatom resting stage cells in bottom sediments of the eastern Bering Sea shelf. *Deep Sea Res. Part II Top. Stud. Oceanogr.* 94, 22–30. doi: 10.1016/j.dsr2.2013.03.020.

Uchimiya, M., Motegi, C., Nishino, S., Kawaguchi, Y., Inoue, J., Ogawa, H., et al. (2016). Coupled response of bacterial production to a wind-induced fall phytoplankton bloom and sediment resuspension in the Chukchi Sea shelf, Western Arctic Ocean. *Front. Mar. Sci.* 3, 231. doi: 10.3389/fmars.2016.00231.

Ueno, H., Komatsu, M., Ji, Z., Dobashi, R., Muramatsu, M., Abe, H., et al. (2020). Stratification in the northern Bering Sea in early summer of 2017 and 2018. *Deep Sea Res. Part II Top. Stud. Oceanogr.* 181–182, 104820. doi: 10.1016/j.dsr2.2020.104820.

Vallis, G. K. (2017). *Atmospheric and Oceanic Fluid Dynamics.* Cambridge University Press.

Vidussi, F., Claustre, H., Manca, B. B., Luchetta, A., and Marty, J.-C. (2001). Phytoplankton pigment distribution in relation to upper thermocline circulation in the eastern Mediterranean Sea during winter. *J. Geophys. Res. Oceans* 106, 19939–19956. doi: 10.1029/1999JC000308.

Vincent, F., Ibarbalz, F. M., and Bowler, C. (2022). "Chapter 15 - Global marine phytoplankton revealed by the Tara Oceans expedition," in *Advances in Phytoplankton Ecology*, eds. L. A. Clementson, R. S. Eriksen, and A. Willis (Elsevier), 531–561. doi: 10.1016/B978-0-12-822861-6.00024-8.

von Quillfeldt, C. H. (2000). Common diatom species in Arctic spring blooms: Their distribution and abundance. *Bot. Mar.* 43, 499–516. doi: 10.1515/BOT.2000.050.

von Quillfeldt, C. H., Ambrose, W. G., and Clough, L. M. (2003). High number of diatom species in first-year ice from the Chukchi Sea. *Polar Biol.* 26, 806–818. doi: 10.1007/s00300-003-0549-1.

Waga, H., Eicken, H., Light, B., and Fukamachi, Y. (2022). A neural network-based method for satellite-based mapping of sediment-laden sea ice in the Arctic. *Remote Sens. Environ.* 270, 112861. doi: 10.1016/j.rse.2021.112861.

Waga, H., Hirawake, T., Fujiwara, A., Grebmeier, J. M., and Saitoh, S.-I. (2019). Impact of spatiotemporal variability in phytoplankton size structure on benthic macrofaunal distribution in the Pacific Arctic. *Deep Sea Res. Part II Top. Stud. Oceanogr.* 162, 114–126. doi: 10.1016/j.dsr2.2018.10.008.

Wang, S. W., Budge, S. M., Iken, K., Gradinger, R. R., Springer, A. M., and Wooller, M. J. (2015). Importance of sympagic production to Bering Sea zooplankton as revealed from fatty acid-carbon stable isotope analyses. *Mar. Ecol. Prog. Ser.* 518, 31–50. doi: 10.3354/meps11076.

Wang, S. W., Springer, A. M., Budge, S. M., Horstmann, L., Quakenbush, L. T., and Wooller, M. J. (2016). Carbon sources and trophic relationships of ice seals during recent environmental shifts in the Bering Sea. *Ecol. Appl.* 26, 830–845. doi: 10.1890/14-2421.

Wang, W., Zhao, S., Pi, X., Kuang, T., Sui, S.-F., and Shen, J.-R. (2020). Structural features of the diatom photosystem II–light-harvesting antenna complex. *FEBS J.* 287, 2191–2200. doi: 10.1111/febs.15183.

Werner, I., Ikävalko, J., and Schünemann, H. (2007). Sea-ice algae in Arctic pack ice during late winter. *Polar Biol.* 30, 1493–1504. doi: 10.1007/s00300-007-0310-2.

Woodgate, R. A., Weingartner, T., and Lindsay, R. (2010). The 2007 Bering Strait oceanic heat flux and anomalous Arctic sea-ice retreat. *Geophys. Res. Lett.* 37. doi: 10.1029/2009GL041621.

Xu, C., Pi, X., Huang, Y., Han, G., Chen, X., Qin, X., et al. (2020). Structural basis for energy transfer in a huge diatom PSI-FCPI supercomplex. *Nat. Commun.* 11, 5081. doi: 10.1038/s41467-020-18867-x.

Yan, D., Endo, H., and Suzuki, K. (2019). Increased temperature benefits growth and photosynthetic performance of the sea ice diatom *Nitzschia* cf. *neglecta* (Bacillariophyceae) isolated from saroma lagoon, Hokkaido, Japan. *J. Phycol.* 55, 700–713. doi: 10.1111/jpy.12846.

Yokoi, N., Matsuno, K., Ichinomiya, M., Yamaguchi, A., Nishino, S., Onodera, J., et al. (2016). Short-term changes in a microplankton community in the Chukchi Sea during autumn: consequences of a strong wind event. *Biogeosciences* 13, 913–923. doi: 10.5194/bg-13-913-2016.

Yoshida, K., Endo, H., Lawrenz, E., Isada, T., Hooker, S. B., Prášil, O., et al. (2018). Community composition and photophysiology of phytoplankton assemblages in coastal Oyashio waters of the western North Pacific during early spring. *Estuar. Coast. Shelf Sci.* 212, 80–94. doi: 10.1016/j.ecss.2018.06.018.

Yoshida, K., Hattori, H., Toyota, T., McMinn, A., and Suzuki, K. (2020a). Differences in diversity and photoprotection capability between ice algae and under-ice phytoplankton in Saroma-Ko Lagoon, Japan: a comparative taxonomic diatom analysis with microscopy and DNA barcoding. *Polar Biol.* 43, 1873–1885. doi: 10.1007/s00300-020-02751-x.

Yoshida, K., Nakamura, S., Nishioka, J., Hooker, S. B., and Suzuki, K. (2020b). Community composition and photosynthetic physiology of phytoplankton in the Western Subarctic Pacific near the Kuril Islands with special reference to iron availability. *J. Geophys. Res. Biogeosciences* 125, e2019JG005525. doi: 10.1029/2019JG005525.

Zhou, Y., Zhang, Y., Li, F., Tan, L., and Wang, J. (2017). Nutrients structure changes impact the competition and succession between diatom and dinoflagellate in the East China Sea. *Sci. Total Environ.* 574, 499–508. doi: 10.1016/j.scitotenv.2016.09.092.